APPLICATION OF THE FAST MARCHING METHOD TO RESERVOIR CHARACTERIZATION AND PRESSURE TRANSIENT ANALYSIS IN STRUCTURED AND CORNER POINT GRID GEOMETRIES

A Dissertation

by

CHEN LI

Submitted to the Office of Graduate and Professional Studies of
Texas A&M University
in partial fulfillment of the requirements for the degree of

DOCTOR OF PHILOSOPHY

Chair of Committee,	Michael J. King
Committee Members,	Akhil Datta-Gupta
	Eduardo Gildin
	Richard Gibson
Head of Department,	Jeffrey B. Spath

December 2018

Major Subject: Petroleum Engineering

ABSTRACT

Well test analysis is a critical tool for evaluation of well and reservoir performance. It is intrinsically an inversion methodology for reservoir parameter estimation and is closely related to the drainage volume evolution around the wellbore. Pressure transient analysis provides insight into our geometric understanding of the reservoir shape and volume, which helps us obtain a volume-averaged estimation of reservoir parameters from the interpretation of the flow regime in the porous media. Though straightforward, the conventional well test methodology can only help us interpret the flow mechanism in an analytic approach with simplified (homogeneous) models. When detailed reservoir information is required, numerical simulation needs to be employed to obtain grid-cell based reservoir parameters from integration of the well pressure or rate data.

To this end, we propose a semi-analytic methodology for simulation of fluid flow in the subsurface and interpretation of the grid-cell based reservoir parameters. It relies upon an asymptotic expansion to the pressure diffusivity equation based on the "diffusive time of flight" (DTOF) calculation, which transforms the three-dimensional diffusivity equation into a reduced one-dimensional formulation. The DTOF (τ) can be calculated from solving the Eikonal equation using the fast marching method (FMM).

In this dissertation, we first discuss the formulation of the drainage volume using the DTOF and prove its relationship with the well test derivative. Different orders of drainage volume discretization schemes in the near-well region are analyzed and combined into a hybrid version, which includes an analytic formulation at the well cell

and ensures sufficiently accurate transient pressure behavior at early times of simulation. Similarly, a hybrid version of cumulative pore volume discretization is used for the DTOF-based transient flow simulation and proves to be able to generate stable and consistent solutions in general heterogeneous porous media.

The second part of this dissertation focuses on exposition of an inverse modeling methodology that can be used to estimate grid-cell based reservoir parameters by integrating pressure transient data into the geologic model. The well test derivative is inversely related to the drainage volume and is treated as the well observation. Its analytic sensitivity coefficients with respect to reservoir parameters are formulated and included into a penalized objective function for inversion. This inversion technique leads to a computational speed orders of magnitude faster than conventional sensitivity-based inverse modeling approaches that would require numerical perturbations.

Finally, we propose a FMM that can be used for reservoir models with faulted corner point grids (CPG). The local Eikonal solution is formulated in a quadratic equation for the DTOF, the coefficients of which are formulated explicitly. This new FMM for CPG applies for general anisotropic heterogeneous media and is easy to implement on triangular and tetrahedral meshes, which constitute the unit CPG. Complex geometric features including the faults and pinch-outs are taken into account when the new FMM is designed.

DEDICATION

To my parents and older sister, for their encouragement, support and love.

ACKNOWLEDGEMENTS

This dissertation would not become possible without the guidance and help of several individuals from both the Department of Petroleum Engineering and beyond, who either provided valuable assistance or contributed to completion of this study.

First and foremost, I would owe my deepest gratitude to my advisor Dr. Michael J. King. Without his challenges, encouragements, inspiring ideas, and financial support, I would not have had the chance to engage in such a novel research project and complete this thesis in the present form. Thoughtful discussions that break research topics into parts and piece them together afterwards have enlightened me and will guide me through my future research activities.

I am grateful to Dr. Akhil Datta-Gupta, whose academic instruction provides me a solid methodological background for my research and enables me to understand the topic from a broader perspective.

I would like to thank Dr. Eduardo Gildin for his hospitality and many inspiring discussions when I visited him for research suggestions.

In addition, I would like to thank Dr. Richard Gibson for taking time to review and comment on my thesis.

Meanwhile, I would like to thank my colleagues Krishna Nunna, Peng Zhou and Zhenzhen Wang (now at Chevron Corporation) in the office of Richardson 703 for their consistent and warm-hearted help during my graduate research.

Many thanks to all MCERI members and friends at Texas A&M University for making my graduate study in College Station a wonderful experience.

Finally, thanks to my beloved parents and older sister for their encouragement and support.

CONTRIBUTORS AND FUNDING SOURCES

Contributors

This work was supervised by a dissertation committee consisting of Professor Michael J. King (advisor), Professor Akhil Datta-Gupta, and Professor Eduardo Gildin of the Department of Petroleum Engineering and Professor Richard Gibson of the Department of Geology and Geophysics.

All work conducted for the dissertation was completed by the student independently.

Funding Sources

This work was made possible by the financial support of the Joint Industry Project (JIP) members of the Model Calibration and Efficient Reservoir Imaging (MCERI) consortium at Texas A&M University.

Graduate study was supported by a fellowship from Texas A&M University.

NOMENCLATURE

k	=	Permeability, md
$\overline{KX}$	=	Average permeability in the x-direction, md
$\overline{KY}$	=	Average permeability in the y-direction, md
$\overline{KZ}$	=	Average permeability in the z-direction, md
ϕ	=	Porosity
$\overline{\phi}$	=	Average porosity
μ	=	Viscosity, cp
c_t	=	Total compressibility, psi^{-1}
α_D	=	Hydraulic diffusivity, ft^2/hr
B_o	=	Oil formation volume factor, res bbl/STB
LX	=	Reservoir length in the x-direction, ft
LY	=	Reservoir length in the y-direction, ft
LZ	=	Reservoir length in the z-direction, ft
h	=	Reservoir thickness, ft
DX	=	Cell length in the x-direction, ft
DY	=	Cell length in the y-direction, ft
DZ	=	Cell length in the z-direction, ft
$\overline{DX}$	=	Average cell length in the x-direction, ft
$\overline{DY}$	=	Average cell length in the y-direction, ft

$\overline{DZ}$	=	Average cell length in the z-direction, ft
NX	=	Number of cells in the x-direction
NY	=	Number of cells in the y-direction
NZ	=	Number of cells in the z-direction
r	=	Distance, ft
τ	=	Diffusive time of flight, $hr^{0.5}$
Δp	=	Pressure drop, psi
$\Delta p'_{wf}$	=	Well test derivative, psi
q_w	=	Well flow rate, res bbl/day
t	=	Time, hr
PV	=	Pore volume, ft^3
$V(t)$	=	Drainage volume, ft^3
$V_p(\tau)$	=	Cumulative pore volume, ft^3
$w(\tau)$	=	Derivative of cumulative pore volume with respect to τ, $ft^3/hr^{0.5}$
J	=	Objective function, psi
VDP	=	Dykstra-Parsons coefficient

TABLE OF CONTENTS

Page

LIST OF FIGURES

Page

LIST OF TABLES

Page

1. INTRODUCTION

Pressure transient analysis (PTA) has long been recognized as a powerful tool for interpretation of transient pressure behavior in the subsurface and it has provided the basis for reservoir parameter estimation using well test data (Lee, 1982; Lee et al., 2003). The pressure variation with time recorded at the production or injection well is a function of the well configuration and reservoir properties. Well test interpretation usually focuses on pressure response under the transient flow condition that will be felt first in the near-well region. The pressure response will be averaged to an increasing extent as the drainage volume keeps expanding, until the finite boundary effect can be observed at later times from the well pressure profile.

Well test analysis provides a dynamic description of the reservoir system as opposed to that provided by the static geologic data. Its objective is to solve an inverse problem by indirect measurements from the well response. From interpretation of the well pressure curve, we can determine the wellbore storage and skin factor of the well (Agarwal et al., 1970; Wattenbarger and Ramey, 1970; Ramey, 1970; Cinco-Ley and Samaniego V, 1977; Gringarten et al., 1979; Chu et al., 1980; Ikoku and Ramey, 1980; Miller, 1980; Tongpenyai and Raghavan, 1981; Joseph and Koederitz, 1985; Blasingame et al., 1989; Chu and Reynolds, 1994), calculate the average permeability of the reservoir being investigated (Miller et al., 1950; Ehlig-Economides and Joseph, 1987; Feitosa et al., 1994; Thompson and Reynolds, 1997), and characterize its heterogeneity as well as complex geologic features (Kazemi et al., 1969; Yaxley, 1987; Abbaszadeh and Cinco-Ley, 1995).

However, in all these instances, relatively homogeneous reservoir descriptions are assumed. When more detailed characterization of reservoir heterogeneity is needed, a robust forward model has to be established first and a numerical inversion technique is required.

Accurate description of drainage volume propagation around the active production well is crucial for understanding of the transient pressure propagation in the petroleum reservoir. Drainage volume characterization frequently relies upon the definition of "radius of investigation" (ROI) in homogeneous media (Johnson, 1988; Daungkaew et al., 2000; Kuchuk, 2009), within which the "bulk-average" reservoir permeability can be estimated from a well test inversion. By means of numerical simulation methods (e.g. finite difference methods, finite volume methods and finite element methods), the concept of ROI can be extended to "depth of investigation" (DOI) for heterogeneous media (Datta-Gupta et al., 2011). With the help of the fast marching method (FMM) (Sethian, 1996), calculation of the drainage volume can be realized quickly and its visualization becomes straightforward under general reservoir conditions (Xie et al., 2015a; Zhang et al., 2016).

Inverse methods for reservoir parameter estimation during history matching may rely on establishing a robust forward model and then determining an objective function to be minimized (Oliver et al., 1996). Many minimization schemes have been devised and used to efficiently calibrate grid-cell reservoir properties by integrating dynamic well test data into the numerical reservoir model, which can be classified into two general categories: derivative-free methods and derivative-related methods. The derivative-free methods such as simulated annealing (Ouenes et al., 1993; Deutsch and Journel, 1994;

Datta-Gupta et al., 1995) or genetic algorithms (Sen et al., 1995; Romero et al., 2000) usually require multiple flow simulations and can become computationally expensive for large-scale field applications. In contrast, the derivative-related approach is a gradient-based optimization method, which usually entails calculation of the sensitivity coefficients of the observational data to the reservoir parameters (Chu et al., 1995a, b; Oliver et al., 1996; Oliver, 1996; Reynolds et al., 1996; Oliver et al., 1997; Reynolds et al., 1999; Oliver et al., 2001; Rodrigues, 2005, 2006).

As alternatives to classic numerical algorithms used for dynamic reservoir simulation, the streamline method (Datta-Gupta et al., 2007) and the FMM have demonstrated the capability to significantly enhance the computational efficiency, which is especially important for inverse modeling where the gradient-based optimization is involved and formulation of the analytic sensitivity coefficients are required. Integrating pressure transient data into reservoir models and calibrating reservoir parameters using the streamline method proves to be successful and provides a convenient means to formulate the sensitivity coefficient in one single dimension (Vasco et al., 2000; Kulkarni et al., 2001; He et al., 2006). In the current study, we replace the streamline method with a new gradient-based inversion scheme devised and implemented for the integration of well test data into reservoir models. The forward model will be designed with the help of the FMM and a semi-analytic asymptotic pressure approximation, which have great advantages over conventional simulation methods in terms of computational efficiency.

Complex grid-cell geometries need to be included into the geologic model design when the structure of the reservoir model can no longer be characterized sufficiently well

by orthogonal-grid based discretization. They are especially important for designing unconventional reservoir models, where detailed analysis of fluid flow around the hydraulic and natural fractures is often required (Kou et al., 2018a, b). Because of their flexibility in adapting irregular geologic features (e.g. stratigraphic thickness variation, faults and pinch-outs), corner point grids (CPG) are widely used in reservoir simulation (Ponting, 1989). Application of the FMM needs to meet the causality requirement, which can be easily satisfied within the orthogonal grid system. But in reservoir models with complex grid geometries, especially those with anisotropic media, the causality condition is often violated. In this case, the local solver within the FMM needs to be carefully designed so that the causality condition can be reasonably enforced.

Given the general background for pressure transient analysis as well as the forward and inverse modeling associated with it, we outline the major research topics included in this dissertation. First, we improve the modeling of early-time (near-well) analytic well test response through improved numerical modeling of the "diffusive time of flight" (DTOF) and the drainage volume. Based on the DTOF that can be calculated by means of the FMM, we then integrate dynamic well test data into 3D reservoir models using a sensitivity-based inversion. After that, the numerical methodology for the FMM development is extended to complex faulted corner point grids for 3D full field reservoir modeling applications.

1.1 Eikonal Equation, Fast Marching Method and Asymptotic Pressure Approximation

Estimation of reservoir parameters from interpretation of the well test data relies upon a good understanding of pressure propagation in a diffusion process in the subsurface porous media. In most cases, the fluid flow in the reservoir media can be adequately described by parabolic partial differential equations, the solution of which can be calculated using numerical methods (e.g. finite element method, finite volume method, finite difference method, etc.). But numerical methods cannot capture the geometric nature of pressure propagation within the heterogeneous media. In addition, although the solution accuracy can be improved by increasing the model resolution, the computational cost will increase. This is especially true for inverse modeling schemes that depend upon sensitivity-based minimization of the objective function, which might make the computational cost prohibitive when the model size is large, as with 3D geologic models.

To enhance the computational efficiency, many approximation approaches are taken to simplify the forward model. Considerable amounts of work had been done to relate the diffusion equation to a wave equation (Pierce, 1986; Philip, 1989; Oliver, 1994). In these efforts made, the concept of "arrival time" is used for matching of wave amplitude, by means of which reservoir parameters can be estimated. Despite the substantial difference between solutions to the diffusion equation and the wave equation, the measured pressure data can be transformed into a wave signal. In the wave domain, the pressure "front" signal propagates at a "velocity" equal to the square root of the diffusivity and the time-like variable has a unit of $(\text{time})^{1/2}$ (Oliver, 1994). This related

body of work provides important insights into pressure transient analysis by means of a wave transform.

The asymptotic expansion technique has been widely used in electromagnetic or elastic wave propagation (Lambare et al., 1992; Jin et al., 1992; Sevink and Herman, 1996; White, 2005; Silin et al., 2006; Silin and Goloshubin, 2010). Many of its concepts associated with propagating fronts provide useful information for reservoir simulation. By taking the high frequency asymptotic expansion of the diffusivity equation using the Fourier transform, the concept of "diffusive time of flight" (DTOF) can be used to describe fluid flow in porous media (Virieux et al., 1994; Vasco et al., 2000; Kulkarni et al., 2001; Vasco et al., 2008). Corresponding to observations from Oliver (1994) about the time-like variable, the DTOF (τ) has a unit of $(\text{time})^{1/2}$ and is closely related with the propagating pressure transient. The DTOF can be calculated by solving the Eikonal equation (which contains the diffusivity information in terms of the reservoir permeability and porosity) using the method of characteristics (Vasco et al., 2000; Vasco et al., 2008). In the method of characteristics, the DTOF solutions are calculated along particular trajectories that can be developed through either a ray tracing technique or a post-processing of the output from a numerical reservoir simulator (Vasco and Finsterle, 2004; Vasco et al., 2004; Vasco, 2004; Vasco et al., 2008). This characteristic trajectory can be approximated by the convective streamline trajectory (Datta-Gupta and King, 1995) along which the analytic sensitivity coefficients can be formulated and included into the objective function to calibrate reservoir parameters by integrating pressure transient data into the reservoir model (Kulkarni et al., 2001; He et al., 2004; Cheng et al., 2005; He et al., 2006).

Based upon the Eikonal equation used for DTOF calculation, the source function for infinite and smoothly varying heterogeneous media can be calculated and a new asymptotic solution to the infinite-acting flow (IAF) is generated (King et al., 2016). Instead of tracking the streamline trajectory, the DTOF is calculated directly from solving the Eikonal equation using the fast marching method (FMM). The DTOF can be treated as a spatial coordinate that transforms the three-dimensional diffusivity equation into an equivalent one-dimensional form (Xie et al., 2015a, b; King et al., 2016; Zhang et al., 2016; Wang et al., 2017). In the newly derived asymptotic pressure approximation to the diffusivity equation, the pressure front is governed by the Eikonal equation, which defines the relationship between the DTOF and reservoir properties (Datta-Gupta et al., 2007). This approximation is a semi-analytic solution to the diffusivity equation and it relies upon an assumption that the pressure gradient is aligned with the DTOF gradient in reservoir media with smoothly varying heterogeneity (King et al., 2016). The methodology we propose relates the Eikonal equation with the drainage volume by means of the DTOF, which governs the propagation of a pressure front in the reservoir. The discretized form of these equations provides the foundation for both fast forward modeling (Nunna et al., 2015; Li, 2016; Nunna, 2017; Nunna and King, 2017; Nunna et al., 2018) and for sensitivity-based inverse problems in reservoir characterization (Li and King, 2016), especially for applications in pressure transient analysis (PTA) of conventional reservoirs and in rate transient analysis (RTA) of unconventional reservoirs (Xue et al., 2016; Iino, 2018; Wang et al., 2018; Xue et al., 2018). We will show that the solution to the Eikonal equation and the calculation of the drainage volume needs to be studied in more detail.

We develop and analyze discretization schemes of these equations, with an emphasis on the near-well region which dominates the accuracy of the solution.

The fast marching method (FMM) is a numerical method designed for solving the Eikonal equation in general heterogeneous and anisotropic media. It is well suited to keeping track of the propagating fronts in a wide variety of settings, including computational geometry, fluid mechanics, computer vision, etc. (Sethian, 1999). Like Dijkstra's algorithm, which can be used for finding the shortest paths between nodes in a graph, the FMM is a construction involving expanding wave fronts based on Huygen's principle. It was initially designed on a rectangular orthogonal mesh system in $O(N \log N)$ steps, where N is the total number of grid points. The scheme relies upon an upwind finite difference approximation to the gradient of the unknown variable and is required to meet a causality condition (Sethian and Vladimirsky, 2000). The local solver within the FMM can be constructed based on either Fermat's principle or an Eulerian discretization.

Drainage volume is frequently used to describe the portion of reservoir volume under depletion by a production well in the oil and gas industry. Accurate and efficient characterization of the drainage volume is fundamental to understanding pressure propagation in porous media and optimizing well-placement for reservoir development. The concept of radius of investigation (ROI) is closely related to drainage volume evolution in homogeneous media and is routinely used to perform well test analysis. Most definitions of ROI are related to the propagation of a pressure disturbance or detectable pressure or rate changes in the subsurface (Datta-Gupta et al., 2011). Lee (1982) defines the ROI and as the "peak" pressure disturbance for an impulse source or sink in

homogeneous porous media. Such a definition can be readily generalized into the depth of investigation (DOI) for a flowing well within the heterogeneous reservoir model (Datta-Gupta et al., 2011). DTOFs calculated from the FMM allow us to formulate the DOI for well production within general heterogeneous reservoir media using the semi-analytic asymptotic solution to the pressure diffusivity equation. With the use of the numerical solution of the Eikonal equation, the drainage volume concept can be extended to heterogeneous and bounded reservoir systems. The asymptotic pressure approximation relies significantly on an accurate characterization of the drainage volume, which is closely related to the well test derivative formulated for pressure transient analysis.

To obtain adequate accuracy for the purpose of well test interpretation, a mixed discretization scheme for the drainage volume that combines analytic, first-order, and zeroth-order volumetric elements was devised. The novel semi-analytic methodology we propose for PTA and RTA drainage volume calculations serves as a bridge between analytic approaches that require many simplified assumptions and conventional numerical simulations that are usually computationally expensive when the reservoir model parameter has excessive degrees of freedom. The hybrid version of the drainage volume discretization is consistent with the DTOF-based transient flow simulation, which is greatly impacted by the inter-cell transmissibility formulation between the "τ-intervals", especially by the transmissibility construction in the near-well region. Implementation of the semi-analytic approach in pressure transient analysis relies upon an understanding of the forward model discretization we prepared for inversion.

1.2 Integration of Pressure Transient Data into Reservoir Models Using the Fast Marching Method

History matching reservoir models and adjusting model parameters with pressure transient data remains an important research topic. Well test data has been recognized as an effective tool that can be used to describe pressure propagation in the subsurface porous media. It is often related to the concepts of radius of investigation (ROI) when a radial or infinite-acting flow occurs and the transient pressure response within the reservoir is visible from the well pressure profile. From the diagnostic plot of the well pressure and production data that interprets transient pressure behavior evolving away from the well, we can easily estimate the bulk-average reservoir permeability. In this research, the well test derivative profile is related to the drainage volume evolution as a function of time and treated as the forward model for inversion. Grid-cell properties within the entire reservoir model will be re-adjusted by reconciliation of the dynamic pressure transient data observed from the production well with a static pre-existing geostatistical data.

Integration of dynamic pressure transient data into reservoir models can be realized using a least-square based optimization scheme (Paige and Saunders, 1982), in which the objective function constructed from the forward model can be matched with the observed well pressure data by means of an iterative minimization procedure. Minimization of the objective function can be achieved through a sensitivity-based method, which requires calculation of partial derivatives of well test data with respect to reservoir parameters. Numerically, sensitivity coefficients can be obtained by evaluating changes in well pressure due to a small perturbation of reservoir parameters. However, this approach will

become computationally infeasible as the model size increases and forward simulations are required for every grid cell. Calculation of the sensitivity coefficients of the objective function with respect to reservoir parameters in an analytic approach is required, which is also one of the major results of this dissertation. Similar to the streamline technique used in inverse modeling (Kulkarni et al., 2001; Datta-Gupta et al., 2001; Cheng et al., 2005; He et al., 2006; Datta-Gupta et al., 2007), we propose a new methodology for calculation of the analytic sensitivity coefficients that can be realized by one single forward simulation using the fast marching method (FMM).

The drainage volume may be directly related to well test derivative data, which serves as the actual objective function used in inversion to calibrate reservoir model parameters. A penalized objective function containing the a priori information generated from geostatistical data and the roughness constraints can be minimized in an iterative approach during history matching. The sensitivity coefficients of the objective function with respect to reservoir properties can be derived analytically and incorporated into the objective function to optimize the inversion. The analytic sensitivity coefficients of the DTOF with respect to reservoir parameters can be generated simultaneously with DTOFs calculated from the FMM algorithm. Our asymptotic pressure approximation provides a formulation of the drainage volume in terms of the DTOF and time. Using the chain rule, sensitivity of the drainage volume as well as the well test derivative can be conveniently formulated by means of DTOF sensitivity calculated via the FMM. The major advantage of formulating analytic sensitivity coefficients using the FMM is its great computational efficiency while inversion is conducted.

1.3 Extension of the Fast Marching Method to Faulted Corner Point Grids

The asymptotic pressure approximation we propose relies heavily upon an accurate calculation of the "diffusive time of flight" (DTOF) that can be obtained by solving the Eikonal equation. The Eikonal equation, which contains the diffusivity information (e.g. permeability, porosity, rock compressibility and fluid viscosity) of the reservoir model, is a reduced form of the general static Hamilton–Jacobi partial differential equation (PDE) when the speed function depends only upon the location in space (which actually becomes the square root of the diffusivity). The key to solving the Eikonal equation is to select the correct viscosity solution by monotone finite difference methods (Crandall and Lions, 1983, 1984).

The fast sweeping method (FSM) and fast marching method (FMM) are the most commonly used numerical algorithms to solve the Eikonal equation. The FSM was first introduced and implemented for solving the Eikonal equation on rectangular meshes in Cartesian coordinates (Zhao, 2004). It was later extended to unstructured triangular meshes that can help generate more accurate solutions because of the better directional resolution (Qian et al., 2007). The FSM has a complexity of order $O(N)$ for N grid points and its numerical implementation relies upon the Gauss-Seidel sweeping algorithm, in which all unknown values will be initialized and require a number of iterations until they converge to the solutions of the discretized system (Zhao et al., 2000; Zhao, 2004; Zhang et al., 2006; Qian et al., 2007; Luo and Qian, 2012; Luo et al., 2014). In contrast, instead of using an iterative algorithm to solve for unknowns, the FMM will update the solution following causality in a sequential way. Similar to Dijkstra's method, the FMM

systematically updates the solution for the time of flight value in an orderly one-pass fashion to find the shortest path on weighted graph of edges and nodes (Sethian, 1996). In the FMM, an upwind finite difference approximation and a heapsort algorithm are needed, which lend itself to a complexity of order $O(N \log N)$ for N grid points (Sethian and Vladimirsky, 2000). If the same local Eikonal solver is implemented, the ultimate DTOF solutions generated from both the FSM and the FMM will also be the same.

In general heterogeneous and anisotropic media, DTOF calculation requires a stable local Eikonal solver that can be implemented within a numerical algorithm. However, there is some difference between pressure propagation in isotropic and anisotropic media when the Eikonal equation is used to describe the propagating pressure front in a diffusion process. In the isotropic media, the characteristic vector has the same direction as the (negative) DTOF gradient. The causality condition is always satisfied and the DTOF gradient can be used as a reliable indicator of fluid flow. This is not the case for anisotropic media, in which the characteristic direction will not coincide with the DTOF gradient direction in general. Without taking into account this essential difference, erroneous solutions may be generated by simply extending the numerical algorithm used to solve the Eikonal equation in isotropic media to DTOF calculation in anisotropic media. The local solver can be constructed based on either Fermat's principle (Sun and Fomel, 1998; Sethian, 1999; Lelievre et al., 2011) or an Eulerian discretization (Sethian and Vladimirsky, 2000; Qian et al., 2007), with the former having a straightforward geometric interpretation and the latter easier for numerical implementations.

The local Eikonal solver developed by Qian et al. (2007) in the FSM demonstrated a general formulation of DTOF calculation based upon known values within a 2D triangular or a 3D tetrahedral element. This formulation provides useful information for updating DTOF values along the characteristic direction based on an Eulerian discretization. When DTOF is updated within anisotropic media, causality can be correctly enforced when it is violated by either reducing the 3D tetrahedral element into the 2D triangular element or even by reducing the 2D tetrahedral element into the 1D Eikonal solution. The causality enforcement often requires calculation of the wave propagation speed from a given ray direction, which cannot be easily obtained using an explicit formula and hence must rely on an iterative algorithm to solve a two-point boundary-value problem (Press et al., 1988; Qian and Symes, 2001).

We modified the local solver within the FSM formulated by Qian et al. (2007) and re-formulated the characteristic direction that is constrained by the data support with known DTOF values. This new local Eikonal solver is causal and easier to implement, eliminating the need for group speed calculation with an iterative procedure. Our motivation is to incorporate the new local solver into a FMM algorithm that can be used to solve the anisotropic Eikonal equation in a reservoir model discretized into a corner point grid (CPG) system.

1.4 Research Objectives and Dissertation Contributions

The motive of this research is to establish a robust numerical method for simulating transient flow in the subsurface and to integrate pressure transient data into reservoir

models using the fast marching method (FMM) in structured and faulted corner point grid geometries. Starting from theoretical development, the research emphases are placed on numerical analysis of the forward mathematical model, design of an efficient inverse modeling scheme and extension of the framework to 3D complex reservoir models, which compose the three major sections of this dissertation.

Section 2 provides the background and motivation for this research. Based upon the asymptotic theory of electromagnetic wave propagation, we first developed the asymptotic pressure approximation to the classic diffusivity equation that governs fluid flow in porous media (King et al., 2016; Wang et al., 2017). This new semi-analytic approach replaces the empirical geometric pressure approximation studied earlier (Xie et al., 2015a) and greatly simplified the calculation of transient flow by using the concept of "diffusive time of flight" (DTOF). The DTOF can be treated as a spatial coordinate that transforms the three-dimensional diffusivity equation into an equivalent one-dimensional formulation. In this new forward model formulation, the drainage volume can be expressed as a function of the DTOF and time, which is directly related to the pressure transient represented by the well test derivative. Thus, it provides us with a geometric understanding of the pressure front propagation in general heterogeneous media.

In **Section 3**, we focus our research attention on establishing a robust forward model based on the DTOF (τ), which can be obtained from solving the Eikonal equation using the FMM. One vertical well with constant production rate is placed at the center of the reservoir and its drainage volume is discretized by evaluating a "$w(\tau)$" term, which is defined as the derivative of the cumulative pore volume with respect to the DTOF. By

computing $w(\tau)$ on each individual grid cell of the reservoir model, we devised a hybrid version of the drainage volume that can better represent pressure transients in the near-well region. This hybrid drainage volume along with the hybrid $w(\tau)$ function prove to be consistent with the transient solution to the DTOF-based pressure diffusivity equation.

In **Section 4**, we performed inversions of reservoir parameters by integrating pressure transient data into reservoir models using the FMM on the basis of the forward model established in the previous section. The well test derivative is shown to be inversely proportional to the drainage volume of the production well and was used as the objective function for history matching of the reservoir model with well pressure data. Its sensitivity coefficients with respect to reservoir parameters are formulated analytically from the functional derivative of the Eikonal equation, which is numerically realized by tracking the characteristic trajectory within the FMM and evaluating reservoir properties within a particular τ-interval. This makes the computational speed orders of magnitude faster than conventional numerical simulations. Sensitivity of the drainage volume with respect to reservoir permeability follows the characteristic trajectory because the characteristic information is implicitly formulated in the Eikonal solver (Li and King, 2016). With an additional constraint to honor the prior model, our inverse modeling approach will adjust the reservoir model to obtain an average permeability as a function of DTOF (τ) distance from the well within the drainage volume (Oliver, 1990, 1992). Our new inversion methodology relies upon only one single production well and it provides a fast and efficient approach to modify reservoir permeability both within and beyond the depth of investigation (DOI).

In **Section 5**, which is the last major section of this dissertation, we developed a three-dimensional anisotropic FMM for corner point grids (CPG) with complex geometries by solving the diagonal-tensor anisotropic Eikonal equation. The diffusivity tensor is formulated in terms of the permeability tensor and tangent vectors of the CPG. A local solution to the Eikonal equation based on an Eulerian discretization was formulated and proved to be consistent with Fermat's principle. The unknown DTOF variable is referenced to a displacement vector measured from the location of the unknown DTOF variable to be solved. The characteristic vector is formulated by the diffusivity tensor and the DTOF gradient evaluated at the unknown DTOF variable. The causality condition is constrained by known data support. General one-dimensional, two-dimensional and three-dimensional local solvers in three-dimensional space for anisotropic media are designed to simulate pressure front propagation in porous media. Discretization of the Eikonal equation for iso-parametric corner point cell geometry with the directional permeability tensor is investigated and extended to include non-neighbor connections (NNC) that are used to represent faulted grids. The new CPG FMM we propose will not only capture complex geologic structures of the reservoir, it can also better represent pressure communications across faulted grids as well as grids with gaps and pinch-outs.

This dissertation is concluded by **Section 6**, in which research contributions from **Section 2** to **Section 5** are summarized and recommendations for future research are provided.

2. ASYMPTOTIC APPROXIMATION TO THE PRESSURE DIFFUSIVITY EQUATION USING THE FAST MARCHING METHOD

Three-dimensional diffusivity equation has been extensively used by both the hydrogeologists and reservoir engineers to characterize pressure propagation when fluids (groundwater, oil and gas) flow in the subsurface porous media. The well pressure and production/injection rate history can be recorded and used for pressure transient analysis (PTA) and rate transient analysis (RTA), which provide us with convenient tools to understand flow regimes in the subsurface. From the fixed well-rate diagnostic curve as a function of time, volume-averaged reservoir properties can be readily estimated.

The diffusivity equation is a parabolic partial differential equation. It can be solved numerically using the finite difference, finite volume, or the finite element method with initial reservoir pressure conditions assigned as well as boundary conditions defined at the production or injection wells. However, the computational cost of conventional reservoir simulation increases significantly as the model size grows. Though its computational speed could be improved either by upscaling of the geologic models or using parallel computing, conventional numerical simulation fails to provide geometric understanding of the pressure front propagation. On the other hand, analytic methods for evaluating reservoir properties from interpreting well test data usually require many simplified assumptions and cannot calibrate grid-cell parameters within the numerical model based on a priori static information. Moreover, the computational cost for inverse modeling usually becomes expensive as the number of degrees of freedom of the reservoir

parameters become large. In this sense, the limitation for PTA or RTA is the lack of an approach for integration of two different fields of analysis: well testing and numerical flow simulation.

We propose a novel semi-analytic approach for calculating reservoir pressure based on the "diffusive time of flight" (DTOF), which can be obtained by solving the Eikonal equation via the fast marching method (FMM) in general heterogeneous media. This semi-analytic formulation is an asymptotic expansion to the pressure diffusivity equation and relies significantly upon the drainage volume characterization. It takes full advantage of the fast computational speed of the FMM and can help us evaluate temporal evolution of the drainage volume from the production well for high-resolution geologic models, with a computational efficiency orders of magnitude greater than conventional numerical simulations. Our proposed approach is especially suited for sensitivity-based inversion and provides a novel method of integrating well test data into prior static 3D geologic models.

2.1 Introduction

Characterization of transient pressure behavior in the subsurface porous media is crucial for prediction of reservoir performance and optimization of well placement. For reservoir under-going primary production or injection, the governing partial differential equation commonly used to describe fluid flow in heterogeneous media is the diffusivity equation. It relates pressure drop and flow rates by Darcy's law and provides the

theoretical basis for both well performance evaluation and integration of well pressure or production data for reservoir parameter estimation.

Most pressure transient analysis (PTA) and rate transient analysis (RTA) rely upon analytic solutions to the diffusivity equation (Lee, 1982; Horne, 1995; Bourdet, 2002; Lee et al., 2003). Though simplified assumptions are used, these analytic solutions provide efficient tools for us to estimate reservoir properties. In contrast, numerical methods used for solving the diffusivity equation often lack the capability to help one gain a quick insight into the reservoir parameters as those analytic approaches. This is especially difficult when the reservoir model size increases and large numbers of reservoir parameters need to be adjusted by integration of pressure transient data or rate transient data (Chu et al., 1995a; Oliver et al., 1996; Reynolds et al., 1996; Oliver et al., 1997; Reynolds et al., 1999; Li et al., 2010).

To strike a balance between the over-simplicity of the analytic solution and the potentially high computational cost of the numerical solution, we have devised an asymptotic formulation of the pressure diffusivity equation. The focus of study in this section will be on development of the semi-analytic formulation and its discretization on a rectangular grid system. Previous studies have used cell-center based DTOFs calculated from the FMM in forward modeling and inversion, but did not provide sufficient analysis of the accuracy of DTOFs calculated and their potential impact on the drainage volume solution (Xie et al., 2015a, b; Zhang et al., 2016). By validating with analytic solutions for the 1D linear flow model, the 2D radial flow model and the 3D full field model, we

demonstrate that detailed characterization of drainage volume both within the near-well region and farther away is required to achieve more accurate semi-analytic solutions.

2.2 Methodology: Forward Model Solutions and Properties

In this section, we review the derivation of the asymptotic limit of the pressure diffusivity equation and demonstrate its relationship with the "diffusive time of flight" (DTOF), which can be obtained by solving the Eikonal equation numerically using the fast marching method (FMM). The asymptotic pressure approximation will provide the semi-analytic forward model used for rapid solutions and which will provide the foundation for our pressure transient inversion.

2.2.1 The Eikonal Equation and the Asymptotic Pressure Approximation

The diffusivity equation that is commonly used to describe transient pressure behavior in heterogeneous porous media is:

$$\phi(\vec{x})\mu c_t \frac{\partial p(\vec{x},t)}{\partial t} - \nabla \bullet \vec{u}(\vec{x},t) = 0 \qquad (2.1)$$

where $\vec{x}$ stands for the physical coordinate in the 3D space; t stands for the flowing time; p is the reservoir pressure; ϕ denotes reservoir porosity; μ and c_t are viscosity and compressibility, respectively; $\vec{u}$ is the Darcy's velocity. Source and sink terms can be treated as boundary conditions of the differential equation (Eq.(2.1)). The diffusivity equation takes advantage of the Darcy's law, which relates the Darcy's velocity with the reservoir permeability and pressure gradient.

$$\vec{u}(\vec{x},t) = -\frac{1}{\mu}\vec{\vec{k}}(\vec{x}) \bullet \nabla p(\vec{x},t) \tag{2.2}$$

Here $\vec{\vec{k}}(\vec{x})$ represents the permeability tensor that applies to the general situation when the porous media is anisotropic in space.

By applying a Fourier transform to Eq.(2.2), we can obtain the diffusivity equation in the frequency domain:

$$\phi(\vec{x})\mu c_t(-i\omega)\tilde{p}(\vec{x},\omega) - \nabla \bullet \left(\vec{\vec{k}}(\vec{x}) \bullet \tilde{p}(\vec{x},\omega)\right) = 0 \tag{2.3}$$

Using concepts from diffusive electromagnetic imaging, the transient pressure response can be represented in the frequency domain (Virieux et al., 1994):

$$\tilde{p}(\vec{x},\omega) = e^{-\sqrt{-i\omega}\tau(\vec{x})} \sum_{k=0}^{\infty} \frac{\tilde{A}_k(\vec{x})}{\left(\sqrt{-i\omega}\right)^k} \tag{2.4}$$

where $\tau(\vec{x})$ in the exponential term of the asymptotic solution is the "diffusive time of flight" (DTOF), which has a unit of square root of time. The quantity $\tilde{A}_k(\vec{x})$ refers to the pressure amplitude at the *k*-th order. After substituting the asymptotic series into the diffusivity equation and taking the high frequency limit, we can derive the Eikonal equation for the DTOF (τ).

$$\nabla\tau(\vec{x}) \bullet \vec{\vec{k}}(\vec{x}) \bullet \nabla\tau(\vec{x}) = \phi(\vec{x})\mu c_t \tag{2.5}$$

or

$$\nabla\tau(\vec{x}) \bullet \vec{\vec{\alpha}}_D(\vec{x}) \bullet \nabla\tau(\vec{x}) = 1 \tag{2.6}$$

where $\vec{\vec{\alpha}}_D(\vec{x})$ is a symmetric tensor for the hydraulic diffusivity, which is defined as

$$\vec{\vec{\alpha}}_D(\vec{x}) = \frac{\vec{\vec{k}}(\vec{x})}{\phi(\vec{x})\mu c_t} \tag{2.7}$$

The wellbore is usually defined as the source point, with the DTOF value assigned to zero. For homogeneous media, it is easy to solve the Eikonal equation analytically; for heterogeneous media, we can use the FMM (Sethian, 1999) to solve for the DTOF. In homogeneous and isotropic media, the DTOF can be calculated as the analytic solution to the Eikonal equation, which is related to the distance r from the source well.

$$\tau = r/\sqrt{\alpha_D} \tag{2.8}$$

We assume that the pressure gradient is aligned with the DTOF gradient, which allows us to use the DTOF as a spatial coordinate (King et al., 2016; Wang et al., 2017). The 3D diffusivity equation can be transformed into a 1D form that combines the pressure and the flux term.

$$c_t \frac{\partial p(\tau,t)}{\partial t} = \frac{\partial q(\tau,t)}{\partial V_p(\tau)} = \frac{1}{w(\tau)} \frac{\partial q(\tau,t)}{\partial \tau} \tag{2.9}$$

where q represents the flux across a "τ-contour" and $V_p(\tau)$ is defined as the cumulative pore volume from the well to the "τ-contour". The shape of V_p is cylindrical in homogeneous media and becomes irregular in heterogeneous media (Figure 2.1).

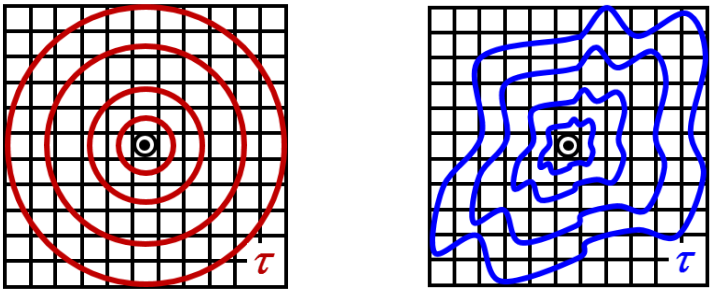

(a) Homogeneous Media **(b) Heterogeneous Media**

Figure 2.1 Cumulative pore volume as a function of the DTOF

Based on the cumulative pore volume (V_p) variation as a function of the DTOF, we define the variable $w(\tau)$ in Eq.(2.9) as its derivative with respect to the DTOF.

$$w(\tau) = \frac{dV_p(\tau)}{d\tau} \tag{2.10}$$

This $w(\tau)$ variable plays a significant role in drainage volume discretization, which we will discuss later in more detail.

2.2.2 Properties of the Fixed Rate Drawdown: Analytic Solution

For fluid flow in a reservoir that has a single well with constant production rate, the solution to the diffusivity equation can be formulated by an asymptotic pressure approximation:

$$c_t \frac{\partial p}{\partial t} = \frac{1}{w(\tau)} \frac{\partial q}{\partial \tau} \approx -\frac{q_w}{V(t)} e^{-\tau^2/4t} \tag{2.11}$$

where q_w represents the constant well production or injection rate; $V(t)$ is the drainage volume that is expressed as a function of time. The quantity ($\tau^2/4$) represents a characteristic time of the propagating pressure front. Instead of solving for the amplitude quantities in Eq.(2.4), we can close our equations with constraints in time. Following the discussion of the Matthews-Brons-Hazebroek (MBH) method for estimation of average pressure in the drainage volume (Matthews et al., 1954), we extended the pseudo-steady state (PSS) definition of MBH to fixed rate transient well test interpretation (King et al., 2016; Wang et al., 2017).

Drainage volume as a function of time is related to its form as a function of the DTOF by the following formula (King et al., 2016):

$$V(t) = \int_{\tau=0}^{\infty} dV_p(\tau) \cdot e^{-\tau^2/4t} = \int_{\tau=0}^{\infty} d\tau \cdot w(\tau) \cdot e^{-\tau^2/4t} \tag{2.12}$$

Eq.(2.12) is the basis of the subsequent drainage volume discretization. This asymptotic pressure approximation can be justified for a "sufficiently smooth" $w(\tau)$ distribution (King et al., 2016; Wang et al., 2017). Since the well is treated as the single source of the entire reservoir model, if the DTOF to the well is defined as zero (Eq.(2.11)), the well test derivative can then be derived:

$$\Delta p'_{wf} \equiv \frac{\partial \Delta p_{wf}}{\partial \ln(t)} = t \cdot \frac{\partial \Delta p_{wf}}{\partial t} \approx \frac{q_w \cdot t}{c_t \cdot V(t)} \tag{2.13}$$

In such a way, the well test derivative is inversely proportional to the drainage volume. The well test derivative is important in the identification of flow geometries (Wong et al., 1986; Tiab and Puthigai, 1988; Bourdet et al., 1989; Tiab, 1994). This new well test

derivative formulation (Eq.(2.13)) not only provides a direct semi-analytic calculation of the well test derivative without solving for the pressure itself, it also forms the basis for calculation of pressure and flux as well as our subsequent inverse modeling.

2.2.3 Fast Marching Method

The fast marching method (FMM) is designed to solve the Eikonal equation (Eq.(2.5)) numerically in a fast and efficient way. The central idea behind the FMM is to systematically construct the $\tau(\vec{x})$ solution using only upwind values. The key to constructing the fast marching algorithm is that the information propagates in "one way". That is, the solution of $\tau(\vec{x})$ can be built in an orderly sequential fashion from smaller to larger values along the characteristic(s) passing through the point $\vec{x}$ (Sethian, 1996).

In general, the progress of the FMM relies on three sets of data points: an *Upwind Side* that stores the *Accepted* values, a *Narrow Band* that stores the *Trial* values, and a *Downwind Side* that stores the *Far* values (Sethian, 1999).

The numerical update procedure for unknowns of the Eikonal equation using the FMM is as follows (Sethian and Vladimirsky, 2000): First, label points in the initial conditions as *Accepted*. Then, label all adjacent points (one grid point away) as *Trial* and compute values at those points by the local Eikonal solution that will be discussed later. Finally, label the remaining grid points as *Far*. Then the loop is:

a) Begin loop: Let *A* be the *Trial* point with the smallest τ value.

b) Add the point *A* to *Accepted* and remove it from *Trial*.

c) Label as *Trial* all neighbors of *A* that are not *Accepted*. If the neighbor is in *Far*, remove it from that set and add it to the set *Trial*.

d) Re-compute the τ values of all neighbors of *Trial* by the local Eikonal solution.

e) Return to top of loop.

The key to successful implementation of the FMM relies on a fast way to find the minimum τ value among the *Neighbor* nodes. Like Dijkstra's method, an efficient implementation of the algorithm can be built by using a heapsort technique. Given *N* nodes to be calculated in the entire modeling domain, the computational efficiency of the FMM is *O(N log N)* (Sethian and Vladimirsky, 2000).

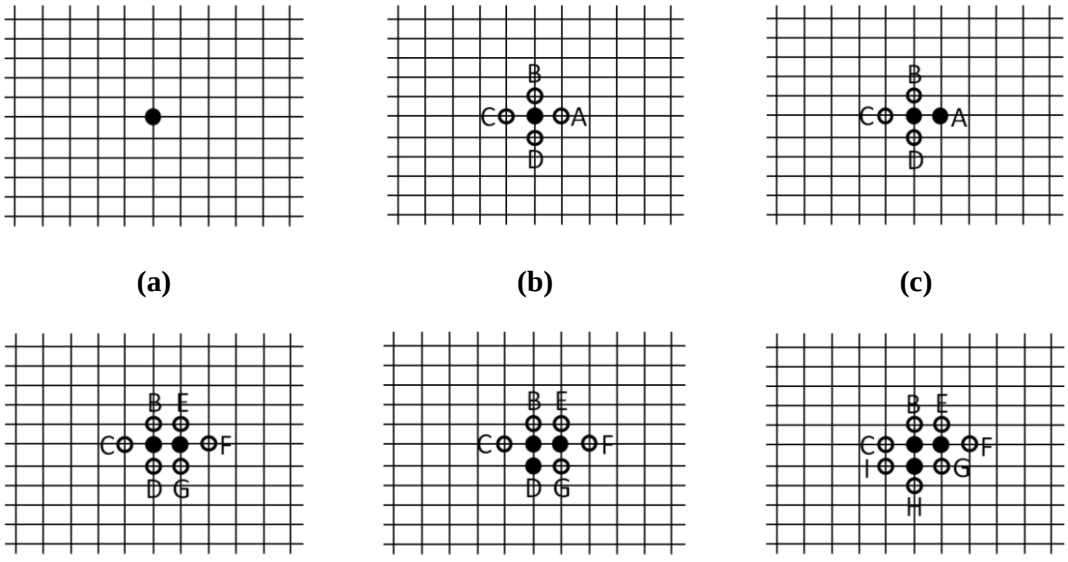

Figure 2.2 Illustration of the FMM within a 2D Cartesian grid system (Xie et al., 2015a)

This fast marching procedure can be illustrated on a 2D, 5-Stencil Cartesian grid system (Figure 2.2). We start from an *Accepted* point in black, which has an initial value of τ assigned (usually zero), and treat it as the initial position of propagating front (a). Its adjacent neighbor node points *A*, *B*, *C*, and *D* are then labeled as *Trial* (b). Once the τ values of *A*, *B*, *C*, and *D* are updated, the point with the minimum solution (suppose it is point A) is labeled as *Accepted* (c). Its adjacent neighbors *E*, *G* and *F* are added into the set *Trial* (d). The same procedure can be applied to the next *Accepted* point (suppose it is D) until all points in the domain are *Accepted* (e and f) (Zhang et al., 2013; Xie et al., 2015a, b).

Updating the τ value of a particular location in space relies upon a local Eikonal solution, which requires a certain way of grid discretization and approximation of the $\tau(\vec{x})$ gradient. Suppose we have a 2D rectangular grid system with uniform mesh size of Δx and Δy in x and y directions, respectively. The media are isotropic and diffusivity α_D is a scalar. We begin to discretize the Eikonal equation on the Cartesian grid and replace the gradient by the first-order approximation (Sethian, 1996):

$$\max\left(D_{ij}^{-x}\tau, -D_{ij}^{-x}\tau, 0\right) + \max\left(D_{ij}^{-y}\tau, -D_{ij}^{-y}\tau, 0\right) = \frac{1}{\alpha_D} \tag{2.14}$$

Here we have used the standard finite difference operator D for notation in the coordinate direction (x direction) as

$$D_{ij}^{-x}\tau = \frac{\tau_{i,j} - \tau_{i-1,j}}{\Delta x}, \quad D_{ij}^{+x}\tau = \frac{\tau_{i+1,j} - \tau_{i,j}}{\Delta x} \tag{2.15}$$

where $\tau_{i,j}$ represents the value of τ on a grid at the point (i, j) with grid spacing Δx. The forward and backward operators D^{-y} and D^{+y} in the other coordinate direction (y direction) are similar. In Eq.(2.14), τ values at unknown points are treated as infinity and the "max" function is used to conform to the "upwind" criteria. This finite difference approximation is numerically consistent and stable, which will make sure that a correct viscosity solution is selected (Sethian and Vladimirsky, 2000).

We illustrate the DTOF calculation on a 2D Cartesian grid system (Figure 2.2e). Suppose a grid point G (hollow circle) with an unknown DTOF has two adjacent grid points (A and D). The pressure front is coming from the two adjacent points A and D with known DTOF values as τ_A and τ_D, respectively. From Eq.(2.14) and Eq.(2.15), the DTOF value of the grid point G to be updated can be calculated as

$$\left(\frac{\tau-\tau_A}{\Delta x}\right)^2+\left(\frac{\tau-\tau_D}{\Delta y}\right)^2=\frac{1}{\alpha_D} \tag{2.16}$$

This discretization leads to a quadratic function of τ, which can be easily extended to 3D space with three known τ values and solved in an efficient way. For a specific grid point, we can calculate its τ value from its four quadrants (2D) or eight octants (3D) and take the minimum solution obtained.

One of the key properties of the FMM used for solving the Eikonal equation is the causality relationship, which means that the solution at each grid point depends only on the smallest adjacent values. This causality relationship guarantees that the solution can be built in an ordered "upwind" direction.

Suppose part of the solutions to the Eikonal equation is known at some time, which can be treated as *Accepted* points. For those points that are not yet *Accepted* but have *Accepted* neighbors, we compute a *Trial* solution to the quadratic equation (Eq.(2.16)) using the known values for τ at *Accepted* neighbor nodes and using values of infinity at all other neighbor nodes not *Accepted*. (Sethian et al., 2000). In implementation, it often requires a reduction of the local Eikonal solution. When updating the τ value of a specific location in 3D space, a 3D local solver will reduce to a 2D local solver if one adjacent neighbor has a τ value of infinity and will even reduce further to a 1D local solver if two adjacent neighbors have τ values of infinity.

2.2.4 Drainage Volume Discretization

From the asymptotic pressure approximation, drainage volume evolution around the production or injection well as a function of time can be calculated analytically using the integral form (Eq.(2.12)). However, the "diffusive time of flight" (DTOF) has to be calculated numerically via the fast marching method (FMM) for reservoir models with heterogeneous media. Thus, the drainage volume formulated in terms of the DTOF and time needs to be discretized.

Suppose we have a reservoir model consisting of n grid cells in total, the DTOF to centers of all those grid cells are calculated from the FMM and can be denoted as τ_j^{cell} ($j = 1, 2, \ldots, n$). If the pore volume of each grid cell is denoted as PV_j, the drainage volume can be evaluated first on each individual grid cell and then be summed.

$$V(t) = \sum_j PV_j \cdot e^{-\left(\tau_j^{cell}\right)^2 / 4t} \tag{2.17}$$

This is a piecewise constant form of the drainage volume discretization, which has been implemented in previous work (Xie et al., 2015a, b; Fujita et al., 2016; Zhang et al., 2016) and is a lowest order approximation whose accuracy has not previously been analyzed. We will validate this piecewise constant form of drainage volume formulation with the analytic solution in 1D, 2D, and 3D flow models and evaluate the potential impact of its accuracy on the forward model construction used for inversion.

2.2.5 Numerical Solutions to the Diffusivity Equation

We have developed the asymptotic pressure approximation, which relies upon an assumption that the pressure contour and the "τ-contour" are identical. In homogeneous and isotropic media, the DTOF can be calculated as the analytic Eikonal solution. This makes the flowing direction of the flux exactly aligned with the DTOF (τ) gradient for the infinite-acting radial flow (IARF). In this case, we can use the asymptotic pressure approximation as the analytic solution to the diffusivity equation and describe transient pressure behavior in homogeneous reservoir models.

In a homogeneous reservoir model that is drained by a fully perforated well, if the pressure gradient is small, the diffusivity equation can then be written in a linearized version as

$$\frac{1}{r}\frac{\partial}{\partial r}\left(r\frac{\partial p}{\partial r}\right) = \frac{\phi \mu c_t}{k}\frac{\partial p}{\partial t} \tag{2.18}$$

where r is the radial distance from the well. A similar formulation based upon the DTOF (τ) coordinate provides the basis for transforming the diffusivity equation into a one-dimensional coordinate system in terms of the DTOF. By multiplying the $w(\tau)$ variable defined above with the pressure gradient in the one-dimensional DTOF (τ) coordinate, we can approximate the flux across a "τ-contour" as:

$$q(\tau,t) \approx c_t w(\tau) \frac{\partial p(\tau,t)}{\partial \tau} \tag{2.19}$$

This new flux approximation is similar to Darcy's law and $w(\tau)$ plays a role similar to that of transmissibility. It enables us to draw an analogy between homogeneous and heterogeneous porous media for the diffusivity equation. Substituting Eq.(2.19) into Eq.(2.9), we can derive the one-dimensional diffusivity equation represented in terms of distance (τ) from the well.

$$\frac{1}{w(\tau)} \frac{\partial}{\partial \tau} \left(w(\tau) \frac{\partial p}{\partial \tau} \right) = \frac{\partial p}{\partial t} \tag{2.20}$$

In such a way, all the spatial heterogeneity of the reservoir model parameters (e.g. permeability and porosity) vanish from the formulation; they only appear through the function $w(\tau)$, which can be calculated using the DTOF from solving the Eikonal equation (King et al., 2016; Wang et al., 2017).

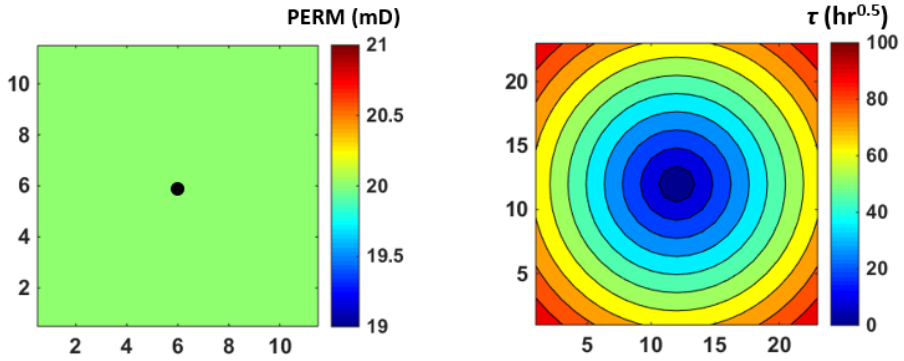

(a) Permeability **(b) Analytic DTOF**

Figure 2.3 "τ-contours" generated from a homogeneous reservoir model for the 2D IARF

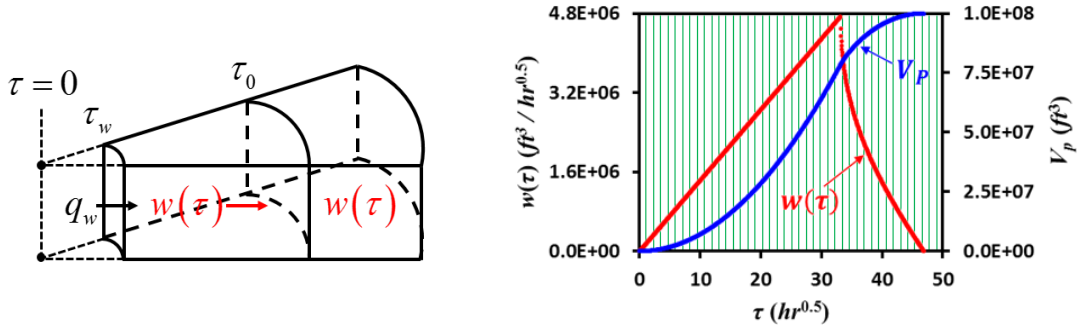

(a) **(b)**

Figure 2.4 Illustration of the IARF within τ-intervals used for discretization of the DTOF-based one-dimensional diffusivity equation

Suppose we have a vertical well placed at the center of a square-shaped 2D homogeneous reservoir model with an equal length and width ($LX = LY$) (Figure 2.3). Grid-cell based DTOFs can be calculated from the analytic Eikonal solution, which can

help discretize the one-dimensional diffusivity equation (Eq.(2.20)) into a limited number of τ-intervals (Figure 2.4). Based upon these radial τ-intervals, we can evaluate inter-cell fluid communication through transmissibility and well index (WI) constructions.

Since the reservoir is homogeneous, the cumulative pore volume, V_p, can be written in an analytic form as

$$V_p(r) = \pi r^2 \phi h \tag{2.21}$$

where r is the distance from the well; ϕ and h are porosity and thickness of the reservoir model. The DTOF can be calculated using the analytic solution to the Eikonal equation, which is related to the distance r from the source well (Eq.(2.8)). Eq.(2.8) indicates that the DTOF at the center of the vertical well is zero. Thus, the analytic $w(\tau)$ function becomes

$$w(\tau) = \frac{dV_p}{d\tau} = \frac{dV_p}{dr} \cdot \frac{dr}{d\tau} = \frac{2\pi kh}{\mu c_t} \cdot \tau \tag{2.22}$$

This linear form of $w(\tau)$ can be conveniently applied to the radial well cell, which starts from τ_w to τ_0 (Figure 2.4a). Here τ_w corresponds to the DTOF to the effective wellbore radius, r_w; τ_0 corresponds to the DTOF to any distance, r_0, that defines the upper limit of the analytic cumulative pore volume (Eq.(2.23)).

$$\tau_w = \frac{r_w}{\sqrt{\alpha_D}}, \quad \tau_0 = \frac{r_0}{\sqrt{\alpha_D}} \tag{2.23}$$

If $r_0 = Min(LX, LY)/2$, then τ_0 can be defined as

$$\tau_0 = Min\left(\frac{LX}{2\sqrt{\alpha_D}}, \frac{LY}{2\sqrt{\alpha_D}}\right) \tag{2.24}$$

The linear form of $w(\tau)$ function (Eq.(2.22)) will hold until the pressure front reaches the outer boundary of the reservoir model. Beyond this upper limit, though the cumulative pore volume will still increase, its DTOF derivative will decrease significantly (Figure 2.4b). This analysis of the linear-form $w(\tau)$ function as well as the applicability of its upper limit is important to our later discussion about improvement of drainage volume discretization.

Suppose the reservoir model is defined by a total number of N τ-intervals, with a cell index range of (0, 1,..., N-1). The first τ-interval defines the radial well cell, which has a lower and upper DTOF limits of τ_w and τ_0, respectively. The pore volume of the radial well cell we defined can be calculated as

$$V_{p,0} = \pi\left(r_0^2 - r_w^2\right)\phi h = \frac{\pi\left(\tau_0^2 - \tau_w^2\right)kh}{\mu c_t} \tag{2.25}$$

If the production or injection well has a constant flow rate of q_w, under pseudo-steady state (PSS) conditions, the flux within the radial well cell can be represented as

$$q(\tau) = \frac{q_w}{V_{p,0}} \int_{\tau'=\tau}^{\tau_0} w(\tau') \cdot d\tau' \tag{2.26}$$

Combining Eq.(2.19), Eq.(2.22) and Eq.(2.25) with Eq.(2.26), we can calculate the pressure drop across the radial well cell as

$$\Delta p_0 = \frac{1}{c_t}\int_{\tau=\tau_w}^{\tau_0}\frac{q(\tau)}{w(\tau)}\cdot d\tau = \frac{q_w}{c_t V_{p,0}}\int_{\tau=\tau_w}^{\tau_0}\frac{d\tau}{w(\tau)}\int_{\tau'=\tau}^{\tau_0} w(\tau')\cdot d\tau' \tag{2.27}$$

Since the $w(\tau)$ function within Eq.(2.27) is linear, we can derive the well index (WI) as

$$\frac{1}{WI} = \frac{\Delta p_0}{q_w} = \frac{\mu}{2\pi kh}\cdot\left[\frac{\tau_0^2}{\tau_0^2-\tau_w^2}\ln\left(\frac{\tau_0}{\tau_w}\right)-\frac{1}{2}\right] \tag{2.28}$$

We define the DTOF to the radial well cell center as τ_c, though there is no need to explicitly calculate its position. In such a way, we can define the half-cell transmissibility from τ_c to τ_0 as T_0, which can be derived following the same procedure when the PSS pressure profile within the radial well cell is applied.

$$\frac{1}{T_0} = \frac{\mu}{2\pi kh}\cdot\left[\frac{1}{2}-\frac{\tau_w^2}{\tau_0^2-\tau_w^2}\ln\left(\frac{\tau_0}{\tau_w}\right)\right] \tag{2.29}$$

Thus, we have the following relationship between the well index and the half-cell transmissibility within the radial well cell, which can be used to depict the steady state pressure drop across it.

$$\frac{1}{WI}+\frac{1}{T_0} = \frac{\mu}{2\pi kh}\left(\frac{\tau_0}{\tau_w}\right) \tag{2.30}$$

Starting from the second to the last τ-interval (which is radial in homogeneous media), we assume that the $w(\tau)$ function across each one of them is constant. That is

$$w_i = \frac{PV_i}{\Delta\tau_i}\ \left(i=1,...,N-1\right) \tag{2.31}$$

where PV_i and $\Delta\tau_i$ represent the pore volume and DTOF difference across the *i*-th τ-interval (i = 1 ,…, N-1). From Eq.(2.31), we can define the half-cell transmissibility beyond the first radial well cell as

$$\frac{1}{T_i} = \frac{\Delta\tau_i}{2c_t w_i} = \frac{(\Delta\tau_i)^2}{2c_t PV_i} \quad (i = 1, ..., N-1) \tag{2.32}$$

After discretization of the one-dimensional diffusivity equation (Eq.(2.20)) using the DTOF, Eq.(2.28), Eq.(2.29) and Eq.(2.32) can be used for inter-cell transmissibility construction by means of the harmonic average of the half-cell transmissibilities between two adjacent τ-intervals. When the boundary condition at the well is defined and an appropriate initial reservoir pressure is assigned to the reservoir model, the pressure or flux profile at the well can be conveniently solved in a numerical approach.

2.3 Validation

From above derivation of the asymptotic pressure approximation, it is evident that drainage volume calculation plays a significant role in pressure transient analysis. Both the drainage volume and the cumulative pore volume constructions rely on an accurate calculation of the "diffusive time of flight" (DTOF). In this section, we will analyze the piecewise constant form of drainage volume discretization using DTOFs calculated from the analytic Eikonal solution and validate it with analytic drainage volume solutions for both 1D linear flow and 2D infinite-acting radial flow (IARF) models. We will also validate the asymptotic pressure approximation for the 2D IARF model using analytic

DTOF solutions. In the end, we test the block-centered FMM on the 3D Brugge full field reservoir model and discuss its potential impact on the forward model construction.

2.3.1 A 1D Linear Flow Model

The analytic solution of drainage volume as a function of time for 1D transient linear flow in the homogeneous media can be formulated as

$$V(t) = A\phi\sqrt{\pi\alpha_D t} \tag{2.33}$$

where A is the uniform cross-sectional area of the 1D flow model.

For drainage volume discretization using the "diffusive time of flight" (DTOF), we start from a 1D linear flow model. Suppose the 1D reservoir model has a total length of 5,000ft and consists of *n* uniform grid cells (DX = (5,000/*n*) ft, DY = DZ = 1ft). The formation porous media are homogeneous and have a uniform permeability value of 20md and a uniform porosity value of 0.1, with a total compressibility of 1.0E-5 psi^{-1}. The formation volume factor is 1 res bbl/STB and the viscosity of fluid within the reservoir is 1cp (Table 2.1).

Table 2.1 Input parameters for the 1D homogeneous linear flow model

LX	5,000	ft	k	20	md
LY	10	ft	ϕ	0.1	
LZ	10	ft	μ	1	cp
q_w	10	res bbl/day	c_t	1.0E-5	psi^{-1}
B_o	1	res bbl/STB			

($\alpha_D = 25835.12\ ft^2/hr$, τ *in* $hr^{0.5}$)

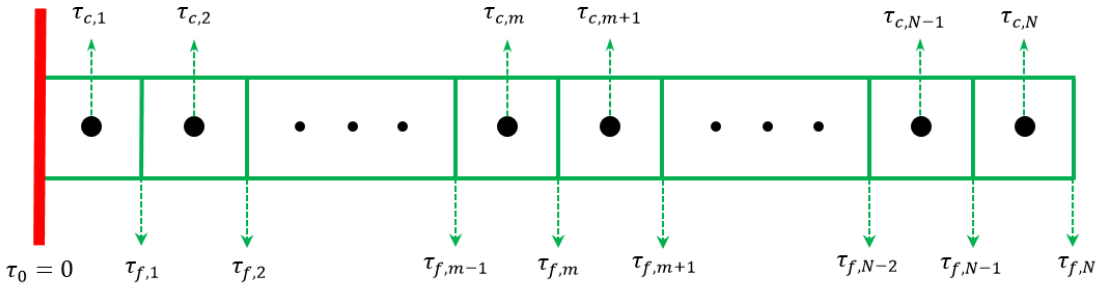

Figure 2.5 Discretization of the 1D linear flow model

A plane-source well with a constant production rate of 10 res bbl/day is placed at the left face of the first grid cell, which ensures that the fluid flows from right to left. DTOFs to cell centers and cell faces can be calculated precisely using the 1D Eikonal solver (Figure 2.5).

Since we have already formulated both the analytic solution and the numerical solution to the drainage volume as a function of time, we can easily estimate the accuracy of the numerical solution by means of the root-mean-square error (RMSE), which can be defined as

$$RMSE\left(V\left(t\right)_{cal}\right)=\sqrt{\frac{\sum_{j=1}^{N_t}\left(V\left(t_j\right)_{cal}-V\left(t_j\right)_{ref}\right)^2}{N_t}} \tag{2.34}$$

where N_t is the total number of time data used for drainage volume calculation; $V\left(t_j\right)_{cal}$ and $V\left(t_j\right)_{ref}$ are the calculated and reference (analytic in this case) drainage volume at the time t_j.

After comparing the numerical solution with the analytic solution to the drainage volume for the 1D linear flow, we can find that the RMSE generated from the piecewise constant form of drainage volume discretization (Eq.(2.17)) decreases fast as the number of cells increases (Figure 2.6a). The numerical drainage volume generates accurate results at later times of flow as long as the number of grid cells is large enough. However, the discrepancy between the numerical solution and the analytic solution at very early times of flow is quite large if the piecewise constant form of $V\left(t\right)$ discretization is adopted, especially when the number of grid cells is small (Figure 2.6b).

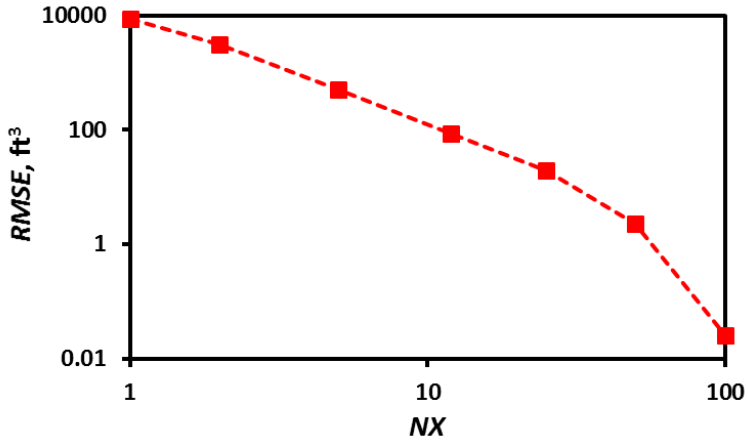

(a) RMSE

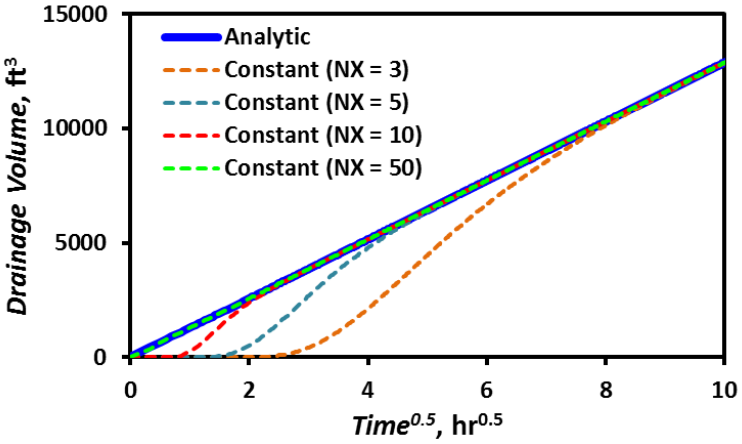

(b) Convergence

Figure 2.6 Convergence and RMSE of the drainage volume under different discretization schemes for the 1D linear flow model based on analytic DTOF solutions

The disagreement between the analytic and numerical solutions indicates that the piecewise constant form of the drainage volume discretization fails to capture the linear flow feature, which varies linearly as a function of square root of time and is not possible to be interpreted by the non-square-root solution. At a later time, dependent upon the resolution of the reservoir model, the piecewise constant form of the drainage volume

converges to the analytic solution. By taking a root-mean-square error analysis, we find that the difference between numerical and analytic solutions becomes negligible only when the number of grid cells becomes large (Figure 2.6b), implying that it cannot be used to accurately model near-well depletion.

2.3.2 A 2D Radial Flow Model

Following the same procedure as taken for the 1D linear flow, we provide a convergence analysis of the drainage volume evolution with time for the 2D infinite-acting radial flow (IARF) model. The analytic form of drainage volume expressed as a function of time for 2D IARF in homogeneous media can be formulated as:

$$V(t) = 4\pi\alpha_D \phi h t \tag{2.35}$$

where h represents the uniform reservoir thickness. This provides us the reference model to validate drainage volume discretization based on the DTOF.

Suppose that we have a 2D square-shaped reservoir model with homogeneous permeability and porosity as well as a uniform thickness. One vertical well with a constant production rate is located at the center of the reservoir domain (Figure 2.3). All other reservoir parameters are listed in Table 2.2. The reservoir has an equal length and width of 10,000ft and a uniform thickness of 10ft. It consists of a total number of n square cells (e.g. DX = DY = 476.1905ft when NX = NY = 21).

Table 2.2 Input parameters for the 2D homogeneous IARF model

DX	476.19	ft	k	20	md
DY	476.19	ft	ϕ	0.1	
DZ	10	ft	μ	1	cp
NX	21		c_t	1.0E-5	psi^{-1}
NY	21		B_o	1	
NZ	1		q_w	100	
Well	(11, 11)				

($\alpha_D = 25835.12\ ft^2/hr$, τ in $hr^{0.5}$)

DTOFs to the center of the reservoir grid cells can be easily calculated using the analytic Eikonal solution (Eq.(2.8)). Thus, we can construct the piecewise constant form of drainage volume based on these analytic DTOFs using Eq.(2.17).

By increasing the resolution of the 2D reservoir model, it can be observed that the discretized drainage volume constructed from the DTOFs converges well to the analytic solution at later times of simulation. However, it is not the same situation for early times; there exists an obvious discrepancy between the discretized $V(t)$ and the analytic formulation, especially when the grid size is large. This convergence analysis once again demonstrates that a higher-order $V(t)$ discretization is needed for more accurate characterization of transient pressure behavior in the near-well region (Figure 2.7).

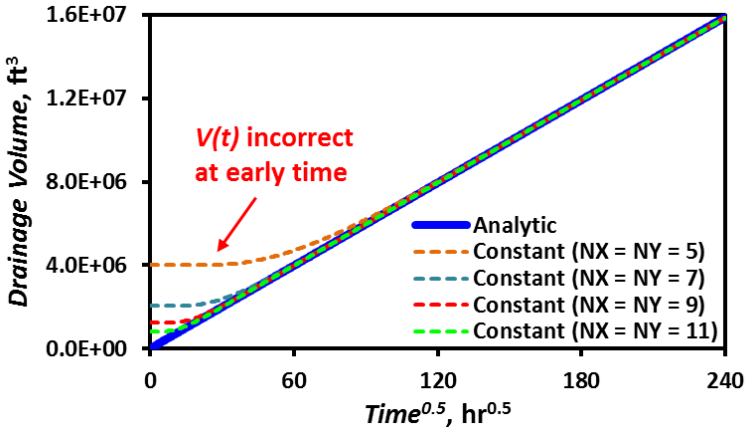

Figure 2.7 Convergence of the drainage volume under the piecewise constant discretization scheme for the 2D radial flow model based on analytic DTOF solutions

To validate our asymptotic pressure approximation, we calculate the pressure drop distribution using the ECLIPSE simulator on a 51x51 grid system and investigate their relationship with the DTOF (τ) values calculated from the analytic Eikonal solution.

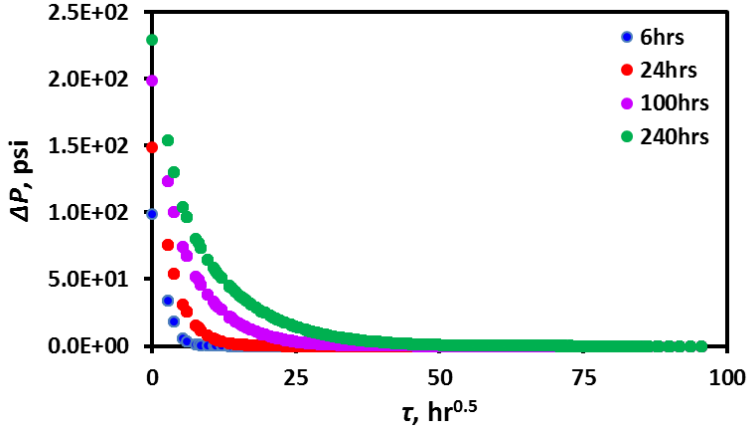

Figure 2.8 Pressure drop (from ECLIPSE) as a distance "τ" from the vertical well for the IARF in a 2D homogeneous reservoir model

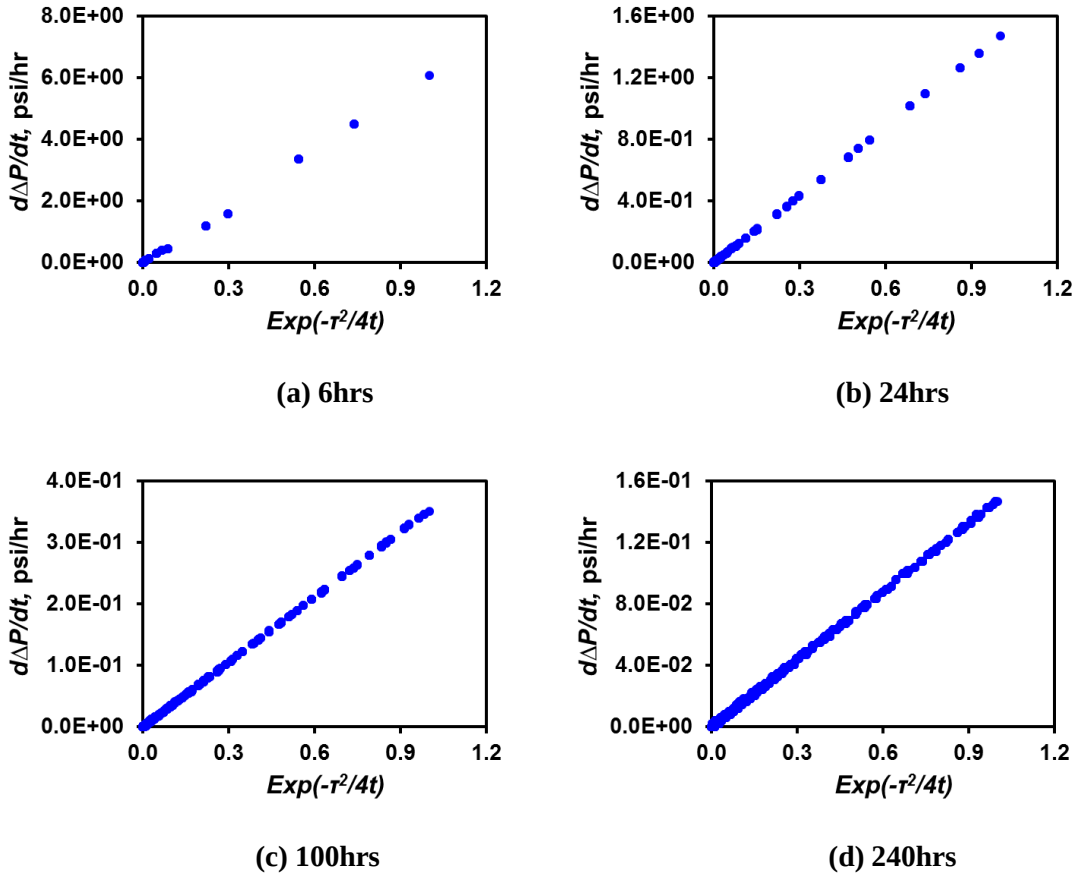

Figure 2.9 Pressure drop derivative (from ECLIPSE) vs. Exp(-τ^2/4t) for the IARF in a 2D homogeneous reservoir model

The reservoir pressure drop has a maximum value at the wellbore and decrease as a function of distance "τ" from the production well (Figure 2.8). Meanwhile, the derivative of pressure drop with respect to time (the pressure drop derivative) has a strong linear relationship with the exponential term in Eq.(2.11), indicating that the flow is under the infinite-acting transient state (Figure 2.9). This is mainly because the pressure contour is exactly aligned with the "τ-contour" for the infinite-acting radial flow (IARF) in

homogeneous media. However, this assumption needs to be validated in heterogeneous media before establishing a robust forward model and conducting inverse modeling.

2.3.3 A 3D Full Field Model

In this section, we test the current FMM method on the Cartesian coordinate system for a 3D full field model. A block-centered discretization scheme is adopted to solve the Eikonal equation for general heterogeneous and anisotropic porous media (Figure 2.10).

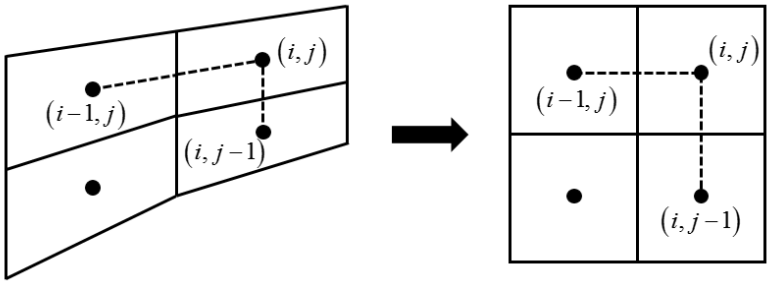

Figure 2.10 Illustration of 2D corner point grid iso-parametric mapping and discretization (Zhang et al., 2013)

For discretization of Eq.(2.5), we assume that the 2D corner point grid (CPG) can be transformed into the rectangular orthogonal grid with an equivalent pore volume (Figure 2.10). Thus, implementing the FMM based on Eq.(2.14) leads to the following discretization:

$$\frac{\left(\tau_{i,j}-\tau_{i-1,j}\right)^2}{s_I^2}+\frac{\left(\tau_{i,j}-\tau_{i,j-1}\right)^2}{s_J^2}=1 \tag{2.36}$$

Here s_I and s_J are the average "slowness" between adjacent grid cells (Zhang et al., 2013), which are inverse to the pressure propagation speed in the reference grid. This discretization scheme can be easily extended to 3D models and will lead to a straightforward FMM calculation for the DTOF.

We implemented this block-centered FMM on a 3D Brugge full field model. Both the permeability and porosity are heterogeneous. The permeability within each grid cell is anisotropic. One vertical well located at (70, 23) penetrates the entire reservoir model. The input parameters for DTOF calculation using the FMM are listed in Table 2.3.

Table 2.3 Input parameters for DTOF calculation from the block-centered FMM for the 3D Brugge full field reservoir model

NX	139	$\overline{DX}$	412.1	ft	μ	1	cp	$\overline{KX}$	476.9	md
NY	48	$\overline{DY}$	405.3	ft	c_t	1.0E-5	psi^{-1}	$\overline{KY}$	475.7	md
NZ	9	$\overline{DZ}$	22	ft				$\overline{KZ}$	34.2	md
Well	(70, 23)							$\bar{\phi}$	0.18	

Based on the permeability and porosity distribution, the 3D nine-layer heterogeneous Brugge field can be classified into four groups. The first group contains the top and second layers, which has an average permeability in I, J, K directions and porosity of 599.8md, 597.3md, 43.2md, and 0.17, respectively. The second group contains Layer 3 to Layer 5, with an average permeability in I, J, K directions and porosity of 82.6md,

82.4md, 5.3md, and 0.15, respectively. The third group contains Layer 6 to Layer 8, with an average permeability in I, J, K directions and porosity of 941.1md, 939.4md, 68.0md, and 0.23, respectively. The last group contains only the bottom layer, with an average permeability in I, J, K directions and porosity of 16.7md, 16.6md, 1.1md, and 0.15, respectively.

Though the permeability and porosity values within the four groups are significantly different, which make the average diffusivity values in the first and third groups much higher than those in the second and last groups, DTOFs generated from the FMM across different layers are generally uniformly distributed (Figure 2.11). This is mainly due to the pressure propagation in the vertical direction. On the other hand, the DTOF values are generally higher in regions where the permeability is distinctively lower than its surrounding areas (e.g. the low permeability areas in Layer 2 and Layer 9.

The original CPGs within the Brugge model are transformed into 3D orthogonal grids, each one of which has a specific length, width and thickness. In such a way, the original fault features within the Brugge model are ignored. Therefore, the DTOF distribution from the block-centered FMM calculation is smooth, without any abrupt changes of DTOF values across the original fault cells. In this 3D full field model, we can see up to an order of magnitude variation in the DTOFs calculated from the FMM corresponding to two orders of magnitude variation in permeability. (Figure 2.11). This is consistent with the analytic Eikonal solution, in which the DTOF value relies upon the square root of the diffusivity (Eq.(2.8)).

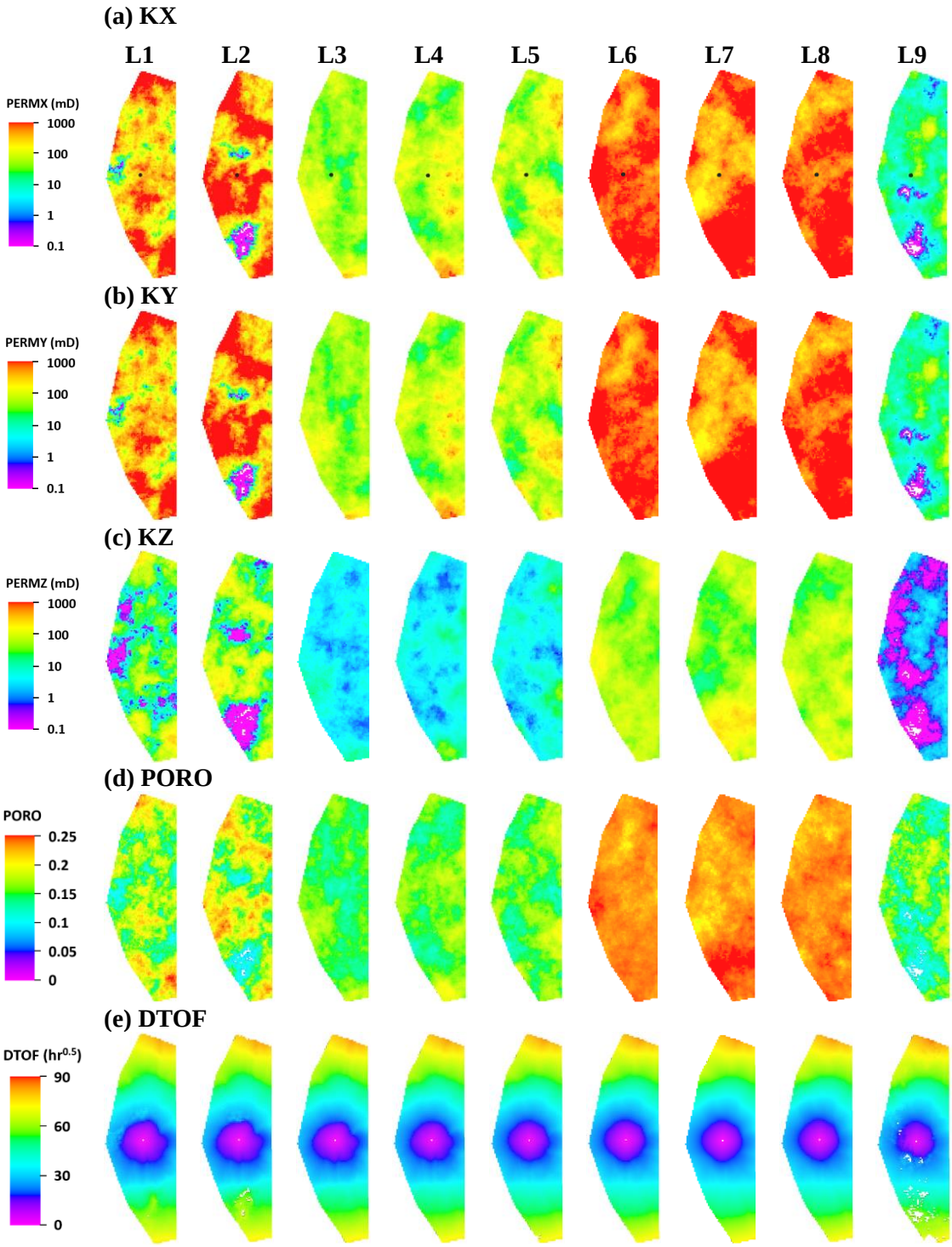

Figure 2.11 DTOFs calculated by the block-centered FMM from the 3D Brugge full field reservoir model with heterogeneous and anisotropic media

2.4 Discussion

The asymptotic pressure approximation is derived from the high frequency limit of the diffusivity equation after Fourier transform. It relies upon an accurate calculation of the "diffusive time of flight" (DTOF), which can be calculated either analytically in homogeneous media or numerically in heterogeneous media by solving the Eikonal equation. The validity of the asymptotic pressure approximation has been demonstrated by the 2D infinite-acting radial flow (IARF) model with homogeneous reservoir media (Figure 2.3), where the DTOFs are calculated analytically. This methodology needs to be further validated in general heterogeneous and anisotropic media.

Studies of drainage volume evolution with time for the 1D linear flow model and the 2D IARF model reveals that the near-well region requires more detailed discretization by means of the DTOF (τ) calculated from the FMM (Figure 2.7). The DTOF-based one-dimensional pressure diffusivity equation can be discretized into a limited number of "τ-intervals", based upon which the inter-cell transmissibility can be constructed in terms of the "$w(\tau)$" function, which is defined as the derivative of the cumulative pore volume with respect to the DTOF. Construction of an accurate and stable $w(\tau)$ function is pivotal when the diffusivity equation is solved using the inter-cell transmissibility formulated in terms of the DTOF. This is especially important for simulation of the transient flow in heterogeneous media, within which the $w(\tau)$ function construction from cumulative pore volume will be discussed in more detail in the next section.

Implementation of the block-centered FMM on orthogonal grids for 3D reservoir models with heterogeneity is straightforward. However, the accuracy of DTOFs calculated is open to discussion. This is important because our forward model for pressure transient calculation relies upon a sufficiently accurate drainage volume construction. Different discretization schemes of the Eikonal equation need to be compared and investigated, so that the DTOF-based drainage volume can better represent the pressure transient. Meanwhile, the causality condition needs to be ensured when the Eikonal equation is solved using the FMM in heterogeneous and anisotropic media. This relies upon an accurate and stable local Eikonal solver within the FMM, which becomes particularly important when it is implemented within the faulted corner point grid (CPG) system.

2.5 Section Summary

In this section, we derived the asymptotic pressure approximation to the diffusivity equation by introducing the concept of "diffusive time of flight" (DTOF), which transforms the 3D diffusivity equation into a reduced 1D formulation. The DTOF serves as a bridging tool devised to guide subsurface pressure propagation in the 3D space through a fast and efficient 1D conduit-a semi-analytic formulation of transient pressure variation as a function of time based on drainage volume characterization.

The results presented provides insights into accurate and efficient discretization schemes for the drainage volume evolution as a function of both the DTOF (τ) and time. Some conclusions can be drawn as follows:

1) Drainage volume formulated from the asymptotic pressure approximation can be discretized using the DTOF and validated with its analytic solution. Both the 1D linear flow and 2D infinite-acting radial flow (IARF) generated from analytic DTOF solutions demonstrate that higher orders of drainage volume discretization schemes are required, especially at the near-well region.
2) Under transient state, the derivative of pressure drop with respect to time for the 2D IARF shows to be linearly related with the exponential term in the asymptotic pressure approximation. This validates our assumption that the pressure gradient is aligned with the DTOF gradient, which needs to be further tested in heterogeneous reservoir model.
3) New discretization schemes for the Eikonal solution need to be designed, which should be consistent with the drainage volume discretization. The DTOFs calculated from the FMM should be able to generate sufficiently accurate drainage volume solutions.
4) The block-center based discretization for DTOF calculation is easy to implement within the FMM. But the accuracy of the calculated DTOFs for drainage volume construction needs to be investigated in more detail. Meanwhile, the DTOFs generated from the block-centered FMM cannot capture faulted features of reservoir models with complex grid geometries. This issue is expected to be resolved by designing new local Eikonal solvers that can be implemented within the FMM for the faulted corner point grid (CPG) system with the causality condition ensured.

3. DRAINAGE VOLUME CHARACTERIZATION AND TRANSIENT FLOW SIMULATION IN POROUS MEDIA USING THE FAST MARCHING METHOD

This section presents the improved pressure transient formulation from the asymptotic pressure approximation and the transient flow simulation in general heterogeneous media using the "diffusive time of flight" (DTOF). The near-well drainage volume is characterized on the basis of the DTOF (τ) that is obtained from solving the Eikonal equation using the fast marching method (FMM). The numerical solution to the DTOF-based one-dimensional diffusivity equation is developed by constructing the inter-cell transmissibility from a more accurate formulation of the cumulative pore volume as well as its DTOF derivative. Multiple discretization schemes for calculating the DTOF and drainage volume have been investigated and compared with the corresponding analytic solution for the 2D infinite-acting radial flow (IARF). The accuracy of the numerical pressure transient solution is found to be dominated by the drainage volume discretization in the near-well region, but also impacted by the discretization of the Eikonal equation.

We study in more detail the "$w(\tau)$" term, which is defined as the DTOF derivative of the cumulative pore volume within a "τ-contour" and relate it to the drainage volume discretization. An efficient way of generating $w(\tau)$ distribution within the full range of DTOF for the entire reservoir model is devised by evaluating its value on each orthogonal grid cell. Mixed-forms of drainage volume that combine an analytic solution with first-order or zeroth-order volumetric elements are developed and their accuracy are tested by

means of the well test derivative. Based on the $w(\tau)$ constructed, the well pressure and flux are calculated as a function of the DTOF from discretization of the equivalent one-dimensional diffusivity equation and verified at the well.

3.1 Introduction

Pressure transient tests are extensively used in petroleum engineering to determine reservoir permeability and porosity, skin factor of the production well as well as the flow regime in the subsurface. Nearly all reservoir limit tests, which are commonly used for obtaining well drainage pore volume, rely on the fact that pressure eventually reaches pseudo-steady state for a closed drainage system with constant drawdown rate at the well (Jones, 1957, 1962; Jones, 1963; Earlougher, 1971). A more popular pressure transient test for evaluating reservoir properties is the pressure buildup test (Miller et al., 1950; Horner, 1951). Using the Horner method, the well drainage pore volume and the effective porosity can be estimated by analysis of pressure buildup data (Denson et al., 1976). Most of these studies of the vertical well performance for transient and pseudo-steady state flow are based on either analytical or analog methods, which applies to idealized reservoir models.

By detecting the maximum pressure change for a given location in space, the concept of radius of investigation (ROI) and depth of investigation (DOI) can be defined for pressure propagation from an impulse source in homogeneous and heterogeneous reservoir media, respectively (Lee, 1982; Datta-Gupta et al., 2011). Using such definitions, the drainage volume variation as a function of time for the infinite-acting flow

can be easily visualized with the help of a numerical simulator (Datta-Gupta et al., 2011). However, the numerical method for DOI calculation and drainage volume characterization is usually computationally-expensive and cannot provide a geometric description of the pressure front propagation in the subsurface.

Though not widely practiced in the oil and gas industry, the use of Green's function for reservoir simulation provides novel insights into transient flow behavior in the subsurface media. Gringarten et al. (1973) applied instantaneous source functions and Green's functions to solve unsteady-flow problems in reservoir models, where the methodology of constructing solutions to complex problems through superposition of simpler solutions were demonstrated. Meanwhile, they provided a comprehensive list of Green's functions and possible source solutions for a wide variety of reservoir geometries and boundary conditions. Since then, mathematical models describing transient pressure response of fractured wells (Gringarten and Ramey, 1974; Gringarten et al., 1974) and naturally fractured reservoirs with arbitrary fracture connectivity (Wijesinghe and Culham, 1984; Wijesinghe, 1985; Wijesinghe and Kececioglu, 1986) are developed by formulating the Green's functions. Although these applications of the Green's functions are limited to isotropic media, they deepens our understanding of the geometric features of the reservoir model from well test analysis.

The asymptotic pressure approximation to the diffusivity equation is actually a variation from the Green's function, but it can be conveniently used to address pressure transient and rate transient problems in heterogeneous reservoir models. In the methodology we proposed, the Eikonal equation is related with the drainage volume

formulation by means of the "diffusive time of flight" (DTOF), which governs the propagation of pressure front in the reservoir for an impulse source. The discretized form of these equations provides the foundation for both fast numerical simulations and for sensitivity-based inverse problems in reservoir characterization, especially for applications in pressure transient analysis (PTA) of conventional reservoirs and in rate transient analysis (RTA) of unconventional reservoirs. The solution to the Eikonal equation and the calculation of the drainage volume are obtained by applying the fast marching method (FMM). We develop and analyze discretization schemes of these equations, with an emphasis on the near-well region which dominates the accuracy of the solutions.

3.2 Methodology: Forward Model Discretization

The "diffusive time of flight" (DTOF) calculated from the fast marching method (FMM) allows us to generalize the concept of the depth of investigation (DOI) to reservoirs with heterogeneous media and complex well geometries. To obtain adequate accuracy for the purpose of well test interpretation, a mixed discretization scheme that uses a combination of analytic, first-order, and zeroth-order volumetric elements is devised. The novel semi-analytic methodology we propose for calculating pressure and rate transient drainage volume calculations serves as a bridge between analytic approaches that require many simplified assumptions and conventional numerical simulation techniques that are usually computationally expensive.

Similar to the mixed structure of drainage volume, a hybrid version of the DTOF derivative of the cumulative pore volume, $w(\tau)$, is included into the one-dimensional form of the diffusivity equation and the solution at the wellbore is calibrated with the conventional reservoir simulator. The implementation of this method relies upon an understanding of the properties of the solutions to discretized forms of the source function, which is the subject of the current study. Consistency between the transient drainage volume solution and the pressure solution from the one-dimensional diffusivity equation using the FMM is achieved. The simplicity and computational efficiency of our proposed approach provide us with a better geometric understanding of pressure transient flow behavior in the subsurface, making it a promising candidate for high resolution reservoir characterization.

3.2.1 Discretization of the Eikonal Equation

The main feature of asymptotic expansion to the diffusivity equation is application of the quantity $\tau(\vec{x})$, which is defined as the "diffusive time of flight" (DTOF). It has a unit of (time)$^{1/2}$ and controls the phase of propagation of the pressure front. The advantage of using the DTOF to simulate reservoir flow is reducing the three-dimensional diffusivity equation to an equivalent one-dimensional form. In heterogeneous and anisotropic porous media, DTOFs can be calculated by solving the Eikonal equation using the fast marching method (FMM).

$$\nabla\tau(\vec{x})\bullet\vec{\vec{k}}(\vec{x})\bullet\nabla\tau(\vec{x})=\phi(\vec{x})\mu c_t \tag{3.1}$$

or

$$\nabla\tau(\vec{x})\bullet\vec{\vec{\alpha}}_D(\vec{x})\bullet\nabla\tau(\vec{x})=1 \tag{3.2}$$

where $\vec{\vec{\alpha}}_D(\vec{x})$ is the diffusivity tensor evaluated at location $\vec{x}$.

$$\vec{\vec{\alpha}}_D(\vec{x})=\frac{\vec{\vec{k}}(\vec{x})}{\phi(\vec{x})\mu c_t} \tag{3.3}$$

The Eikonal equation shows that the pressure front propagates in the subsurface with a velocity given by the square root of diffusivity. It is solved numerically subject to the boundary condition of a zero DTOF value at the well. To get more accurate DTOF solutions, we will discuss in more detail about the FMM design as well as the local Eikonal solver it contains.

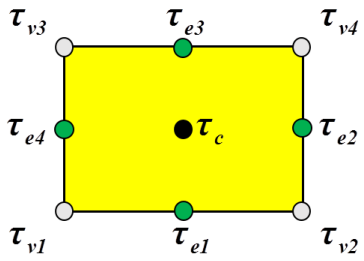

Figure 3.1 Illustration of 2D rectangular grid cell and its potential locations for DTOF evaluation

Suppose we have a 2D reservoir model that consists of rectangular grid cells. For each orthogonal grid cell, the DTOF can be evaluated at the cell center, cell vertex and

edge center (Figure 3.1). Each node can have connections with neighboring nodes in the X (or I) direction, Y (or J) direction and XY (or IJ) direction.

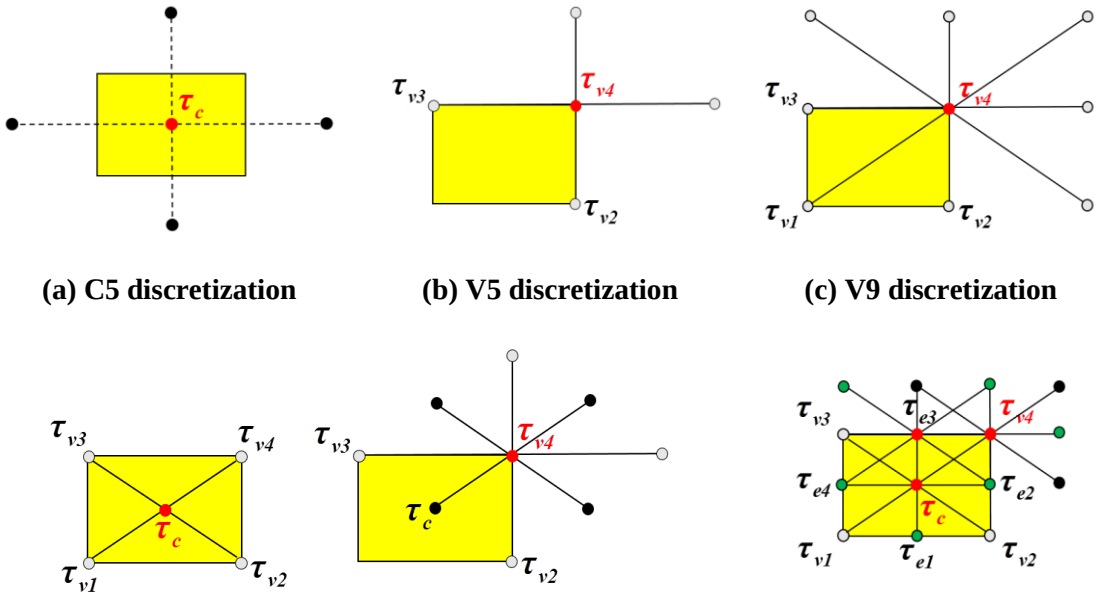

(a) C5 discretization **(b) V5 discretization** **(c) V9 discretization**

(d) C5V9 discretization **(e) CVE9 discretization**

Figure 3.2 Illustration of discretization schemes for the Eikonal equation on 2D reservoir models that consist of uniform rectangular grid cells

For the 2D DTOF calculation, we mainly investigate five discretization schemes for the Eikonal equation (Figure 3.2).

- In the first scheme, only cell centers are calculated and the cell-center node has direct connections with only cell-center nodes of its adjacent neighbor cells in the X (or I) and Y (or J) directions. This scheme is named as the **2D C5 discretization** (Figure 3.2a).

- In the second scheme, only DTOFs to cell vertices are calculated and the cell-vertex node has direct connections with only cell-vertex nodes of its adjacent neighbor cells in the X (or I) and Y (or J) directions. This scheme is named as the **2D V5 discretization** (Figure 3.2b).
- In the third scheme, only DTOFs to cell vertices are calculated and the cell-vertex node has direct connections with only cell-vertex nodes of its adjacent neighbor cells in the X (or I), Y (or J) directions and XY (or IJ) directions. This scheme is named as the **2D V9 discretization** (Figure 3.2c).
- In the fourth scheme, DTOFs to both cell vertices and cell centers are calculated. The cell-vertex node not only has direct connections with cell-vertex nodes of its adjacent neighbor cells in the X (or I) and Y (or J) directions, it also has direct connections with cell-center nodes of its diagonal neighbor cells in the XY (or IJ) direction. The cell-center node has only direct connections with the four vertex nodes of the cell itself. This scheme is named as the **2D C5V9 discretization** (Figure 3.2d).
- In the fifth scheme, DTOFs to cell centers, cell vertices and edge centers are calculated. The nodes at all these locations have direct connections with nodes located at cell centers, cell vertices and edge centers of adjacent and diagonal neighbor cells as well as the cell itself. This scheme is named as the **2D CVE9 discretization** (Figure 3.2e). Such a scheme provides the most complex node connections among the five discretizations to be investigated and thus is

expected to help generate the most accurate local DTOF solutions using the FMM for general heterogeneous media.

Table 3.1 Discretization schemes for the 2D Eikonal equation

Discretization Scheme (2D)	Nodes Per Cell	Equations Per Cell	Description
C5	1	4	1 Center node per cell 5-point discretization
V5	1	4	1 Vertex node per cell (shared) 5-point discretization
V9	1	8	1 Vertex node per cell (shared) 9-point discretization
CVE9	4	4x8	1 Center node per cell 1 Vertex node per cell (shared) 2 Edge nodes per cell (shared) 9-point discretization for each unknown
C5V9	2	4+8	1 Center node per cell 1 Vertex node per cell (shared) Center 5-point discretization Vertex 9-point discretization

Table 3.1 lists the computational information about the unknown DTOF variable for each of the five discretization schemes of the Eikonal equation (Figure 3.2), which includes the number of nodes per cell and the number of quadratic equations it required to solve for the unknown nodal DTOFs. We implemented the five discretization schemes for the Eikonal equation within the FMM algorithm and tested them on 2D homogeneous and heterogeneous reservoir models that consist of uniform square cells.

For all the five discretization schemes demonstrated above (Figure 3.2, Table 3.1), one basic rule underlying the DTOF calculation is that all pressure fronts have a constant speed of propagation within each element (with either a rectangular or triangular shape). In reservoir models discretized by all the five schemes, a vertical well is located at the reservoir center so that the DTOF information will propagate from the wellbore regions with lower DTOF values towards regions farther away with higher DTOF values.

At given locations in space, DTOFs are updated in such a way that they only depend upon points with smaller DTOF values. These discretization schemes for the Eikonal equation were analyzed and implemented either using the fast marching method (FMM) (Sethian, 1996; Sun and Fomel, 1998; Sethian, 1999; Sethian and Vladimirsky, 2000; Rawlinson and Sambridge, 2004, 2005; Konukoglu et al., 2007; Lelievre et al., 2011) or the fast sweeping method (FSM) (Zhao, 2004; Zhang et al., 2006; Qian et al., 2007; Luo and Qian, 2012; Luo et al., 2014).

Table 3.2 Input parameters for the 2D reservoir model

LX	10,000	ft	ϕ	0.1	
LY	10,000	ft	μ	1	cp
h	10	ft	c_t	1.0E-05	psi^{-1}
NX	199		B_o	1	res bbl/STB
NX	199		Well	(100, 100)	

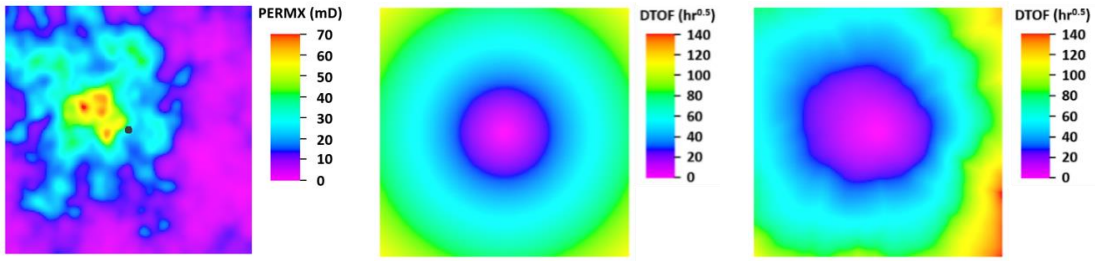

(a)
Heterogeneous KX
VPD = 0.5573

(b)
DTOFs within
homogeneous media

(c)
DTOFs within
heterogeneous media

Figure 3.3 Permeability and DTOFs calculated from the CVE9 FMM within a 199x199 square grid system

By applying the 2D CVE9 FMM to solve the Eikonal equation for a homogeneous reservoir and a heterogeneous reservoir (Figure 3.3a) (both with a grid resolution of 199x199 and with a vertical well located at (100,100)), we calculated the DTOFs for the reservoir model with input parameters listed in Table 3.2. DTOFs are radially distributed in homogeneous media (Figure 3.3b). In contrast, the DTOF distribution has a more irregular shape in the heterogeneous media (Figure 3.3c). In both cases, DTOF values are smallest at the central source region (the DTOF to the well is assigned as zero) and become increasingly large to the outer boundary of the reservoir domain. DTOF solutions for both the homogeneous and heterogeneous models can capture the pressure front propagating in the porous media (Figure 3.3b and c).

For both the homogeneous media and the heterogeneous media, we study the accuracy of the numerical DTOF solutions calculated from 2D FMMs under the five discretization schemes mentioned above. In the homogeneous reservoir model, the reference DTOF solution is analytic. In the sufficiently smooth heterogeneous reservoir

model (Figure 3.3a), which has a permeability field with a Dykstra-Parsons coefficient (VDP) of 0.5573, the reference DTOF solution is calculated from the 2D CVE9 FMM (Figure 3.3c). Within the entire modeling region of both the homogeneous and heterogeneous model which are decomposed into a 199 x 199 grid system, we select a central subdomain consisting of a 5x5 grid system to investigate the DTOF accuracy in the near-well region. The well is located at (100, 100) and (3, 3) within the entire reservoir domain and the near-well subdomain, respectively.

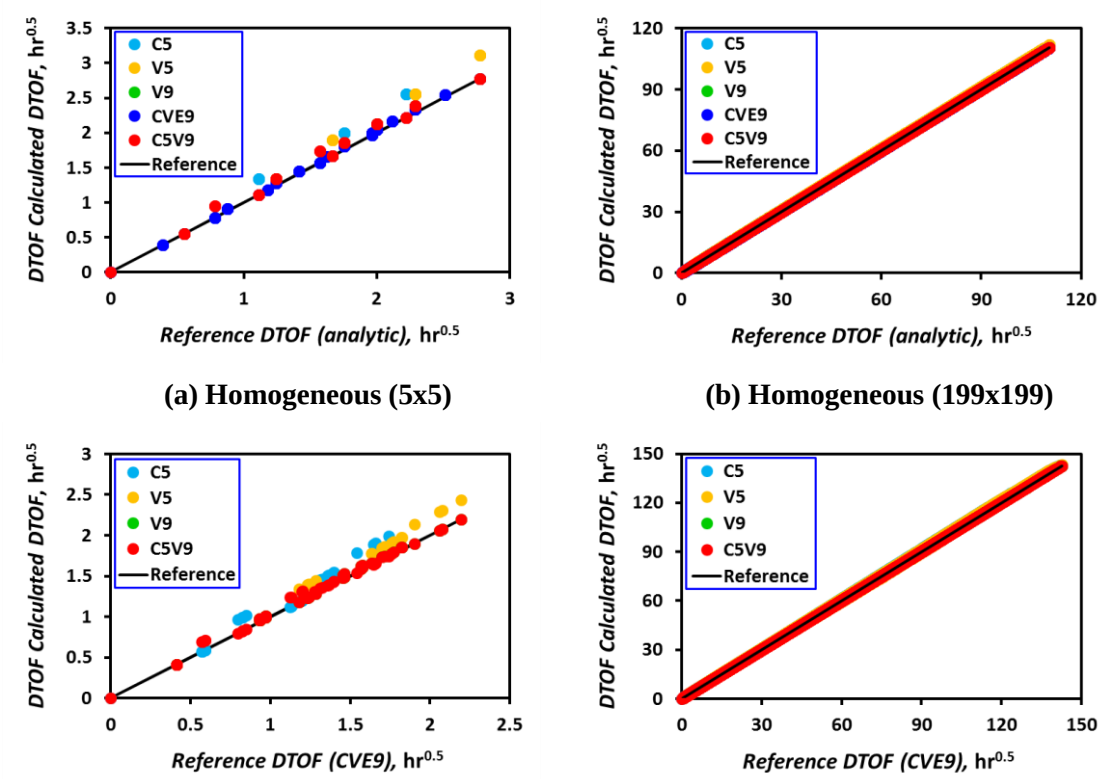

(a) Homogeneous (5x5)

(b) Homogeneous (199x199)

(c) Heterogeneous (5x5)

(d) Heterogeneous (199x199)

Figure 3.4 DTOFs calculated from FMMs under different discretization schemes within the near-well (5x5) and entire (199x199) 2D square reservoir domain

Figure 3.4 shows the scatter plots between DTOFs generated under different discretization schemes for the Eikonal equation and those generated from the reference FMM for both the homogeneous (Figure 3.4a and b) and heterogeneous models (Figure 3.4c and d). Particularly in the near-well region, the cell-vertex DTOFs generated from the 2D C5V9 FMM overlap all the DTOFs generated from the 2D V9 FMM and are closest to the reference model (Figure 3.4a and c). Based on DTOFs generated from the different FMMs, we can calculate the corresponding relative computational error in terms of the root-mean-square error (RMSE) for each discretization.

Suppose that the total number of DTOF data to be calculated using the FMM is N_τ. Then we can define the RMSE of the calculated DTOFs as

$$RMSE\left(\tau_{cal}\right)=\sqrt{\frac{\sum_{j=1}^{N_\tau}\left(\tau_{cal,j}-\tau_{ref,j}\right)^2}{N_\tau}} \tag{3.4}$$

where $\tau_{cal,j}$ and $\tau_{ref,j}$ represent the numerical DTOF calculated from the FMM and reference DTOF (analytic in the homogeneous reservoir model) at a node with index $j\left(j=1,2,\cdots,N_\tau\right)$ within the 2D coordinate system. If we only consider the 2D homogeneous square reservoir model with an equal number cells in the x and y directions (*NX* = *NY* = 101, 201, 401, 801, 1601), we can easily conduct a convergence rate analysis of the DTOF values calculated from the five different FMMs (Figure 3.5).

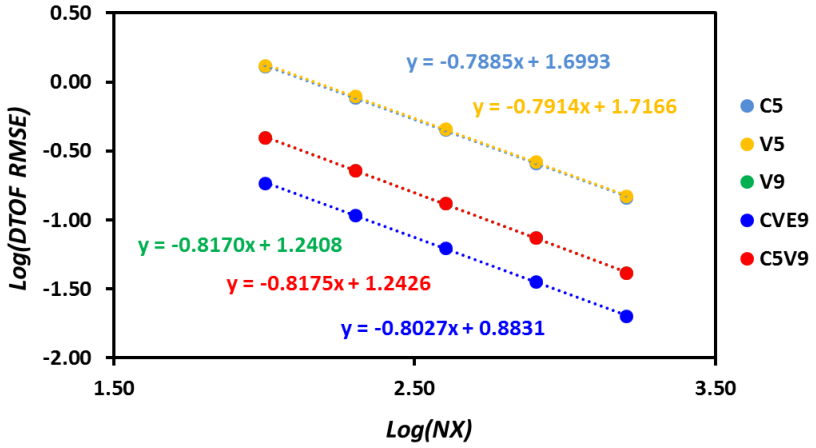

Figure 3.5 Convergence rate analysis of DTOFs generated from different discretization schemes of the Eikonal equation within a 2D homogeneous square reservoir model

In Figure 3.5, we can easily find that the C5 and V5 discretization schemes of the Eikonal equation generate the most inaccurate DTOF solutions and the truncation errors they introduced are quite close. The V9 and C5V9 discretization schemes can significantly improve the numerical solutions to the Eikonal equation and their computational accuracy are also very similar. This explains why the V5 scheme is overlapping the C5 scheme and the C5V9 scheme is overlapping the V9 scheme in Figure 3.5. The CVE9 FMM generates the most accurate DTOF solution with the least truncation errors since it involves the most computational costs compared with the other four schemes.

This result is also listed in Table 3.3, where the correlation coefficients between the numerical solutions of the Eikonal equation and the corresponding analytic solution are also demonstrated. In particular, the convergence rates we estimated from the RMSE calculation for each of the five FMMs is approximately 0.8, which is not quite close to 1.

This is different from the convergence rate generated from the numerical solutions to the Eikonal equation in triangular elements using the fast sweeping method (FMM) by Qian et al. (2007), where a first order convergence rate can be obtained using the L1 error estimation by means of a so called "wrapping technique". The reason for this convergence rate discrepancy in numerical calculation of the Eikonal solution is worthy of further investigation in the future research work.

Table 3.3 Numerical errors and convergence rate of DTOFs calculated from FMMs in the 2D homogeneous reservoir model (KX = 15.5272md)

Discretization Schemes (2D)	Correlation Coefficients		RMSE ($hr^{0.5}$)		Convergence Rate (Confidence Interval)
	(5x5)	(199x199)	(5x5)	(199x199)	
C5	1.119862	1.011107	0.2123	0.7776	0.7885 (0.7616, 0.8153)
V5	1.100708	1.011598	0.1983	0.7971	0.7914 (0.7642, 0.8185)
V9	1.035780	1.003036	0.0862	0.2320	0.8170 (0.7978, 0.8361)
C5V9	1.039944	1.003045	0.0964	0.2322	0.8175 (0.7989, 0.8362)
CVE9	1.015687	1.001427	0.0340	0.1100	0.8027 (0.7784, 0.8270)

We also compared the numerical solutions generated from the C5, V5, V9 and C5V9 FMMs with the DTOFs calculated from the CVE9 FMM in the 2D heterogeneous reservoir model (Figure 3.3a). The correlation coefficient and RMSE between them are generalized in Table 3.4. Discretization analysis of the DTOF calculation within the heterogeneous media also shows that Eikonal solutions from the V9 and C5V9 FMMs have similar convergence rates and almost the same accuracy. But the C5V9 FMM requires less computational cost compared to the V9 FMM (Figure 3.2).

Table 3.4 Numerical errors of DTOFs calculated from FMMs in the 2D heterogeneous reservoir model (Average KX = 15.5272md, VDP = 0.5573)

Discretization Schemes (2D)	Correlation Coefficients		RMSE ($hr^{0.5}$)	
	(5x5)	(199x199)	(5x5)	(199x199)
C5	1.106959	1.011930	0.1443	0.7954
V5	1.075322	1.009768	0.1204	0.6924
V9	1.015790	1.001509	0.0303	0.1054
C5V9	1.021544	1.001486	0.0497	0.1045

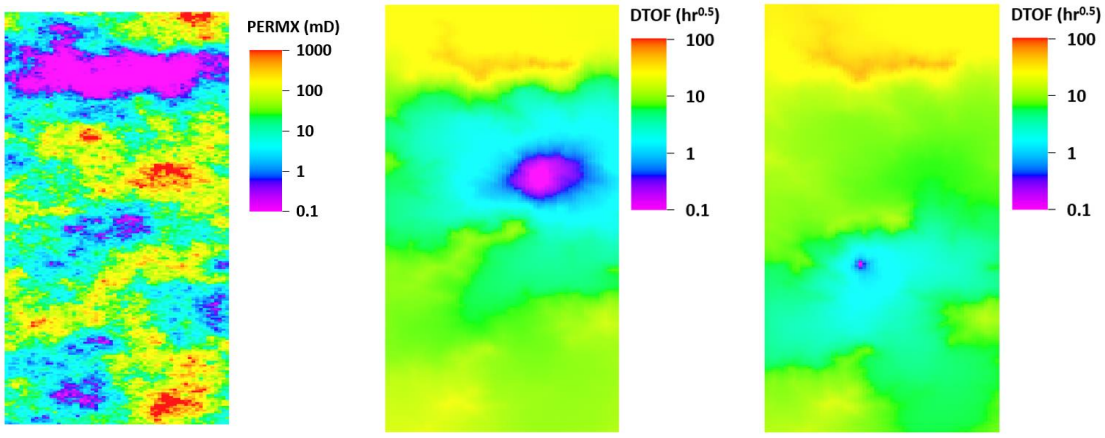

(a)
Permeability in Layer 1
(Average KX = 74.33md)
(VDP = 0.9191)

(b)
DTOFs in Layer 1
Well (40, 90)

(c)
DTOFs in Layer 1
Well (24, 134)

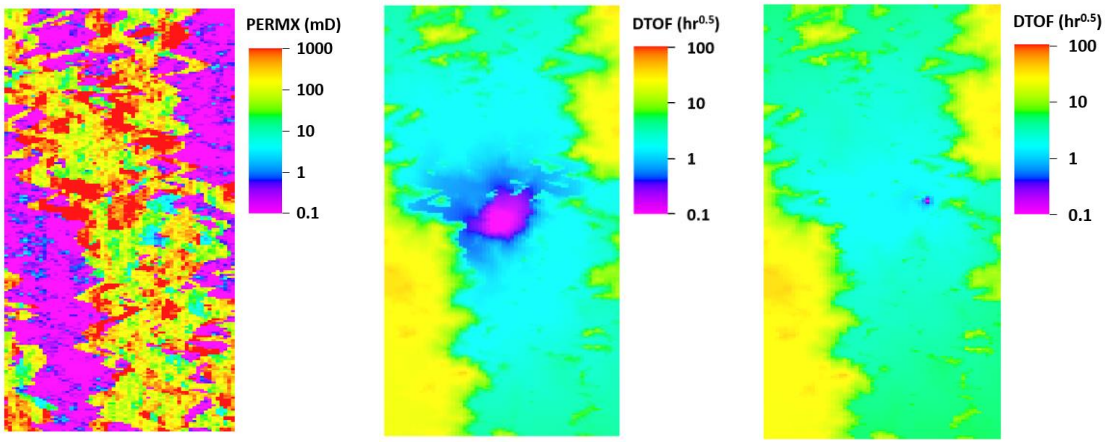

(d)
Permeability in Layer 72
(Average KX = 475.90md)
(VDP = 0.9982)

(e)
DTOFs in Layer 72
(Well (33, 103)

(f)
DTOFs in Layer 72
Well (42, 100)

Figure 3.6 DTOFs calculated from the 2D CVE9 FMM for the permeability fields of the 1st layer and 72nd layer within the SPE10 model (60x220 rectangular grid systems; grid cell aspect ratio = 2:1)

Following the same procedure above, we test the four FMMs (C5, V5, V9 and C5V9) against the CVE9 FMM in much more heterogeneous reservoir media. The permeability fields of the 1st layer (Figure 3.6a) and 72nd layer (Figure 3.6d) within the SPE10 model (with VDPs of 0.9191 and 0.9982, respectively) are taken as examples to test the computational accuracy of the four candidate FMMs.

Table 3.5 Input parameters for the 2D reservoir fields within the SPE10 model

LX	1,200	ft	ϕ	0.1	
LY	2,200	ft	μ	1	cp
h	2	ft	c_t	1.0E-05	psi^{-1}
NX	60		B_o	1	res bbl/STB
NY	220				

Table 3.6 Well locations in the 1st layer and the 72nd layer of the SPE10 model as well as the maximum DTOF values calculated from the 2D CVE9 FMM

Reservoir Layers	Well-cell Permeability (md)		Maximum DTOF Value ($hr^{0.5}$)	
Layer 1	Well (40, 90)	Well (25, 134)	Well (40, 90)	Well (25, 134)
	993.06	7.71	51.27	57.50
Layer 72	Well (33, 103)	Well (42, 100)	Well (33, 103)	Well (42, 100)
	3430.85	3.40	43.83	45.16

Reservoir porosity, viscosity, compressibility and the formation volume factor are assumed to be uniform as listed in Table 3.5. In each layer, the well is placed at two different cells of the 2D reservoir model, with a higher and lower permeability values, respectively (Table 3.6). The distributions of the DTOF values calculated from the CVE9 FMM are different due to different well locations (Figure 3.6b, c, e and f).

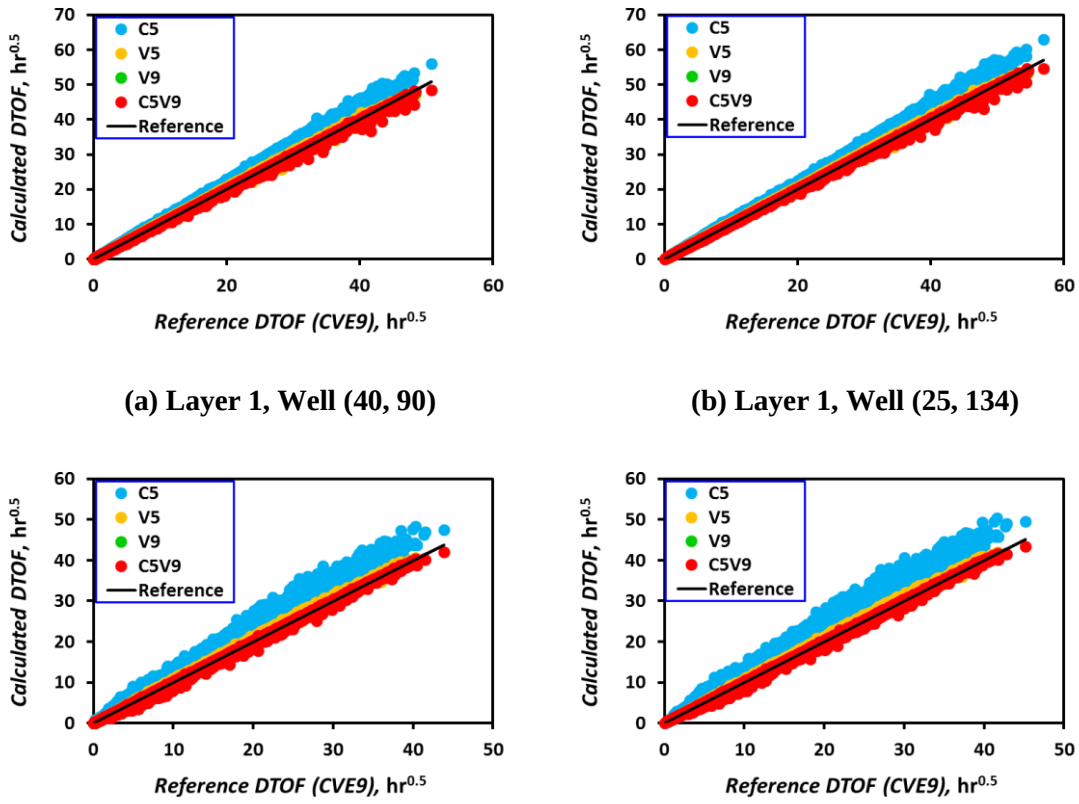

(a) Layer 1, Well (40, 90)

(b) Layer 1, Well (25, 134)

(c) Layer 72, Well (33, 103)

(d) Layer 72, Well (42, 100)

Figure 3.7 DTOFs calculated from the FMM under different discretization schemes for the 2D reservoir fields (60x220) within the SPE10 model

In Figure 3.7, we also make the scatter plots between the DTOFs calculated from the candidate discretization schemes against that calculated from the reference scheme (CVE9) of the Eikonal equation for the 2D SPE10 models. It should be noted that the DTOF calculated from the C5 FMM deviates significantly from the reference solution compared with the other three FMMs.

Table 3.7 Numerical errors of DTOFs calculated using FMMs from the permeability field of the 1st layer within the SPE10 model (VDP = 0.9191)

Discretization Schemes (2D)	Correlation Coefficients		RMSE ($hr^{0.5}$)	
	Well (40, 90)	Well (25, 134)	Well (40, 90)	Well (25, 134)
C5	1.115987	1.114111	1.5035	1.7425
V5	1.011137	1.014595	0.2351	0.2991
V9	0.999081	1.002075	0.0452	0.0695
C5V9	0.998585	1.002143	0.1412	0.1534

Table 3.8 Numerical errors of DTOFs calculated using FMMs from the permeability field of the 72nd layer within the SPE10 model (VDP = 0.9982)

Discretization Schemes (2D)	Correlation Coefficients		RMSE ($hr^{0.5}$)	
	Well (33, 103)	Well (42, 100)	Well (33, 103)	Well (42, 100)
C5	1.181338	1.209014	2.0368	2.5230
V5	1.024296	1.025083	0.3267	0.3501
V9	1.001788	1.002830	0.0450	0.0532
C5V9	1.000336	1.001442	0.1603	0.1613

By comparing the RMSE of the DTOF values generated from the C5, V5, V9 and C5V9 FMMs against the CVE9 reference FMM for the 2D SPE models, we can see that the C5 and V5 FMM solutions are least accurate, especially the former scheme (which has a RMSE significantly greater than the other three schemes) (Table 3.7 and Table 3.8). This is consistent with previous results generated from homogeneous and relatively smooth heterogeneous models. DTOFs generated from the V9 and C5V9 FMMs have almost the same correlation coefficients with DTOFs calculated from the reference scheme (CVE9 FMM).

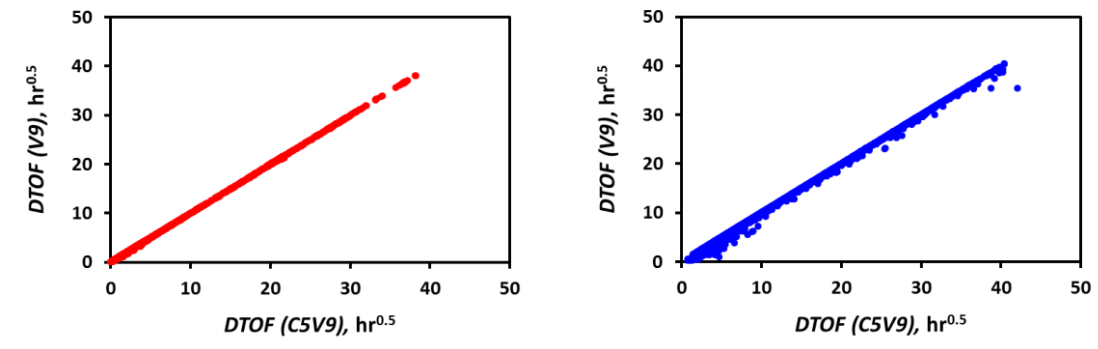

(a) High-permeability region **(b) Low-permeability region**

Figure 3.8 Correlations between maximum grid-cell DTOFs calculated from the 2D V9 and C5V9 FMMs within the 72nd layer in the SPE10 model (VDP = 0.9982) with a vertical well located at Cell (33, 103)

Figure 3.8 shows the scatter plots of maximum grid-cell DTOFs calculated from the C5V9 FMM against the V9 FMM in high-permeability cells (Figure 3.8a) and low-permeability cells (Figure 3.8b) within the 72nd layer of the SPE10 model, respectively. There are a total number of 13,200 cells within the 2D SPE10 model. The low-permeability cells are defined as the 4,400 cells with the lowest permeability values, which have a minimum, maximum and mean permeability values of 8.69E-4md, 0.36md and 0.12md, respectively. The remaining 8,800 cells are defined as the high-permeability cells with a minimum, maximum and mean permeability values of 0.36md, 20,000md and 713.80md, respectively. The vertical well is located at the high-permeability cell (33, 103).

Although the V9 FMM has some advantages over the C5V9 FMM in terms of the DTOF accuracy within the entire highly heterogeneous reservoir model (Table 3.7 and Table 3.8), it performs less well compared with the C5V9 FMM within the low-permeability cells (Figure 3.8b). In cells with higher permeability values, the maximum DTOF values evaluated on every grid cell calculated from the V9 FMM (at the cell vertex) has a strong linear relationship with those calculated from the C5V9 FMM (either at the cell vertex or cell center) (Figure 3.8a). However, this linear relationship become worse if the maximum grid-cell DTOFs are calculated within those cells with lower permeability values. Especially in grid cells that are far away from the well and have much smaller permeability values compared with the high-permeability cells close to the well, the maximum grid-cell DTOFs evaluated from the C5V9 FMM can be distinctly higher than the V9 FMM (Figure 3.8b).

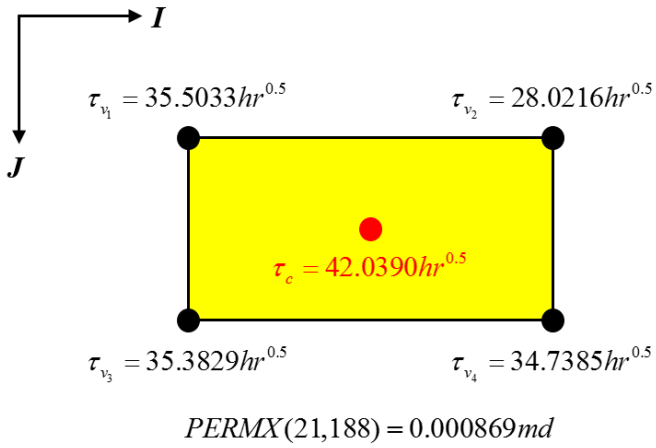

Figure 3.9 DTOFs evaluated at the four vertices and the center of Cell (21, 188) within the 72nd layer in the SPE10 model with a vertical well located at Cell (33, 103) using the 2D C5V9 FMM

This deviation of maximum grid-cell DTOF values calculated using the C5V9 FMM from those calculated using the V9 FMM is mainly due to the an additional degree of freedom of the DTOF introduced at the cell center by the C5V9 FMM. Figure 3.9 shows the DTOFs evaluated at the vertices and center of Cell (21, 188) within the 72nd layer in the SPE10 model. Using the C5V9 FMM to solve the Eikonal equation, the DTOF to the center of Cell (21, 188), which has a very low permeability value of 8.69E-4md, is greater than the DTOFs to its four vertices. This indicates that the pressure front will finally enter into the low-permeability Cell (21, 188) after it passes the four vertices. On the contrary, the pressure front will circumvent this low-permeability cell if the DTOFs are only evaluated at the cell vertices using the V9 discretization, which may not reflect the real circumstances of fluid flow in low-permeability cells within the reservoir model.

From Figure 3.8 and Figure 3.9, it is evident that an additional degree of freedom of DTOF evaluated at the cell center is significant for accurate characterization of pressure front propagation in heterogeneous reservoir models that have low-permeability cells. These results show that the C5V9 FMM is the best candidate for DTOF calculation compared with the C5, V5 and V9 FMMs. It can not only help generate sufficiently accurate Eikonal solutions without much computational cost (Table 3.3, Table 3.4, Table 3.7 and Table 3.8) but can also more realistically capture pressure front propagation in general heterogeneous media (Figure 3.9).

From above analysis of DTOF calculation using different discretization schemes for the Eikonal equation, we can obtain following observations both for the porous media with smoothly varying heterogeneity (Figure 3.3) and the porous media with high heterogeneity (Figure 3.6):

- The C5 and V5 discretization schemes designed for the Eikonal equation generates the DTOF solutions with the greatest errors, with the latter slightly more accurate than the former (Figure 3.4 and Figure 3.7).
- DTOFs generated from the V9, C5V9 and CVE9 discretization schemes for the Eikonal equation have comparable magnitudes of accuracy (Table 3.3, Table 3.4, Table 3.7 and Table 3.8).
- For the 2D reservoir model that has a large grid-cell resolution, the C5V9 discretization scheme should be mostly recommended for solving the Eikonal equation using the FMM. It can generate a sufficiently accurate DTOF solution

among the five discretization schemes we suggested for DTOF calculation without introducing much additional computational cost.

- The 2D C5V9 discretization scheme for the FMM ensures an additional degree of freedom of DTOF value at the cell center, which connects DTOFs evaluated at the four cell vertices and proves to be suited for describing pressure propagation in highly heterogeneous reservoir models (Figure 3.8 and Figure 3.9).

3.2.2 Discretization of the Drainage Volume

From the asymptotic pressure approximation, it is evident that characterization of the drainage volume evolution as a function of time relies largely on both the calculation of the DTOF and the differential of the cumulative pore volume.

$$V(t) = \int_0^\infty dV_p(\tau) \cdot e^{-\tau^2/4t} = \int_0^\infty d\tau \cdot w(\tau) \cdot e^{-\tau^2/4t} \tag{3.5}$$

Sufficient attention needs to be paid to the $w(\tau)$ term that is defined as the DTOF derivative of the cumulative pore volume $V_p(\tau)$ within a specific "τ-contour". We have demonstrated in **Section 2** that a higher-order $w(\tau)$ formulation is required to generate more accurate drainage volume as well as pressure transient solutions at early times of simulation, when the pressure front propagates mainly in the near-well region.

As mentioned in **Section 2**, we can use the analytic Eikonal solver to calculate the DTOF in reservoir models with homogeneous and isotropic media when a vertical well is located at the center of the reservoir domain and the radial flow occurs.

$$\tau = \frac{r}{\sqrt{\alpha_D}}, \ \tau_w = \frac{r_w}{\sqrt{\alpha_D}} \tag{3.6}$$

Here r represents the radial distance from the well and r_w represents the effective wellbore radius; τ_w represents the DTOF to the r_w location. Then, the analytic cumulative pore volume can be formulated in terms of the DTOF as

$$V_p(\tau) = \pi\left(r^2 - r_w^2\right)\phi h = \pi\alpha_D\phi h\left(\tau^2 - \tau_w^2\right) \tag{3.7}$$

where α_D , ϕ , and h are the uniform diffusivity, porosity and thickness of the homogeneous reservoir model, respectively. This $V_p(\tau)$ function can be non-negative only when $\tau \geq \tau_w$. The corresponding analytic DTOF derivative of the cumulative pore volume can then be formulated as

$$w(\tau) = 2\pi\alpha_D\phi h\tau \tag{3.8}$$

Analytic formulation of the cumulative pore volume using the DTOF is the key to ensuring accurate analysis of the pressure transient behavior near the well, especially within the well cell.

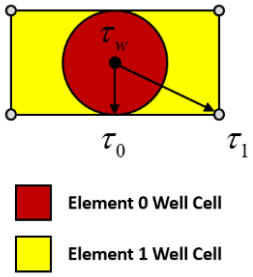

(a) Hybrid discretization within the well cell

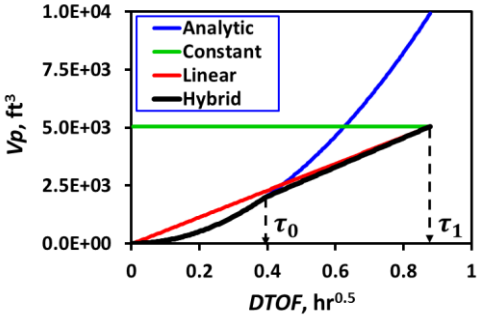

(b) $V_p(\tau)$ within the well cell

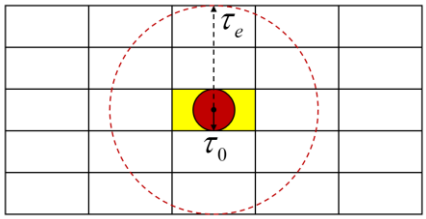

(c) DTOF (τ) calculation beyond the well cell

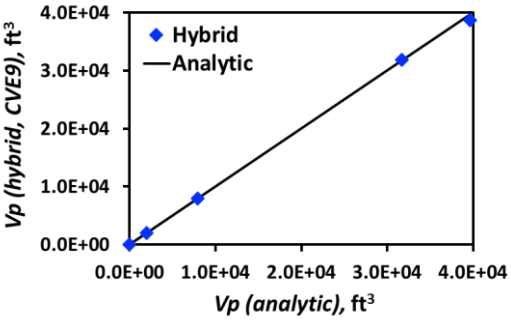

(d) $V_p(\tau)$ beyond the well cell

Figure 3.10 Hybrid cumulative pore volume as a function of the DTOF within the rectangular cells (with an aspect ratio of 2:1) for the 2D radial flow

Suppose there is a rectangular grid cell in a 2D reservoir model with a uniform thickness of h and a vertical well with an effective wellbore radius of r_w is located at the grid-cell center. From the wellbore radius to the nearest boundary of the rectangular well cell, it is easy to construct an inscribed annular cell, which has an inner radius equal to r_w

and an outer radius equal to one half of the width of the rectangular cell (the shorter length of the rectangular well cell), r_0.

$$r_0 = \frac{1}{2}\min(\Delta x_0, \Delta y_0) \tag{3.9}$$

where Δx_0 and Δy_0 represent the lengths of the rectangular well cell in the x and y directions, respectively. Using Eq.(3.6), the DTOF to the outer radius of the annular cell as well as the vertex of the rectangular well cell can be calculated as τ_0 and τ_1, respectively (Figure 3.10a).

$$\tau_0 = \frac{r_0}{\sqrt{\alpha_{D,0}}}, \quad \tau_1 = \frac{\sqrt{\Delta x_0^2 + \Delta y_0^2}}{2\sqrt{\alpha_{D,0}}} \tag{3.10}$$

where $\alpha_{D,0}$ is the diffusivity of the well cell. Then, the pore volume of the annular cell within the well cell can be calculated using Eq.(3.7) As

$$PV_0 = \pi\alpha_{D,0}\phi_0 h\left(\tau_0^2 - \tau_w^2\right) \tag{3.11}$$

where $\alpha_{D,0}$ and ϕ_0 are the diffusivity and porosity of the well cell, respectively. This annular cell can be defined as the Element 0 well cell (which is represented as the red-colored region in Figure 3.10a). The remaining region beyond the Element 0 well cell within the rectangular well cell can be defined as the Element 1 well cell (which is represented as the yellow-colored region in Figure 3.10a), which has a pore volume that can be calculated as

$$PV_1 = \left[\Delta x_0 \cdot \Delta y_0 - \pi\alpha_{D,0}\left(\tau_0^2 - \tau_w^2\right)\right]\phi_0 h \tag{3.12}$$

In general 3D reservoir models, if we use (i, j, k) to represent the grid-cell index, the grid-cell pore volume can be represented as PV_{ijk}. We can also represent the DTOF to the center of each grid cell as τ_{ijk}^{cell}. Meanwhile, the minimum and maximum DTOF (τ) values for each grid cell (which can be evaluated at the cell center, cell vertex, cell face center, or cell edge center) can be represented as $\tau_{ijk}^{\min}$ and $\tau_{ijk}^{\max}$, respectively. The grid-cell based τ_{ijk}^{cell}, $\tau_{ijk}^{\min}$, and $\tau_{ijk}^{\max}$ can be conveniently calculated using the fast marching method (FMM). If we only evaluate the DTOF to the center of each grid cell, a piecewise constant form of cumulative pore volume function can be constructed as

$$V_p(\tau) = \sum_{ijk} PV_{ijk} \cdot H\left(\tau - \tau_{ijk}^{cell}\right) \tag{3.13}$$

If we evaluate both the minimum and maximum DTOF values for each grid cell, we can generate a piecewise constant $w(\tau)$ function on each grid cell (i, j, k) as

$$w(\tau)_{ijk} = \frac{PV_{ijk}}{\tau_{ijk}^{\max} - \tau_{ijk}^{\min}} \tag{3.14}$$

Then, we are able to generate a piecewise linear form of the cumulative pore volume function as

$$V_p(\tau) = \sum_{ijk} PV_{ijk} \cdot Max\left(Min\left(1, \frac{\tau - \tau_{ijk}^{\min}}{\tau_{ijk}^{\max} - \tau_{ijk}^{\min}}\right), 0\right) \tag{3.15}$$

If a vertical well perforates a certain number of N orthogonal well cells, we can generate a hybrid version of the cumulative pore volume function in a complete form as

$$V_p(\tau) = \sum_{\substack{Perforated \\ ijk}} \left[\begin{array}{l} PV_{0,ijk} \cdot Min\left(1, \dfrac{\tau^2 - \tau_w^2}{\tau_{0,ijk}^2 - \tau_w^2}\right) \\ +PV_{1,ijk} \cdot Max\left(Min\left(1, \dfrac{\tau - \tau_{0,ijk}}{\tau_{1,ijk} - \tau_{0,ijk}}\right), 0\right) \end{array} \right] + \sum_{ijk} PV_{ijk} \cdot Max\left(Min\left(1, \frac{\tau - \tau_{ijk}^{\min}}{\tau_{ijk}^{\max} - \tau_{ijk}^{\min}}\right), 0\right) \tag{3.16}$$

Here, $PV_{0,ijk}$ and $PV_{1,ijk}$ represent the pore volume of the Element 0 and Element 1 well cells with index (i, j, k) where the vertical well perforates, respectively; PV_{ijk} represents the orthogonal non-well cells with index (i, j, k). Eq.(3.16) is a combination of Eq.(3.7) and Eq.(3.15), which indicates that this hybrid version of cumulative pore volume function utilizes the analytic solution within the Element 0 well cell and the piecewise linear solution beyond it.

The accuracy of the analytic (Eq.(3.7)), piecewise constant (Eq.(3.13)), piecewise linear (Eq.(3.15)), and hybrid (Eq.(3.16)) forms of cumulative pore volume construction can be compared and analyzed in the near-well region in the homogeneous reservoir model.

We first compare the different formulations of $V_p(\tau)$ within the rectangular well cell (with an aspect ratio of 2:1) with its analytic solution. It is easy to find that the piecewise constant form of $V_p(\tau)$ construction generates the most inaccurate solution when $\tau \le \tau_1$. Though being able to significantly improve the $V_p(\tau)$ construction within the well cell, the piecewise linear solution is still insufficiently accurate within the Element 0 well cell. By applying the hybrid construction of the $V_p(\tau)$ function, the cumulative

pore volume can match exactly with the analytic solution within the Element 0 well cell (Figure 3.10b). This precise solution to the cumulative pore volume within the Element 0 well cell is important for later pressure transient formulation as well as the one-dimensional diffusivity equation solution using the DTOF.

Then, we extend the hybrid formulation of the cumulative pore volume (Eq.(3.16)) to a larger near-well region (5x5 grids with a uniform aspect ratio of 2:1) and investigate the $V_p(\tau)$ function within an upper limit of the DTOF, τ_e, which signifies that the pressure front reaches the outer boundary of the region (Figure 3.10c).

$$\tau_e = \frac{5 \cdot \min(\Delta x, \Delta y)}{2\sqrt{\alpha_D}} \tag{3.17}$$

Here Δx and Δy represent the lengths of the uniform rectangular grid cell in the x and y directions, respectively. We use the 2D CVE9 FMM to solve the Eikonal equation and calculate the DTOF. The hybrid $V_p(\tau)$ solution can then be obtained based on the τ_w and τ_0 values as well as those τ_{ijk}^{cell} values less than τ_e. By comparing with the analytic solution, we find that the hybrid cumulative pore volume construction can help generate a sufficiently accurate $V_p(\tau)$ solution both within (Figure 3.10b) and beyond the rectangular well cell in the near-well region (Figure 3.10d).

Though the hybrid version of the cumulative pore volume proves to be able to significantly improve the solution accuracy in the near-well region, we still need to investigate the potential impact of the FMM-based DTOF calculation on the $V_p(\tau)$ function, especially in regions farther away from the wellbore. Since DTOF values within

the well cell (at the wellbore, cell center, cell vertex, or edge center) can be calculated analytically (Eq.(3.6)), the hybrid $V_p(\tau)$ construction (Eq.(3.16)) can be applied to all the five discretization schemes listed above (Figure 3.2). However, only cell-center DTOF values can be obtained for grid cells beyond the well cell if the 2D C5 discretization scheme is used for solving the Eikonal equation (Figure 3.2). So, we can modify Eq.(3.16) and apply the cell-center DTOF values for those non-well cells and formulate the hybrid cumulative pore volume function in a reduced form.

$$V_p(\tau) = \sum_{\substack{Perforated \\ ijk}} \left[\begin{array}{l} PV_{0,ijk} \cdot Min\left(1, \dfrac{\tau^2 - \tau_w^2}{\tau_{0,ijk}^2 - \tau_w^2}\right) \\ +PV_{1,ijk} \cdot Max\left(Min\left(1, \dfrac{\tau - \tau_{0,ijk}}{\tau_{1,ijk} - \tau_{0,ijk}}\right), 0\right) \end{array} \right] + \sum_{ijk} PV_{ijk} \cdot H\left(\tau - \tau_{ijk}^{cell}\right) \tag{3.18}$$

In this new formulation, the Element 0 and Element 1 well cells still rely on the minimum and maximum DTOF values evaluated on them to construct the cumulative pore volume; only cell-center DTOF values are calculated for the remaining orthogonal non-well cells.

We use Eq.(3.18) for subsequent reduced hybrid $V_p(\tau)$ construction based on all the five discretization schemes (C5, V5, V9, C5V9 and CVE9) for the Eikonal equation. For the 2D V5 and V9 FMMs, we evaluate the cell-center DTOF values (τ_{ijk}^{cell}) by taking the arithmetic average of the four vertex DTOF values of the cell. The $\tau_{0,ijk}$ values for all the five discretization schemes can be calculated analytically (Eq.(3.6)) within the well cell.

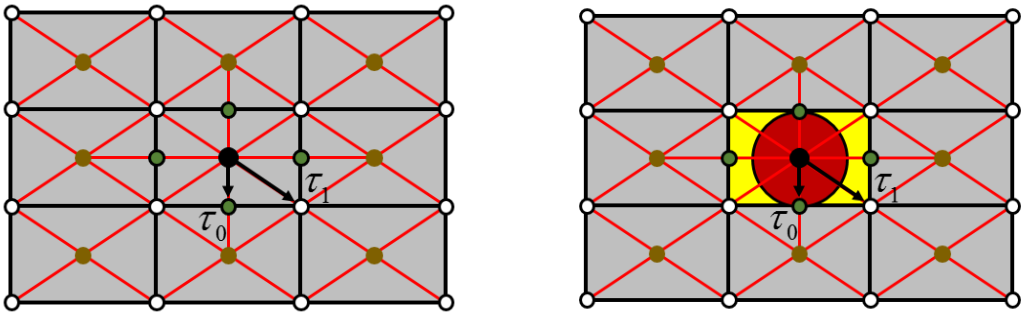

(a) LGR on well cell and its four adjacent cells within the C5V9 FMM

(b) Hybrid cumulative pore volume within the C5V9 (LGR) FMM

Figure 3.11 Extension of the C5V9 FMM by LGR on 2D uniform rectangular grid cells and the corresponding hybrid cumulative pore volume construction

Since the 2D C5V9 FMM shows to be able to generate DTOF values with almost the same accuracy compared with the 2D V9 FMM but with less computational cost required, we extend the investigation on the C5V9 discretization scheme for the Eikonal equation by applying a local grid refinement (LGR) to the well cell as well as its adjacent four cells. In particular, the DTOFs to the edge center of the well cell are calculated simultaneously with all other DTOF values evaluated at the cell center and cell vertex (Figure 3.11).

Thus, the hybrid of $V_p(\tau)$ function can be constructed in a reduced form (Eq.(3.18)) using DTOFs calculated from six FMMs (C5, V5, V9, C5V9, C5V9 (LGR), and CVE9). Using the same homogeneous and heterogeneous reservoir models (Figure 3.3) with the same input parameters (Table 3.2), we investigate the hybrid $V_p(\tau)$ function

within both the near-well region (5x5 uniform square grids) and the entire reservoir domain (199x199 uniform square grids).

In homogeneous media, the reference hybrid cumulative pore volume model is constructed based on the DTOF that is calculated by solving the Eikonal equation analytically. Analytic DTOF values are evaluated at the cell center, vertex and edge center of grid cells within the reservoir model. Only unique values of these DTOFs, which are first sorted in an ascending order, are kept as the DTOF samples to evaluate the hybrid cumulative pore volume (Eq.(3.16) and Eq.(3.18)). In heterogeneous media, the reference hybrid cumulative pore volume model is constructed based on the DTOF that is calculated from solving the Eikonal equation using the CVE9 FMM. In such a way, it can be guaranteed that the same DTOF input is used when comparing the cumulative pore volume constructed from different FMMs.

In both the homogeneous and heterogeneous media, we construct the hybrid cumulative pore volume model in the reduced and complete forms. Hybrid cumulative pore volume models constructed from FMMs under different discretization schemes are compared consistently with the corresponding reference model, either in the reduced or complete form. For the C5 FMM, only the hybrid cumulative pore volume model in the reduced form is investigated. For the remaining V5, V9, C5V9, CVE9 and C5V9 (LGR) FMMs, both the reduced and complete forms of the hybrid cumulative pore volume models are investigated (Figure 3.12).

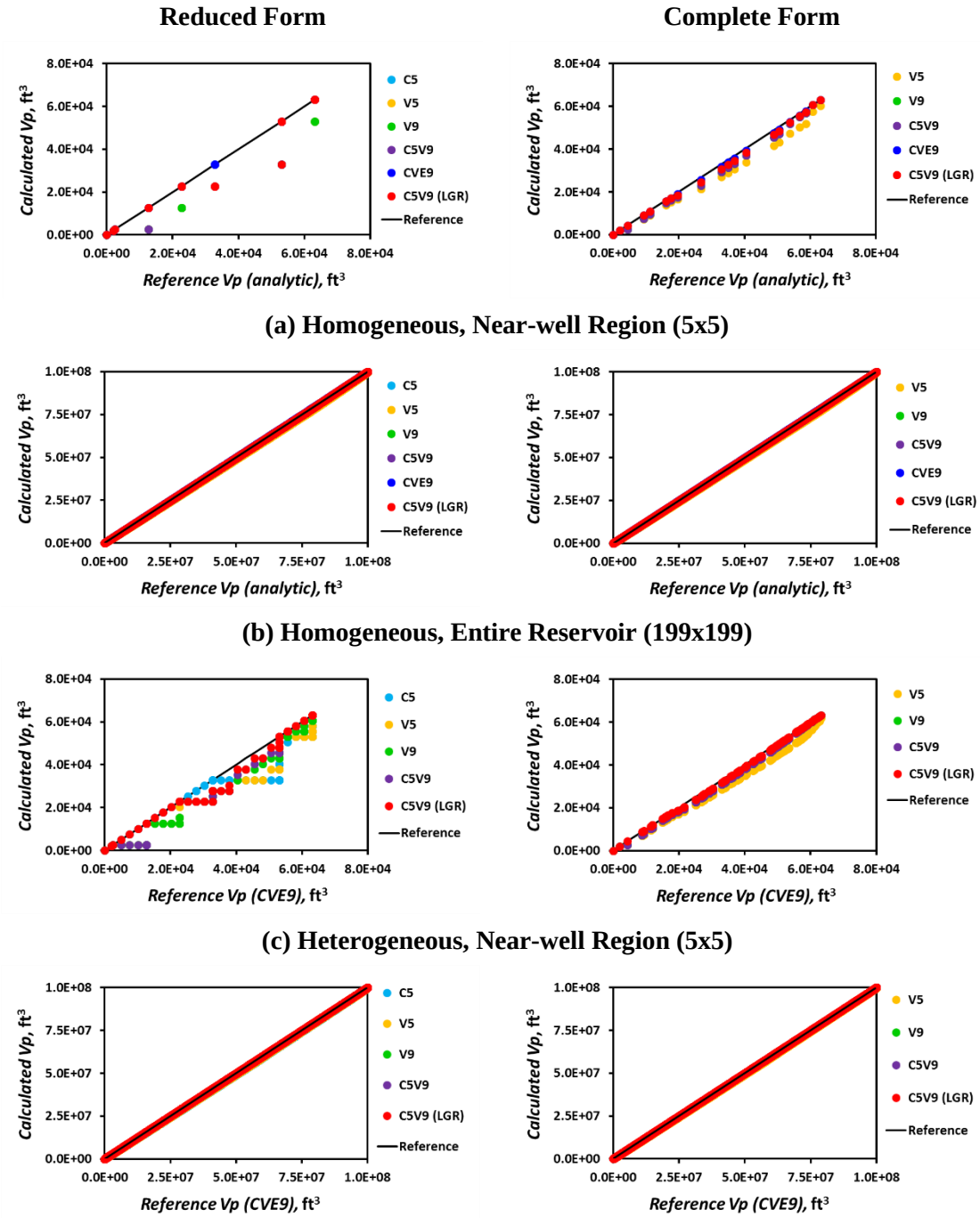

(a) Homogeneous, Near-well Region (5x5)

(b) Homogeneous, Entire Reservoir (199x199)

(c) Heterogeneous, Near-well Region (5x5)

(d) Heterogeneous, Entire Reservoir (199x199)

Figure 3.12 Hybrid cumulative pore volume calculated for a vertical well at the center of the homogeneous and heterogeneous reservoirs models using FMMs under different discretization schemes

From the near-well region (Figure 3.12a and c), we can observe that the reduced hybrid cumulative pore volume calculated from the FMMs under different discretization schemes are significantly smaller than the reference model. The complete hybrid cumulative pore volume function is more capable of capturing the pressure front propagation in the near-well region by taking the minimum and maximum grid-cell DTOF values to interpolate the sampling DTOFs. This provides important information for our later discretization of the one-dimensional diffusivity equation based on the DTOF calculated from the FMM and calibration of the well pressure or production response. Within the entire reservoir domain, both the reduced and complete forms of the hybrid cumulative pore volumes can generate solutions close to the reference model in both the homogeneous and the smooth heterogeneous models (Figure 3.12b and d).

Suppose there are a total number of N_τ sampling DTOF data used as independent input variables to evaluate the hybrid $V_p(\tau)$ function, which are the same for both the reference and the calculated functions. Similar to the RMSE analysis of the DTOF calculation, we can also define the RMSE of the calculated hybrid $V_p(\tau)$ function as

$$RMSE\left(V_p(\tau)_{cal}\right)=\sqrt{\frac{\sum_{j=1}^{N_\tau}\left(V_p(\tau_j)_{cal}-V_p(\tau_j)_{ref}\right)^2}{N_\tau}} \tag{3.19}$$

where $V_p(\tau_j)_{cal}$ and $V_p(\tau_j)_{ref}$ represent the hybrid $V_p(\tau)$ using grid-cell DTOFs (evaluated at the cell center, cell vertex or edge center) calculated from the different FMMs

and from the reference DTOFs (analytic in the homogeneous reservoir model), respectively, for a particular input DTOF value with index $j\ (j=1,2,\cdots,N_\tau)$.

If we only consider the 2D homogeneous square reservoir model, we can conduct a convergence rate analysis of the complete hybrid $V_p(\tau)$ function (Eq.(3.16)) calculated using the five different FMMs (V5, V9, C5V9, C5V9 with LGR and CVE9) (Figure 3.13).

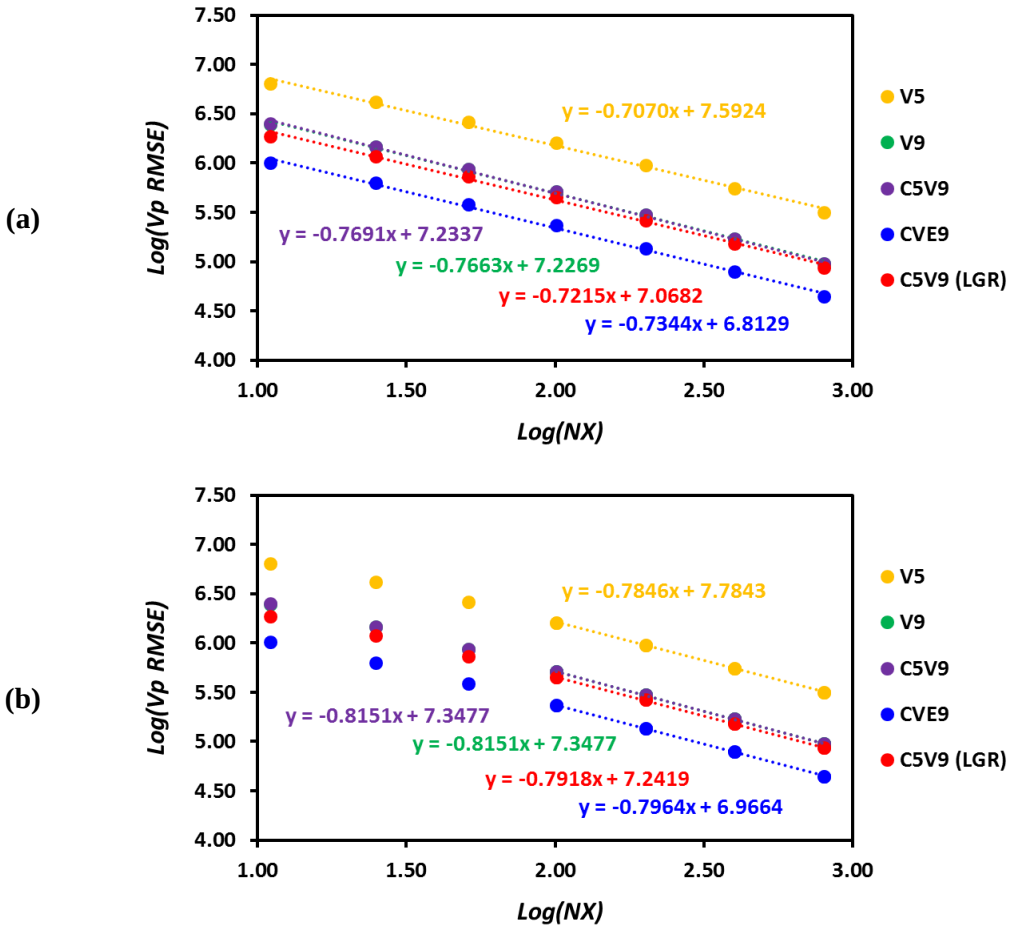

Figure 3.13 Convergence rate analysis of the hybrid cumulative pore volume as a function of the DTOF calculated from FMMs in the homogeneous reservoir model: (a) including coarse grids; (b) excluding coarse grids

In Figure 3.13, the 2D homogeneous reservoir model is discretized using different grid numbers ($NX = NY$ = 11, 25, 51, 101, 201, 801) with a fixed outer boundary length and width. We define the grids as coarse if the number of grid cells in the x and y directions is less than 100 ($NX = NY < 100$) and compare the convergence rates of the hybrid $V_p(\tau)$ function with (Figure 3.13a) and without (Figure 3.13b) the coarse grid refinement. As can be observed from Figure 3.13, the hybrid cumulative pore volume constructed based on DTOFs calculated using the V5 FMM generates the largest truncation errors compared with the analytic solution. The results generated from the V9, C5V9 and C5V9 (LGR) FMMs have significantly improved computational accuracy for the hybrid $V_p(\tau)$ function. The solution generated from the C5V9 FMM significantly overlaps the solution generated from the V9 FMM, especially when the reservoir model is discretized into fine grids (Figure 3.13b). The hybrid $V_p(\tau)$ function calculated from the C5V9 (LGR) FMM can slightly decrease the truncation error compared with the solutions generated from the V9 and C5V9 FMMs because of a more accurate calculation of the DTOF in the near-well region (Figure 3.11). The CVE9 FMM generates the hybrid $V_p(\tau)$ function with the least truncation error mainly because of the most accurate DTOFs used as the input variables. It is also worth noting that the convergence rates estimated for the hybrid $V_p(\tau)$ function using the five different FMMs when the coarse grids are included (Figure 3.13a) are quite close to those estimation when only the fine grids are used (Figure 3.13b).

Using the same reservoir model and grid discretization schemes, we also make the convergence rate analysis for the reduced hybrid $V_p(\tau)$ function (Eq.(3.18)) using the

RMSE estimation. The C5 FMM is added into the convergence rate estimation for the reduced $V_p(\tau)$ function since the cell-center DTOF values are mainly used (Figure 3.14).

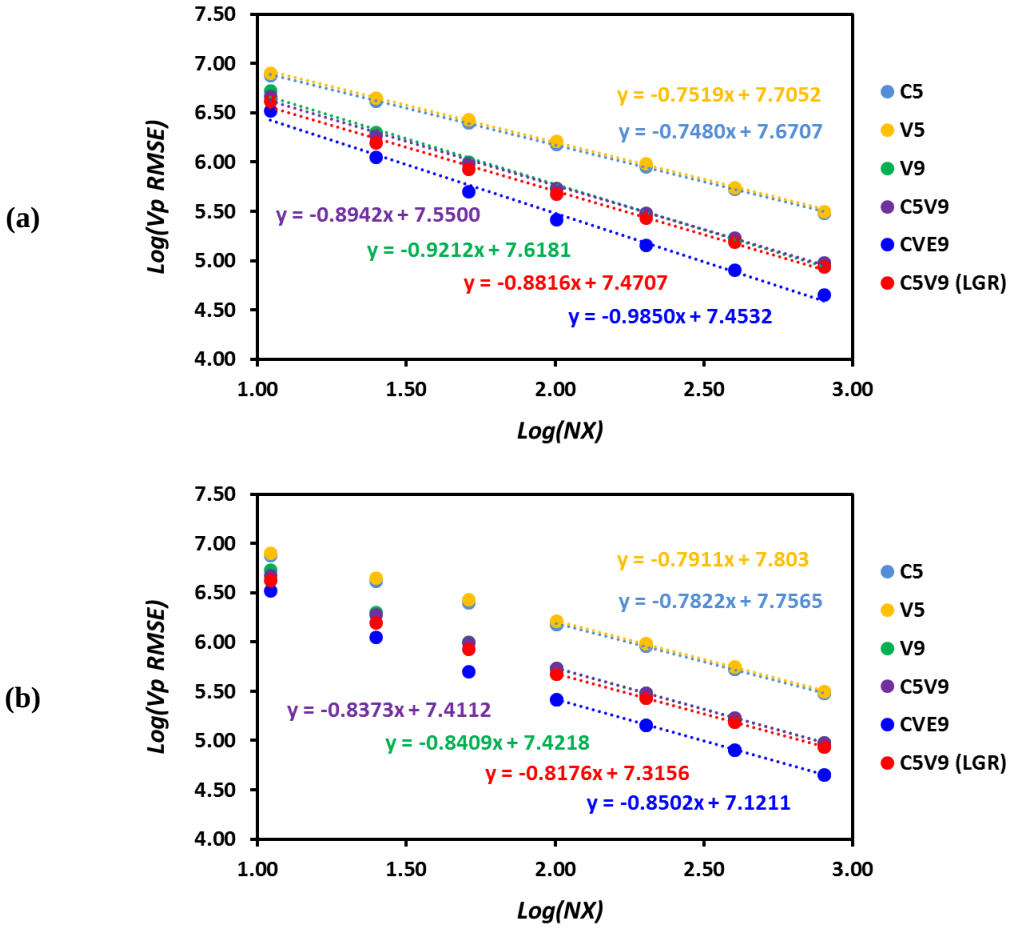

Figure 3.14 Convergence rate analysis of the reduced hybrid cumulative pore volume as a function of the DTOF calculated from FMMs in the homogeneous reservoir model: (a) including coarse grids; (b) excluding coarse grids

From Figure 3.14, we can observe that the C5 FMM generates the reduced hybrid $V_p(\tau)$ function with almost the same accuracy compared with that generated from the V5 FMM. Truncation errors of the reduced hybrid $V_p(\tau)$ functions generated from the C5 and V5 FMMs are significantly higher than those errors generated from the V9, C5V9, C5V9 (LGR) and CVE9 FMMs. Similar to the complete form (Figure 3.13), the reduced hybrid $V_p(\tau)$ function generated from the C5V9 FMM overlaps largely the solution generated from the V9 FMM. Using the C5 and V5 FMMs, the convergence rates of the reduced hybrid $V_p(\tau)$ function estimated when both the coarse and fine grids are included (Figure 3.14a) are slightly lower than the estimation from only fine grid refinements (Figure 3.14b). In contrast, the convergence rates estimated for the reduced hybrid $V_p(\tau)$ function by means of the remaining four FMMs when only fine grids are used are significantly lower than the convergence rates estimated when both coarse and fine grids are employed.

Using only the fine grid refinements, the truncation errors estimated from the hybrid $V_p(\tau)$ function (Figure 3.13b) and its reduced form (Figure 3.14b) are quite similar. This result indicates that the reduced hybrid $V_p(\tau)$ function will decrease the computational accuracy when the grid size is large but can be as accurate as its complete form when the resolution of the reservoir model is high.

Table 3.9 Numerical errors and convergence rate of the hybrid cumulative pore volume as a function of the DTOF calculated from FMMs in the 2D homogeneous reservoir model

Discretization Schemes (2D)	Correlation Coefficients		RMSE (ft^3)		Convergence Rate (Confidence Interval)
	(5x5)	(199x199)	(5x5)	(199x199)	
V5	0.882247	0.985469	4.8701E+3	9.6636E+5	0.7846 (0.7458, 0.8234)
V9	0.951925	0.996009	2.4417E+3	2.9985E+5	0.8151 (0.7887, 0.8416)
C5V9	0.951925	0.996009	2.4417E+3	2.9985E+5	0.8151 (0.7887, 0.8416)
C5V9 (LGR)	0.971002	0.996419	1.4312E+3	2.6655E+5	0.7918 (0.7566, 0.8271)
CVE9	0.982425	0.998123	8.1595E+2	1.3784E+5	0.7964 (0.7631, 0.8298)

Table 3.10 Numerical errors and convergence rates of the reduced hybrid cumulative pore volume as a function of the DTOF calculated from FMMs in the 2D homogeneous reservoir model

Discretization Schemes (2D)	Correlation Coefficients		RMSE (ft^3)		Convergence Rate (Confidence Interval)
	(5x5)	(199x199)	(5x5)	(199x199)	
C5	0.855438	0.986107	8.4509E+3	9.1641E+5	0.7822 (0.7491, 0.8152)
V5	0.817355	0.985389	9.8450E+3	9.7271E+5	0.7911 (0.7591, 0.8231)
V9	0.876423	0.995942	8.1435E+3	3.0692E+5	0.8409 (0.8322, 0.8496)
C5V9	0.929274	0.995958	6.7758E+3	3.0582E+5	0.8373 (0.8309, 0.8436)
C5V9 (LGR)	0.937046	0.996364	5.9757E+3	2.7279E+5	0.8176 (0.8113, 0.8239)
CVE9	0.967357	0.998067	4.5172E+3	1.4557E+5	0.8502 (0.8265, 0.8739)

In Table 3.9 and Table 3.10, we generated the correlation coefficients between the hybrid $V_p(\tau)$ function (in both the complete and reduced forms) and its analytic solution within the near-well region (5x5 grids) and the entire modeling domain (199x199) of the 2D homogeneous reservoir model. Estimated from only the fine grid refinements (Figure 3.13b and Figure 3.14b), the convergence rates of the hybrid $V_p(\tau)$ functions base on the RMSE analysis are also included in Table 3.9 and Table 3.10.

Following the same procedure, we calculated the hybrid cumulative pore volume function and its reduced form on the 2D heterogeneous reservoir model (Figure 3.3a). The hybrid $V_p(\tau)$ functions generated from the CVE9 FMM is used as the reference model to compare with solutions from other four FMMs (C5, V5, V9, C5V9, and C5V9 with LGR). The correlation coefficients between the calculated hybrid $V_p(\tau)$ functions using different FMMs and the reference model are listed in Table 3.11 and Table 3.12.

Table 3.11 Numerical errors of the hybrid cumulative pore volume as a function of the DTOF calculated from FMMs in the 2D heterogeneous reservoir model (VDP = 0.5573)

Discretization Schemes (2D)	Correlation Coefficients		RMSE (ft^3)	
	(5x5)	(199x199)	(5x5)	(199x199)
V5	0.907328	0.992053	4.2771E+3	5.4114E+5
V9	0.975410	0.998737	1.5281E+3	8.6825E+4
C5V9	0.975410	0.998737	1.5281E+3	8.6825E+4
C5V9 (LGR)	0.989352	0.998927	7.0601E+2	7.2683E+4

Table 3.12 Numerical errors of the reduced hybrid cumulative pore volume as a function of the DTOF calculated from FMMs in the 2D heterogeneous reservoir model (VDP = 0.5573)

Discretization Schemes (2D)	Correlation Coefficients		RMSE (ft^3)	
	(5x5)	(199x199)	(5x5)	(199x199)
C5	0.869905	0.990187	7.8272E+3	6.6082E+5
V5	0.876858	0.992089	7.3960E+3	5.3919E+5
V9	0.939947	0.998771	5.0874E+3	8.5599E+4
C5V9	0.977816	0.998762	4.0702E+3	8.6089E+4
C5V9 (LGR)	0.976744	0.998952	2.7954E+3	7.1964E+4

From the RMSE analysis results of the hybrid $V_p(\tau)$ functions listed in Table 3.11 and Table 3.12, we can see that the reduced hybrid cumulative function can be almost as accurate as its complete form if fine grid cells (199x199) are used to discretize the

smoothly varying heterogeneous reservoir model (VPD = 0.5573). This is consistent with previous RMSE analysis of the hybrid $V_p(\tau)$ functions in homogeneous media (Table 3.9 and Table 3.10).

Table 3.9 to Table 3.12 demonstrate that the reduced form of hybrid $V_p(\tau)$ might provide sufficient accuracy for the drainage volume calculation compared with the complete form, which will be validated later for pressure transient analysis. Meanwhile, the root-mean-square error (RMSE) analysis of the cumulative pore volume calculated shows that DTOFs generated from the C5V9 (LGR) FMM will lead to sufficiently accurate hybrid $V_p(\tau)$ solutions without adding much computational cost. Moreover, the convergence rate of the hybrid $V_p(\tau)$ function constructed from the C5V9 (LGR) FMM is closest to that generated from the CVE9 FMM (Table 3.9 and Table 3.10), which indicates that the DTOFs generated from C5V9 (LGR) discretization of the Eikonal equation is most accurate compared with the other four discretization schemes (C5, V5, V9 and C5V9).

Similar to analysis of the DTOF calculation, we test the hybrid $V_p(\tau)$ function within more heterogeneous media in the 1st layer and the 72nd layer within the SPE10 model (Figure 3.15). The DTOF samples are generated from the CVE9 FMM (which is also used to generate the reference model) for a fixed well location in the 2D SPE10 reservoir model.

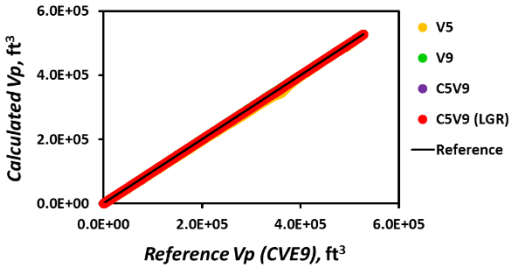

(a) Complete Form Layer 1, Well (40, 90)

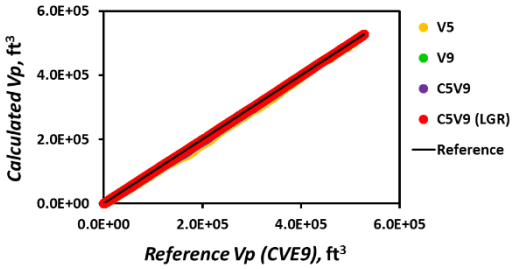

(b) Complete Form Layer 1, Well (25, 134)

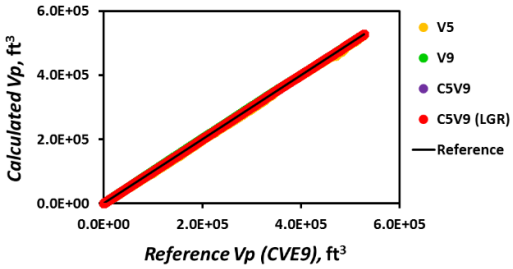

(c) Complete Form Layer 72, Well (33, 103)

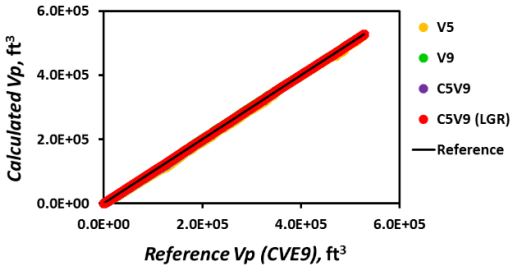

(d) Complete Form Layer 72, Well (42, 100)

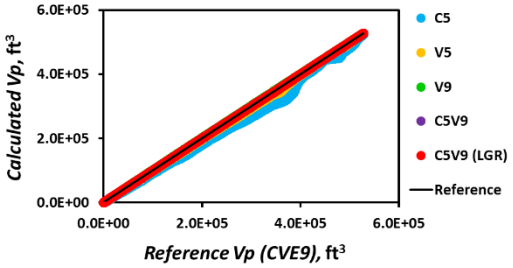

(e) Reduced Form Layer 1, Well (40, 90)

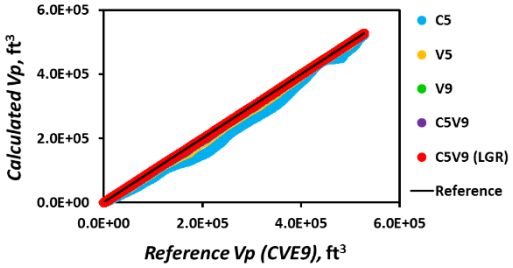

(f) Reduced Form Layer 1, Well (25, 134)

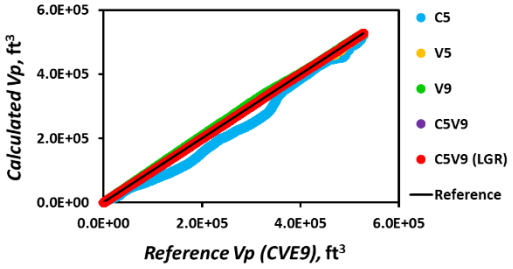

(g) Reduced Form Layer 72, Well (33, 103)

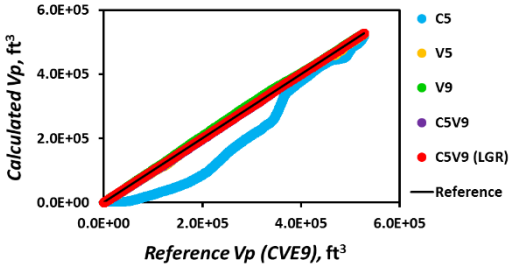

(h) Reduced Form Layer 72, Well (42, 100)

Figure 3.15 Hybrid cumulative pore volume as a function of the DTOF calculated for the 1st layer and 72nd layer within the SPE10 model using FMMs under different discretization schemes

If the hybrid cumulative pore volume function is calculated in the complete form (Figure 3.15a, b, c, and d), the $V_p(\tau)$ solutions generated from all four FMMs (V5, V9, C5V9 and C5V9 with LGR) are closely correlated with the reference model. The solution generated from the V5 FMM shows to be slightly smaller than the reference model at some grid cells of the highly heterogeneous reservoir, which is mainly due to the overestimation of the vertex DTOF values. The results are generalized in Table 3.13 and Table 3.14.

Table 3.13 Numerical errors of the hybrid cumulative pore volume calculated from the FMM in the 1st layer within the SPE10 model (VDP = 0.9191)

Discretization Schemes (2D)	Correlation Coefficients		RMSE (ft^3)	
	Well (40, 90)	Well (25, 134)	Well (40, 90)	Well (25, 134)
V5	0.989343	0.981577	4.6472E+3	8.5804E+3
V9	1.000581	0.995879	2.6041E+2	2.2704E+3
C5V9	0.999207	0.993800	4.5756E+2	3.0867E+3
C5V9 (LGR)	0.999425	0.998229	3.7374E+2	8.4986E+2

Table 3.14 Numerical errors of the hybrid cumulative pore volume calculated from the FMM in the 72nd layer within the SPE10 model (VDP = 0.9982)

Discretization Schemes (2D)	Correlation Coefficients		RMSE (ft^3)	
	Well (33, 103)	Well (42, 100)	Well (33, 103)	Well (42, 100)
V5	0.994607	0.989759	2.6276E+3	5.3532E+3
V9	1.003950	1.001835	1.8568E+3	1.2275E+3
C5V9	1.000788	0.998872	6.4712E+2	1.5542E+3
C5V9 (LGR)	1.000979	1.000807	6.5388E+2	6.6514E+2

If the hybrid cumulative pore volume function is calculated in the reduced form (Figure 3.15e, f, g and h), it is easy to discover an underestimated $V_p(\tau)$ using the C5 FMM. This is more obvious in the 72nd layer of the SPE10 model, where the permeability is more heterogeneous than the 1st layer, especially when the well is located at a low-permeability grid cell (Figure 3.15g and h). It is mainly due to an overestimation of the cell-center DTOF values using the C5 FMM, which proves once again inappropriate for description of the pressure propagation within highly heterogeneous media. All other discretization schemes show much better characterizations of the hybrid $V_p(\tau)$ function in the reduced form compared with the reference model CVE9 FMM. Particularly in the 72nd layer, the V5 and V9 FMMs used for DTOF calculation in the reduced form of the hybrid $V_p(\tau)$ construction show to overestimate the cumulative pore volume at some DTOF values compared with the reference model (Figure 3.15c and d). This indicates an underestimation of the DTOF values at some places in the reservoir model due to a lack of DTOF evaluation at the cell center using the V5 and V9 FMMs. This result is consistent with previous analysis from Figure 3.8 and Figure 3.9, which once again demonstrates the importance of the cell-center DTOF evaluation.

By comparing the correlation coefficients with the reference model and calculating the RMSE, it is easy to find that the C5V9 (LGR) scheme for DTOF calculation (Figure 3.11) generates the most accurate solution for the cumulative pore volume solution (Table 3.15 and Table 3.16).

Table 3.15 Numerical errors of the reduced hybrid cumulative pore volume calculated from the FMM in the 1st layer within the SPE10 model (VDP = 0.9191)

Discretization Schemes (2D)	Correlation Coefficients		RMSE (ft^3)	
	Well (40, 90)	Well (25, 134)	Well (40, 90)	Well (25, 134)
C5	0.937578	0.919439	2.2875E+4	3.1973E+4
V5	0.991900	0.984004	3.8288E+3	7.7145E+3
V9	1.003169	0.998326	1.1621E+3	1.4864E+3
C5V9	1.000109	0.994547	3.4966E+2	2.8440E+3
C5V9 (LGR)	1.000327	0.998974	3.3394E+2	6.5655E+2

Table 3.16 Numerical errors of the reduced hybrid cumulative pore volume calculated from the FMM in the 72nd layer within the SPE10 model (VDP = 0.9982)

Discretization Schemes (2D)	Correlation Coefficients		RMSE (ft^3)	
	Well (33, 103)	Well (42, 100)	Well (33, 103)	Well (42, 100)
C5	0.918605	0.847231	3.3417E+4	7.1534E+4
V5	1.007271	1.002245	4.2814E+3	3.7216E+3
V9	1.016738	1.014442	7.2361E+3	6.1561E+3
C5V9	1.001125	0.999225	9.3355E+2	1.7577E+3
C5V9 (LGR)	1.001314	1.001140	9.1900E+2	9.3492E+2

Table 3.13 to Table 3.16 show that the reduced hybrid $V_p(\tau)$ function is almost as accurate as its complete form for each of the FMMs compared in highly heterogeneous media. This is important information for later hybrid drainage volume as well as well test derivative construction using the DTOF. Because it provides the possibility to construct

the drainage volume forward model in a less complex form and makes the inversion computationally more efficient. On the other hand, the complete form of the hybrid $V_p(\tau)$ function provides a solid basis for later calculation of a piecewise constant DTOF derivative of the cumulative pore volume, which plays an important role in solving the DTOF-based one-dimensional diffusivity equation.

Above analysis demonstrates that the hybrid cumulative pore volume is significantly impacted by the accuracy of DTOFs calculated from the FMM. In this sense, selection of an appropriate discretization scheme for the Eikonal equation needs to meet the demand for computational accuracy and require a computational cost as low as possible. The C5V9 (LGR) FMM (Figure 3.11) proves to be an appropriate fit for the DTOF-based cumulative pore volume calculation.

From the RMSE of the calculated hybrid $V_p(\tau)$ function to the reference model as well as the correlation coefficients between them, it is easy to provide the subsequent observations along with the DTOF discretization analysis in this section.

- By applying the analytic solution to the drainage volume function within the well cell, the cumulative pore volume has a significantly improved solution when a hybrid version of the function is constructed, either in a complete form or a reduced form.
- In the homogeneous media, the 2D CVE9 FMM proves to be able to generate the most accurate $V_p(\tau)$ solution, which validates its candidacy as the reference FMM for $V_p(\tau)$ calculation in heterogeneous media.

- In both homogeneous and heterogeneous media, the 2D V9, C5V9 and C5V9 (LGR) discretization schemes show to generate more accurate DTOF values, which correspondingly give rise to more accurate cumulative pore volume solutions in the hybrid form than the 2D C5 and V5 discretization schemes for the Eikonal equation.
- Adding an additional degree of freedom of the DTOF at the cell center can not only help generate more accurate Eikonal solutions without much computational cost introduced, it will also lead to a more accurate construction of the cumulative pore volume. This is especially important for heterogeneous reservoir models that have regions with very low permeability values.
- The 2D C5V9 (LGR) scheme shows to be an ideal candidate for both the DTOF calculation and the hybrid cumulative pore volume construction.

3.2.3 Extension to the Fast Marching Method

Accurate DTOF solutions will definitely help generate accurate drainage volume solutions (Eq.(3.5)). After analysis of cumulative pore volume calculation using the DTOF from different FMMs, it is easily to find that the numerical DTOF solution will lose accuracy if DTOFs are evaluated merely in the X (or I) and Y (or J) directions in the Cartesian coordinate (Figure 3.16a). However, the accuracy of the solution to the Eikonal equation can be significantly improved if the DTOF can also be updated in the XY (or IJ) direction (Figure 3.16b).

(a) 5 Stencil (4 Quadrants) **(b) 9 Stencil (8 Octants)**

Figure 3.16 Illustration of the DTOF calculation using the 2D FMM with different discretization orientations

If we analyze the computational accuracy as well as the computational cost for each FMM discretization in both the homogeneous and heterogeneous media, the 2D V9, C5V9 and CVE9 FMMs prove to be better algorithms compared with the 2D C5 and V5 FMMs (Table 3.3 and Table 3.4) among the five discretization schemes for the Eikonal equation listed before (Figure 3.2). Because each unknown DTOF value will be updated by 8 octants around it, the CVE9 FMM provides the most accurate DTOF solution to the Eikonal equation. Meanwhile, it also requires the most computational efforts among all the five schemes. The V9 scheme can also provide an accurate DTOF solution because each unknown at the cell vertex will also be updated by 8 surrounding octants. However, it lacks the capability of describing pressure front propagation within low-permeability cells due to its lack of the cell-center DTOF value. The C5V9 FMM can meet the requirement of both computational accuracy and efficiency, with vertex DTOF values providing most accurate Eikonal solutions and cell-center DTOF values “capturing” the pressure propagation across the grid cell it occupies.

Since the accuracy of the DTOF solution within the near-well region plays a significant role in ensuring that the pressure (drop) gradient can be approximated by the DTOF gradient, which the asymptotic pressure approximation relies heavily upon, the C5V9 FMM is extended to a modified version. Within the modification, the DTOF to the edge center of the well cell is also evaluated (C5V9 discretization with LGR) and is updated simultaneously with all other DTOF values within the FMM algorithm (Figure 3.11). By such a slight modification of the C5V9 discretization of the Eikonal equation, the accuracy of DTOFs to centers of the four cells adjacent to the well cell can be significantly improved without much computational cost added. This makes sure that the pressure front within the near-well region can propagate along the shortest path, which will have a great impact on the next-step DTOF-based pressure transient calculation. Thus, the C5V9 (LGR) FMM is selected in the following sections to calculate the DTOF, which is used for validation of the asymptotic pressure approximation. This C5V9 (LGR) FMM will also contribute to a more accurate construction of the DTOF derivative of the cumulative pore volume, by means of which the transient flow simulation based on the inter-cell transmissibility between the "τ-contours" generated from the FMM calculated DTOF can be realized.

3.3 Flow Simulation

In above discussion on cumulative pore volume discretization, we compared the analytic form, piecewise linear form and piecewise constant form of $V_p(\tau)$ using the DTOF. The hybrid version of the $V_p(\tau)$ construction, which combines the three forms of

the formulation, proves to be able to generate much more accurate solutions. In this section, we start with the construction of the $w(\tau)$ variable, which is defined as the DTOF derivative of the cumulative pore volume. It is calculated based on the hybrid the $V_p(\tau)$ function discussed before and included into the pressure transient simulation by means of the drainage volume formulation (Eq.(3.5)). The impact of $V_p(\tau)$ calculation on transient flow simulation using the DTOF will be analyzed in more detail.

3.3.1 $V_p(\tau)$ and $w(\tau)$

The asymptotic pressure approximation relies upon an accurate characterization of the drainage volume $V(t)$, which can be used to represent the pressure transient and is greatly influenced by calculation of the $w(\tau)$ variable (Eq.(3.5)). By definition, the $w(\tau)$ variable is the derivative of the cumulative pore volume $V_p(\tau)$ with respect to the DTOF.

$$w(\tau) = \frac{dV_p(\tau)}{d\tau} \tag{3.20}$$

Its numerical solution relies upon the DTOF (τ) values calculated from solving the Eikonal equation and the construction of the cumulative pore volume within the "τ-contour". Similar to the permeability and porosity values of orthogonal grid cells within the Cartesian coordinate, the $w(\tau)$ function can be used to reflect the heterogeneity of the reservoir media. It also plays a pivotal role in pressure transient formulation in terms of the DTOF and transient flow simulation based on the inter-cell transmissibility constructed within the τ-intervals.

For a 2D homogenous field with one single well located at the center of the square reservoir model, it is easy to generate the DTOF distribution by solving the Eikonal equation analytically (Figure 3.3b). The $w(\tau)$ function increases linearly with the DTOF before the pressure front reaches the outer boundary of the reservoir model and begins to decrease sharply afterwards (Figure 3.17a).

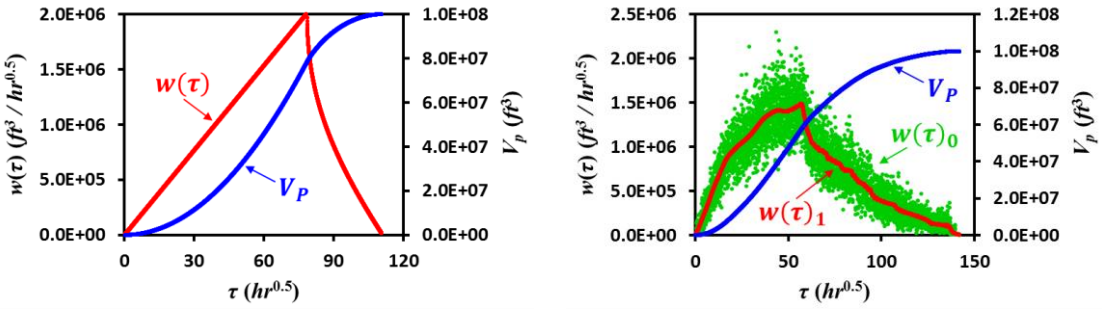

(a) Homogeneous media **(b) Heterogeneous media**

Figure 3.17 Cumulative pore volume and its DTOF derivative for the 2D square reservoir model (199x199) with a vertical well located at Cell (100, 100)

Since the "τ-contour" for infinite-acting flow in heterogeneous media appears near-circular in shape (Figure 3.3c), it is intuitively reasonable to analyze the distribution of $w(\tau)$ by means of a local differentiation of the cumulative pore volume, $V_p(\tau)$, with respect to the corresponding DTOF series. However, it is hard to obtain a straightforward relationship between the DTOF and $w(\tau)$ because the data are not locally smooth. A smoothing technique has been used to process the raw data sets of DTOFs against the $w(\tau)$ generated from the FMM calculation (Zhang et al., 2016). The bandwidth of the

smoother can be tuned to the DTOF value in order to maximize the signal and reduce the noise of calculation (Figure 3.17b). Though straightforward, the smoothing procedure for the $w(\tau)$ calculation could be time-consuming by trial and error and might not provide a stable solution.

Given these concerns on stability and efficiency of $w(\tau)$ construction from the smoothing technique, we designed an alternative strategy for generation of the $w(\tau)$ function. This new approach is based upon the hybrid $V_p(\tau)$ construction in the complete form (Eq.(3.16)). A limited number of τ-intervals independent of the DTOFs calculated from the FMM could be created. They may range from the effective wellbore radius location (where the DTOF value is τ_w as calculated from Eq.(3.10)) to the maximum DTOF value calculated from the FMM for the entire reservoir model (which is usually located at the outer boundary of the reservoir). After that, we can calculate the cumulative pore volume within each of those τ-contours by a linear interpolation of the minimum and maximum grid-cell DTOFs generated from the FMM. Finally, the $w(\tau)$ function can be created by taking an average of the incremental $V_p(\tau)$ values over each τ-interval.

Suppose there are a total number of N τ-intervals ($i = 0,1,\cdots,N-1$) used to generate the hybrid $V_p(\tau)$ function in the complete form (Eq.(3.16)). Then the $w(\tau)$ within a specific τ-interval can be calculated in a piecewise constant form as

$$w_i = \frac{\Delta V_{p,i}}{\Delta \tau_i}, \quad i = 0,1,\cdots,N-1 \tag{3.21}$$

where $\Delta V_{p,i}$ and $\Delta \tau_i$ are the incremental pore volume and the incremental DTOF of the *i*-th τ-interval, respectively. The first τ-interval can be designed to range from τ_w to τ_0 (Figure 3.10a and Figure 3.11b), which corresponds to the Element 0 well cell introduced previously in Section 3.2 (which has a pore volume and DTOF derivative that can be calculated using Eq.(3.11) and Eq.(3.21), respectively).

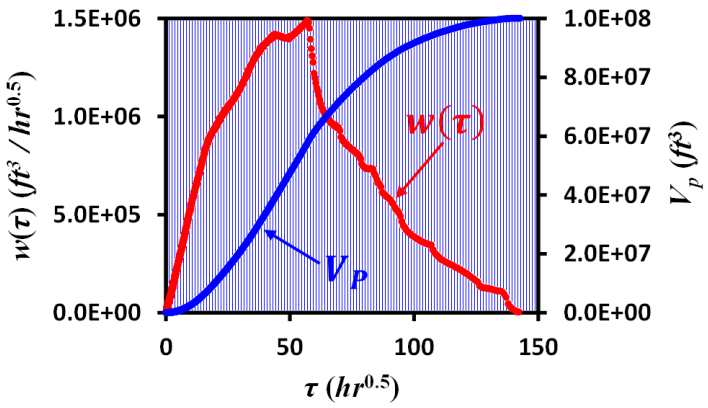

Figure 3.18 Illustration of w(τ) generated from the hybrid $V_p(\tau)$ function constructed using the C5V9 (LGR) FMM within τ-intervals for a 2D heterogeneous reservoir model (199x199) with a vertical well located at Cell (100, 100)

This leads to a $w(\tau)$ function close to the results from the smoothing technique in both homogeneous and heterogeneous media (Figure 3.18). Particularly, the fixed DTOF width of the first τ-interval will help generate a stable well pressure/flux profile after solving the DTOF-based one-dimensional diffusivity equation that will be discussed later. Since the pressure drop in the near-well region has a gradient higher than regions far away,

it is reasonable to generate logarithmically distributed τ-intervals. Thus, the τ-intervals near the well have smaller DTOF widths compared with others. This new method for $w(\tau)$ construction help us generate a solution similar in shape to that generated from the smoothing technique (Figure 3.17), but with an improved stability (Figure 3.18).

From Figure 3.19 to Figure 3.24, we applied this new methodology for $w(\tau)$ function generation to the 2D synthetic models (Figure 3.3) as well as the 1st and 72nd layers of the SPE10 reservoir model (Figure 3.6). Within each of the two layers of the SPE10 model, two models are set up corresponding to two different well placements. In both the synthetic models and the 2D SPE10 models, $w(\tau)$ functions generated from this new method are stable and provide a solid basis for subsequent transient flow simulation. Because of the logarithmically distributed τ-intervals created, the $w(\tau)$ function generated from local differentiation of the hybrid $V_p(\tau)$ function can be stable even with a limited number of τ-intervals.

According to the theory of the asymptotic pressure approximation, an increasing $w(\tau)$ function represents an outward propagation of the pressure front from the production well without much hindrance. In contrast, the decreasing $w(\tau)$ function represents the local "reflection" of the pressure front due to the high contrast porous media or the reservoir boundary (King et al., 2016; Wang et al., 2017).

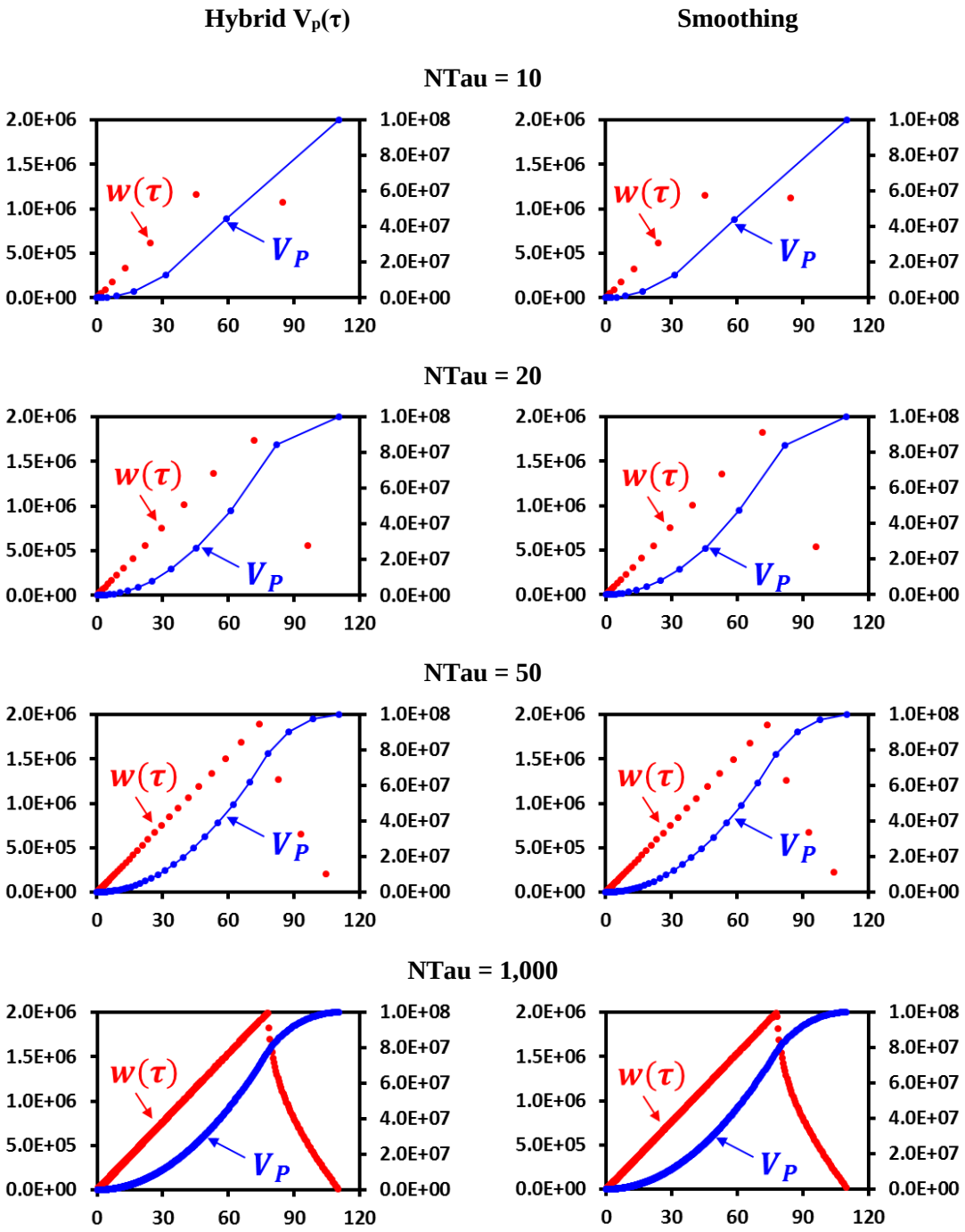

Figure 3.19 w(τ) functions constructed from the hybrid cumulative pore volume and the smoothing technique within the logarithmically distributed τ-intervals of the homogeneous reservoir model (199x199, Well (100, 100))

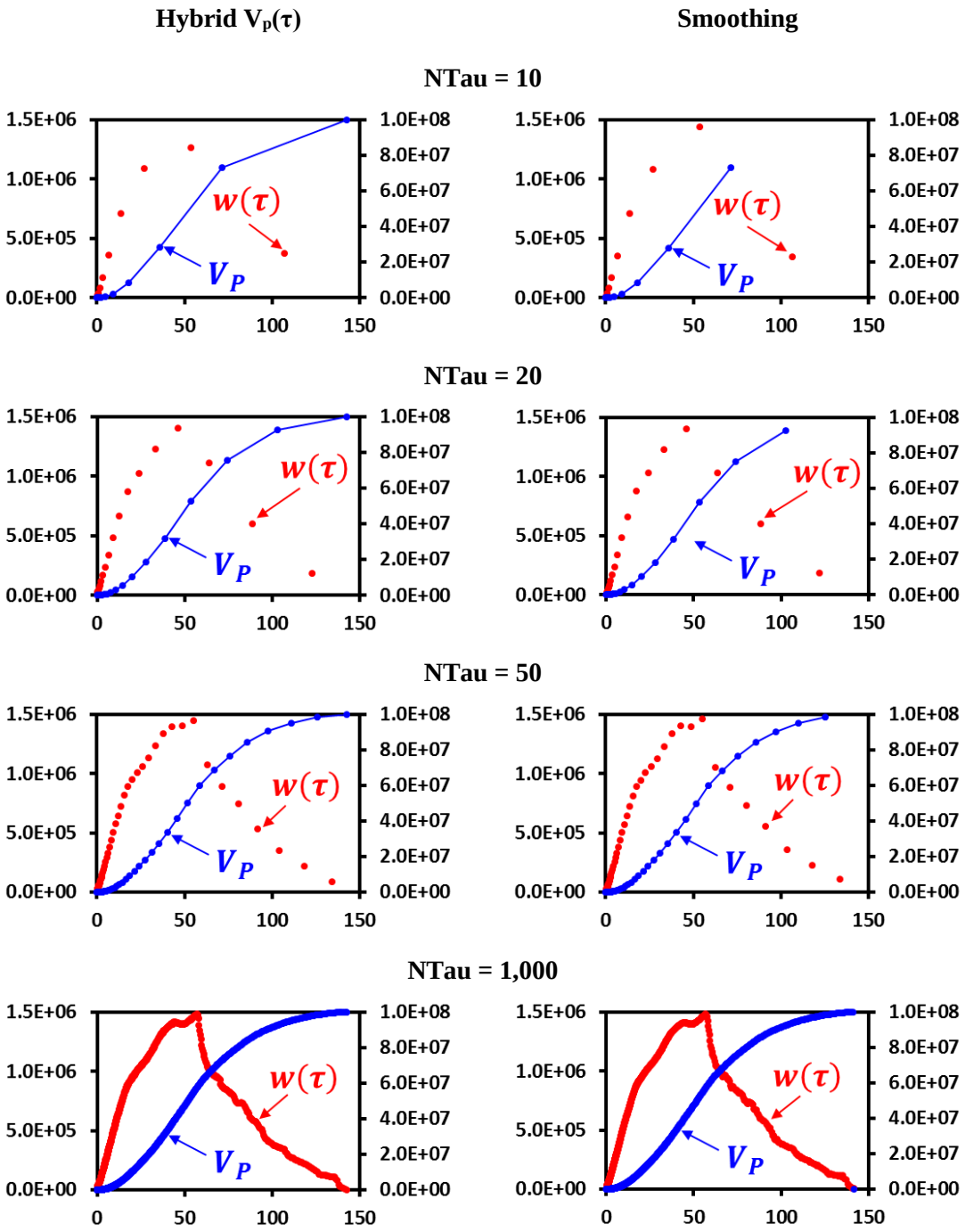

Figure 3.20 w(τ) functions constructed from the hybrid cumulative pore volume and the smoothing technique within the logarithmically distributed τ-intervals of the heterogeneous reservoir model (199x199, Well (100, 100))

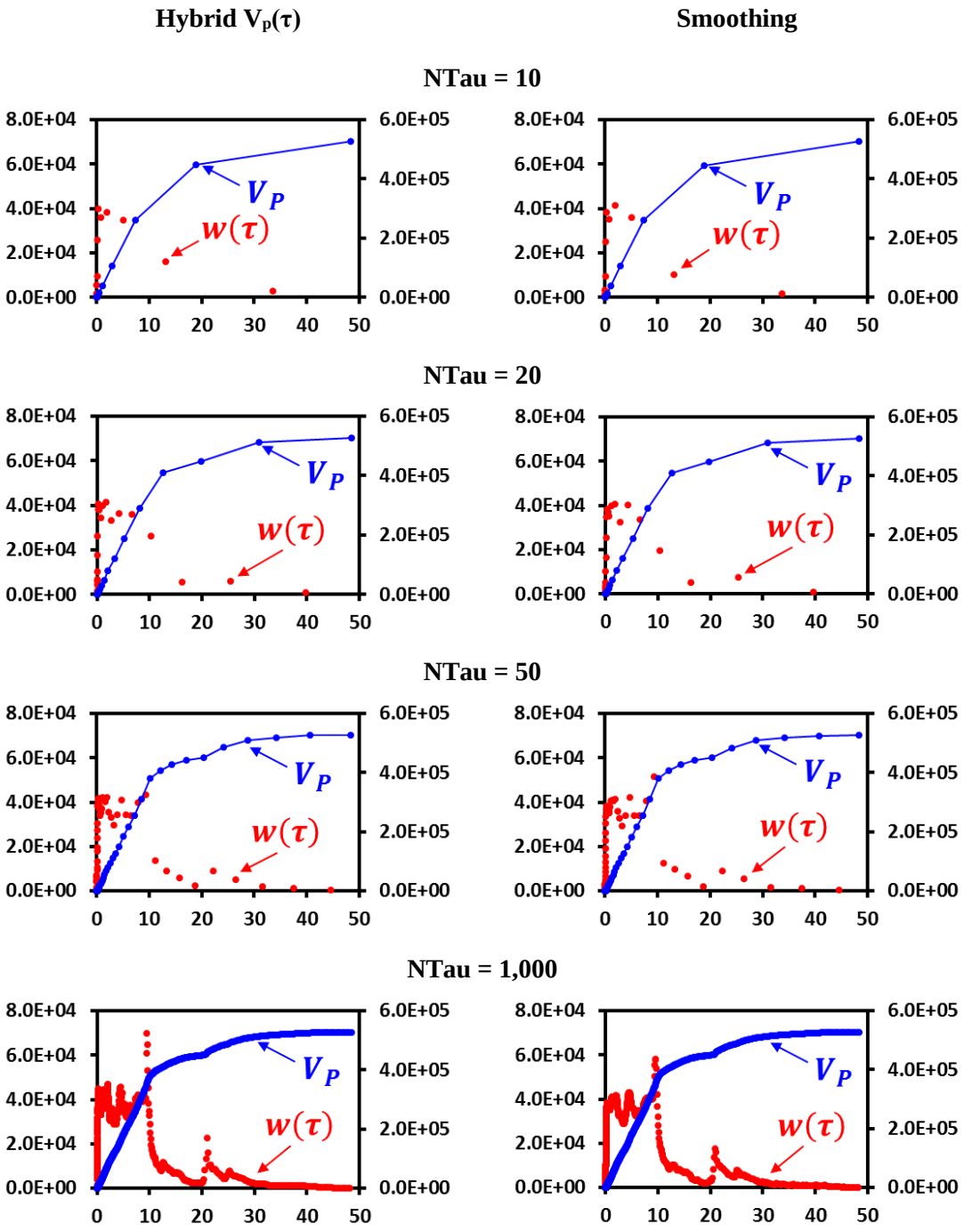

Figure 3.21 w(τ) functions constructed from the hybrid cumulative pore volume and the smoothing technique within the logarithmically distributed τ-intervals of the 1st layer within the SPE10 model (Well (40, 90))

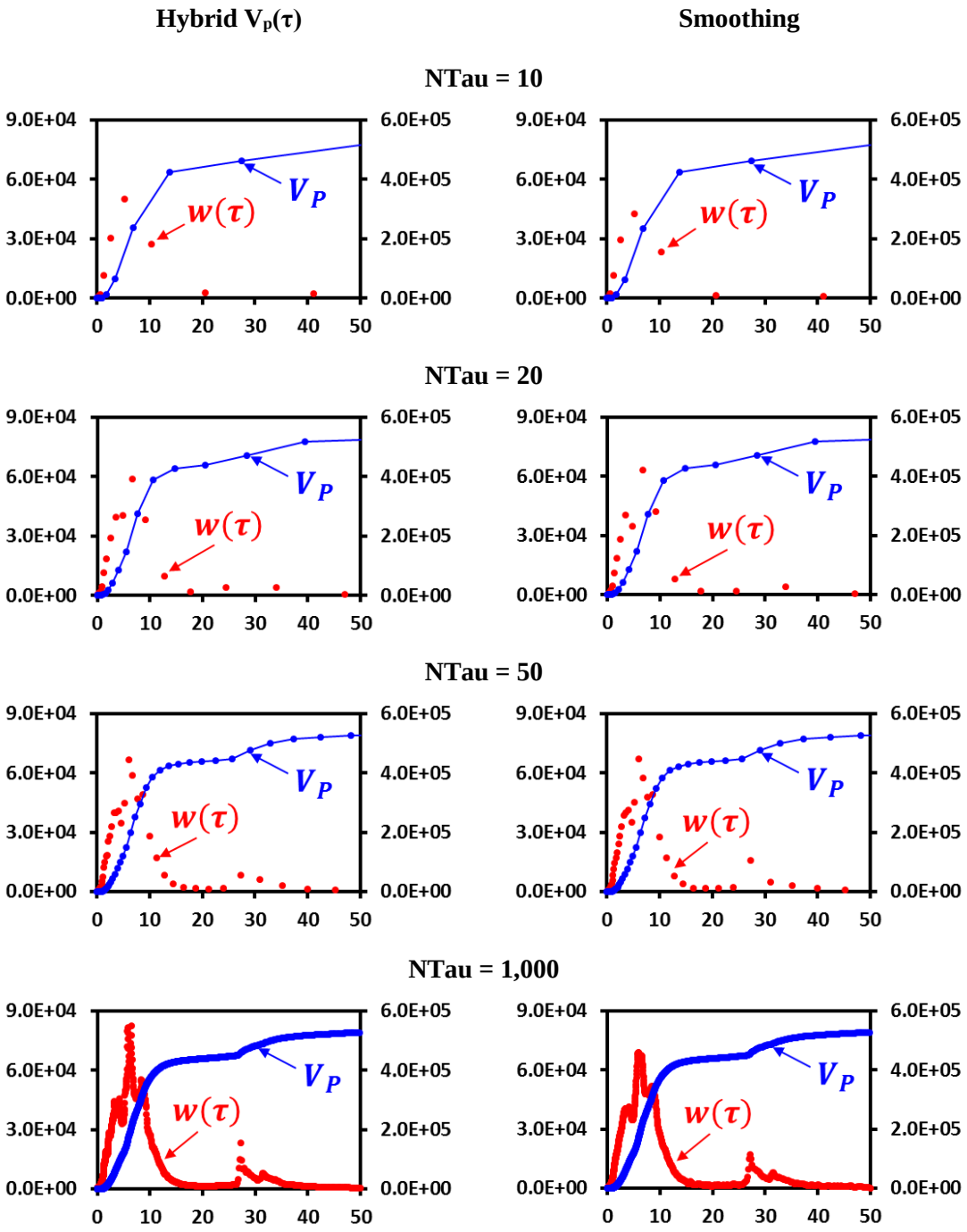

Figure 3.22 w(τ) functions constructed from the hybrid cumulative pore volume and the smoothing technique within the logarithmically distributed τ-intervals of the 1st layer within the SPE10 model (Well (25, 134))

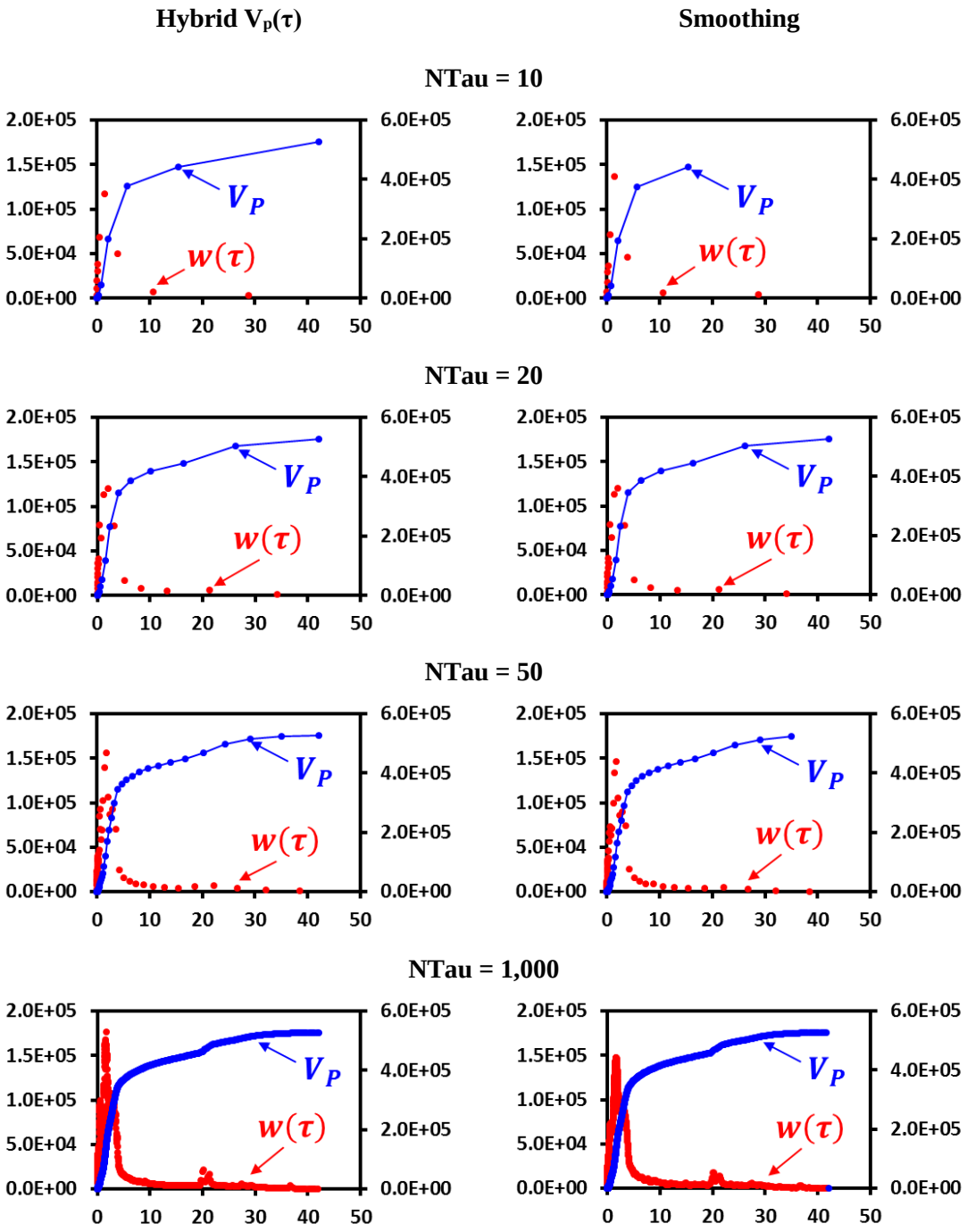

Figure 3.23 w(τ) functions constructed from the hybrid cumulative pore volume and the smoothing technique within the logarithmically distributed τ-intervals of the 72nd layer within the SPE10 model (Well (33, 103))

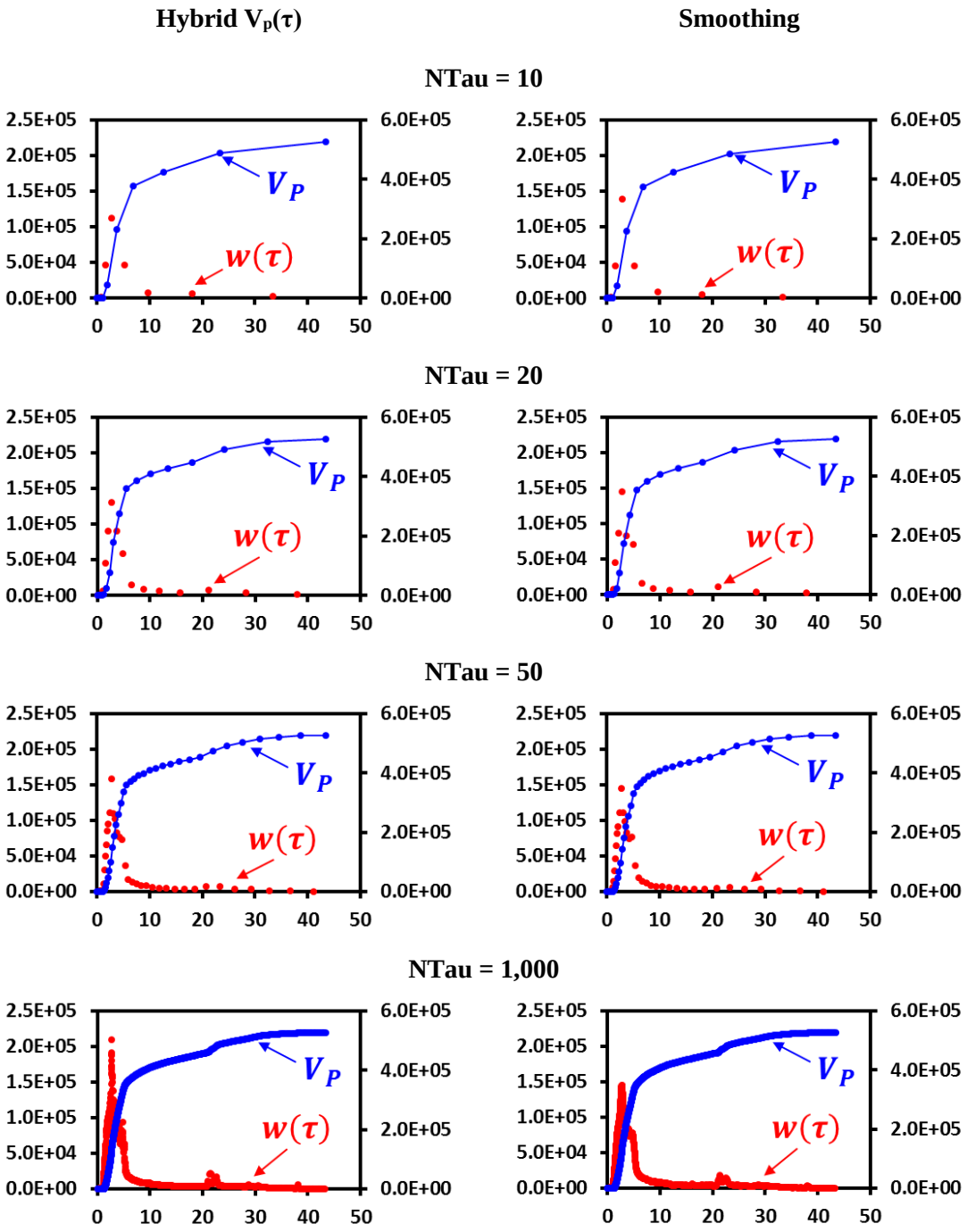

Figure 3.24 w(τ) functions constructed from the hybrid cumulative pore volume and the smoothing technique within the logarithmically distributed τ-intervals of the 72nd layer within the SPE10 model (Well (42, 100))

In the homogeneous and smoothly varying heterogeneous porous media, the $w(\tau)$ function decreases mainly when the pressure front arrives at the no-flow boundary of the reservoir model (Figure 3.19 and Figure 3.20). However, multiple decreasing trends of the $w(\tau)$ function can be observed in the 2D SPE10 model, which represent multiple reflections of the pressure front within the highly heterogeneous porous media before it reaches the outer boundary (Figure 3.21 to Figure 3.24).

After comparing the $w(\tau)$ function generated from the smoothing technique and that generated from direct local differentiation of the hybrid $V_p(\tau)$ function in the complete form (Eq.(3.16)), we can observe that the second method for $w(\tau)$ generation we propose can better keep all signatures of reservoir heterogeneity, especially for highly heterogeneous media (Figure 3.21 to Figure 3.24). This new method for $w(\tau)$ function generation does not introduce any unsatisfactory under-smoothing or over-smoothing artifacts, which is particularly important for near-well pressure transient analysis.

3.3.2 Pressure Transient Simulation: V(t)

Analysis of the analytic, first-order and zero-order volumetric elements for the cumulative pore volume as a function of the DTOF provides useful insights into designing discretization schemes for drainage volume evolution with time, especially at the near-well region. The hybrid construction of $V_p(\tau)$ function indicates that formulation of the

pressure transient might also need a combination of the analytic solution in the near-well region and numerical solution at other locations.

For the 2D infinite-acting radial flow (IARF) in homogeneous and isotropic media, the drainage volume increases linearly as a function of time.

$$V(t) = 4\pi\alpha_D \phi h t \tag{3.22}$$

Since the minimum and maximum grid-cell DTOF values can be easily calculated by solving the Eikonal equation using the C5V9 (LGR) FMM, a piecewise linear form of drainage volume as a function of time can be formulated when the piecewise constant $w(\tau)$ evaluated on each grid cell is substituted into the integral form of the drainage volume (Eq.(3.5)).

$$V(t) = \sqrt{\pi t} \sum_{ijk} \left(\frac{PV_{ijk}}{\tau_{ijk}^{\max} - \tau_{ijk}^{\min}} \right) \cdot \left(erf\left(\frac{\tau_{ijk}^{\max}}{2\sqrt{t}} \right) - erf\left(\frac{\tau_{ijk}^{\min}}{2\sqrt{t}} \right) \right) \tag{3.23}$$

Correspondingly, a piecewise constant form of drainage volume as a function of time can be formulated when only DTOFs to the grid-cell centers are used for pressure transient formulation.

$$V(t) = \sum_{ijk} PV_{ijk} \cdot e^{-\left(\tau_{ijk}^{cell}\right)^2 / 4t} \tag{3.24}$$

The analytic, piecewise linear and piecewise constant formulations of the drainage volume provide the basis for the hybrid formulation of the pressure transient, which is expected to better represent the pressure propagation as a function of time, especially in the near-well region.

Within the well cell, $V(t)$ can be represented by a combination of the analytic (Eq.(3.22)) and piecewise linear forms of the drainage volume (Eq.(3.23)). Beyond the well cell, $V(t)$ can be calculated by summing up all the individual integral values evaluated on each orthogonal grid cell, either in a piecewise linear (Eq.(3.23)) or a piecewise constant form (Eq.(3.24)).

In a 3D reservoir model that consists of orthogonal grid cells, the construction of a hybrid version of $V(t)$ can be achieved in the following procedure.

- When $0 \le \tau \le \tau_0$, the drainage volume can be formulated as

$$V_0(t) = \int_0^{\tau_0} d\tau \cdot w(\tau) \cdot e^{-\tau^2/4t} = \sum_{ijk} 4\pi\phi_{0,ijk}\alpha_{D0,ijk} DZ_{ijk} \cdot t \cdot \left(1 - e^{-\tau_{0,ijk}^2/4t}\right) \qquad (3.25)$$

  where DZ_{ijk} represents the height of a particular orthogonal well cell. This first part of drainage volume formulation corresponds to the Element 0 well cell mentioned before.

- When $\tau_0 \le \tau \le \tau_1$, the drainage volume can be evaluated on the Element 1 well cell beyond the annular Element 0 well cell, which can be calculated in a piecewise linear form.

$$\begin{aligned} V_1(t) &= \int_{\tau_0}^{\tau_1} dV_p(\tau) \cdot e^{-\tau^2/4t} \\ &= \sum_{ijk} \left(\frac{PV_{1,ijk}}{\tau_{1,ijk} - \tau_{0,ijk}} \right) \cdot \sqrt{\pi t} \cdot \left(erf\left(\frac{\tau_{1,ijk}}{2\sqrt{t}} \right) - erf\left(\frac{\tau_{0,ijk}}{2\sqrt{t}} \right) \right) \end{aligned} \qquad (3.26)$$

- For the remaining non-well cells, the drainage volume can be calculated either in a piecewise linear form (Eq.(3.23)), which can be represented as

$$V_2(t) = \sqrt{\pi t} \sum_{ijk} \left(\frac{PV_{ijk}}{\tau_{ijk}^{\max} - \tau_{ijk}^{\min}} \right) \cdot \left(erf\left(\frac{\tau_{ijk}^{\max}}{2\sqrt{t}} \right) - erf\left(\frac{\tau_{ijk}^{\min}}{2\sqrt{t}} \right) \right) \tag{3.27}$$

or in a piecewise constant form (Eq.), which can be represented as

$$V_2(t) = \sum_{ijk} PV_{ijk} \cdot e^{-\left(\tau_{ijk}^{cell}\right)^2 / 4t} \tag{3.28}$$

This piecewise constant formulation of the drainage volume within the non-well cells leads to a much simpler computation of the pressure transient model using the DTOF.

- Then the hybrid version of drainage volume can be obtained by combining the three parts together.

$$V(t) = V_0(t) + V_1(t) + V_2(t) \tag{3.29}$$

If the third part of the hybrid drainage volume, $V_2(t)$, is calculated in a piecewise linear form (Eq.(3.27)), the hybrid drainage volume is constructed in a complete form. Otherwise, the hybrid drainage volume is constructed in a reduced form if $V_2(t)$ is calculated in a piecewise constant form (Eq.(3.28)). This corresponds well with the hybrid construction of the cumulative pore volume function, $V_p(\tau)$. The hybrid formulation of drainage volume as a function of time is expected to generate a more accurate pressure transient formulation, especially in the near-well region.

For the infinite-acting flow around the vertical well with a constant production rate, q_w, the asymptotic pressure approximation can be formulated using the DTOF calculated from the FMM and the drainage volume constructed.

$$c_t \frac{\partial p}{\partial t} = \frac{1}{w(\tau)} \frac{\partial q}{\partial \tau} \approx -\frac{q_w}{V(t)} e^{-\tau^2/4t} \tag{3.30}$$

By taking a zero value of DTOF at the vertical well center, we can derive the well test derivative.

$$\Delta p'_{wf} \equiv \frac{\partial \Delta p_{wf}}{\partial \ln(t)} = t \cdot \frac{\partial \Delta p_{wf}}{\partial t} \approx \frac{q_w \cdot t}{c_t \cdot V(t)} \tag{3.31}$$

Within homogeneous and smoothly varying heterogeneous media, the well test derivative curve will be horizontal at early times of flow on a diagnostic plot of constant well production rate. The hybrid version of drainage volume construction will help validate the asymptotic pressure approximation for infinite-acting flow around the production well with constant flow rate using the well test derivative. Accurate constructions of both the drainage volume and the well test derivative are crucial for our understanding of the transient flow near the wellbore.

3.3.3 Transient Flow Simulation: w(τ) and transmissibility

The DTOF (τ) calculated from solving the Eikonal equation has a unit of square root of time and provides an effective means of describing the pressure front propagation in homogeneous and smoothly varying heterogeneous media. It can also be treated as a spatial coordinate that transforms the 3D pressure diffusivity equation in the Cartesian coordinate into an equivalent 1D form in the "τ-contour" system (Figure 3.25).

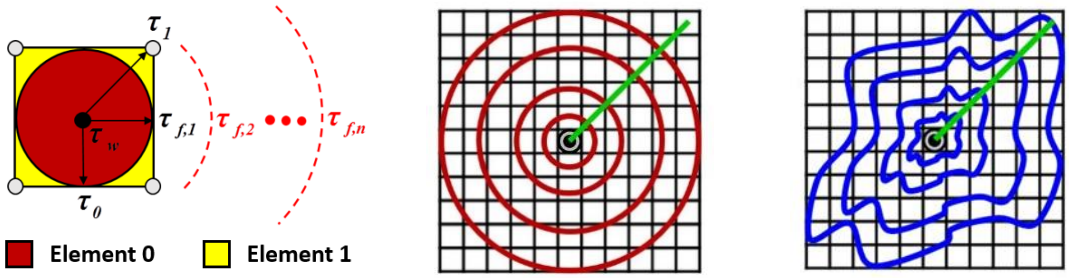

(a)
τ-intervals within and beyond the well cell

(b)
"τ-contours" in homogeneous media

(c)
"τ-contours" in heterogeneous media

Figure 3.25 "τ-contours" generated under the Cartesian coordinate system

This transformed one-dimensional diffusivity equation relies upon an assumption that the pressure (drop) contour is aligned with the τ-contour (Eq.(3.32)).

$$\frac{1}{w(\tau)}\frac{\partial}{\partial\tau}\left(w(\tau)\frac{\partial p}{\partial\tau}\right)=\frac{\partial p}{\partial t} \tag{3.32}$$

This assumption is valid for transient flow in homogeneous and "sufficiently" smooth heterogeneous reservoir models. Under such circumstances, the $w(\tau)$ function can be used to describe the reservoir heterogeneity, which is similar to the role played by permeability. By evaluating the pressure gradient along the DTOF (τ) coordinate, we can formulate an approximation to the Darcy's equation using $w(\tau)$ and the total compressibility of the reservoir model.

$$q(\tau,t)\approx c_t w(\tau)\frac{\partial p(\tau,t)}{\partial\tau} \tag{3.33}$$

Eq.(3.32) and Eq.(3.33) provide the governing equation and the basic law of mass conservation for transient flow in the presence of reservoir heterogeneity, respectively.

Taking advantage of the DTOF (τ) coordinate, it is straightforward to apply various boundary conditions to the one-dimensional diffusivity equation and calculate the pressure and flux solution under appropriate discretization schemes.

For a fixed flow-rate constraint at the wellbore, the flux boundary condition can be expressed as

$$\left[c_t w(\tau) \frac{\partial p}{\partial \tau} \right]_{\tau=\tau_w} = q_w \tag{3.34}$$

For a fixed bottom-hole flowing pressure (BHP) constraint at the wellbore, the pressure boundary condition can be expressed as

$$p\big|_{\tau=\tau_w} = p_{wf} \tag{3.35}$$

Under transient flow conditions, the outer-boundary pressure is kept constant as the initial reservoir pressure and does not need to be specified. These governing equations along with corresponding boundary conditions constrained at the well make it possible to perform a rapid simulation of transient flow in reservoir models using DTOFs as the spatial coordinate. From the FMM calculated DTOFs, the hybrid cumulative pore volume in the complete form (Eq.(3.16)) can be constructed using the minimum and maximum grid-cell DTOF values (Eq.(3.15)). Then the piecewise constant $w(\tau)$ can be easily obtained from dividing the incremental pore volume by the incremental DTOF value across each of those τ-intervals (Eq.(3.21)), which are independent of the DTOFs calculated from the FMM.

In the following discussion, we will focus on demonstrating how the one-dimensional diffusivity equation (Eq.(3.32)) can be discretized into a series of τ-intervals

as well as the way pressure values within those τ-intervals are solved. This procedure relies heavily upon the $w(\tau)$ function evaluated on each of those τ-intervals and the inter-cell transmissibility construction.

Suppose the entire reservoir model is discretized into a total number of N τ-intervals ($j = 0,1,\cdots,N-1$), which range from a minimum DTOF value evaluated at the wellbore, τ_w, to a maximum DTOF (τ) value evaluated at the outer boundary of the reservoir model (Figure 3.25). The first τ-interval (Element 0 well cell) has a lower limit of τ_w and an upper limit of τ_0, which is actually the Element 0 well cell discussed before (Figure 3.26a).

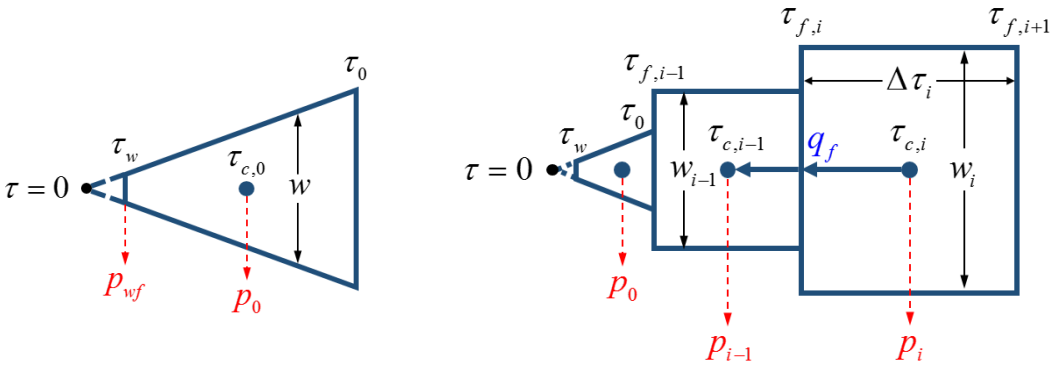

(a) Flow within Element 0 **(b) Inter-cell flow beyond Element 0**

Figure 3.26 Flow within the τ-intervals generated from the FMM calculated DTOFs for the reservoir model with one single vertical well

The $w(\tau)$ within the Element 0 well cell is a linear function of τ (Figure 3.26a).

$$w(\tau) = \frac{2\pi k_0 h}{\mu c_t} \cdot \tau \tag{3.36}$$

We formulate the well index (WI) to ensure flow communication between the vertical well (with an effective wellbore radius of r_w) and the first τ-interval.

$$\frac{1}{WI} = \frac{\Delta p_{pss}}{q_w} = \frac{\mu}{2\pi k_0 h} \cdot \left[\frac{\tau_0^2}{\tau_0^2 - \tau_w^2} \ln\left(\frac{\tau_0}{\tau_w}\right) - \frac{1}{2} \right] \tag{3.37}$$

During flow simulation, it is not required to know the location where the pressure at the first Element 0 well cell is evaluated. From this location to the upper boundary of the first τ-interval, we formulate a half-cell transmissibility similar to the way the well index is derived.

$$\frac{1}{T_0} = \frac{\mu}{2\pi k_0 h} \cdot \left[\frac{1}{2} - \frac{\tau_w^2}{\tau_0^2 - \tau_w^2} \ln\left(\frac{\tau_0}{\tau_w}\right) \right] \tag{3.38}$$

Beyond τ_0, there are $N-1$ τ-intervals. Across each of those τ-intervals, the DTOF value can be evaluated at the cell face $\tau_{f,i}$ (Figure 3.26b). This makes it possible to evaluate the $w(\tau)$ value for each τ-interval beyond the first one by local differentiation of the incremental pore volume to the DTOF difference across it.

$$\Delta\tau_i = \tau_{f,i+1} - \tau_{f,i}, \quad i = 0,1,...,N-1 \tag{3.39}$$

Then the $w(\tau)$ for each τ-interval beyond the Element 0 well cell can then be calculated as

$$w_i = \frac{PV_i}{\Delta\tau_i}, \quad i = 1, ..., N-1 \tag{3.40}$$

Here PV_i represents the pore volume of the *i*-th τ-interval beyond the Element 0 well cell. Across the *i*-th τ-interval beyond Element 0, the $w(\tau)$ function evaluated on it (w_i) is constant. The τ-intervals beyond τ_0 can be discretized with any resolution. When solving the DTOF-based one-dimensional diffusivity equation (Eq.(3.32)), it is recommended to use logarithmically distributed τ-intervals beyond Element 0 since they can make the pressure solution within them converge fast. Based on Eq.(3.40), we can construct the inter-cell transmissibility beyond the annular Element 0 well cell as

$$\frac{1}{T_i} = \frac{\Delta\tau_i}{2c_t w_i} = \frac{(\Delta\tau_i)^2}{2c_t PV_i} \quad (i = 1, ..., N-1) \tag{3.41}$$

The pressure within those τ-intervals beyond the Element 0 well cell is evaluated at the cell center. The flow communication between τ-intervals beyond τ_0 relies upon an inter-cell transmissibility that can be constructed as

$$\frac{1}{T_{n-1,n}} = \left(\frac{1}{2c_t}\right) \cdot \left(\frac{\Delta\tau_{n-1}}{w_{n-1}} + \frac{\Delta\tau_n}{w_n}\right) \tag{3.42}$$

Using Eq.(3.42), we can calculate the inter-cell transmissibility by means of a harmonic average of the half-cell transmissibility values between adjacent τ-intervals beyond Element 0 (Eq.(3.41)).

Between the Element 0 well cell and its adjacent τ-interval, the flow communication relies upon an inter-cell transmissibility that can be constructed as

$$\frac{1}{T_{0,1}} = \left(\frac{\mu}{2\pi k_0 h}\right) \cdot \left(\frac{1}{2} - \frac{\tau_w^2}{\tau_0^2 - \tau_w^2} \ln\left(\frac{\tau_0}{\tau_w}\right)\right) + \frac{\Delta\tau_1}{2c_t \cdot w_1} \tag{3.43}$$

This construction of the inter-cell transmissibility between the first and second τ-intervals will lead to a well pressure or flux profile more accurate than the Pedrosa and Aziz's method (1986), which will be demonstrated when validating the transient flow simulation.

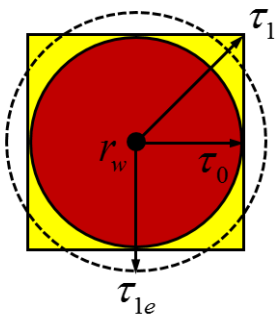

Figure 3.27 Illustration of the effective DTOF value calculated for the Element 1 well cell using the Petrosa and Aziz's method (Pedrosa and Aziz, 1986)

As an alternative approach to constructing the inter-cell transmissibility between the first and second τ-intervals, the Pedrosa and Aziz's method (1986) takes advantage of the DTOF value evaluated at the vertex of the well cell (τ_1) to obtain an effective DTOF (τ) value (τ_{1e}) used as the upper limit of the second τ-interval beyond τ_0 (Figure 3.27). This second τ-interval has an equal pore volume as the Element 1 well cell (Figure 3.10a and Figure 3.25a).

$$V_p(\tau_1) - V_p(\tau_0) = \left(\frac{\pi k_0 h}{\mu c_t}\right) \cdot \left(\tau_{1e}^2 - \tau_0^2\right) \tag{3.44}$$

Here $V_p(\tau_1)$ can be calculated using Eq.(3.16) and must take into account of the adjacent cells of the well cell. The inter-cell transmissibility between Element 0 and its adjacent τ-interval can then be calculated using τ_{1e}.

$$\frac{1}{T_{0,1}} = \left(\frac{\mu}{2\pi k_0 h}\right) \cdot \left(\frac{\tau_{1e}^2}{\tau_{1e}^2 - \tau_0^2} \ln\left(\frac{\tau_{1e}}{\tau_0}\right) - \frac{\tau_w^2}{\tau_0^2 - \tau_w^2} \ln\left(\frac{\tau_0}{\tau_w}\right)\right) \tag{3.45}$$

The inter-cell transmissibility construction for the remaining τ-intervals stays in the same constant form (Eq.(3.42)).

By applying appropriate boundary conditions at the wellbore (Eq.(3.34) or Eq.(3.35)) and assigning a reasonable initial pressure to the reservoir model, the pressure values distributed within those discretized τ-intervals can be efficiently solved for the DTOF-based one-dimensional transient flow equation (Eq.(3.32)).

3.4 Convergence and Validation

In this section, we validate the pressure transient represented by the drainage volume and the DTOF-based transient flow simulation by either the analytic solution for homogenous reservoir models or the numerical solution from a reservoir simulator (ECLIPSE) for heterogeneous reservoir models.

3.4.1 Validation of the Pressure Transient

The asymptotic pressure approximation (Eq.(3.30)) relies significantly upon an accurate formulation of the drainage volume as a function of time (Eq.(3.5)) based on the DTOF calculated from solving the Eikonal equation (Eq.(3.1)). It can reflect the pressure transient behavior by means of the well test derivative, which demonstrates to be inversely proportional to the drainage volume, $V(t)$ (Eq.(3.31)). Previous convergence analyses of DTOFs calculated from different discretization schemes of the Eikonal equation have proved that the 2D C5V9 (LGR) FMM can help generate sufficiently accurate DTOF solutions without much computational cost involved. So, we use this discretization scheme to calculate the DTOF and construct the drainage volume in the analytic, piecewise linear, piecewise constant as well as hybrid forms. By comparing different discretization schemes for the drainage volume, we can determine an ideal strategy for the pressure transient analysis using the DTOF.

We investigate the pressure transient behavior for a constant flow rate well test on a 2D homogeneous reservoir model using the asymptotic pressure approximation to the well test derivative (Eq.(3.31)). The input parameters for the homogeneous reservoir are listed in Table 3.2, except for the permeability value (15.53md), which is the same as that used for DTOF calculation shown in Figure 3.3b. The production well is located at the reservoir center with a constant flow rate of 100 res bbl/day.

Figure 3.28 demonstrates the drainage volume calculated using four discretization schemes during the well test performed within a short period of 100hrs and a long period of 1000hrs, respectively. The homogeneous reservoir model is discretized into a 7x7 and

51x51 uniform square grid systems, respectively. Within each one of the two discretized reservoir models, we compare the drainage volume constructed in four different forms, which include the piecewise constant form (represented as "Constant", Eq.(3.24)), the piecewise linear form (represented as "Linear", Eq.(3.23)), the complete hybrid form (represented as "Hybrid", Eq.(3.22), Eq.(3.26), Eq.(3.27) and Eq.(3.29)), and the reduced hybrid form (represented as "Reduced Hybrid", Eq.(3.22), Eq.(3.26), Eq.(3.28) and Eq.(3.29)). The four discretized drainage volumes are compared with the analytic solution (Eq.(3.22), which is represented as "Analytic"). The corresponding well test derivatives can be calculated straightforwardly using Eq.(3.31).

Comparing the four different discretization schemes of drainage volume variation as a function time (the left column of plots in Figure 3.28), we can hardly differentiate them because they significantly overlaps each other except for the 100hrs simulation under the 7x7 grid discretization. However, we can more easily differentiate the four forms of pressure transient if they are interpreted in terms of the well test derivative (the right column of plots in Figure 3.28), where only the hybrid pressure transient is largely overlapping its reduced form (Eq.(3.29)).

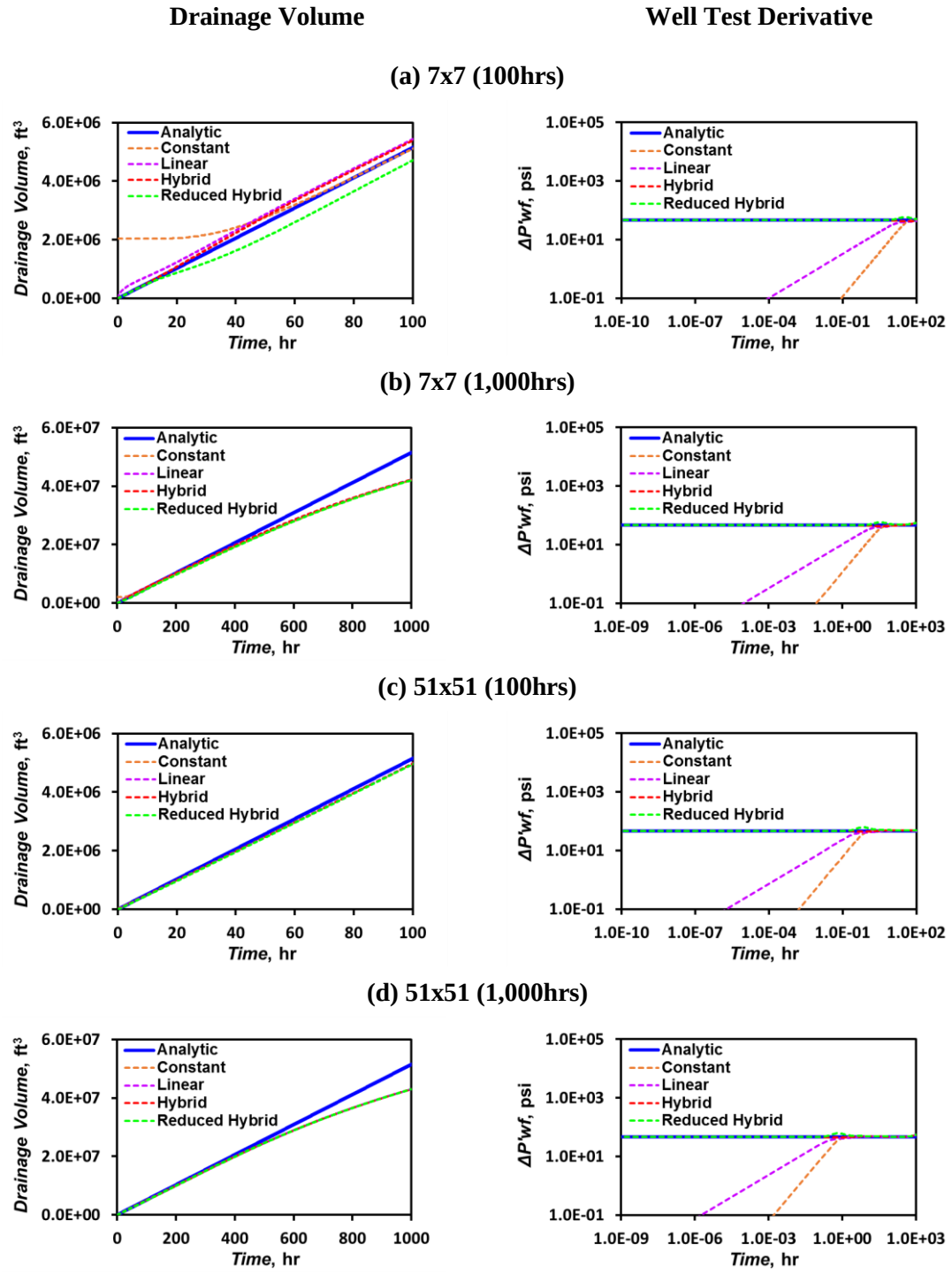

Figure 3.28 Calibration of the pressure transient for a constant flow rate well test within a 2D homogeneous reservoir model using DTOFs calculated from the C5V9 (LGR) FMM

We can easily find that the piecewise constant form of drainage volume discretization leads to a numerical solution that is significantly higher than the analytic formulation at very early times of flow. The discrepancy between numerical and analytic solutions can be decreased by applying the piecewise linear formulation of drainage volume (Figure 3.28a). The divergence of constant and linear forms of drainage volume from the analytic solution can be decreased by increasing the numbers of grid cells within the reservoir model (Figure 3.28c and d). However, early-time errors still exist and become particularly visible when the pressure transient is interpreted by means of the well test derivative. The hybrid versions of drainage volume discretization can help generate far more accurate numerical solutions at early times of simulation. The complete hybrid drainage volume construction gives rise to an overestimation of the numerical solution when the pressure front passes from the well cell to adjacent cells, which leads to an underestimation of the well test derivative. On the contrary, the well test derivative shows to be a little higher than the analytic solution when the pressure front passes across the well cell due to an underestimation of the drainage volume when it is constructed in the reduced hybrid form.

As the number of grid cells increases, the divergence of well test derivatives from the analytic solution due to a hybrid construction of the drainage volume occurs at an earlier time. Particularly, the complete form of hybrid drainage volume leads to a more accurate well test derivative compared with the reduced hybrid formulation. However, the reduced hybrid formulation of the drainage volume requires less computational efforts, which is important for establishing the forward model and performing rapid inversion that

will be discussed in the next section. The errors caused by both forms of hybrid construction of the drainage volume are negligible as long as the well test time is short enough and the transient flow can be ensured.

As the well test time increases and boundary effect is being felt, the hybrid drainage volume formulated in terms of the DTOF will diverge significantly from the analytic solution, making the well test derivative curve not horizontal anymore (Figure 3.28b and d). This circumstance should be avoided for reservoir parameter estimation from pressure transient analysis, because much more errors will be introduced by inaccurate forward modeling.

The hybrid drainage volume construction using the DTOF calculated from the C5V9 (LGR) FMM shows to converge very fast to the analytic solution and proves to be able to generate sufficiently accurate numerical solutions as long as resolution of the reservoir model is high enough. It provides a useful tool for pressure transient analysis in heterogeneous reservoir models and can be efficiently used to validate the transient flow based on the asymptotic pressure approximation.

3.4.2 Validation of the Transient Flow Simulation

The solution from the DTOF-based transient flow simulation can be validated with the bottom-hole flowing pressure (BHP) and well production rate generated from the reservoir simulator (ECLIPSE) under fixed well production rate and fixed bottom-hole flowing pressure conditions, respectively. Using the inter-cell transmissibility constructed from the complete form of hybrid cumulative pore volume (Eq.(3.16) as well as the

corresponding $w(\tau)$ function generated, we solve the DTOF-based one-dimensional diffusivity equation (Eq.(3.32)) and calibrate the pressure and flux response at the production well.

On the basis of the same reservoir models used for $w(\tau)$ function construction as shown in Figure 3.3 and Figure 3.6, we conduct numerical simulations of the single-phase transient flow with one vertical production well placed within the 2D reservoir model. An initial reservoir pressure of 1,000 psi is assigned to all cases. The boundary condition is defined by constraining the production rate or BHP at the well, which is located at the center of the 2D synthetic reservoir model but might be located at different locations within the 1st and 72nd layers of the SPE10 reservoir model (Table 3.17). The well placement in all cases is consistent with previous $w(\tau)$ function construction (Figure 3.19 to Figure 3.24).

Table 3.17 2D Reservoir dimensions and boundary conditions constrained at the production well

Reservoir Model	Reservoir Dimension	Well Location	Initial reservoir Pressure (psi)	Fixed Well Rate (res bbl/d)	Fixed Well BHP (psi)
Homogeneous	199x199	(100, 100)	5000	100	4300
Heterogeneous	199x199	(100, 100)	5000	100	4500
SPE10, Layer01	60x220	(40, 90)	5000	10	4900
SPE10, Layer01	60x220	(25, 134)	5000	10	4000
SPE10, Layer72	60x220	(33, 103)	5000	10	4900
SPE10, Layer72	60x220	(42, 100)	5000	10	4000

In all the six 2D reservoir models (Table 3.17), logarithmically distributed τ-intervals (ranging from DTOF evaluated at the wellbore to DTOF evaluated at the reservoir outer boundary) are used to discretize the one-dimensional pressure diffusivity equation (Eq.(3.32)). The pressure values are correspondingly evaluated within the τ-intervals, with the output pressure or flux at the well compared with that calculated from a numerical simulator (ECLIPSE).

In order to determine the best scheme designed for the $w(\tau)$ function calculation, we compared three different methods for the $w(\tau)$ generation and their applications in the transient flow simulation using the C5V9 (LGR) FMM. They use the same set of logarithmically distributed τ-intervals, which has a fixed DTOF width across the first Element 0 well cell ranging from τ_w to τ_0. The τ-intervals have a maximum DTOF value equal to the maximum DTOF calculated from the C5V9 (LGR) FMM for the entire

reservoir model, but are independent of the FMM calculated DTOFs beyond the Element 0 well cell. The method we proposed (Eq.(3.37) to Eq.(3.43)) for the DTOF-based transient flow simulation is compared with the Petrosa and Aziz's method (PA) and the smoothing technique (SM) for $w(\tau)$ and inter-cell transmissibility constructions.

Simulations of the six reservoir models (Table 3.17) are demonstrated from Figure 3.29 to Figure 3.40. The results are compared with the ECLIPSE simulation, which is represented by the blue solid curve as "ECL". The well BHP and flux generated from the method we propose for τ-interval generation and inter-cell transmissibility calculation is represented by the red dash line as "FMM". The well responses generated from the method used by Pedrosa and Aziz (1986) for hybrid τ-interval generation near the well is represented by the green dash line as "FMM (PA)". The well responses generated from the method that relies on the smoothing technique to generate the $w(\tau)$ function and calculate the inter-cell transmissibility is represented by the pink dash line as "FMM (SM)". The numbers of logarithmically distributed τ-intervals used for simulation are 10, 20, 50 and 1000, respectively.

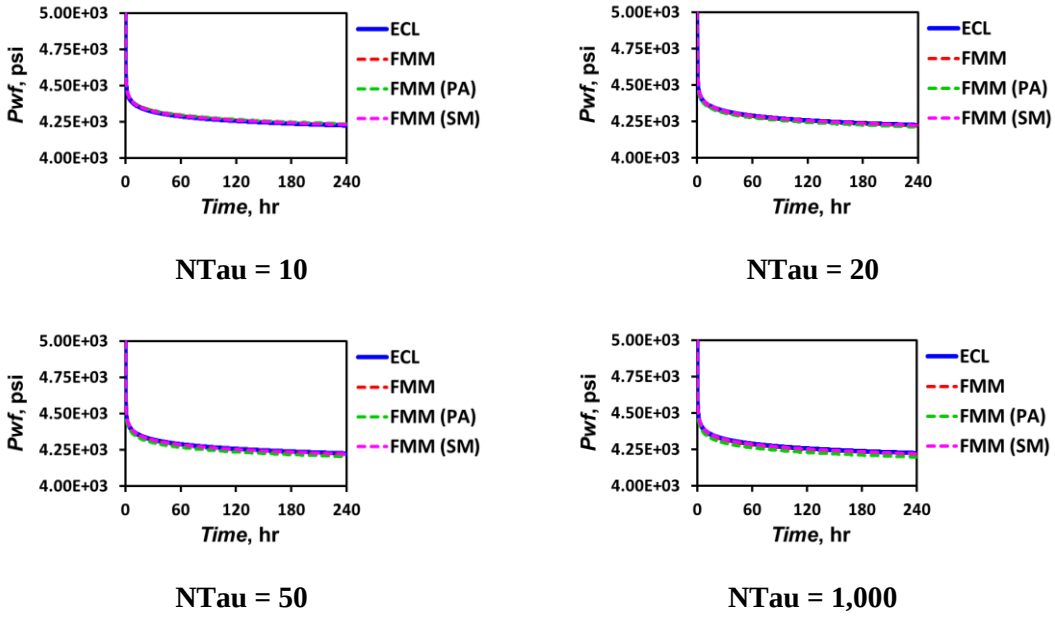

Figure 3.29 Calibration of BHP in the homogeneous reservoir model (199x199) by solving the DTOF-based one-dimensional diffusivity equation using the 2D C5V9 (LGR) FMM with a fixed well production rate

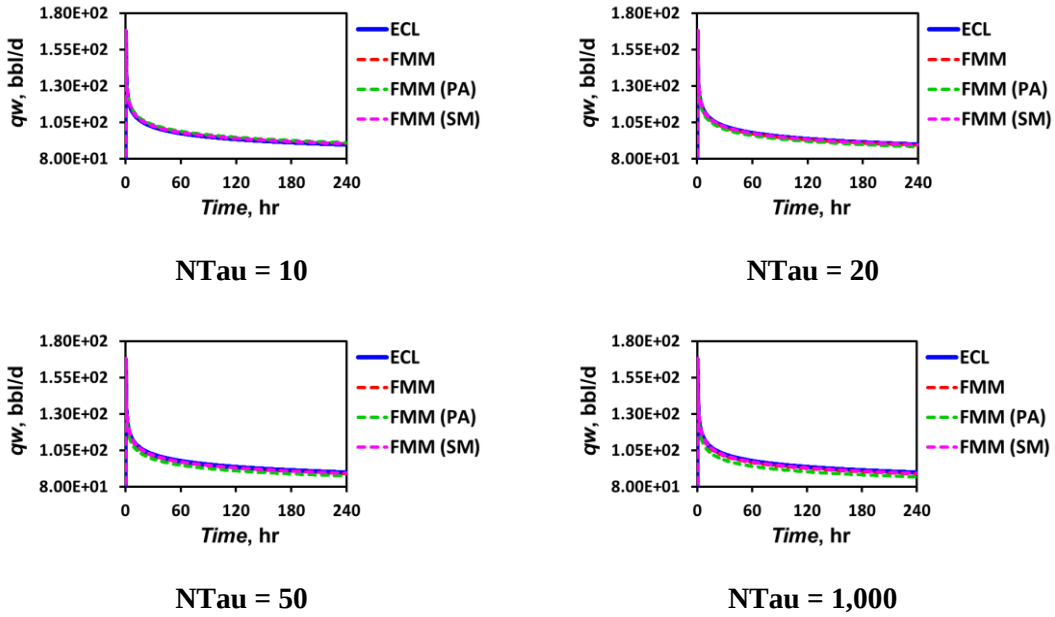

Figure 3.30 Calibration of well production rate in the homogeneous reservoir model (199x199) by solving the DTOF-based one-dimensional diffusivity equation using the 2D C5V9 (LGR) FMM with a fixed BHP

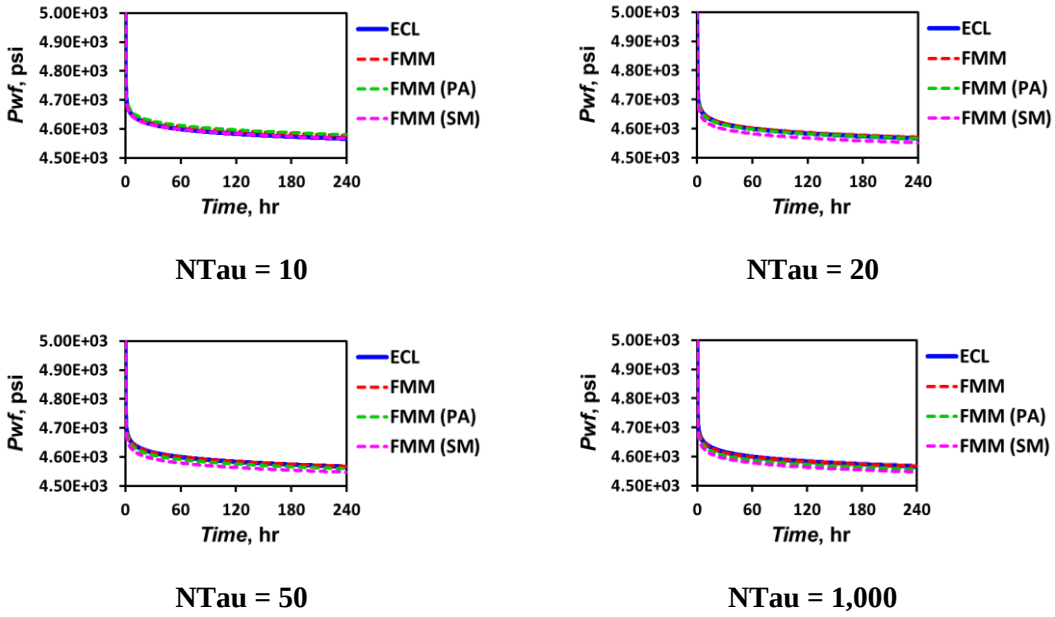

Figure 3.31 Calibration of BHP in the heterogeneous reservoir model (199x199) by solving the DTOF-based one-dimensional diffusivity equation using the 2D C5V9 (LGR) FMM with a fixed well production rate

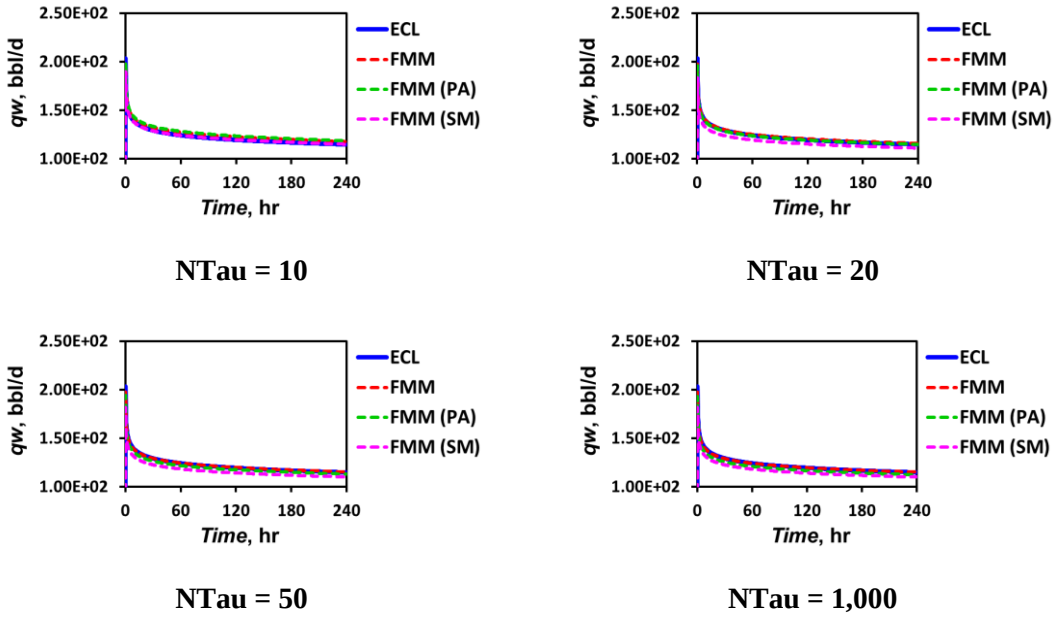

Figure 3.32 Calibration of well production rate in the heterogeneous reservoir model (199x199) by solving the DTOF-based one-dimensional diffusivity equation using the 2D C5V9 (LGR) FMM with a fixed BHP

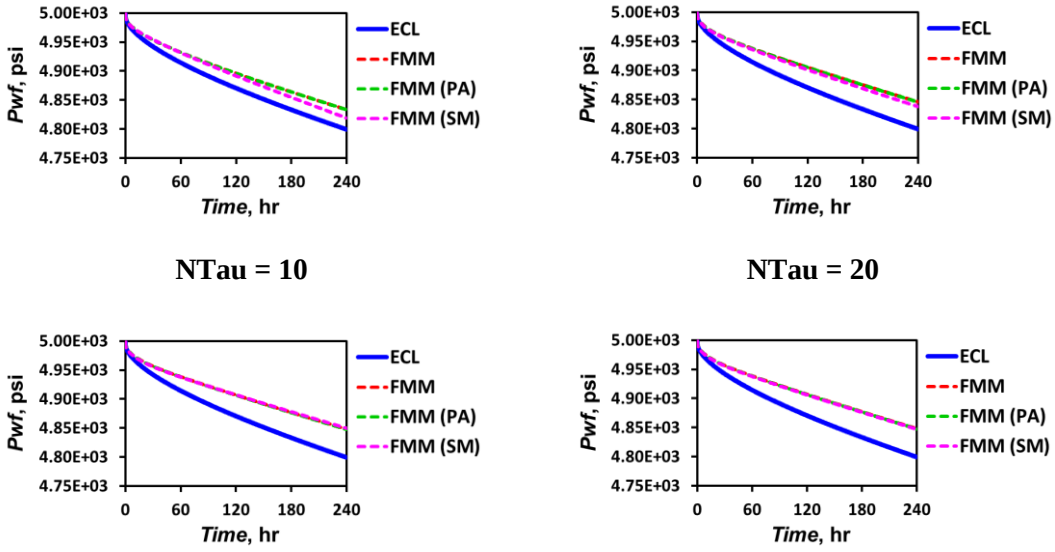

NTau = 10 **NTau = 20**

NTau = 50 **NTau = 1,000**

Figure 3.33 Calibration of BHP in the 1st layer of the SPE10 model with a well (40, 90) by solving the DTOF-based one-dimensional diffusivity equation using the 2D C5V9 (LGR) FMM with a fixed well production rate

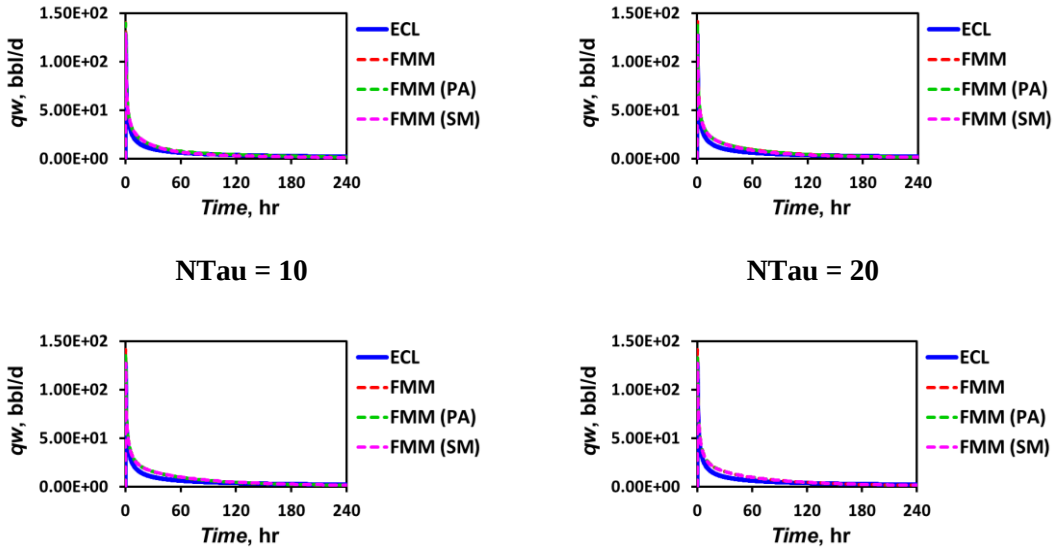

NTau = 10 **NTau = 20**

NTau = 50 **NTau = 1,000**

Figure 3.34 Calibration of well production rate in the 1st layer of the SPE10 model with a well (40, 90) by solving the DTOF-based one-dimensional diffusivity equation using the 2D C5V9 (LGR) FMM with a fixed BHP

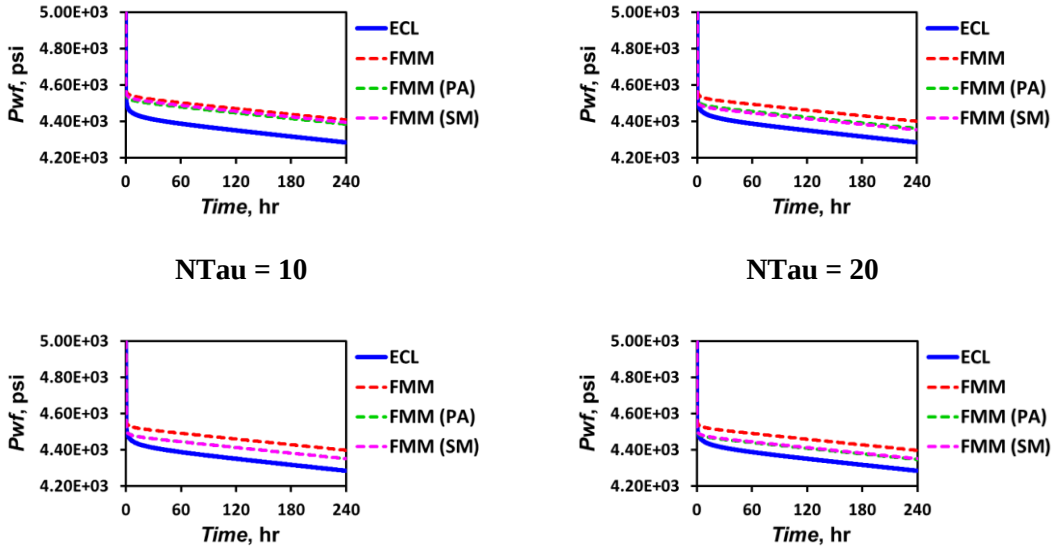

Figure 3.35 Calibration of BHP in the 1st layer of the SPE10 model with a well (25, 134) by solving the DTOF-based one-dimensional diffusivity equation using the 2D C5V9 (LGR) FMM with a fixed well production rate

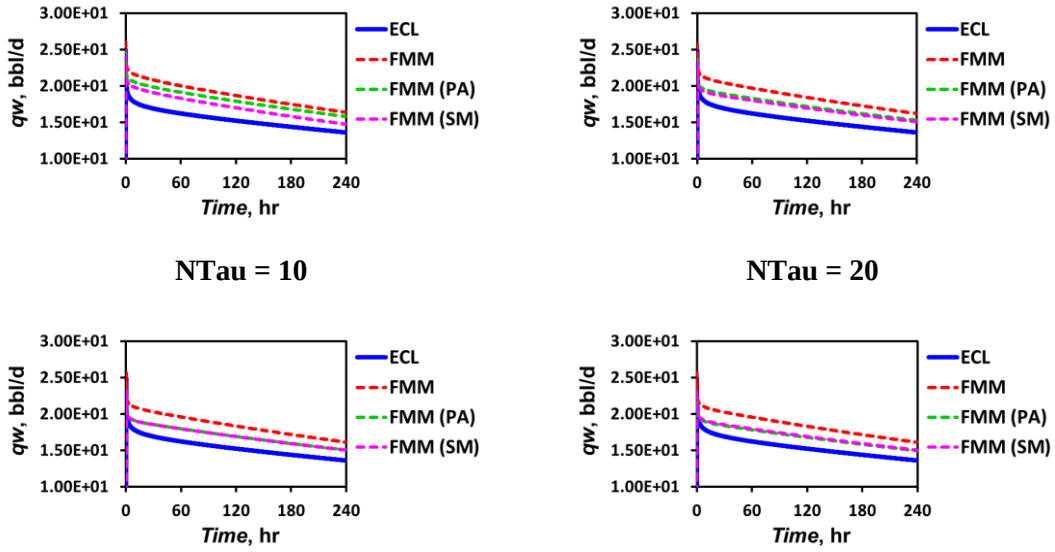

Figure 3.36 Calibration of well production rate in the 1st layer of the SPE10 model with a well (25, 134) by solving the DTOF-based one-dimensional diffusivity equation using the 2D C5V9 (LGR) FMM with a fixed BHP

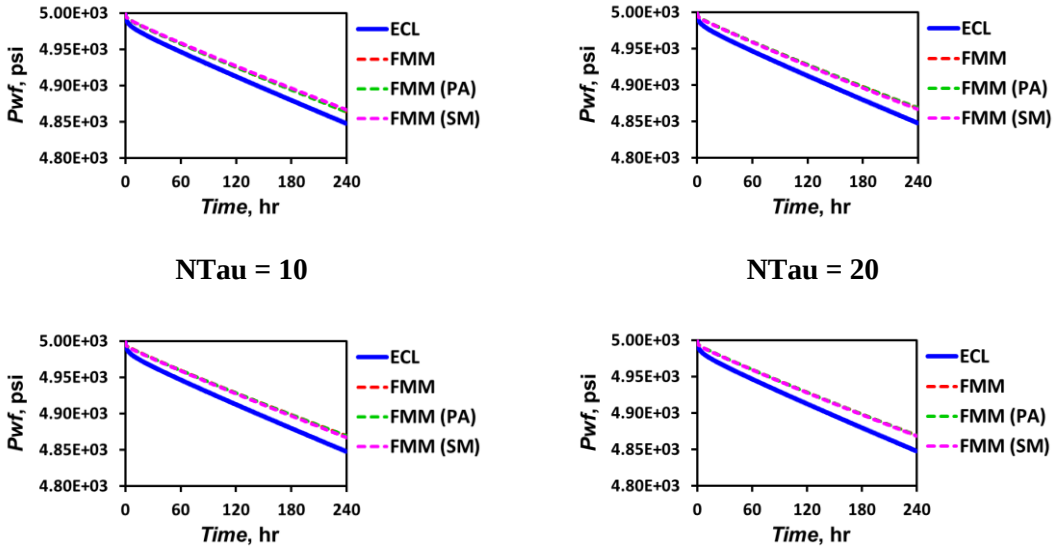

Figure 3.37 Calibration of BHP in the 72nd layer of the SPE10 model with a well (33, 103) by solving the DTOF-based one-dimensional diffusivity equation using the 2D C5V9 (LGR) FMM with a fixed well production rate

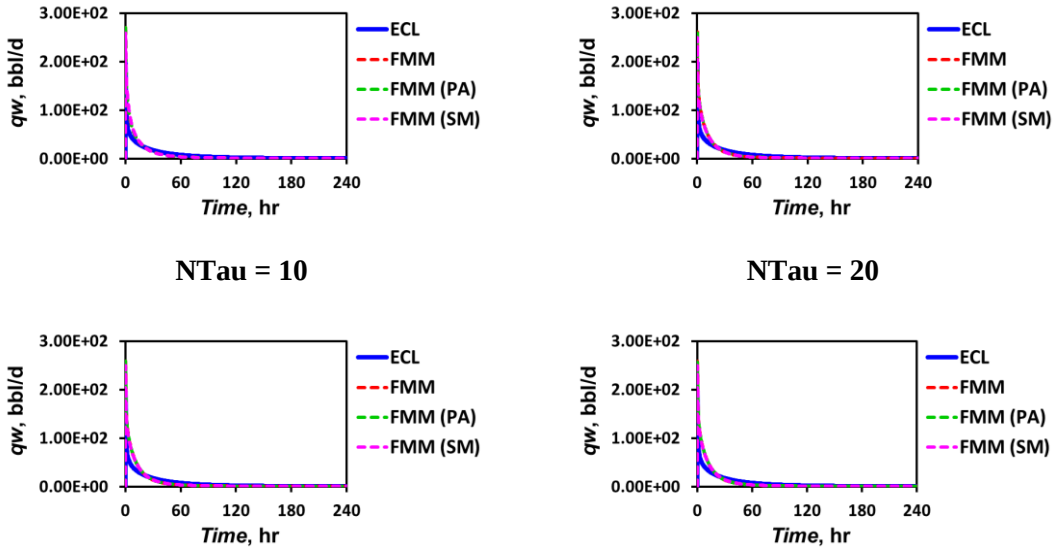

Figure 3.38 Calibration of well production rate in the 72nd layer of the SPE10 model with a well (33, 103) by solving the DTOF-based one-dimensional diffusivity equation using the 2D C5V9 (LGR) FMM with a fixed BHP

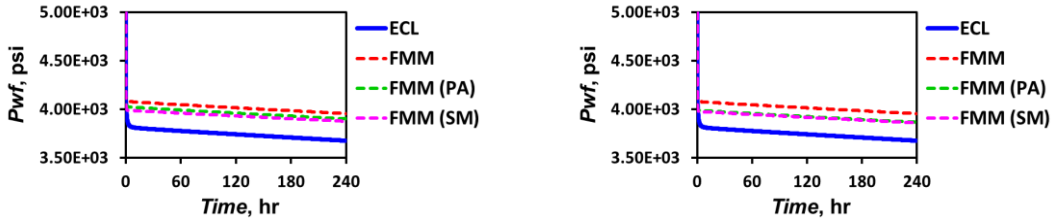

NTau = 10 **NTau = 20**

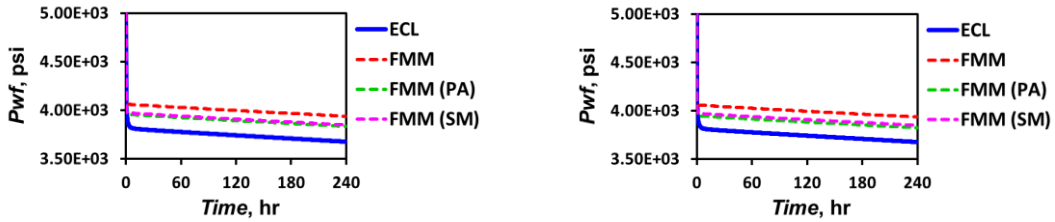

NTau = 50 **NTau = 1,000**

Figure 3.39 Calibration of BHP in the 72nd layer of the SPE10 model with a well (42, 100) by solving the DTOF-based one-dimensional diffusivity equation using the 2D C5V9 (LGR) FMM with a fixed well production rate

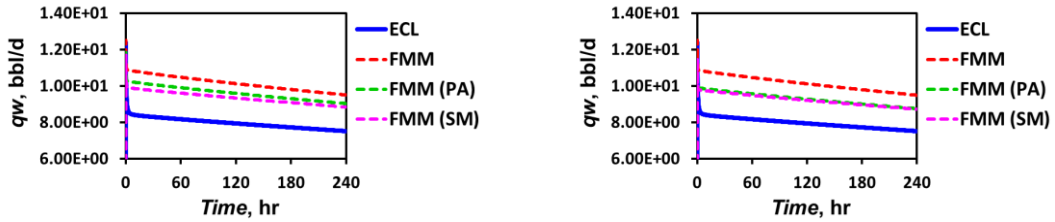

NTau = 10 **NTau = 20**

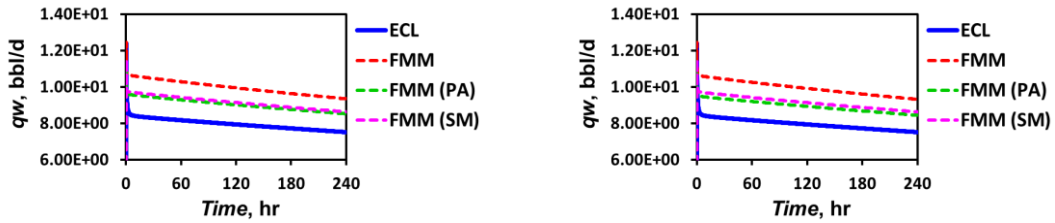

NTau = 50 **NTau = 1,000**

Figure 3.40 Calibration of well production rate in the 72nd layer of the SPE10 model with a well (42, 100) by solving the DTOF-based one-dimensional diffusivity equation using the 2D C5V9 (LGR) FMM with a fixed BHP

The simulation is first performed on the 2D homogeneous reservoir model (Figure 3.29 and Figure 3.30). The well BHP and flux calculated from the method we propose significantly overlaps that calculated from the smoothing technique under the four resolutions of the τ-intervals. The results generated from the two methods match excellently with the ECLIPSE simulation. As the number of τ-intervals increases, the well pressure and flux generated from the Pedrosa and Aziz's method begins to "drift" away from the ECLIPSE result. Although the well pressure and flux profiles will converge as the number of τ-intervals increases, the Pedrosa and Aziz's method proves to generate less accurate transient flow solutions compared to the other two methods.

Figure 3.31 and Figure 3.32 show the simulation results from the 2D heterogeneous reservoir model (Figure 3.3a) with smoothly varying heterogeneity (VDP = 0.5573). Well pressure and flux profiles will converge using all three methods, but the results generated from the Pedrosa and Aziz's method and the smoothing technique show to "drift" away from the ECLIPSE result. The method we propose generates the most accurate well BHP and flux profiles compared with ECLPSE simulation under all the four τ-interval resolutions.

Figure 3.33 to Figure 3.40 show the simulation performed on the 2D SPE10 reservoir models. The calibration results with the ECLIPSE simulation are far from satisfactory using all three methods for transient flow simulation, which correspond well to the multiple $w(\tau)$ decreasing trends observed before (Figure 3.21 to Figure 3.24) that indicates strong local reflections of the pressure front within the highly heterogeneous media.

After comparing the pressure or flux profile at the well using different methods of $w(\tau)$ calculation, we can make the following observations.

- The Petrosa and Aziz's method for calculating the effective DTOF value for the upper limit of the Element 1 well cell and its application in the inter-cell transmissibility construction (Eq.(3.45)) between the first and second τ-intervals cannot improve the computational accuracy for the transient flow simulation. When high resolution τ-intervals are used, the Petrosa and Aziz's method leads to a consistently lower well pressure or flux profile in homogeneous and smooth heterogeneous media compared with the ECLIPSE simulation (Figure 3.29 to Figure 3.32).
- Though performing well in homogeneous media (Figure 3.29 and Figure 3.30), the $w(\tau)$ function generated from the smoothing technique fails to generate accurate numerical solutions for transient flow simulation in heterogeneous media, even with a fixed DTOF width across the first τ-interval (Figure 3.31 to Figure 3.40).
- The method we propose for $w(\tau)$ and inter-cell transmissibility calculations provides the most accurate solution for the transient flow simulation in reservoir models with smoothly varying heterogeneity. The result is in excellent agreement with the ECLIPSE simulation (Figure 3.29 to Figure 3.32).

- Due to strong local reflections of the pressure front, all three methods fail to generate a transient flow solution that can match well with the ECLIPSE simulation in highly heterogeneous reservoir models, even when the well is placed at a cell with a high permeability value (Figure 3.33 to Figure 3.40).

To get a deeper understanding of the excellent simulation results for the first two synthetic models and the unsatisfactory performance in the 2D SPE10 models, we investigate the pressure drop behavior within the entire reservoir model and its relationship with the FMM calculated DTOFs. The asymptotic pressure approximation is compared with ECLIPSE simulation in both well cells (where the well test derivatives can be compared) and non-well cells (where the pressure drop derivatives can be compared) during the constant flow rate well test.

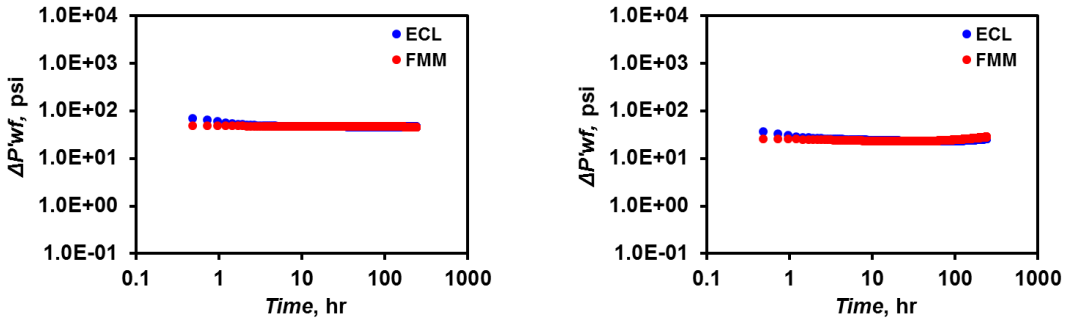

Figure 3.41 Calibration of the well test derivative calculated from the DTOF-based asymptotic pressure approximation with the ECLIPSE simulation during a constant flow rate well test on the 2D reservoir model

From Figure 3.41, it is easy to find that both the asymptotic pressure approximation and the ECLIPSE simulation reflect an infinite-acting flow within a 240hrs of constant flow rate well test in the homogeneous and smoothly varying heterogeneous media. The good agreement between FMM and ECLIPSE calculated well test derivatives corresponds well with the BHP agreements from the transient flow simulations (Figure 3.29 and Figure 3.31). We can also compare the pressure drop values generated from the asymptotic pressure approximation (Eq.(3.30)) with the ECLPSE simulation within the entire reservoir model. By taking a scatter plot of the pressure drop derivative against the DTOF and against the drainage volume weighted exponential term (Eq.(3.30)) for each grid cell, we test the validity of the asymptotic pressure approximation in both homogeneous and smoothly varying heterogeneous media (Figure 3.42).

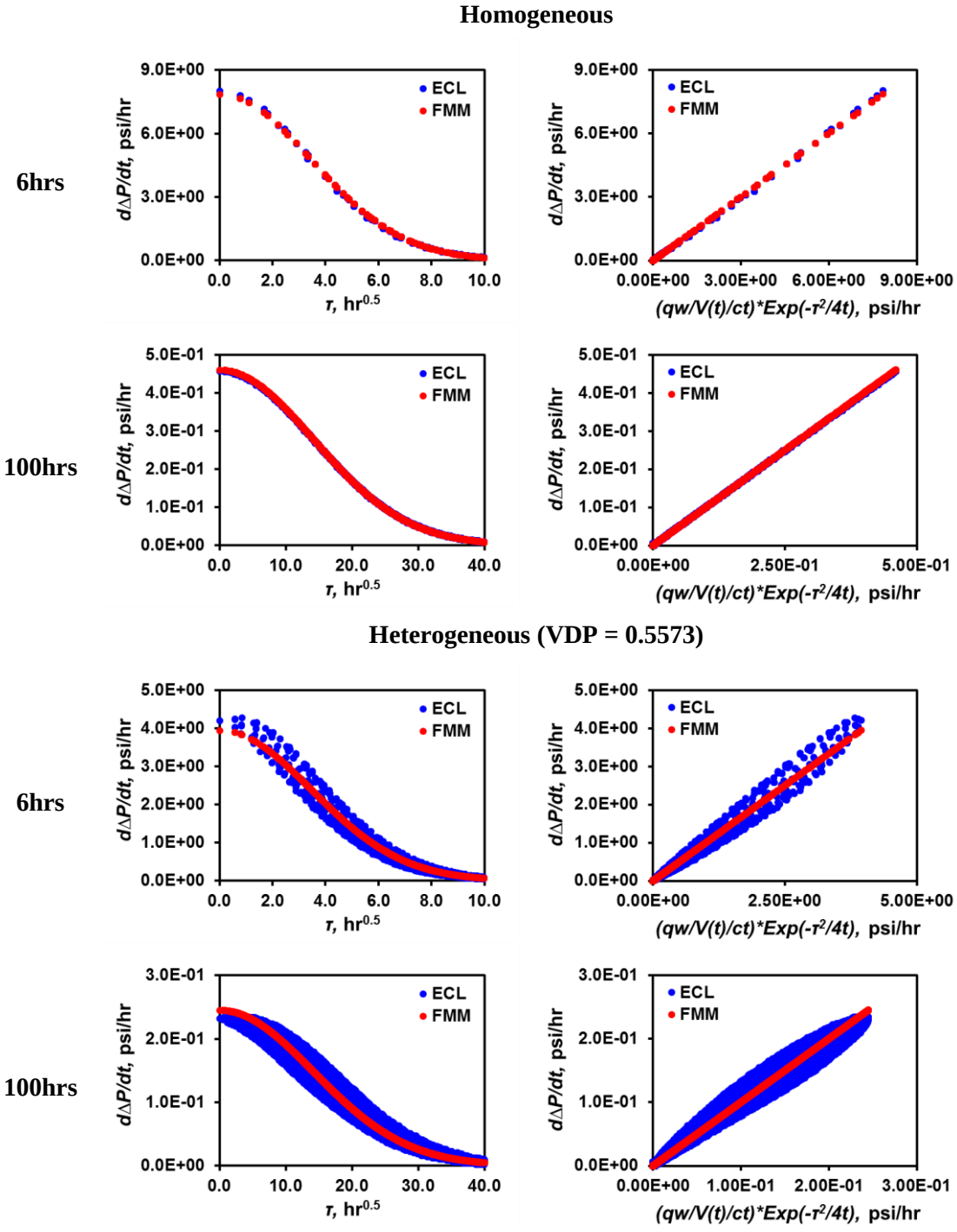

Figure 3.42 Comparison of the pressure drop derivatives calculated from the FMM and ECLIPSE within the entire homogeneous and heterogeneous reservoir models (199x199) during a constant flow rate well test

From the left column of Figure 3.42, it can be observed that the pressure drop derivative with respect to time generated from the ECLIPSE simulation and that from the FMM calculation are matching well with each other, especially in the homogeneous reservoir model. Within a distance "τ" less than $40hr^{0.5}$ from the well, the ECLIPSE generated pressure drop derivative is gradually decreasing, which indicates the out-going pressure front propagation from the well without much local reflection. This is consistent with the increasing $w(\tau)$ function within the "τ" distance of $40hr^{0.5}$ from the well in Figure 3.19 and Figure 3.20. From the right column of Figure 3.42, we can find that the pressure drop derivatives calculated from the FMM have a strong linear relationship with those calculated from the ECLISPE simulation within the entire reservoir domain, especially for the homogeneous model. This indicates that our assumption of the agreement between the pressure contour and the DTOF contour is valid for homogenous and "sufficiently" smooth heterogeneous reservoir media.

Pressure transient analysis using both the ECLPSE simulation and the asymptotic pressure approximation can also be conducted on the 2D SPE10 models. Figure 3.43 shows the well pressure interpreted by the well test derivative for the four constant flow rate well tests within the 1st layer (Figure 3.42a and b) and 72nd layer (Figure 3.42c and d) of the SPE10 model. The well test derivative calculated from the FMM is close to the ECLIPSE simulation at early times of simulation only if the permeability within the well cell is high (Figure 3.43a and c; Table 3.6). The discrepancy between the FMM and ECLIPSE generated results becomes larger when the well is placed in low-permeability cells (Figure 3.43b and d; Table 3.6).

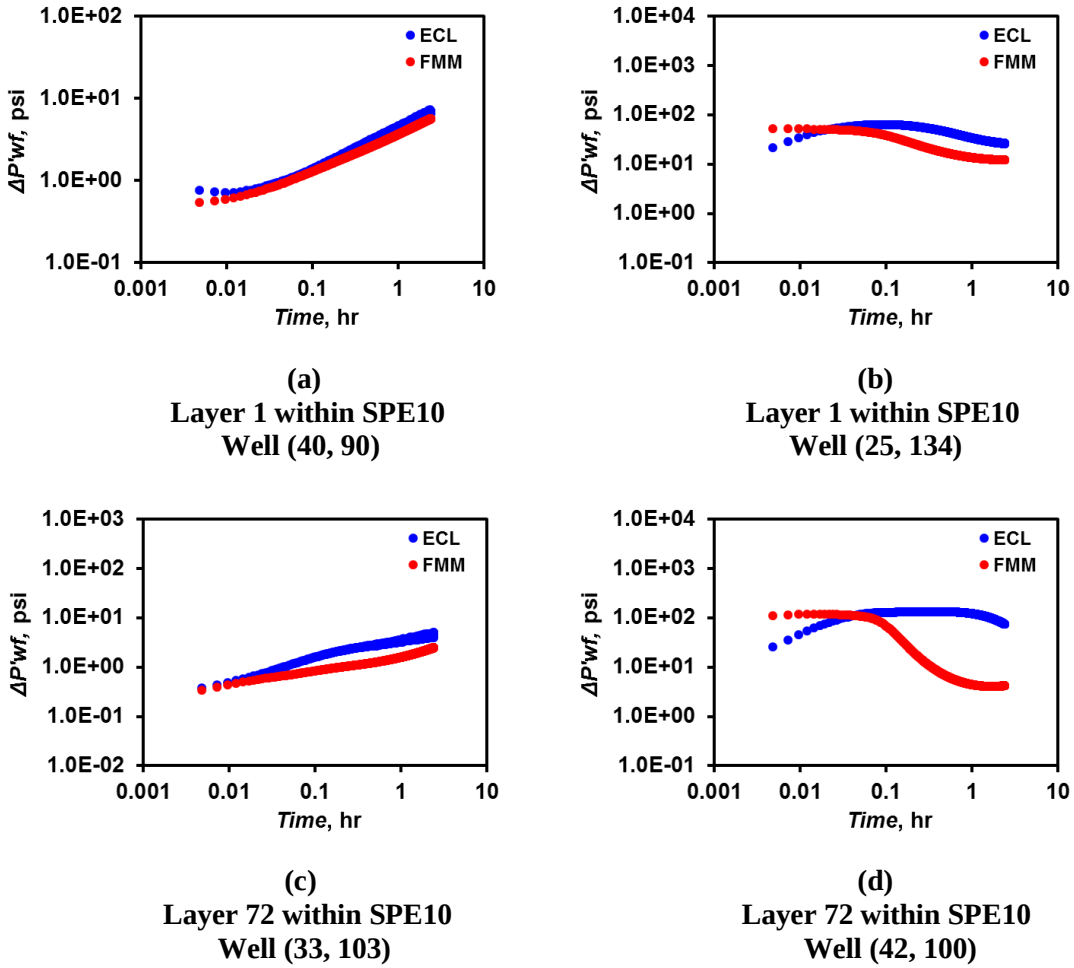

(a)
Layer 1 within SPE10
Well (40, 90)

(b)
Layer 1 within SPE10
Well (25, 134)

(c)
Layer 72 within SPE10
Well (33, 103)

(d)
Layer 72 within SPE10
Well (42, 100)

Figure 3.43 Calibration of the well test derivative calculated from the DTOF-based asymptotic pressure approximation with the ECLIPSE simulation during a constant flow rate well test on the 2D SPE10 model

In Figure 3.43, we can see the quick reflection of the pressure front at the no-flow reservoir boundary interpreted from the ECLIPSE simulated well test derivative with non-zero slope. The reason for the discrepancy between the FMM and ECLIPSE simulations can be further investigated by analysis of the pressure drop derivative within the entire reservoir model (Figure 3.44 to Figure 3.47).

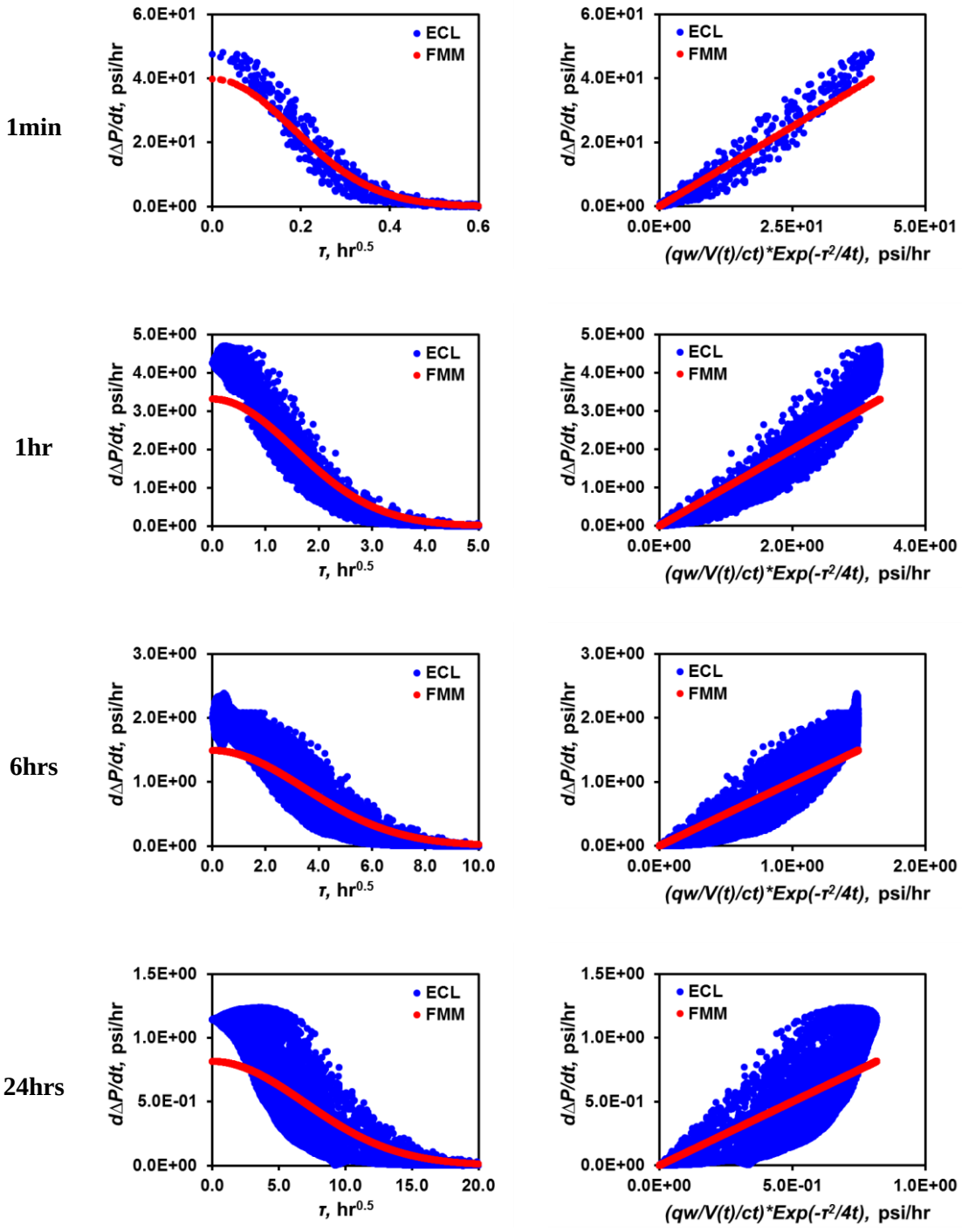

Figure 3.44 Comparison of the pressure drop derivatives calculated from the FMM and ECLIPSE within the entire reservoir field of the 1st layer within the SPE10 model during a constant flow rate well test with the well located at Cell (40, 90)

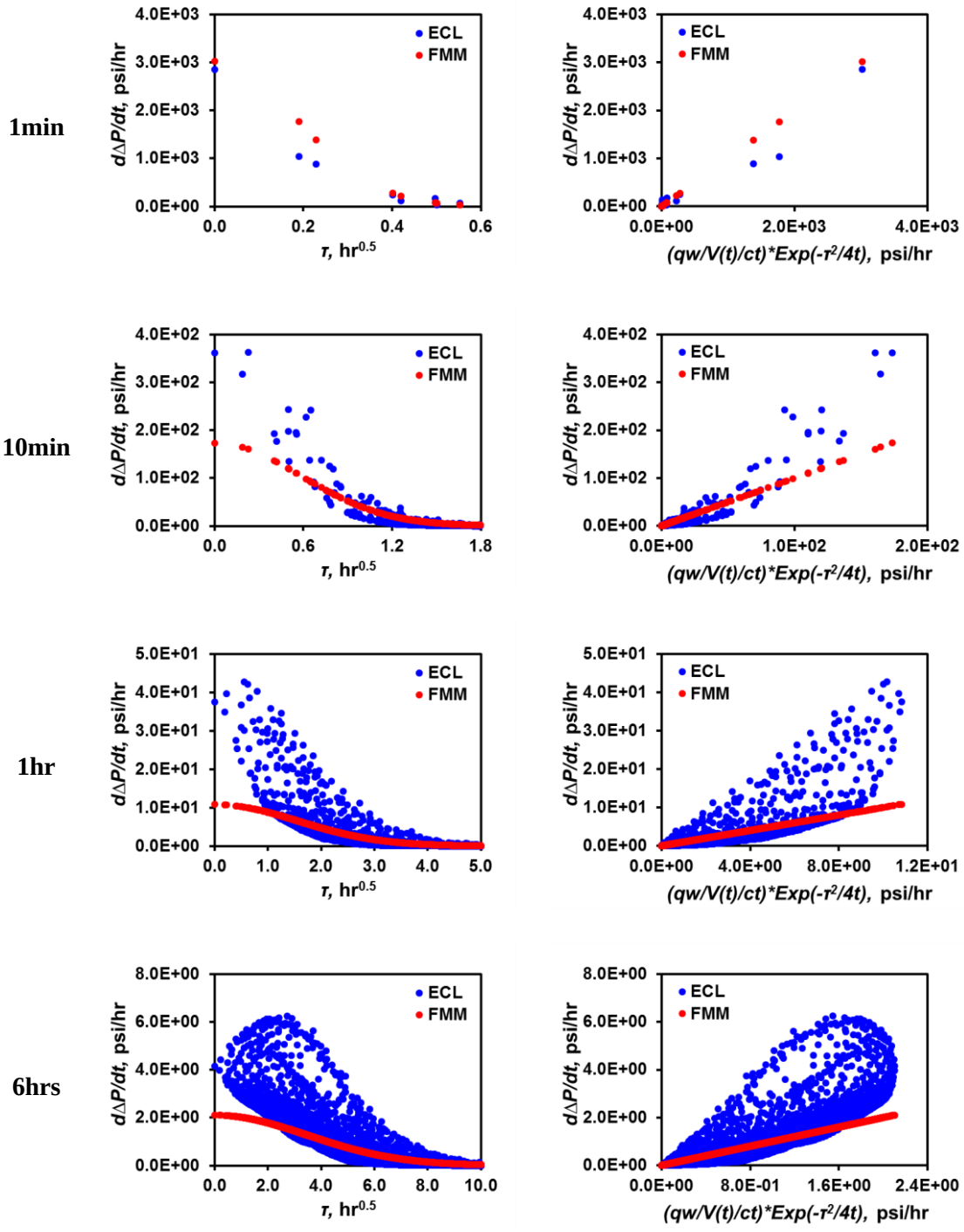

Figure 3.45 Comparison of the pressure drop derivatives calculated from the FMM and ECLIPSE within the entire reservoir field of the 1st layer within the SPE10 model during a constant flow rate well test with the well located at Cell (25, 134)

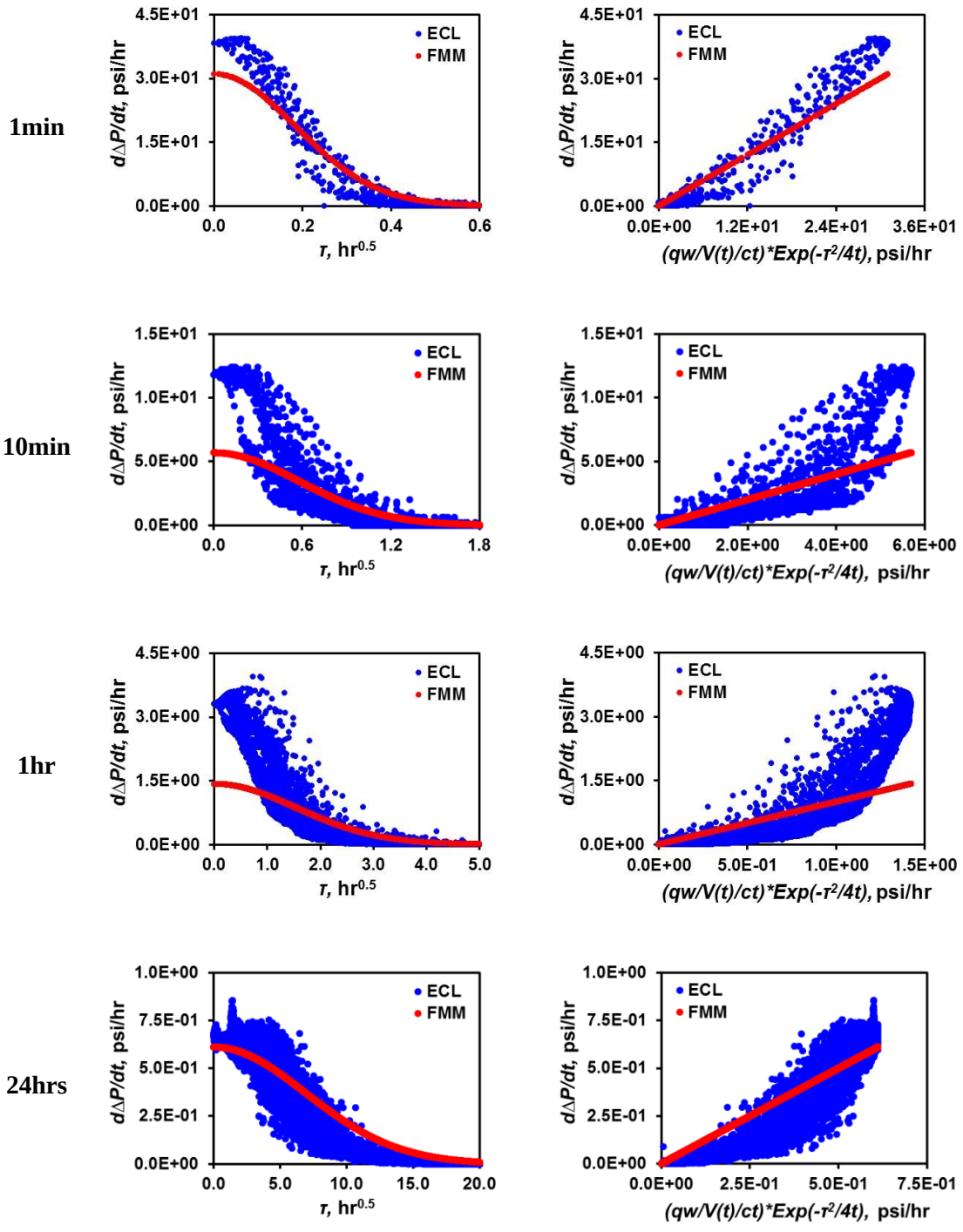

Figure 3.46 Comparison of the pressure drop derivatives calculated from the FMM and ECLIPSE within the entire reservoir field of the 72nd layer within the SPE10 model during a constant flow rate well test with the well located at Cell (33, 103)

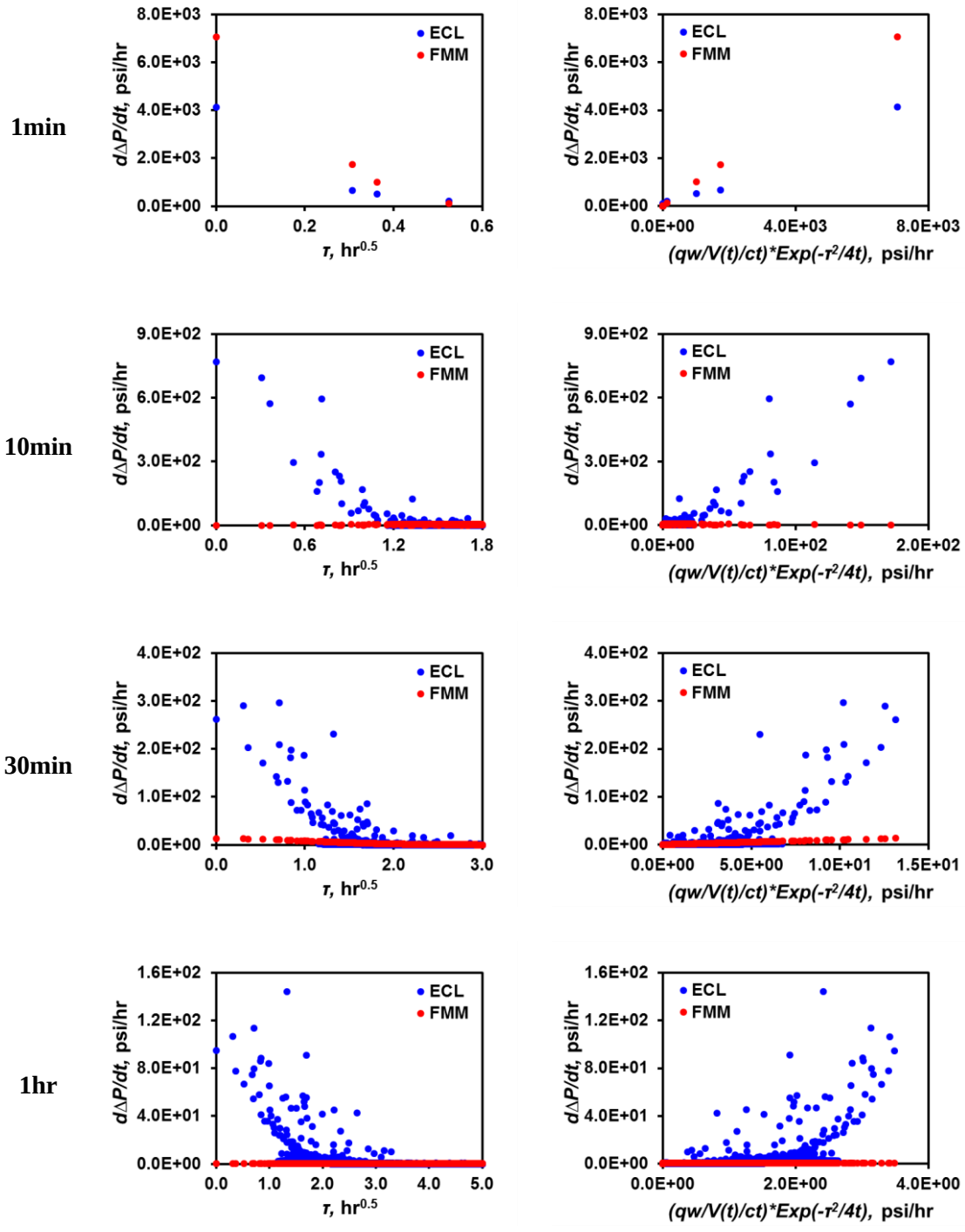

Figure 3.47 Comparison of the pressure drop derivatives calculated from the FMM and ECLIPSE within the entire reservoir field of the 72nd layer within the SPE10 model during a constant flow rate well test with the well located at Cell (42, 100)

In Figure 3.44, the production well is placed at a high-permeability cell within the 1st layer of the SPE10 model (Table 3.6). At the very early times of simulation (within one minute) when the pressure front propagates within a "τ" distance less than $0.6hr^{0.5}$ from the well, the pressure drop derivative with respect to time calculated from the FMM matches very well with the ECLIPSE simulation. The linear relationship between the FMM calculated pressure drop derivative and the drainage volume weighted exponential term within the asymptotic pressure approximation can approximately represent the ECLIPSE pressure simulation within all reservoir grid cells. This corresponds well with the increasing $w(\tau)$ function where the "τ" distance from the well is less than $0.6hr^{0.5}$ in Figure 3.21. Before the pressure front reaches the "τ" distance of $10hr^{0.5}$, multiple decreasing trends of the $w(\tau)$ function can be observed (Figure 3.21). This represents multiple local reflections of the pressure front within the highly heterogeneous media, which corresponds to the degraded approximation to the reservoir pressure derivative using the asymptotic pressure approximation at 1hr and 6hrs shown in Figure 3.44. After the pressure front has arrived at the "τ" distance of $10hr^{0.5}$, the reflection from the no-flow boundary of the reservoir can be more felt, which can be represented by the sharp decreeing $w(\tau)$ function when the "τ" distance is greater than $10hr^{0.5}$ (Figure 3.21).

Figure 3.45 to Figure 3.47 show that the asymptotic pressure approximation can barely represent the ECLIPSE calculated pressure transient behavior only within a short period of 1min. Beyond this very early time of simulation, multiple local reflections of the pressure front can be observed from the multiple decreasing trends of the $w(\tau)$ function

that occurs at short "τ" distances from the well (Figure 3.22 to Figure 3.24). These correspond to the rapidly deteriorated correlation between the pressure drop derivatives calculated from the asymptotic pressure approximation and those from ECLIPSE simulation (Figure 3.45 to Figure 3.47). This situation becomes even worse if the production well is located at the low-permeability cells within the two layers of the SPE10 model (Figure 3.45 and Figure 3.47; Table 3.6), in which cases the asymptotic pressure approximation shows to be invalid during most of the simulation time.

The asymptotic pressure approximation relies upon an assumption that the DTOF contour generated from solving the Eikonal equation is aligned with the pressure contour around the production well. When transient flow occurs in homogeneous and "sufficiently" smooth heterogeneous media, local reflections of the pressure front will not be strongly felt. But the pressure front "reflection" becomes more obvious when the reservoir media are highly heterogeneous. By testing the methodology from the highly heterogeneous SPE10 model, we can see that the asymptotic pressure approximation is more appropriate for describing transient pressure behavior in reservoir models with smoothly varying heterogeneity.

3.5 Discussion

The asymptotic pressure approximation to the diffusivity equation proves to be an efficient methodology for characterization of the transient pressure behavior in the reservoir porous media. It relies significantly upon the DTOF calculation and the drainage volume formulation, which could provide us a geometric understanding of the pressure

front propagation in the subsurface. This cannot be easily achieved by the conventional reservoir simulation (e.g. the finite difference method, finite volume method and finite element method, etc.). Accurate calculation of the drainage volume is crucial for DTOF-based pressure transient analysis as well as the transient flow simulation.

Discretization analysis of the Eikonal equation and the potential DTOF solutions proves that an extension of the FMM from the block-centered scheme (C5) to a discretization scheme capable of describing pressure propagation in more directions is needed. Evaluation of the DTOFs at both the grid-cell vertex and center can not only significantly improve the accuracy of the Eikonal solution, it can also better capture pressure propagation in low permeability regions. In addition, the near-well pressure gradient can be better represented by adding one more degree of freedom of the DTOF at the edge center of the well cell. Ensuring both computational accuracy and efficiency, the C5V9 (LGR) FMM proves to be the most appropriate discretization scheme for solving the Eikonal equation and constructing the 2D drainage volume.

Our study shows that the drainage volume is mainly affected by the discretization scheme at early times of flow simulation and relies more on the accuracy of DTOFs calculated from the FMM at later times. A hybrid construction of the drainage volume which utilizes the analytic, piecewise linear as well as piecewise constant formulations of the cumulative pore volume leads to a significantly improved numerical solution. The complete form of hybrid drainage volume is more appropriate for $w(\tau)$ calculation based upon the minimum and maximum grid-cell DTOFs calculated from the FMM. The

reduced form of hybrid drainage volume construction can improve the computational efficiency for pressure transient analysis without losing much accuracy.

One primary limitation of our methodology is the assumption that the porous media are "sufficiently" smooth and the heterogeneity is not quite large. So that the pressure (drop) gradient can be approximated by the DTOF gradient and the pressure transient can be efficiently calculated. This assumption is valid when the $w(\tau)$ function generated from the cumulative pore volume is "smoothly" increasing with the DTOF (τ). However, this assumption becomes less valid if the asymptotic pressure approximation is applied in highly heterogeneous reservoir models. Multiple decreasing trends of the $w(\tau)$ function represent multiple local reflections of the pressure front within the highly heterogeneous porous media.

3.6 Section Summary

We proposed a novel method to characterize drainage volume and simulate transient flow in porous media by means of the "diffusive time of flight" (DTOF) calculated from the fast marching method (FMM). Application of the FMM to DTOF (τ) calculation and transient flow simulation in the reservoir can make the computational speed orders magnitude faster than conventional reservoir simulators. This method relies heavily upon construction of the cumulative pore volume as a function of the DTOF and calculation of its DTOF derivative, $w(\tau)$.

Based on above analysis of drainage volume and transient flow simulation using the DTOF, following conclusions can be drawn:

1) Discretization analysis of the drainage volume for the 2D infinite-acting flow shows that application of the piecewise constant or piecewise linear form of drainage volume will generate an inaccurate solution, especially at very early times of simulation.
2) Application of an analytic form of drainage volume within the orthogonal well cell can help significantly reduce the discrepancy between the numerical and analytic solutions.
3) Hybrid versions of drainage volume, in which different orders of $w(\tau)$ are applied on rectangular cells, help generate a consistently horizontal well test derivative curve for the infinite-acting radial flow (IARF) in homogeneous media.
4) Discretization of the Eikonal equation proves to have great impacts upon the accuracy of DTOF calculation, which will also affect the accuracy of the drainage volume solution.
5) Following the hybrid construction of the cumulative pore volume as a function of the DTOF, $V_p(\tau)$, a hybrid $w(\tau)$ function can be calculated by a local differentiation of the incremental pore volume to the incremental DTOF (τ) value across each one of the τ-intervals. Generation of the τ-intervals can be independent of the FMM calculated DTOFs within the grid cells.
6) The hybrid $w(\tau)$ function converges to a stable distribution after the grid refinement beyond the first analytic τ-interval achieves a certain level. This

$w(\tau)$ function can help generate a stable pressure solution to the DTOF-based one-dimensional diffusivity equation.

7) The $w(\tau)$ function generated from the hybrid cumulative pore volume function can be used to describe the reservoir heterogeneity. A smoothly increasing $w(\tau)$ function represents the pressure front propagation from the well without much hindrance. The decreasing $w(\tau)$ function represents the reflection of the pressure front from either the no-flow reservoir boundary or the high-contrast porous media within the reservoir model.
8) When the infinite-acting flow occurs in the reservoir, the transient drainage volume calculated from the DTOF proves to be consistent with the pressure solution from the one-dimensional diffusivity equation.
9) The validity of the asymptotic pressure approximation proves to be significantly affected by the reservoir heterogeneity. Thus, it is recommended to evaluate the reservoir heterogeneity first before applying this methodology to pressure transient analysis in heterogeneous reservoir models.

4. INTEGRATION OF PRESSURE TRANSIENT DATA INTO RESERVOIR MODELS USING THE FAST MARCHING METHOD*

Calibration of reservoir model properties by integration of well test data remains an important research topic. Well test data has been recognized as an effective tool that can be used to describe transient flow behavior in petroleum reservoirs. It is also closely related to the drainage volume of the well and the pressure front propagation in the subsurface. Traditional analytic means of estimating reservoir permeability relies on an interpretation of the diagnostic plot of the well pressure and production data, which usually leads to a bulk average estimation of the reservoir permeability. When more detailed characterization of reservoir heterogeneity is needed, a robust forward model needs to be established and a numerical inversion technique is required.

We utilize the concept of the "diffusive time of flight" (DTOF) to formulate an asymptotic solution of the diffusivity equation that describes transient flow behavior in petroleum reservoirs. The DTOF is obtained from the solution of the Eikonal equation using the fast marching method (FMM). It may be used as a spatial coordinate which reduces the three dimensional diffusivity equation to an equivalent one dimensional formulation. We investigate the drainage volume evolution as a function of time in terms

---

*Material adapted with permission from "Integration of Pressure Transient Data Into Reservoir Models Using the Fast Marching Method" by Li, C. and King, M.J., 2016: Paper SPE-180148-MS Presented at the SPE Europec featured at 78th EAGE Conference and Exhibition in Vienna, Austria, 30 May-2 June 2016.

of the DTOF. The drainage volume may be directly related to the well test derivative which may be used in an inversion calculation to calibrate reservoir model parameters.

The analytic sensitivity coefficients of well test derivative with respect to reservoir properties are derived and incorporated into the objective function to perform history matching. The key to formulating the sensitivity coefficients is to utilize the functional derivative of the Eikonal equation to derive the analytic sensitivity of the DTOF to reservoir permeability. Its solution is implemented by tracking the characteristic trajectory of the local Eikonal solver within the FMM. The major advantage of formulating sensitivity coefficients using the FMM is its great computational efficiency while inversion is conducted.

This inverse modeling approach is tested on a two-dimensional synthetic heterogeneous reservoir model and then applied to the three-dimensional Brugge field, where a single well with constant flow rate is simulated. The well test derivative is shown to be inversely proportional to the drainage volume and is treated as the objective function for inversion. With an additional constraint to honor the prior model, our inverse modeling approach will adjust the reservoir model to obtain permeability as a function of distance from the well within the drainage volume. It provides a modification of reservoir permeability both within and beyond the depth of investigation (DOI).

4.1 Introduction

Adjusting reservoir model parameters frequently involves integrating dynamic data to characterize subsurface heterogeneity. Pressure transient information is widely

used in history matching of reservoir models because of its ready availability and rapid response at the well. The well pressure response can be affected by both geometry and flow properties of the reservoir. One may estimate bulk reservoir properties around the injection or production well by analyzing the well test curve (Miller et al., 1950; Ehlig-Economides and Joseph, 1987). Though merely applying to a limited amount of idealized models, the analytic approach provides the simplest way to obtain reservoir parameters through analysis of pressure changes. Many definitions about the concept of radius of investigation (ROI) relate to the propagation of a pressure disturbance or detectable pressure or rate changes in space (Kuchuk, 2009; Datta-Gupta et al., 2011). Based on the ROI, the near-well effective permeability can be estimated as a function of distance from the well from pressure transient data (Oliver, 1990, 1992; Feitosa et al., 1994; Sagar et al., 1995; Thompson and Reynolds, 1997).When more detailed characterization of reservoir heterogeneity is needed, a numerical inversion technique is required to integrate the dynamic observational data into reservoir models (Tarantola, 2005).

Reservoir parameter estimation from inverse modeling usually relies upon establishment of a robust forward model and determination of an objective function to be minimized. The forward model formulated in differential equations that governs the physical process of subsurface flow in the reservoir media requires numerical simulation of pressure and fluid communications between discretized grid cells. The objective function is frequently used to measure the difference between the observational data and calculated reservoir response at the well, which can be predicted by the forward model (Tarantola, 2005; Oliver et al., 2008). Minimization of the objective function can be

achieved using a gradient-based algorithm, which requires calculation of the sensitivity coefficients of the objective function with respect to reservoir parameters. Sensitivity-based inversion often entails calculation of partial derivatives of the objective function to reservoir properties in all grid cells of the model, which becomes considerably expensive and even computationally infeasible as the model grows to a large size (Yeh, 1986; Oliver et al., 2008).

Given the crucial role played by sensitivity calculation in gradient-based inversion, extensive research efforts have been made to calculate the sensitivity coefficient using more efficient approaches when integrating pressure transient data into reservoir models (e.g. the Modified Generalized Pulse Spectrum Technique (MGPST) (Chu et al., 1995a) and the linear search procedure (Landa and Horne, 1997; Landa et al., 2000)). The Bayesian approach is the most popular probabilistic inversion methodology, where the a priori static geologic information is contained in a prior probability density function (PDF) and the a posteriori PDF provides the solution to the inverse problem (Duijndam, 1988a, b; Oliver et al., 2008). The sensitivity coefficients of the well pressure data to reservoir model parameters can be included into a composite objective function to be minimized using the Maximum a Posteriori (MAP) estimation of reservoir parameters (e.g. the Gauss-Newton and Levenberg-Marquardt algorithms). By using models that are linearized about the maximum likelihood point, multiple generalizations of the permeability field conditioned to the well test data can be realized (Oliver, 1996) and extended to the three-dimensional reservoir model (He et al., 1997). The computational cost in inversion can be decreased by implementing a subspace method to reparameterize the reservoir model

(Reynolds et al., 1996; Abacioglu et al., 2001). Stochastic modeling and geostatistics can be used to reduce uncertainty when calibrating reservoir model parameters and provide optimization algorithms for automatic history matching of reservoir models with well pressure and production data (Reynolds et al., 1999; Zhang et al., 2002; Zhang and Reynolds, 2002). The gradient-based history matching of reservoir models with pressure transient data can also be connected with the application of the the Monte Carlo (MC) method (Oliver, 1996), the Markov chain Monte Carlo (MCMC) method (Oliver et al., 1996; Oliver et al., 1997; Bonet-Cunha et al., 1998), and the ensemble Kalman filter (EnKF), where the sensitivity coefficients are approximated through an ensemble of realizations of the observational data and model parameters at each analysis step (Chen and Zhang, 2006; Zafari and Reynolds, 2007; Oliver et al., 2008; Oliver and Chen, 2011).

The asymptotic approach has been widely used in geometric optics and seismology. Many of its concepts related to propagating interfaces also prove to be valuable in reservoir engineering. Both the concept of radius of investigation (ROI) in homogeneous media (Lee, 1982) and its extension to depth of investigation (DOI) in heterogeneous media (Datta-Gupta et al., 2011) can be interpreted as the propagation distance of the "peak" pressure disturbance for an impulse source or sink. By deriving the high frequency asymptotic expansion form of the diffusivity equation, Vasco et al. (1999 and 2000) and Kulkarni et al. (2001) introduced the concept of "diffusive time of flight" (DTOF) that has a unit of (time)1/2. Based on the asymptotic method and the DTOF, pressure transient data were integrated into reservoir models by formulating analytic sensitivity coefficients along the pressure gradient trajectories, which can be approximated

as the streamline trajectory (Datta-Gupta and King, 1995). Thus, the sensitivity matrix required for solving the inverse problem can be constructed in an analytic form using one single forward simulation and the computational speed will be tremendously accelerated. Xie et al. (2015a, b) developed a new asymptotic approach to formulating the "drainage volume" using the DTOF and integrated production history of shale gas into the reservoir model. This methodology associates the propagation of the peak of a pressure pulse with the DTOF that can be calculated by solving the Eikonal equation using the fast marching method (FMM). By taking a high-frequency asymptotic solution of the classic three-dimensional diffusivity equation for general heterogeneous reservoir models, a one-dimensional diffusivity equation was formulated in terms of the DTOF, which provides a convenient forward modeling approach for rapid field-scale performance assessment and reservoir parameter estimation in history matching by use of a genetic algorithm (Zhang et al., 2016). King et al. (2016) and Wang et al. (2017) improved this asymptotic methodology by redefining the "drainage volume" and reformulating the ROI and DOI in terms of the DTOF.

In this section, we propose a novel methodology for integrating well test data with a prior geologic model for inverse modeling. The approach is based upon the use of the DTOF (τ) to characterize the geologic model. The forward model is established by using an approximate pressure solver, from which the initial and predicted well test data are calculated analytically. One single production well is placed in the reservoir to record pressure and construct the well test derivative as the objective function in history matching. By tracking the characteristic trajectory of the local Eikonal solver proposed by

Qian et al. (2007), which is included in the FMM algorithm we propose, an analytic calculation of the sensitivity of well test derivative to reservoir properties is performed to support the inversion for reservoir permeabilities. The main advantage of using the FMM to solve the Eikonal equation and run the forward model is its great computational efficiency that makes the inversion tremendously faster than those traditional gradient-based methods. By means of evaluating the sensitivity coefficient of the well test derivative with respect to reservoir permeability on each "τ-interval" instead of each Cartesian grid cell, sensitivity calculation becomes independent of the size of the 3D reservoir inversion problem. Comparing with the numerical perturbation scheme, this new approach for analytic sensitivity coefficients construction makes the computational speed orders of magnitudes faster.

4.2 Methodology: Inversion Approach

The methodology we propose relies upon the asymptotic pressure approximation to the diffusivity equation that can be used to describe transient pressure behavior in heterogeneous porous media. It transforms the 3D diffusivity equation into an equivalent 1D form using the "diffusive time of flight" (DTOF), which can be calculated from solving the general anisotropic Eikonal equation. Based upon the DTOF, we set up the forward mathematical model in the form of the drainage volume as well as the well test derivative, which can be treated as the objective function for inverse modeling. Then their sensitivity coefficients with respect to reservoir permeability are formulated analytically by taking the functional derivative of the Eikonal equation, which are then included in a penalized

form of the objective function that is used for history matching of the reservoir model with well test data.

4.2.1 Validation of the Forward Model

The forward model used for inversion is derived from the asymptotic pressure approximation for the constant flow-rate well test.

$$c_t \frac{\partial p}{\partial t} = \frac{1}{w(\tau)} \frac{\partial q}{\partial \tau} \approx -\frac{q_w}{V(t)} e^{-\tau^2/4t} \tag{4.1}$$

where the DTOF (τ) is obtained by solving the Eikonal equation.

$$\nabla \tau(\vec{x}) \bullet \vec{\vec{k}}(\vec{x}) \bullet \nabla \tau(\vec{x}) = \phi(\vec{x}) \mu c_t \tag{4.2}$$

or

$$\nabla \tau(\vec{x}) \bullet \vec{\vec{\alpha}}_D(\vec{x}) \bullet \nabla \tau(\vec{x}) = 1 \tag{4.3}$$

where $\vec{\vec{\alpha}}_D(\vec{x})$ is the diffusivity tensor evaluated at location $\vec{x}$, which can expressed as

$$\vec{\vec{\alpha}}_D(\vec{x}) = \frac{\vec{\vec{k}}(\vec{x})}{\phi(\vec{x}) \mu c_t} \tag{4.4}$$

The numerical DTOF (τ) solution to the Eikonal equation is calculated using the FMM. Then, the forward model is obtained from the drainage volume as a function of time and from the corresponding well test derivative.

$$V(t) = \int_{\tau=0}^{\infty} dV_p(\tau) \cdot e^{-\tau^2/4t} = \int_{\tau=0}^{\infty} d\tau \cdot w(\tau) \cdot e^{-\tau^2/4t} \tag{4.5}$$

$$\Delta p'_{wf} \equiv \frac{d\Delta p_{wf}}{d\ln(t)} = t \cdot \frac{d\Delta p_{wf}}{dt} \approx \frac{q_w \cdot t}{c_t \cdot V(t)} \tag{4.6}$$

The drainage volume (Eq.(4.5)) used for inversion is constructed in the reduced hybrid form as discussed in **Section 3**. Then the well test derivative is formulated as inversely proportional to the drainage volume with a constant production rate at the well (Eq.(4.6)).

Suppose there is a 2D reservoir model with an equal length and width of 10,000ft as well as a uniform thickness of 10ft. It is discretized into a 51x51 square grid system, with a vertical well placed at the center of the model (26, 26). The reservoir media are homogeneous and isotropic, with a uniform permeability of 20md and porosity of 0.1. All other reservoir geometry information and fluid properties are listed in Table 4.1.

Table 4.1 Input parameters for the 2D radial flow in a square-shaped reservoir model

LX	10,000	ft	k	20	md
LY	10,000	ft	ϕ	0.1	
h	10	ft	μ	1	cp
NX	51		c_t	1.0E-5	psi^{-1}
NY	51		B_o	1	res bbl/STB
Well	(26, 26)		q_w	100	res bbl/day

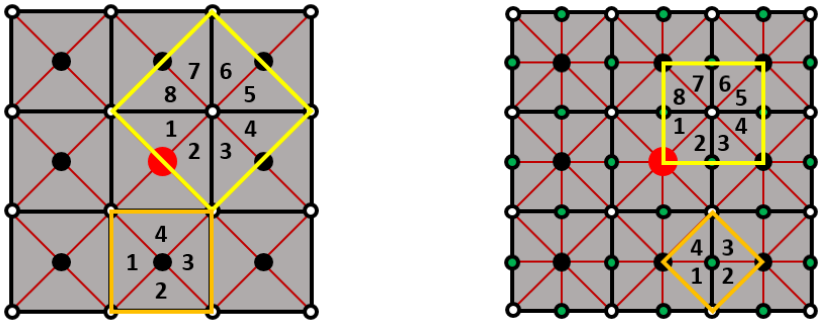

(a) 2D C5V9 FMM **(b) 2D C9V9E5 FMM**

Figure 4.1 Illustration of triangulation of square cells that comprise the 2D reservoir model where the FMM can be implemented (reprinted with permission from Li and King, 2016)

In Section 3, the 2D C5V9 (LGR) discretization scheme for the Eikonal equation is extended from the 2D C5V9 discretization scheme. In such a way, the pressure gradient close to the wellbore can be better approximated by the DTOF gradient when the DTOF values to the centers of grid cells adjacent to the well cell are more accurately calculated from the FMM. In this section, we further extended the 2D C5V9 FMM (Figure 4.1a) to a 2D C9V9E5 FMM by adding more degrees of freedom of the DTOF to the edge center of the 2D orthogonal grids (Figure 4.1b). Each unknown DTOF value in the 2D space will be determined from its neighboring four or eight local Eikonal solutions. Only the minimum local Eikonal solution among the neighboring four our eight candidate solutions will be used to update the unknown DTOF. The index of the minimum local Eikonal solution can also be recorded when DTOFs are calculated within the FMM algorithm, which will help generate analytic sensitivity coefficients of DTOFs with respect to reservoir model parameters in the inversion (Figure 4.1). Accuracy of FMM calculated

DTOFs to reservoir regions far away from the wellbore can be further improved, which will make the hybrid drainage volume (in the reduced form) converge faster to the analytic solution. The C9V9E5 discretization scheme is used for DTOF calculation from the FMM, which provides the basis for the 2D drainage volume forward model construction and the subsequent inverse modeling (Figure 4.1b).

We first conduct a convergence analysis for the numerical drainage volume by comparing it with the infinite-acting analytic solution for 2D radial flow in homogeneous reservoir media. The hybrid drainage volume under different grid-cell resolutions (3x3, 5x5, 11x11, and 51x51, respectively) is analyzed under two well tests of 240 hours and 1200 hours, respectively (Figure 4.2).

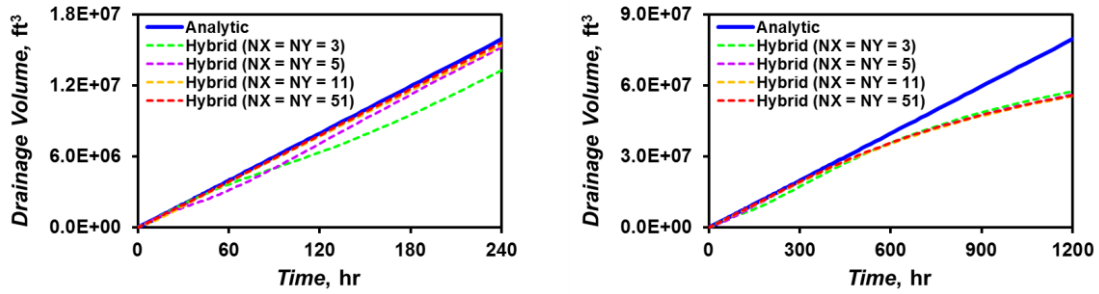

(a) 240hrs **(b) 1200hrs**

Figure 4.2 Convergence analysis of hybrid drainage volume discretization using the C9V9E5 FMM for 2D radial flow (reprinted with permission from Li and King, 2016)

After comparing the simulations, it is easy to find that the hybrid drainage volume matches well with its analytic solution at very early times of flow (Figure 4.2a). Meanwhile, it converges to the analytic solution with DTOFs calculated from the C9V9E5

FMM, even on a coarse grid. However, as expected, the hybrid solution will diverge from the infinite-acting analytic solution as the flowing time becomes longer than when the pressure front has arrived at the no-flow reservoir boundary (Figure 4.2b).

This flow regime transition can also be reflected in the diagnostic plot, when the well test derivative changes from an early horizontal line representing IARF to a later curve with a non-zero slope. It is quite important to validate the flow regime as transient infinite-acting flow before establishing the forward model for inversion, making sure that no significant boundary effects can be felt during history matching. On the basis of the hybrid drainage volume, the well test derivative for 2D/3D IARF can be set up and its sensitivity coefficients with respect to reservoir parameters can be derived in an analytic form.

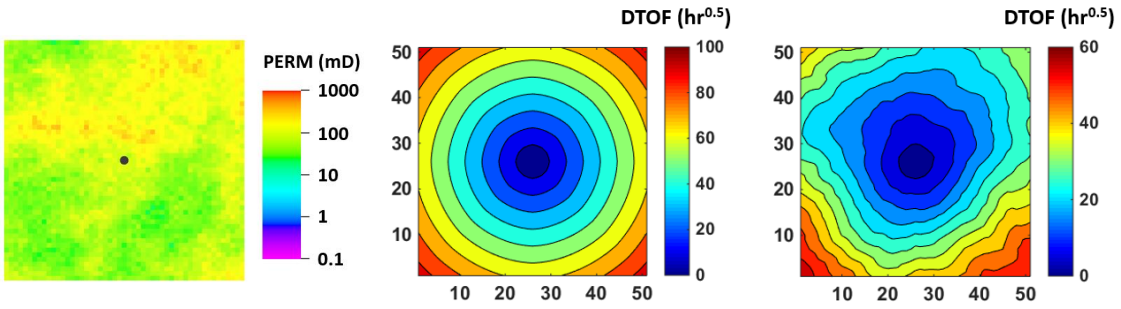

(a) Heterogeneous KX VPD = 0.4617

(b) DTOFs within homogeneous media

(c) DTOFs within heterogeneous media

Figure 4.3 Permeability and DTOFs calculated from C9V9E5 FMM within a 51x51 uniform square grid system (reprinted with permission from Li and King, 2016)

Calculation of the DTOF using the FMM provides the basis for understanding of the pressure front propagation using the depth of investigation (DOI). We calculate the DTOFs for both a homogeneous reservoir (with a uniform permeability value of 20md) and a heterogeneous reservoir (Figure 4.3) with one vertical well located at the reservoir center by solving the Eikonal equation (Eq.(4.2)) using the C9V9E5 FMM (Figure 4.1b). In both cases, the DTOF has a minimum zero value at the well location and increases monotonically to the outer boundary. In particular, the DTOF distribution in the homogenous reservoir is radial because of the isotropy of the permeability (Figure 4.3b). The maximum DTOF values calculated from the C9V9E5 FMM in the homogenous and heterogeneous reservoir models are 97.4hr$^{0.5}$ and 59.7hr$^{0.5}$, respectively.

Based on the asymptotic pressure approximation, we can define the concepts of depth of investigation (DOI) and "limit of detectability" (LOD) using the DTOF, which can both be expressed as a function of time (King et al., 2016; Wang et al., 2017). The DOI can be calculated based on the hybrid drainage volume formulation that has been discussed in **Section 3**.

$$\tau_{DOI}^2 = \frac{\int_{\tau=0}^{\infty} dV_p(\tau)\cdot\tau^2\cdot e^{-\tau^2/4t}}{\int_{\tau=0}^{\infty} dV_p(\tau)\cdot e^{-\tau^2/4t}} = \frac{\int_{\tau=0}^{\infty} dV_p(\tau)\cdot\tau^2\cdot e^{-\tau^2/4t}}{V(t)} \tag{4.7}$$

The numerator in Eq.(4.7) can also be calculated in a hybrid version, which is similar to the way drainage volume is discretized. For the infinite-acting flow occurring in the homogeneous models and sufficiently smooth heterogeneous models (VPD =

0.4617 in this case), there exists an approximate relationship between the DOI expressed in terms of the DTOF and the time (King et al., 2016; Wang et al., 2017).

$$\frac{\tau_{DOI}^2}{4t} \cong 1 \tag{4.8}$$

Similarly, the LOD can be defined as (King et al., 2016; Wang et al., 2017)

$$\frac{\tau_{LOD}^2}{4t} = 4 \tag{4.9}$$

For an infinite-acting flow in homogeneous and smooth heterogeneous media, it can be estimated that the LOD is approximately twice as large as the DOI in terms of the DTOF at a given time (Eq.(4.8) and Eq.(4.9)). Defining the DOI and LOD using the DTOF provides a convenient way to characterize the pressure front propagation in the subsurface.

The validity of asymptotic pressure approximation for the infinite-acting radial flow (IARF) in homogeneous media has been demonstrated in **Section 3**. We need to validate its application within the heterogeneous reservoir model (Figure 4.3a), which has a Dykstra-Parsons coefficient (VDP) of 0.4167, before it can be treated as the reference model for inversion. After calculating the DTOF values generated from the heterogeneous reservoir model using the FMM, we can construct the hybrid drainage volume (Eq.(4.5)) and the well test derivative (Eq.(4.6)).

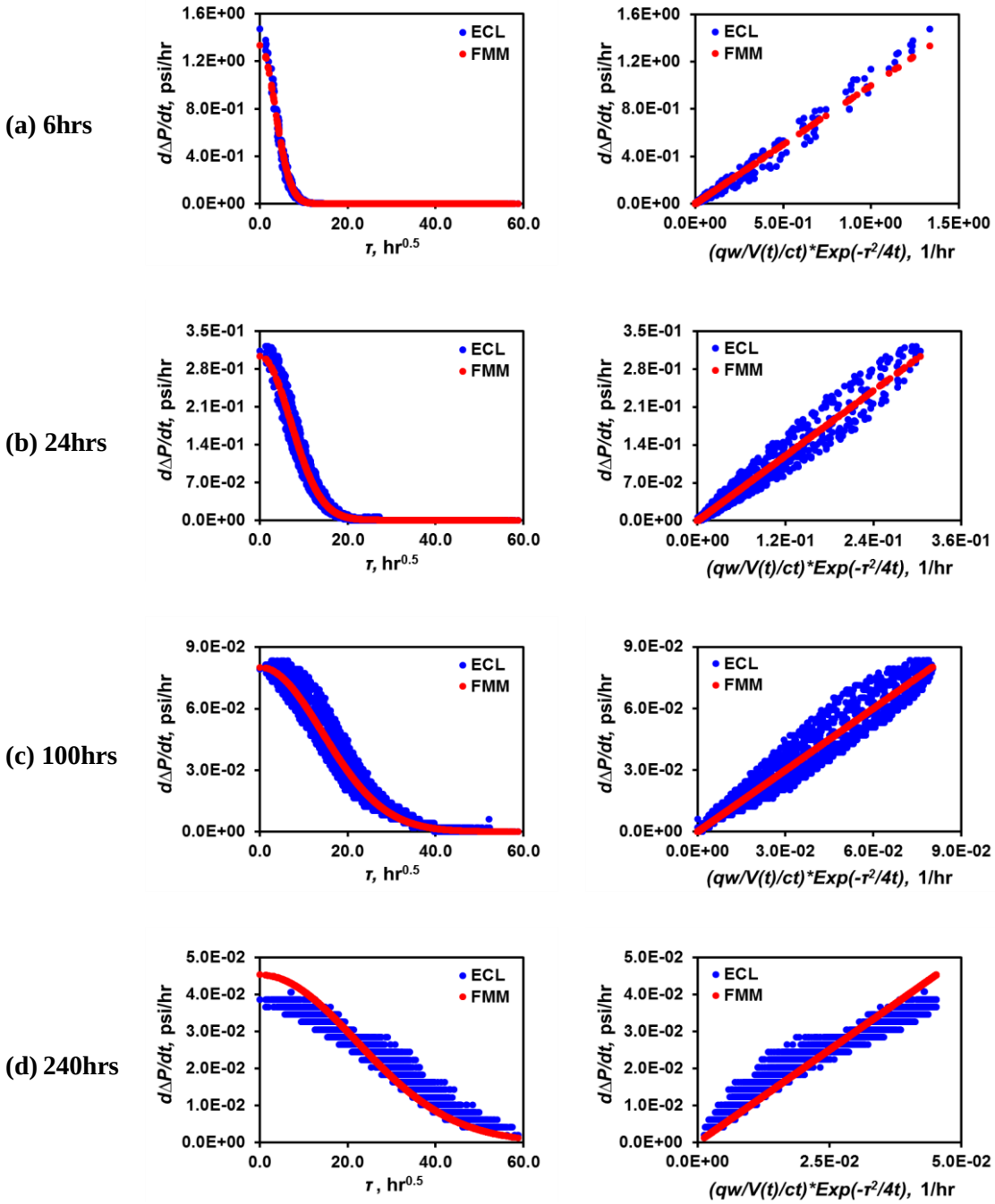

Figure 4.4 Validation of the asymptotic pressure approximation with ECLIPSE simulation within the 2D heterogeneous reservoir model (51x51, Well (26, 26), VDP = 0.4167) under a constant flow rate well test (q_w = 100 res bbl/day)

Figure 4.4 shows the validation of pressure generated from the asymptotic pressure approximation with that generated from the numerical reservoir simulator (ECLIPSE) in the 2D heterogeneous reference model. The production well is placed at the reservoir center with a constant rate of 100 res bbl/day. Other input parameters for the 2D reservoir models are listed in Table 4.1. We plot the time derivative of the pressure drop against the DTOFs calculated from the FMM and against the drainage volume weighted exponential terms of the asymptotic pressure approximation (Eq.(4.1)). The overall performance of the asymptotic pressure approximation can reflect the real transient flow behavior within a 100hrs of constant flow rate well test, without significant boundary effects being felt (Figure 4.4a, b and c). Beyond 100hrs, the linear relationship between FMM and ECLIPSE calculated reservoir pressures deteriorates and the transient state of flow can no longer be ensured (Figure 4.4d).

Within 100hrs, the pressure drop derivative with respect to time generated from the asymptotic pressure approximation is in good agreement with the ECLIPSE calculation. The pressure drop calculated from the asymptotic pressure approximation has a strong linear relationship with that from the ECLIPSE simulation (Figure 4.4a, b and c). Even at 100hrs, the LOD approximately estimated as $40hr^{0.5}$ (Eq.(4.9)) is still less than the maximum reservoir DTOF value of $59.7hr^{0.5}$. Thus, a well test period of time up to 100 hours is used for pressure transient analysis so that no much boundary effect will be felt when the pressure front propagates in the reservoir media.

4.2.2 Sensitivity Coefficient Formulation

Formulation of the analytic sensitivity coefficients of the objective function with respect to reservoir parameters plays a crucial role in inverse modeling and history matching. They relate reservoir response at the well to reservoir property disturbance at other locations within the reservoir model. We consider variations in the permeability tensor that maintain the local anisotropy but which modify the magnitude of the permeability:

$$\delta\vec{\vec{\boldsymbol{k}}}(\vec{x}) = \left(\delta \ln k(\vec{x})\right)\cdot\vec{\vec{\boldsymbol{k}}}(\vec{x}) \tag{4.10}$$

where $\delta \ln k(\vec{x})$ is the variation in the natural logarithm of the permeability tensor $\vec{\vec{\boldsymbol{k}}}(\vec{x})$. Formulation of analytic sensitivity coefficients for permeability inversion in 2D/3D reservoir models can be achieved by taking the functional derivative of the Eikonal equation with respect to the reservoir parameter.

$$\left(\frac{\vec{\vec{\boldsymbol{k}}}(\vec{x})}{\phi(\vec{x})\mu c_t}\bullet\nabla\tau(\vec{x})\right)\bullet\left(\nabla\delta\tau(\vec{x};\vec{x}')\right) = -\frac{1}{2}\cdot\delta\ln k(\vec{x}')\cdot\delta(\vec{x}-\vec{x}') \tag{4.11}$$

The left hand side of Eq.(4.11) consists of two parts. The first part indicates the characteristic direction within the local Eikonal solver and the second part represents the gradient of the DTOF sensitivity. The right hand side of Eq.(4.11) includes the variations in reservoir parameters. This formulation for the sensitivity coefficients relates DTOF changes in one location ($\vec{x}$) to reservoir property changes in another location ($\vec{x}'$). Numerical realization of the analytic sensitivity coefficient formulation relies upon tracing the characteristic vector direction of the local Eikonal solution within the FMM.

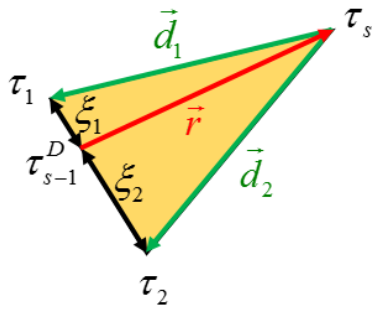

Figure 4.5 Lagrangian formulation of the local Eikonal solution

The local Eikonal solution within the FMM can be expressed using a Lagrangian formulation (Figure 4.5). If the solutions at two nodes of a specific triangular element are known (τ_1 and τ_2 in Figure 4.5), the DTOF to a parametric point on the upstream boundary of the domain is obtained by a linear interpolant

$$\tau_{s-1}^D = \sum_{m=1}^{N} \xi_m \tau_m \tag{4.12}$$

where ξ_m are non-negative weights ($\xi_m \geq 0$) and sum to unity, $\sum_{m=1}^{N} \xi_m = 1$. Here N can be 1, 2, or 3, depending on the 1D/2D/3D local Eikonal solution used within the FMM. Based upon Fermat's Principle, the unknown DTOF value at the remaining node of the triangular element (τ_s in Figure 4.5) can be updated along the characteristic direction. If we define $\vec{d}_m$ as the displacement vector measured from the location of the unknown τ_s, we will know the parametric point in terms of the displacement vectors.

$$\vec{r} = \sum_{m=1}^{N} \xi_m \vec{d}_m \tag{4.13}$$

Then we can calculate the DTOF difference distance between the upstream unknown node and downstream boundary within a triangular element as

$$\tau_s = \sqrt{\vec{r} \bullet \vec{\vec{\alpha}}_D^{-1} \bullet \vec{r}} + \tau_{s-1}^D = \sqrt{\vec{r} \bullet \vec{\vec{\alpha}}_D^{-1} \bullet \vec{r}} + \sum_m^N \xi_m \cdot \tau_m \tag{4.14}$$

If we use (i, j, k) as the index for a grid cell in 3D space, we can calculate the DTOF sensitivity with respect to the permeability within that particular cell as

$$\frac{\delta \tau_s}{\delta \ln k_{ijk}} = -\frac{1}{2}\left(\sqrt{\vec{r} \bullet \vec{\vec{\alpha}}_D^{-1} \bullet \vec{r}}\right) \cdot \delta_{ijk}^{Cell} + \sum_m^N \xi_m \cdot \frac{\delta \tau_m}{\delta \ln k_{ijk}} \tag{4.15}$$

Here, both the diffusivity $\vec{\vec{\alpha}}_D$ tensor and the weight ξ_m can be obtained from the local Eikonal solution. In such a way, formulation of the analytic sensitivity coefficient with respect to reservoir permeability through the functional derivative of the Eikonal equation can be realized on the grid-cell basis using Eq.(4.15). It can be readily achieved by post-processing the non-negative weights for each nodal DTOF value updated within the FMM in a sequential approach after one single forward simulation of the FMM.

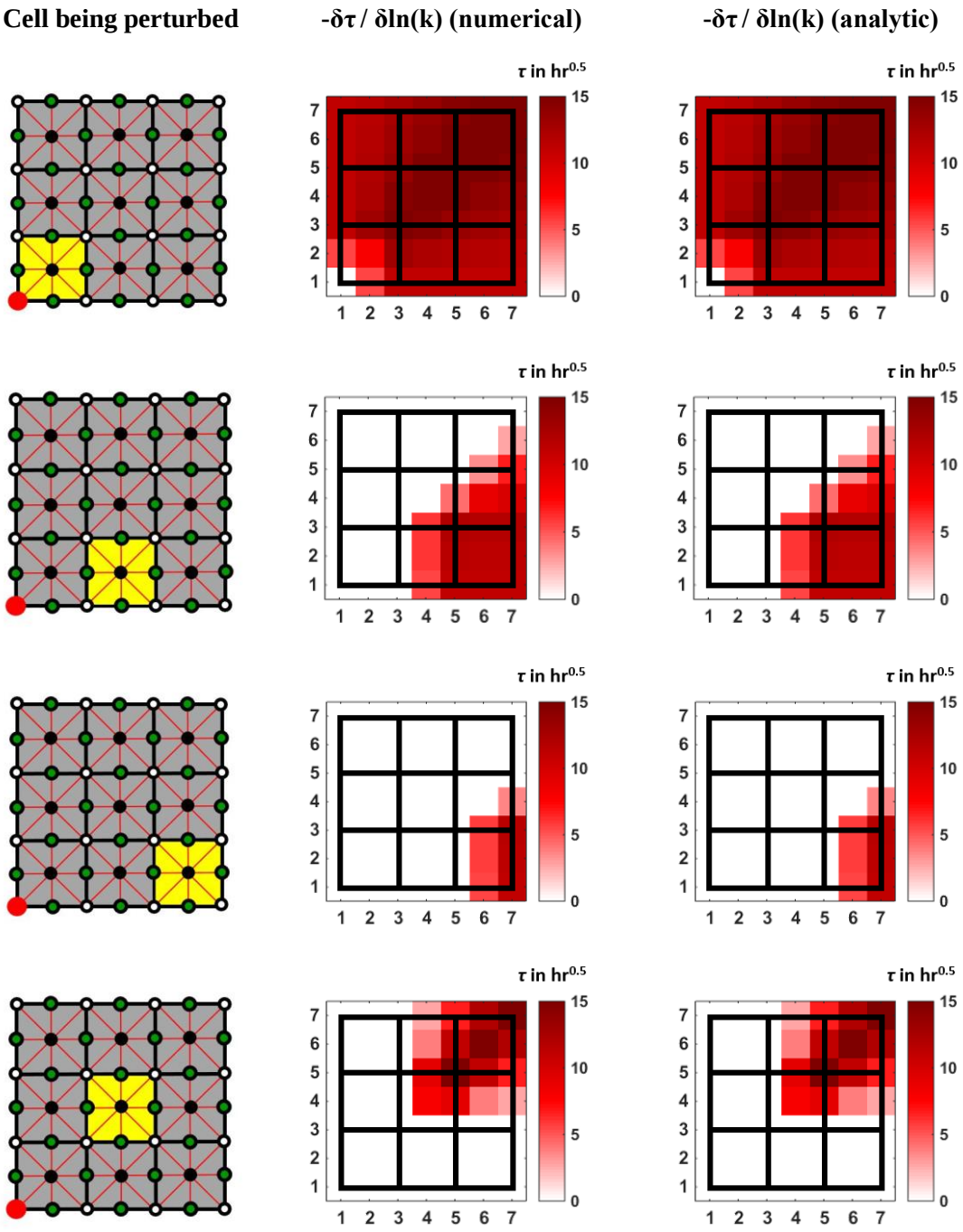

Figure 4.6 Dependence of the 2D sensitivity coefficients of the DTOFs with respect to the cell permeability for various positions of the perturbed cell using the 2D C9V9E5 FMM (δτ / δln(k) in $hr^{0.5}$) (reprinted with permission from Li and King, 2016)

To estimate the impact of grid-cell permeability disturbance on DTOF response of the reservoir model, a 2D model with homogeneous and isotropic media is investigated (Figure 4.6). It is discretized into a 3x3 square-grid system, within which each grid cell is subdivided into eight identical triangular elements so that the C9V9E5 FMM method can be applied. A line-source well is placed at the bottom-left corner of the reservoir model. The yellow cell represents the location where the reservoir permeability is being perturbed. From the bottom left to the top right of the modeling domain, the magnitude of DTOF disturbance in each grid cell is different. Only cells behind the cell being perturbed will be affected. We can also observe that the grid-cell based analytic sensitivity coefficients of DTOFs to reservoir parameters (Eq.(4.15)) obtained from the functional derivative of the Eikonal equation (Eq.(4.11)) show an excellent match with their numerical counterparts.

When the infinite-acting flow (IARF) occurs in "sufficiently" smooth heterogeneous media, there exists a strong relationship between the pressure contour and the DTOF contour (King et al., 2016). In such situations, it is reasonable to assume that the pressure gradient and the DTOF gradient are aligned and the Darcy velocity stays parallel to the scalar product between the permeability tensor and the DTOF gradient (Wang et al., 2017). The asymptotic pressure approximation we propose is suitable to establishing the forward model used for inversion. When the well test data is treated as the objective function, its sensitivity coefficients with respect to reservoir properties can be formulated analytically using the chain rule based on the DTOF sensitivity coefficients formulated (Eq.(4.11)).

Since we have constructed a hybrid form of the drainage volume as a function of time, $V(t)$, which consists of three parts that include an analytic form, a piecewise linear form and a piecewise constant form, it can be used to formulate the pressure transient sensitivity coefficients with respect to the grid-cell reservoir permeability.

$$\frac{\delta V(t)}{\delta \ln k_{ijk}} = \frac{\delta V_0(t)}{\delta \ln k_{ijk}} + \frac{\delta V_1(t)}{\delta \ln k_{ijk}} + \frac{\delta V_2(t)}{\delta \ln k_{ijk}} \tag{4.16}$$

Using the chain rule, the well test derivative sensitivity coefficients can be derived as

$$\frac{\delta \Delta p'_{wf}}{\delta \ln k_{ijk}} = -\frac{q_w \cdot t}{c_t \cdot V^2(t)} \cdot \frac{\delta V(t)}{\delta \ln k_{ijk}} \tag{4.17}$$

The analytic sensitivity coefficient of the pressure transient data with respect to reservoir permeability can later be included into a penalized objective function for inversion.

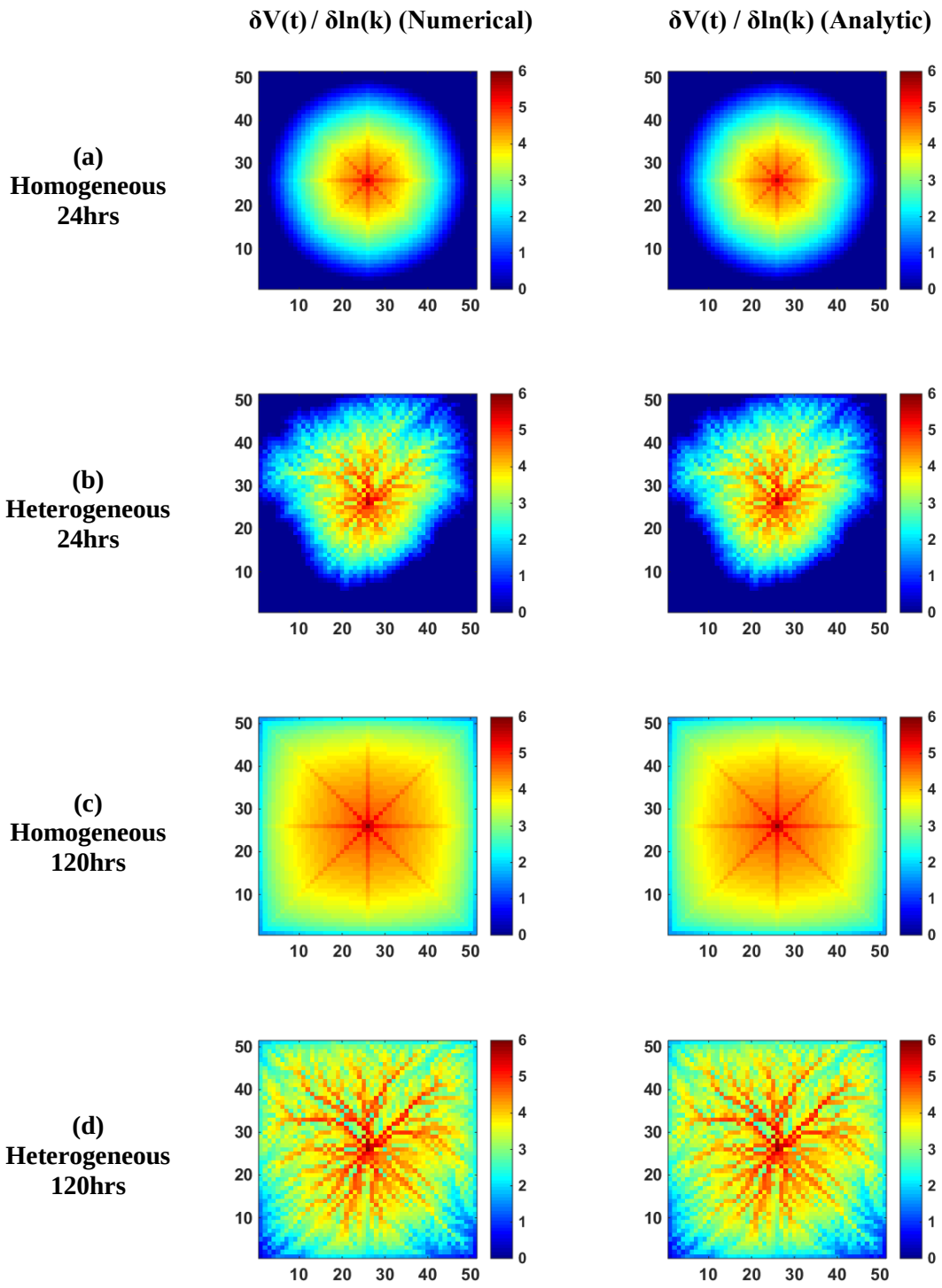

Figure 4.7 Sensitivity of the drainage volume with respect to the grid-cell reservoir permeability (reprinted with permission from Li and King, 2016)

In Figure 4.7, we demonstrate investigation of the sensitivity of drainage volume with respect to the grid-cell permeability with a homogeneous and heterogeneous reservoir model based on Eq.(4.16). The homogeneous model has a uniform permeability of 86.31md, which is the same as the average permeability value of the heterogeneous model. Both models are represented on a 51x51 square grid system, with the remaining reservoir properties listed in Table 4.1. The drainage volume sensitivity with respect to the grid-cell permeability for the entire reservoir model are evaluated numerically and analytically.

It can be easily observed that the analytic sensitivity coefficient of drainage volume with respect to reservoir permeability matches excellently with the numerical sensitivity coefficient. However, the drainage volume sensitivity coefficient evaluated on a grid-cell basis demonstrates a "dendritic" effect in both the homogeneous and heterogeneous models (Figure 4.7). This reflects the sensitivity preference along certain directions that might have adverse impacts upon the inversion results.

Assuming that there is a 2D reservoir model discretized into a limited number of grid cells and each grid cell has its unique reservoir properties (e.g., permeability and porosity). DTOFs to cell centers, cell vertices and cell edge centers can be calculated using the C9V9E5 FMM (Figure 4.1b). The local Eikonal solver can be easily implemented upon the basic triangular element within the square cell, so that the DTOF values can be updated in the upwind direction (Figure 4.8a).

Instead of calculating the sensitivity of DTOF to the permeability of a specific grid cell, we can analyze the DTOF sensitivity with respect to the permeability within a particular τ-interval that might have a DTOF range overlapping with it (Figure 4.8b).

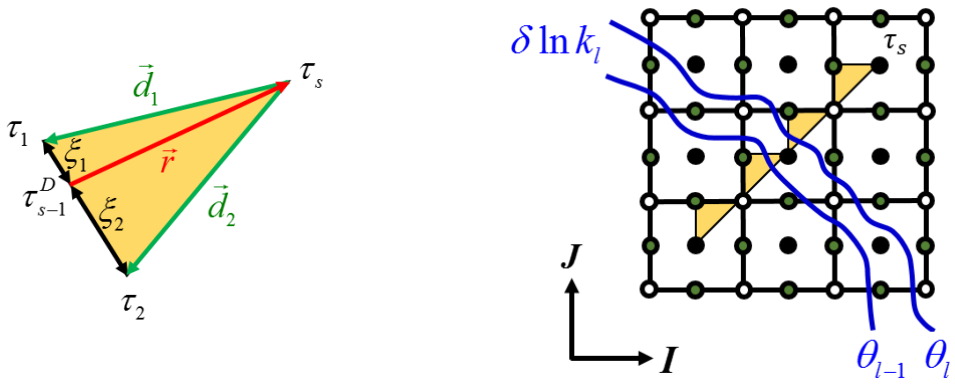

(a) local Lagrangian Eikonal solver **(b) τ-interval based sensitivity**

Figure 4.8 Calculation of the analytic sensitivity coefficient of the DTOF with respect to reservoir parameters within a τ-interval based on the functional derivative of the Eikonal equation

Combining with DTOFs calculated from the FMM in the upwind direction along the characteristic vector, sensitivity of DTOFs of the entire reservoir model with respect to the permeability within a specific τ-interval perturbed can be calculated sequentially.

$$\frac{\delta \tau_s}{\delta \ln k_l} = \frac{\delta \tau_{s-1}^D}{\delta \ln k_l} - \frac{1}{2} Max\left(Min\left(\tau_s, \theta_l\right) - Max\left(\tau_{s-1}^D, \theta_{l-1}\right), 0\right) \qquad (4.18)$$

Here θ_{l-1} and θ_l represent the lower and upper DTOF limits of the τ-interval being perturbed. Eq.(4.18) shows the sensitivity relationship between the upstream point and a downstream point, which essentially is the functional derivative of the Eikonal equation (Eq.(4.11)) discretized in a 1D form. It can be easily extended to multi-dimensional implementations if the causality information is retained when the DTOF is calculated using the FMM algorithm. More importantly, the sensitivity perturbation occurs only to

permeabilities within a limited number of τ-intervals so that the sensitivity coefficients can be generated without dependence upon the model size. In other words, the degrees of freedom of the reservoir parameters to be calibrated in inversion can be significantly reduced, which will make the computational efficiency of inverse modeling tremendously improved.

Based on the same homogeneous and heterogeneous reservoir models used for grid-cell based drainage volume sensitivity analysis (Figure 4.7), we investigate the DTOF sensitivity with respect to permeability perturbation within τ-intervals. In both cases, one single vertical well is located at the center (26, 26) of the 51x51 uniform square grid system and DTOFs are calculated using the C9V9E5 FMM (Figure 4.1b). From the FMM calculated DTOFs, the lower and upper limits of a particular τ-intervals can be set and used to calculate the sensitivity of DTOFs with respect to permeability within it for the entire reservoir model (Figure 4.9).

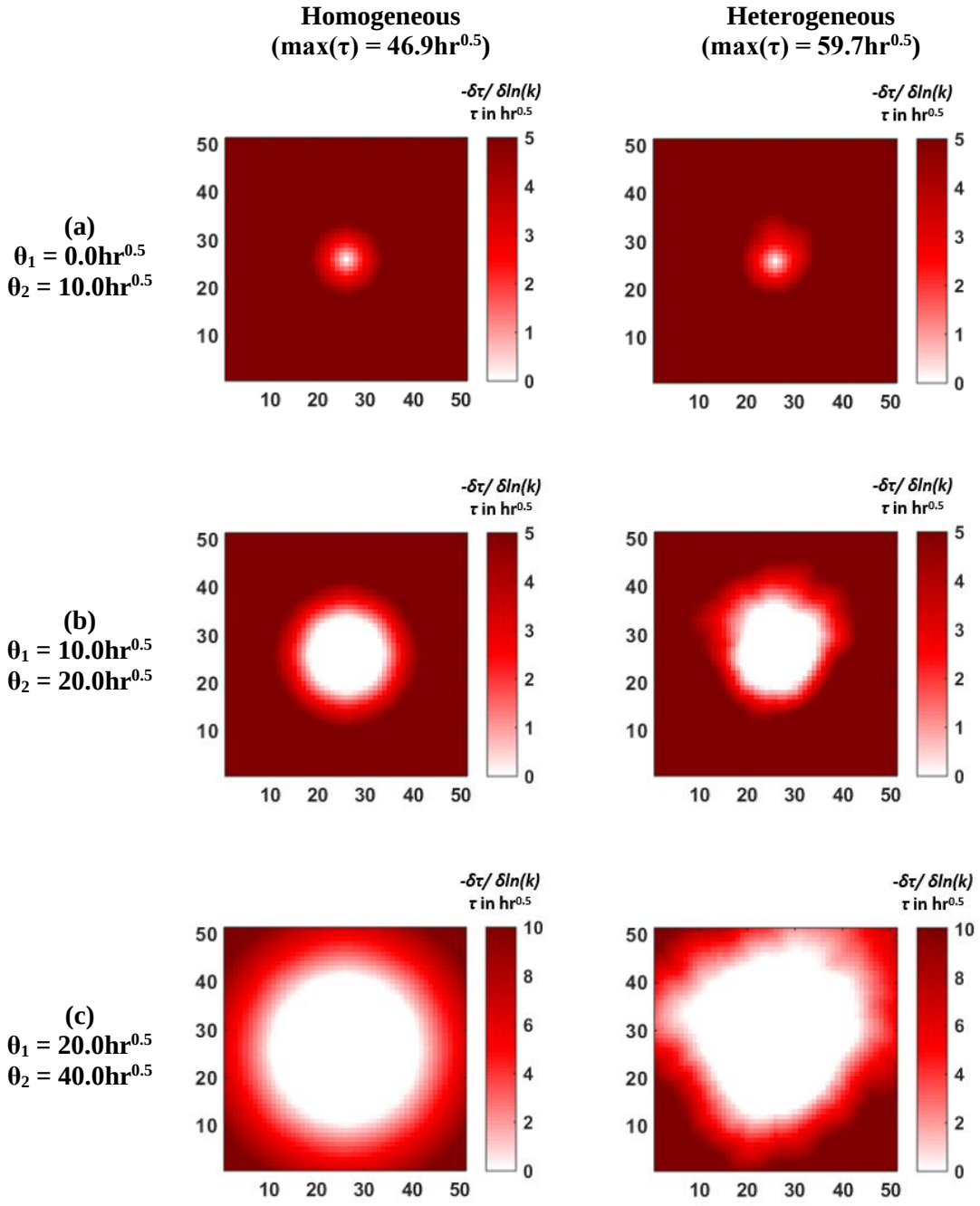

Figure 4.9 Analytic sensitivity of the DTOF with respect to reservoir permeability within the τ-interval calculated from C9V9E5 FMM for the 2D square reservoir model (51x51) with one production well at the reservoir center (26, 26)

If the lower τ-interval limit is set as zero and its upper limit is set as a positive value less than the maximum DTOF value of the reservoir model, the magnitude of DTOF sensitivity with respect to permeability keeps increasing to the outer reservoir boundary. Gradation of DTOF sensitivity within the τ-interval is more obvious than the remaining reservoir region, where the magnitudes of DTOF sensitivities are almost the same (Figure 4.9a). If both the lower and upper limits of the τ-interval are set as positive values that are less than the maximum reservoir DTOF value (τ), DTOF sensitivities at regions within the lower DTOF (τ) limit become zero; only DTOF sensitivities within the τ-interval being perturbed and behind it are non-zero (Figure 4.9b and c). This is consistent with previous grid-cell based sensitivity analysis (Figure 4.6). Meanwhile, larger lower and upper DTOF limits of the τ-interval being perturbed lead to higher magnitudes of DTOF disturbance within the reservoir model (Figure 4.9c).

From above analysis of DTOF sensitivities with respect to the reservoir permeability in the 2D homogeneous reservoir model, it is evident that only areas behind the perturbed cell have DTOF disturbance; areas in front of the perturbed cell have zero values of DTOF sensitivities. This is consistent with the asymptotic pressure approximation which utilizes the DTOF to reduce the 2D/3D reservoir model to a simplified 1D form. It also meets our expectation on DTOF sensitivity formulation based on functional derivative of the Eikonal equation, which can be readily expressed in terms of a discretized DTOF (τ) sequence.

From the DTOF sensitivity calculated analytically (Eq.(4.11) and Eq.(4.18)), the drainage volume and well test derivative sensitivity coefficients with respect to reservoir

parameters within the τ-interval can also be formulated analytically using the chain rule (Eq. (4.19) and Eq.(4.20)).

$$\frac{\delta V(t)}{\delta \ln k_l} = \frac{\delta V_0(t)}{\delta \ln k_l} + \frac{\delta V_1(t)}{\delta \ln k_l} + \frac{\delta V_2(t)}{\delta \ln k_l} \tag{4.19}$$

$$\frac{\delta \Delta p'_{wf}}{\delta \ln k_l} = -\frac{q_w \cdot t}{c_t \cdot V^2(t)} \cdot \frac{\delta V(t)}{\delta \ln k_l} \tag{4.20}$$

The real benefit of the τ-interval based sensitivity formulation is that it can generate a stable inversion which the grid-cell based sensitivity formulation cannot provide. This sensitivity formulation method will prove later to be more efficient than the grid-cell based scheme for calibrating reservoir model parameters, especially for 3D reservoir models which usually consists of a large number of grid cells.

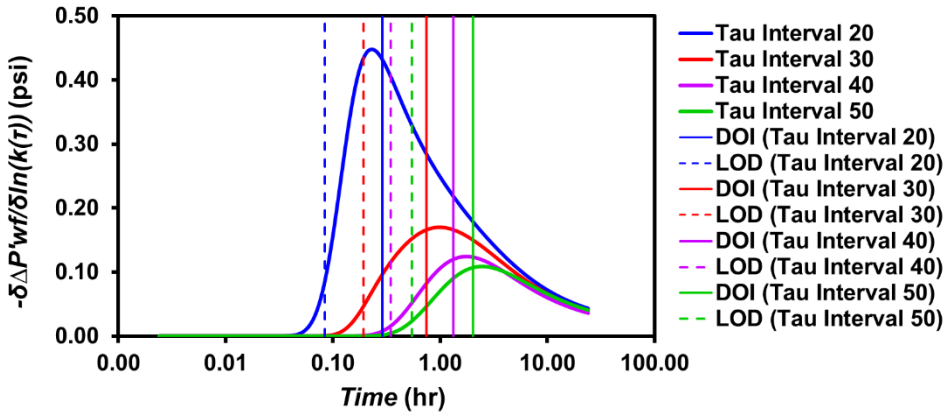

Figure 4.10 Sensitivity of the well test derivative with respect to the permeability within τ-intervals in a 2D heterogeneous reservoir model (DOI = Depth of Investigation; LOD = Limit of Detectability) (reprinted with permission from Li and King, 2016)

Figure 4.10 demonstrates sensitivity coefficients of the well test derivative with respect to permeabilities within the τ-intervals as a function of time (Eq.(4.20)) within the 2D heterogeneous reservoir model (Figure 4.3a). One single production well is located at the reservoir center with a constant production rate of 100 res bbl/day during a well test period of 24hrs. From the reservoir center to the outer boundary, 1,000 linearly distributed τ-intervals with equal widths are defined. Taking the average DTOF values of the 20^{th}, 30^{th}, 40^{th}, and 50^{th} τ-intervals near the wellbore, we can estimate the times when the DOI and LOD pass them (Eq.(4.8) and Eq.(4.9)). The solid vertical lines represent the DOI and dashed lines represent the LOD.

In Figure 4.10, it can be easily observed that the maximum magnitude of well test derivative sensitivity at a given location occurs approximately when the DOI passes by. This result is consistent with previous investigations of the sensitivity of well test data to radially symmetric non-uniform reservoir properties (Oliver, 1993). For a specific τ-interval, the LOD occurs much earlier than the DOI. This indicates that a major proportion of well test derivative sensitivity occurs after the LOD passes a particular location in space. In other words, the magnitude of well test derivative sensitivity is negligibly small before the LOD passes by a specific "τ" distance from the well. The sensitivity occurs much earlier in τ-intervals closer to the well compared to τ-intervals far away. Among the four demonstrated τ-intervals, only the 20^{th} τ-interval from the wellbore has sensitivities at a very early time of 0.1hr. The other three τ-intervals farther away from the wellbore will have non-zero sensitivities at a later time as the pressure front passes by.

From above sensitivity analysis, it is easy to define a certain number of τ-intervals from the wellbore to the outer boundary of the reservoir model, with a lower DTOF limit of zero and an upper DTOF limit equal to the maximum DTOF value calculated from the FMM for the entire model. In such a way, degrees of freedom of reservoir parameters to be updated can be efficiently reduced to the limited number of τ-intervals. It also enables us to extend the pressure transient analysis beyond the DOI estimated from the maximum well test time (Eq.(4.8)) to the maximum DTOF value of the reservoir model. In other words, not only reservoir permeability within the DOI will be updated, remaining grid cells beyond it in the reservoir model can also be calibrated since there are still some non-zero sensitivities in that region (Figure 4.10). Reservoir parameters within the DOI are expected to be updated fast during history matching because of the relatively large magnitude of the well test derivative sensitivity with respect to permeability within it (Figure 4.10).

Since the C9V9E5 FMM (Figure 4.1b) is used for DTOF calculation, it is easy to identify the minimum and maximum DTOF values evaluated for each grid cell. We use τ_{ijk}^{Min} and τ_{ijk}^{Max} to represent the minimum and maximum DTOF values for the grid cell within the 3D Cartesian coordinates, which can be evaluated at the cell center, cell vertex, face center as well as edge center. Then we can establish the relationship between the grid-cell based sensitivity and the τ-interval based sensitivity.

$$\frac{\delta \ln k_{ijk}}{\delta \ln k_l} = Max\left[0, \frac{Min\left[\tau_{ijk}^{Max}, \theta_l\right] - Max[\tau_{ijk}^{Min}, \theta_{l-1}]}{\theta_l - \theta_{l-1}}\right] \tag{4.21}$$

Using Eq.(4.21), grid-cell based reservoir permeability values will be updated by projecting permeability changes within the τ-interval back to the spatial grid cells using a pore volume weighted scheme, which relies upon the proportion of DTOF each grid cell overlaps with a τ-interval. For reservoir models with anisotropic media, permeabilities in I, J and K directions are updated with the same magnitude. Definition of the τ-intervals can be completely independent of the time used for estimation of the DOI (Eq.(4.8)) and LOD (Eq.(4.9)). Specifically, linearly instead of logarithmically distributed τ-intervals with equal DTOF width are recommended to be used for inversion. Densely distributed τ-intervals with narrow width around the wellbore will easily give rise to unstable inversion results that will be demonstrated in later discussions.

4.2.3 Extension to the Fast Marching Method

From the forward model set up above, it is evident that extension of the Eikonal equation discretization from the C5V9 scheme to the C9V9E5 scheme makes the hybrid drainage volume converge to the analytic solution for 2D infinite-acting radial flow (IARF) in homogenous media (Figure 4.2). By adding extra degrees of freedom of DTOF values at the edge center of the rectangular cells, the pressure front propagation can be better characterized by the Eikonal solution. An equivalent discretization scheme for the Eikonal equation is required for drainage volume and well test derivative constructions for 3D infinite-acting flow. Since the asymptotic pressure approximation relies upon an assumption that the pressure gradient is aligned with the DTOF gradient (King et al., 2016; Wang et al., 2017), it is important to capture the shape of the pressure front by more

accurate DTOF calculation. To this end, we extend the 2D C9V9E5 FMM to (Figure 4.1b) an equivalent 3D C27V27F11E11 FMM (Figure 4.11).

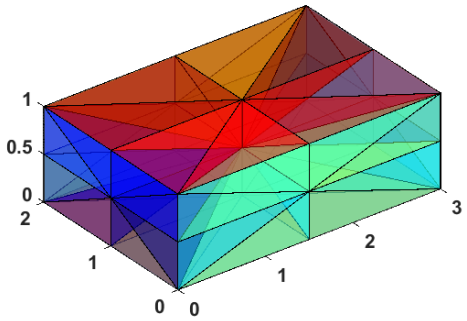

Figure 4.11 Illustration of the 3D C27V27F11E11 discretization scheme for the Eikonal equation

In the C27V27F11E11 discretization scheme for the Eikonal equation, each orthogonal grid is subdivided into 48 equivalent tetrahedral elements. DTOF values are evaluated at the cell center, cell vertex, face center as well as the edge center. In such a way, the DTOF values calculated in each of the three horizontal slices within the orthogonal grid will be identical to those calculated from the equivalent 2D C9V9E5 FMM if a vertical well perforates the face center from the top to the bottom. This C27V27F11E11 FMM forms the basis for the DTOF calculation in subsequent 3D full field inversion.

4.2.4 Integration of Pressure Transient Data

Based on the methodology we proposed above for asymptotic expansion to the diffusivity equation and the hybrid drainage volume constructed from the DTOF calculation, high-resolution geostatistical reservoir models can be reconciled with well production history. The asymptotic approach in combination with the FMM provides us with an efficient way to integrate pressure transient data into the reservoir models. Sensitivity coefficients of the objective function with respect to reservoir parameters required for inversion can be formulated analytically in one single forward simulation. The DTOF and its analytic sensitivity with respect to reservoir parameters can be updated simultaneously within the FMM algorithm.

In this study, the well test derivative (which is inversely proportional to the drainage volume formulated in terms of the DTOF and time) is treated as the objective function to be optimized in inversion. It is included in a penalized form of the objective function, which consists of three terms as follows:

$$J = \left\| \delta \boldsymbol{d} - \boldsymbol{S}\delta \boldsymbol{R} \right\| + \beta_1 \left\| \delta \boldsymbol{R} \right\| + \beta_2 \left\| \boldsymbol{L}\delta \boldsymbol{R} \right\| \tag{4.22}$$

In this objective function, $\delta \boldsymbol{d}$ is the data residual vector which is the difference between observed data and calculated results; $\boldsymbol{S}$ is the sensitivity matrix containing well production response due to a small disturbance in reservoir parameters; $\delta \boldsymbol{R}$ refers to the updating of reservoir parameters during inversion; $\boldsymbol{L}$ is a second-spatial-difference operator which computes the spatial gradient of the model by taking differentiations between adjacent block values (Parker, 1994). The first term represents the data misfit that minimize the observed well response and calculated pressure data. The second term is

called a "norm" constraint, which penalizes deviations from the prior model. It helps preserve the geologic information that has already been incorporated into the prior model. The third term is the "roughness penalty" ensuring that production data are best suited to resolving large-scale property variations.

The minimization of Eq.(4.22) can be realized by an iterative least-square solution to the augmented linear system (Vasco et al., 2000; Kulkarni et al., 2001).

$$\begin{pmatrix} \boldsymbol{S} \\ \beta_1 \boldsymbol{I} \\ \beta_2 \boldsymbol{L} \end{pmatrix} \delta \boldsymbol{R} = \begin{pmatrix} \delta \boldsymbol{d} \\ \boldsymbol{0} \\ \boldsymbol{0} \end{pmatrix} \tag{4.23}$$

The coefficients β_1 and β_2 are weights that determine the relative strengths of the prior model and roughness term. The inverse modeling result will be affected by these weighting coefficients. Reasonable weighting coefficients should be assigned to the regularization term that controls the prior information so that the pressure profile at the well can match with the observational data, even at very early times of flow. As long as comparable magnitudes of the prior and roughness terms are used, the penalized objective function can be easily minimized during data integration. This is important for achieving optimized inversion results in history matching reservoir models with the well test data. Since the augmented matrix is large and sparse, an iterative sparse-matrix solver, LSQR, can be used for solving this linear system in an accurate and efficient way.

4.3 Validation and Application

On the basis of the forward model we set up and the analytic sensitivity coefficients formulated, history matching can be tested for reservoir models where infinite-acting flow occurs. In all subsequent inverse modeling cases, one single vertical well with a constant production rate is located at the center of the 2D/3D reservoir model during integration of pressure transient data.

4.3.1 Synthetic Illustrative Examples

The inversion technique is tested first on a 2D synthetic permeability field with the same heterogeneous permeability distribution shown in Figure 4.3a, which is used as the reference model to generate the "observational" well test derivative data. It has a maximum, minimum and average permeability values of 432.41md, 22.38md and 86.31md, respectively. One vertical well is located at (26, 26) of the 51x51 grid system, with a constant production rate of 100 res bbl/day. All other reservoir parameters are listed in Table 4.1. Before conducting history matching of the reservoir model with the well test data, it is important to validate the asymptotic pressure approximation by comparing the FMM generated well pressure profile with a numerical reservoir simulator (ECLIPSE).

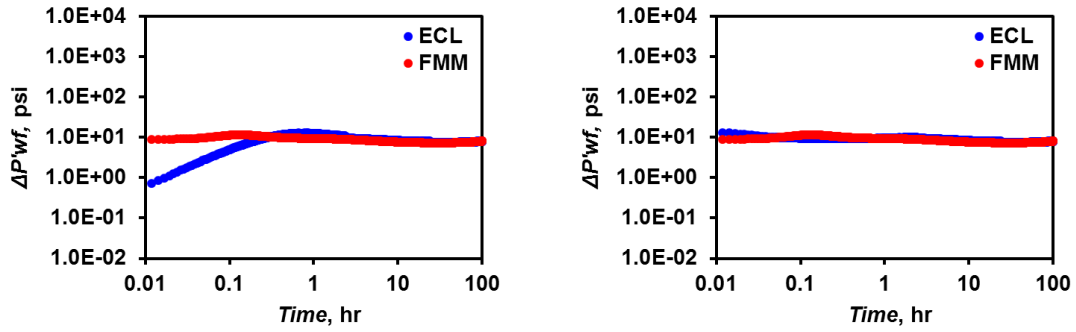

(a) Without LGR around the well in ECLIPSE

(b) With LGR around the well in ECLIPSE

Figure 4.12 Validation of the well test derivative calculated within the 2D heterogeneous reservoir field (51x51) used as the reference model for inversion.

In Figure 4.12, we validate the FMM generated well test derivative with the ECLIPSE simulation result. If no local grid refinement (LGR) around the well is applied within the ECLISPE simulation, an obvious non-zero slope of the well test derivative can be observed at very early times of the well test due to the effective wellbore radius (Figure 4.12a). By applying LGR around the wellbore within the ECLIPSE simulation, the FMM generated well test derivative can match very well with the ECLIPSE result, even at very early times of simulation (Figure 4.12b). Thus, it is recommended to apply the LGR around the wellbore within the ECLIPSE simulation when it is used to validate the asymptotic pressure approximation before inversion.

The good agreement between the ECLIPSE and FMM generated well pressure profiles (Figure 4.12b) corresponds well with previous validation of the forward model on the entire 2D modeling domain within 100hrs (Figure 4.4a, b and c). Because of the "sufficiently" smooth permeability distribution within the 2D heterogeneous reference

model (VDP = 0.4167), there is little local reflection being felt when the pressure front propagates from the wellbore into the reservoir. Moreover, both the ECLIPSE and FMM generated well test derivative curves keep a horizontal shape during the 100hrs well test. This indicates that radial flow dominates the entire inversion process, which can make the calibrated permeability more uniformly distributed after history matching the reservoir model with the well test data (Figure 4.12).

Three sets of permeability fields are used to test the integration of well test data into the reservoir model and calibrate the grid-cell permeabilities using the FMM. The reference model, which is heterogeneous (Figure 4.3a), is the same for all three sets of inversion. In the first and second sets, the prior models are homogeneous with a low permeability value of 20md and a high permeability value of 200md, respectively. In the third set, the prior model is heterogeneous and has an average permeability value of 36.31md. The homogeneous and heterogeneous prior models are treated as the a priori information, based on which reservoir permeabilities are calibrated. The "observational" well test derivative data are generated from the heterogeneous reference model using ECLIPSE (Figure 4.12b).

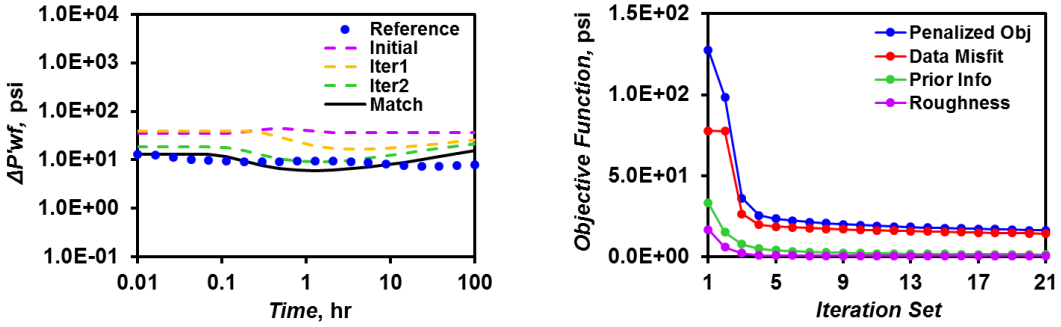

(a) Well Test Derivative **(b) Objective Function**

Figure 4.13 Integration of pressure transient data into the 2D homogeneous model (KX = 20md) during a constant flow rate well test with a heterogeneous reference model using grid-cell based sensitivity coefficients (β_1 = 5 and β_2 = 15) (reprinted with permission from Li and King, 2016)

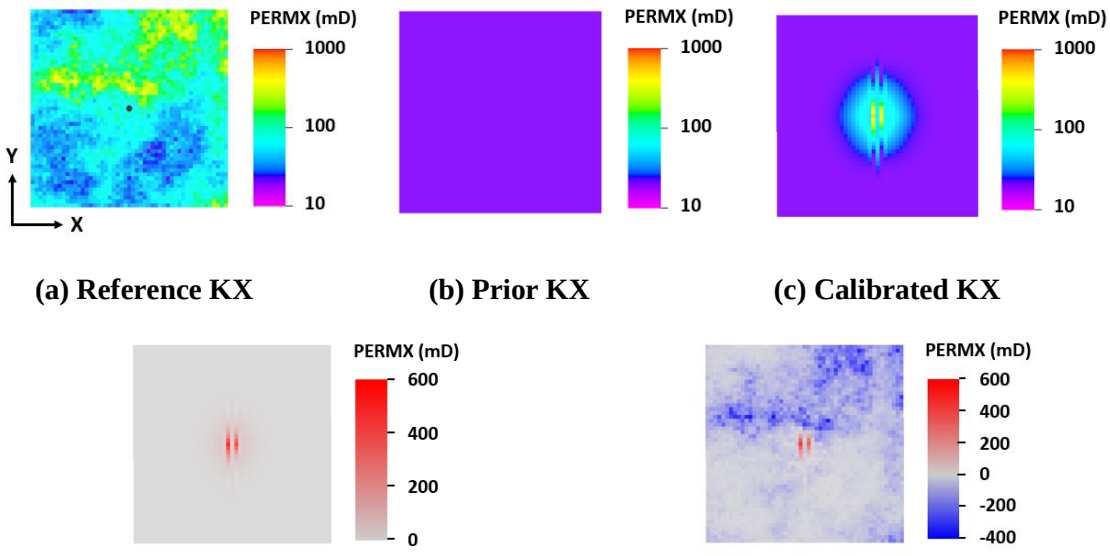

(a) Reference KX **(b) Prior KX** **(c) Calibrated KX**

(d) Calibrated KX − Prior KX **(e) Calibrated KX − Reference KX**

Figure 4.14 Calibration of permeability values within the 2D reservoir model during a constant flow rate well test with a homogeneous prior model (KX = 20md) and a heterogeneous reference model using grid-cell based sensitivity coefficients (reprinted with permission from Li and King, 2016)

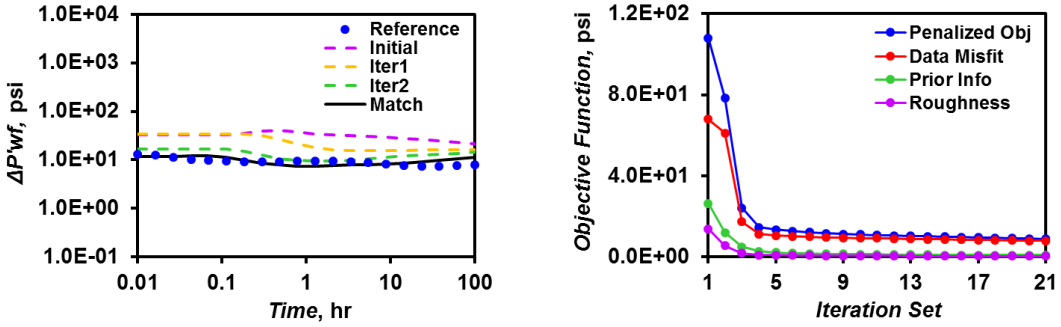

(a) Well Test Derivative **(b) Objective Function**

Figure 4.15 Integration of pressure transient data into the 2D heterogeneous model (average KX = 36.31md) during a constant flow rate well test with a heterogeneous reference model using grid-cell based sensitivity coefficients (β_1 = 5 and β_2 = 15) (reprinted with permission from Li and King, 2016)

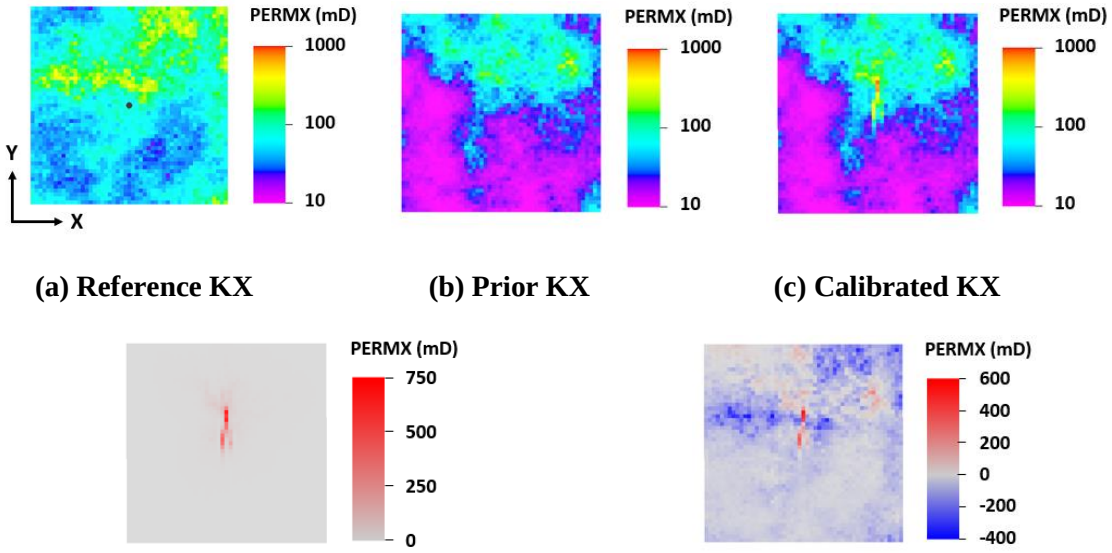

(a) Reference KX **(b) Prior KX** **(c) Calibrated KX**

(d) Calibrated KX − Prior KX **(e) Calibrated KX − Reference KX**

Figure 4.16 Calibration of permeability values within the 2D reservoir model during a constant flow rate well test with a heterogeneous prior model (average KX = 36.31md) and a heterogeneous reference model using grid-cell based sensitivity coefficients (reprinted with permission from Li and King, 2016)

As demonstrated from Figure 4.13 to Figure 4.16, we first test the data integration procedure within the first and third sets of permeability fields using the grid-cell based sensitivity coefficients. The degrees of freedom of reservoir permeabilities to be calibrated in both cases are 2601. After a limited sets of iterations, the penalized objective function decreases and converges to an almost constant value (Figure 4.13b and Figure 4.15b).

The well test derivatives obtained from inversion match well with the "observational" data generated from the reference permeability field in both cases, even at the early times of simulation (Figure 4.13a and Figure 4.15a). However, this good agreement between the well test derivative profile after inversion and the "observational" data cannot represent a "good" adjustment of the permeability values in the near-well region to the static prior geologic model (Figure 4.14c and Figure 4.16c).

Regularization coefficients are assigned to the penalized objective function (Eq.(4.22) and Eq.(4.23)) to investigate the impact of the prior information and roughness upon history matching results. Though a sufficiently high value of coefficient (β_2 = 15 in both cases) has been assigned to the roughness term of the penalized objective function, an obvious "spike" can still be observed in the calibrated permeability (Figure 4.14c and Figure 4.16c). This results mainly from the directional preference of the sensitivity coefficients evaluated on the grid-cell basis (Figure 4.7) using FMM calculated DTOFs, which leads to significantly higher magnitudes of permeability updates in certain directions than others. Since only one production well is employed to record the pressure transient data, an alternative method of calculating the analytic sensitivity coefficients is

required so that the preference of updating reservoir parameters in certain directions can be avoided and more stable inversion results can be obtained.

From Figure 4.17 to Figure 4.26, we try alternatively to calibrate the reservoir permeability using the τ-interval based sensitivity formulation in view of the inherent "drawback" in grid-cell based sensitivity calculation. Similar to the transient flow simulation by solving the DTOF-based one-dimensional diffusivity equation discussed in Section 3, the τ-intervals defined for inversion are independent of the grid-cell DTOF values calculated from the FMM, except for the upper and lower limits.

We first test the new inversion scheme on the second set of permeability fields (with a homogeneous prior permeability of 200md). A total number of 20 τ-intervals are used for inversion, which has a lower limit of zero and an upper limit equal to the maximum reservoir DTOF value calculated from the FMM. We compare the inversion results based on two ways of defining the 20 τ-intervals, which are linearly and logarithmically distributed, respectively. In both approaches, the upper limit of the first τ-interval is fixed at τ_0 evaluated at the well cell (Figure 3.10). The purpose of fixing the width of the first τ-interval is to avoid the unstable permeability calibration near the wellbore when the τ-intervals are logarithmically distributed.

Since the prior permeability value is significantly higher than the average permeability value within the reference model (86.31md), a higher regularization coefficient is assigned to the roughness terms within the penalized objective function (β_1 = 10; β_2 = 350) so that the well test derivative profile after inversion can match that generated from the reference model.

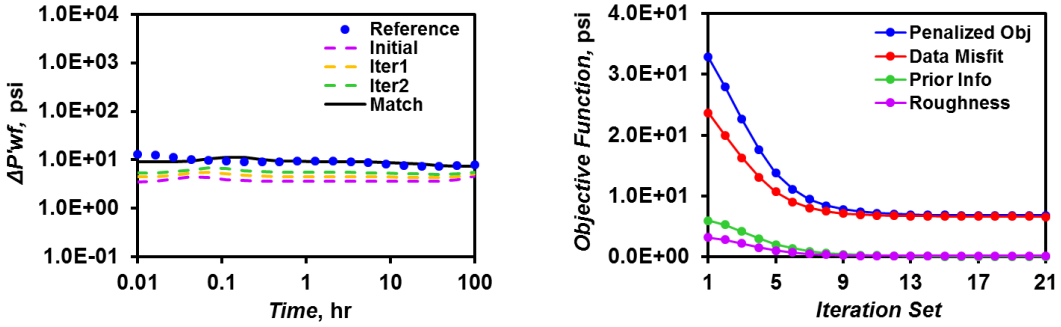

(a) Well Test Derivative **(b) Objective Function**

Figure 4.17 Integration of pressure transient data into the 2D homogeneous model (KX = 200md) during a constant flow rate well test with a heterogeneous reference model using τ-interval based sensitivity coefficients (β_1 = 10 and β_2 = 350; linearly distributed τ-intervals; NTau = 20) (reprinted with permission from Li and King, 2016)

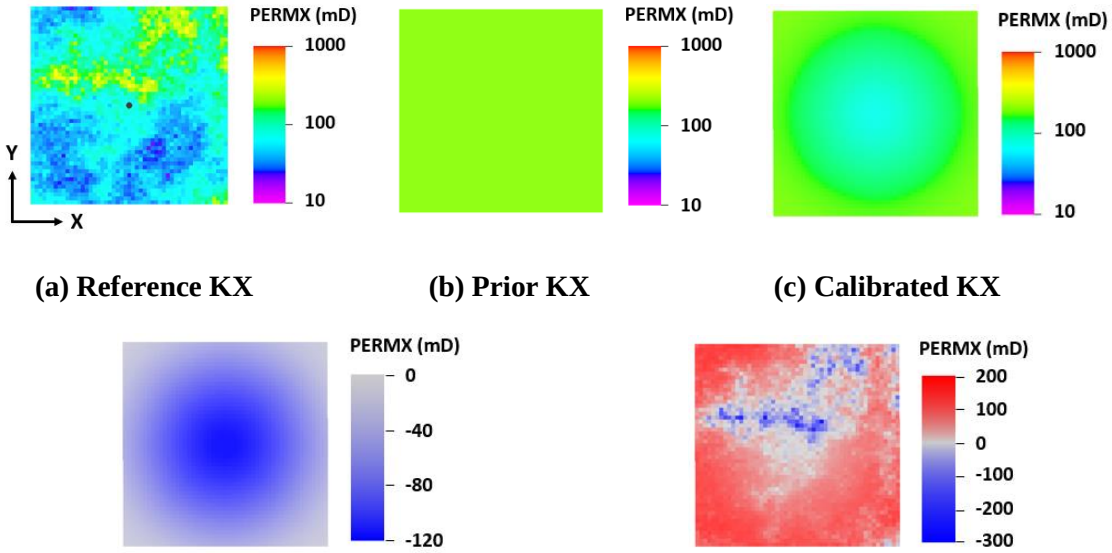

(a) Reference KX **(b) Prior KX** **(c) Calibrated KX**

(d) Calibrated KX − Prior KX **(e) Calibrated KX − Reference KX**

Figure 4.18 Calibration of permeability values within the 2D reservoir model during a constant flow rate well test with a homogeneous prior model (KX = 200md) and a heterogeneous reference model using τ-interval based sensitivity coefficients (linearly distributed τ-intervals; NTau = 20) (reprinted with permission from Li and King, 2016)

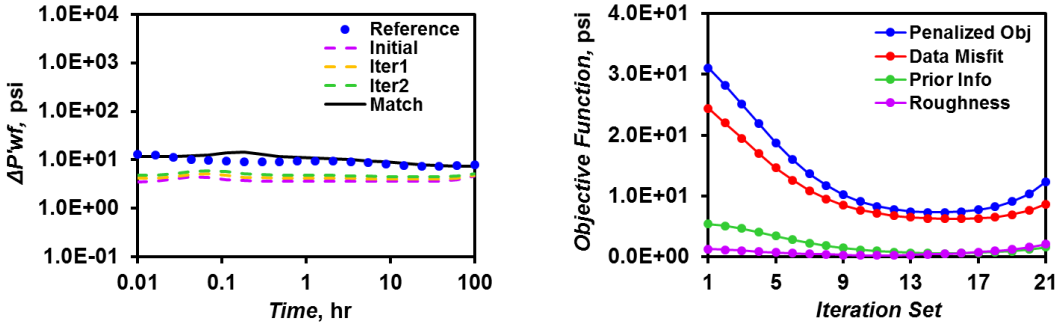

(a) Well Test Derivative **(b) Objective Function**

Figure 4.19 Integration of pressure transient data into the 2D homogeneous model (KX = 200md) during a constant flow rate well test with a heterogeneous reference model using τ-interval based sensitivity coefficients (β_1 = 10 and β_2 = 350; logarithmically distributed τ-intervals; NTau = 20) (reprinted with permission from Li and King, 2016)

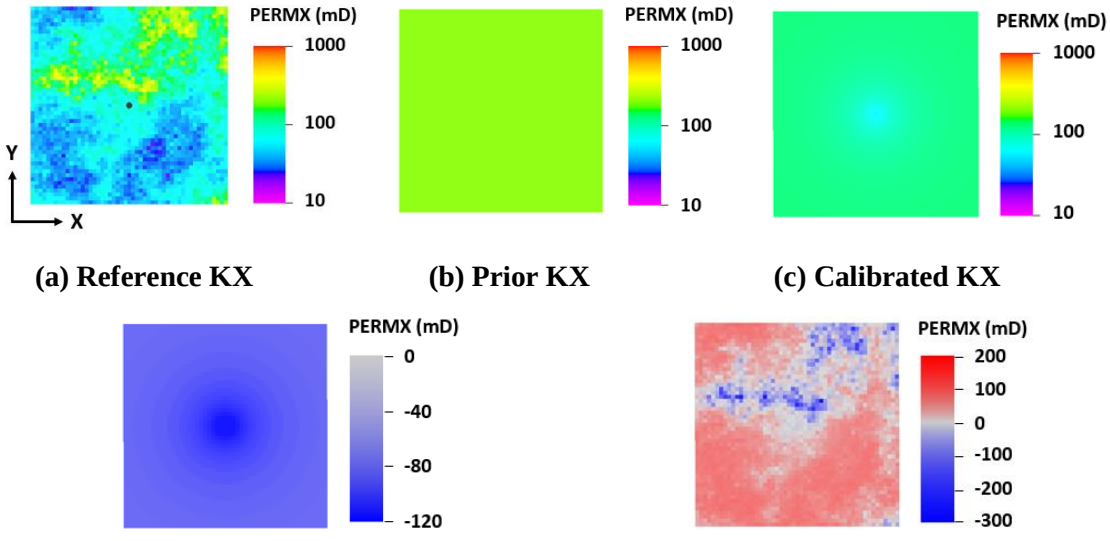

(a) Reference KX **(b) Prior KX** **(c) Calibrated KX**

(d) Calibrated KX − Prior KX **(e) Calibrated KX − Reference KX**

Figure 4.20 Calibration of permeability values within the 2D reservoir model during a constant flow rate well test with a homogeneous prior model (KX = 200md) and a heterogeneous reference model using τ-interval based sensitivity coefficients (logarithmically distributed τ-intervals; NTau = 20) (reprinted with permission from Li and King, 2016)

In Figure 4.17 and Figure 4.18, we can see that the linearly distributed τ-intervals used for sensitivity calculation leads to a good history matching of the reservoir models with pressure transient data. The well test derivative after inversion matches well with the ECLIPSE generated "observational" data from the reference model (Figure 4.17a). The penalized objective function decreases very fast to a constant value after a limited sets of iterations (Figure 4.17b). The calibrated permeability is radially symmetric to the well located at the reservoir center (Figure 4.18c), with major modifications of the permeability values within the near-well region (Figure 4.18d). No sensitivity preference is observed from the calibrated permeability field, which indicates that the linearly defined τ-intervals from the wellbore to the reservoir boundary can help generate stable inversions.

However, this is not the case for the inversion that relies on logarithmically distributed τ-intervals to calculate the sensitivity coefficients (Figure 4.19 and Figure 4.20). Assigning the same regularization coefficients to the penalized objective function, we can observe a calibrated permeability field (Figure 4.20c) that is closer to a "bulk average" change from the homogeneous prior model (Figure 4.20d). The gradation of the calibrated permeability from the wellbore to the reservoir boundary is less similar to the pressure front propagation. More importantly, all three terms of the penalized objective functions are not converging to constant values and even begin to increase again after several sets of iterations (Figure 4.19b). Although the calibrated permeability can still generate a well test derivative matching well with the "observational" data (Figure 4.19a), the logarithmically defined τ-intervals proves less capable to generate stable inversion results compared with the linearly defined τ-intervals.

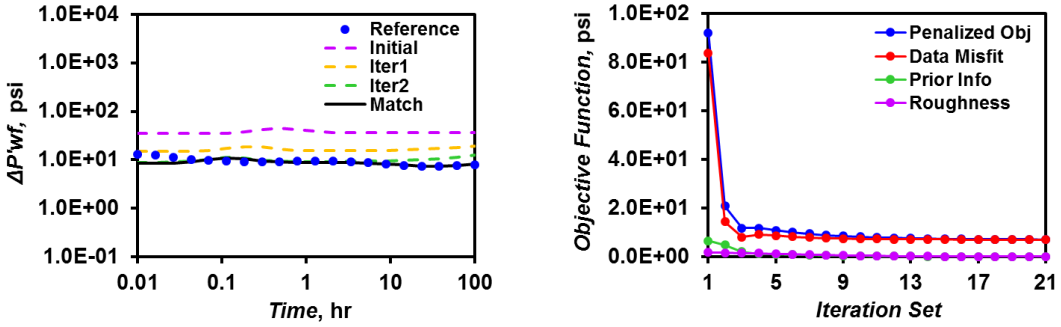

(a) Well Test Derivative **(b) Objective Function**

Figure 4.21 Integration of pressure transient data into the 2D homogeneous model (KX = 20md) during a constant flow rate well test with a heterogeneous reference model using τ-interval based sensitivity coefficients (β_1 = 5 and β_2 = 10; linearly distributed τ-intervals; NTau = 10) (reprinted with permission from Li and King, 2016)

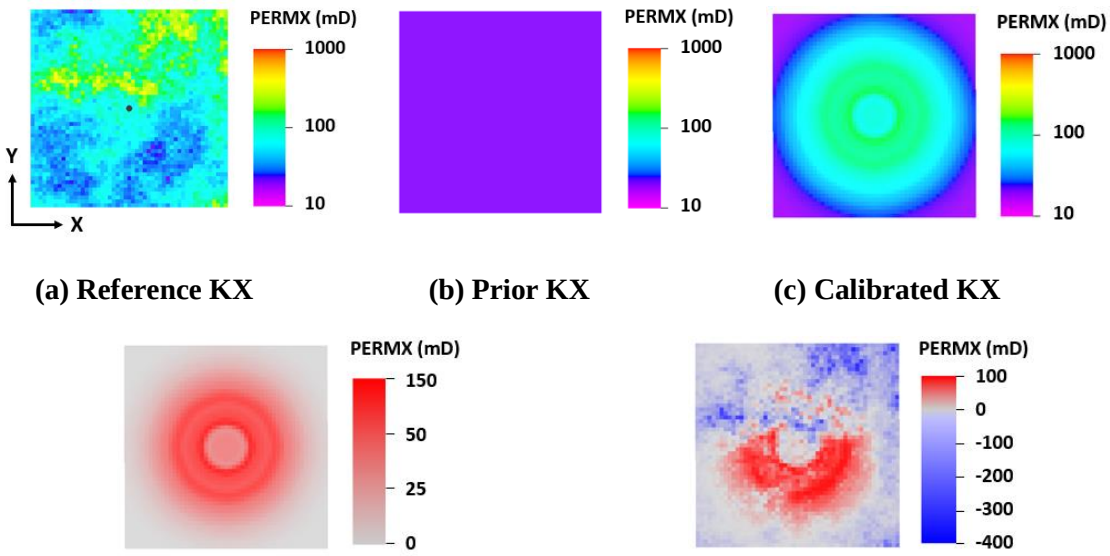

(a) Reference KX **(b) Prior KX** **(c) Calibrated KX**

(d) Calibrated KX − Prior KX **(e) Calibrated KX − Reference KX**

Figure 4.22 Calibration of permeability values within the 2D reservoir model during a constant flow rate well test with a homogeneous prior model (KX = 20md) and a heterogeneous reference model using τ-interval based sensitivity coefficients (linearly distributed τ-intervals; NTau = 10) (reprinted with permission from Li and King, 2016)

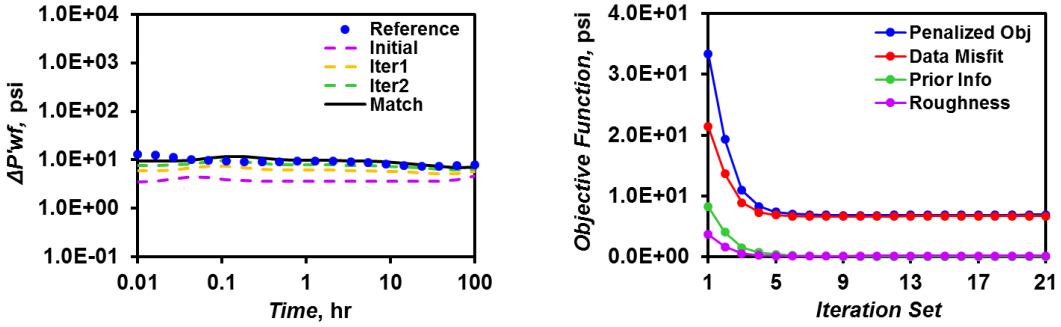

(a) Well Test Derivative **(b) Objective Function**

Figure 4.23 Integration of pressure transient data into the 2D homogeneous model (KX = 200md) during a constant flow rate well test with a heterogeneous reference model using τ-interval based sensitivity coefficients (β_1 = 10 and β_2 = 40; NTau = 10; linearly distributed τ-intervals; NTau = 10) (reprinted with permission from Li and King, 2016)

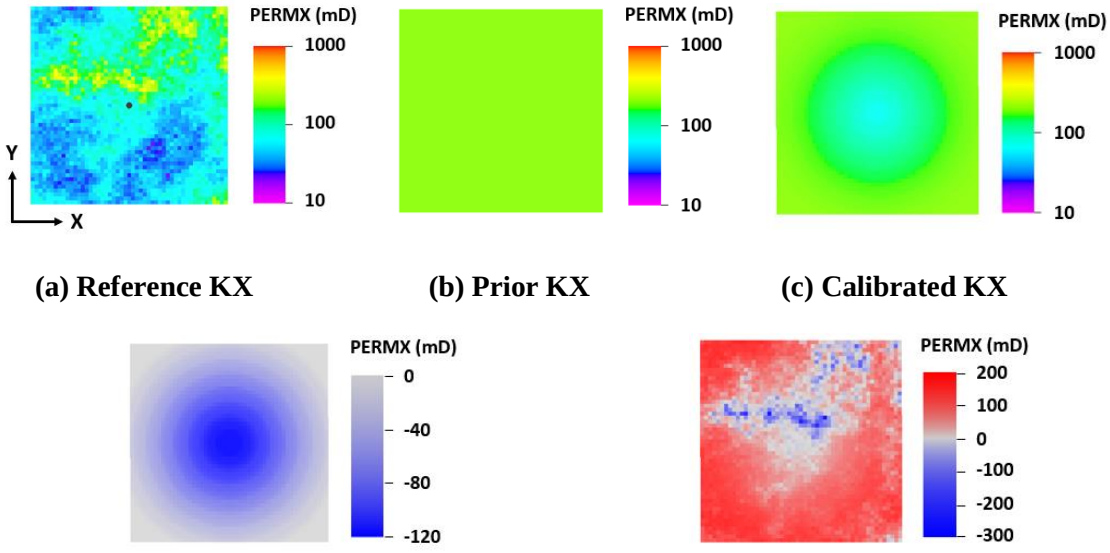

(a) Reference KX **(b) Prior KX** **(c) Calibrated KX**

(d) Calibrated KX − Prior KX **(e) Calibrated KX − Reference KX**

Figure 4.24 Calibration of permeability values within the 2D reservoir model during a constant flow rate well test with a homogeneous prior model (KX = 200md) and a heterogeneous reference model using τ-interval based sensitivity coefficients (linearly distributed τ-intervals; NTau = 10) (reprinted with permission from Li and King, 2016)

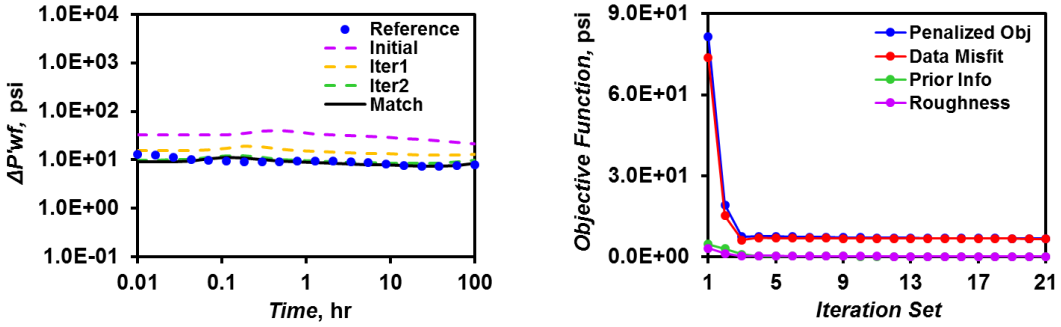

(a) Well Test Derivative **(b) Objective Function**

Figure 4.25 Integration of pressure transient data into the 2D heterogeneous model (average KX = 36.31md) during a constant flow rate well test with a heterogeneous reference model using τ-interval based sensitivity coefficients (β_1 = 5 and β_2 = 10; linearly distributed τ-intervals; NTau = 10) (reprinted with permission from Li and King, 2016)

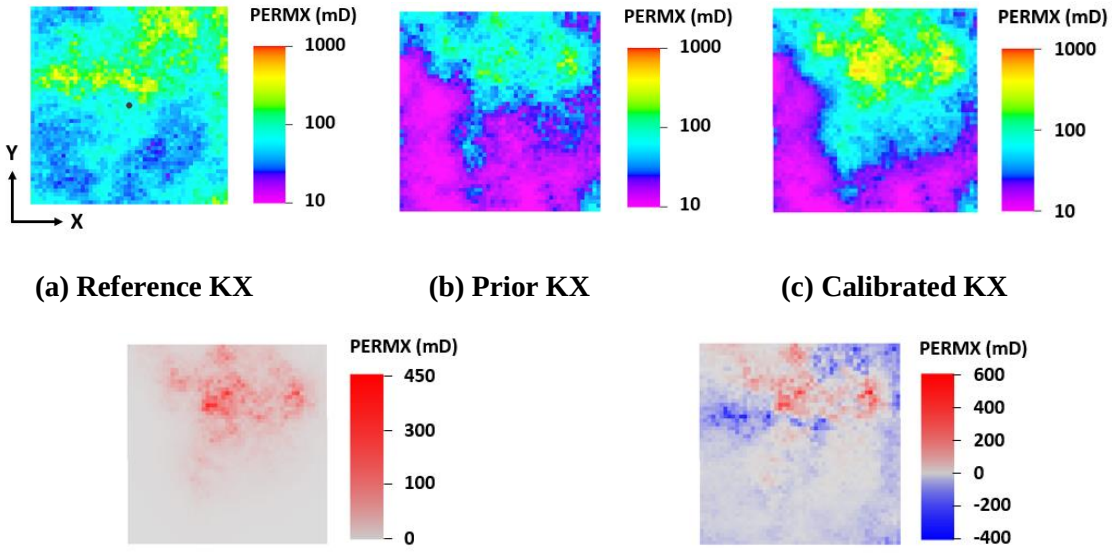

(a) Reference KX **(b) Prior KX** **(c) Calibrated KX**

(d) Calibrated KX − Prior KX **(e) Calibrated KX − Reference KX**

Figure 4.26 Calibration of permeability values within the 2D reservoir model during a constant flow rate well test with a heterogeneous prior model (average KX = 36.31md) and a heterogeneous reference model using τ-interval based sensitivity coefficients (linearly distributed τ-intervals; NTau = 10) (reprinted with permission from Li and King, 2016)

After above analysis, we determine to use linearly distributed τ-intervals to calculate the well test derivative sensitivity coefficients and perform history matching of the 2D reservoir models with pressure transient data (Figure 4.21 to Figure 4.26). A total number of 10 linearly distributed τ-intervals with equal widths are defined from the wellbore at the reservoir center to the reservoir outer boundary. The lower and upper limits of the τ-intervals are still defined as zero at the wellbore and the maximum reservoir DTOF value, respectively. The upper limit of the first τ-interval is not fixed anymore and can be defined beyond the well cell. Since the number of τ-intervals to be used to adjust reservoir parameters during pressure transient analysis has decreased from 20 to 10, we try to assign less weights to the regularization terms when the penalized objective function is iteratively minimized during inversion (Figure 4.21, Figure 4.23 and Figure 4.25).

From the homogeneous prior models, we can get an inversion result that has a permeability radially symmetric to the vertical well and is distributed as a function of distance "DTOF (τ)" to the center of the reservoir domain (Figure 4.22 and Figure 4.24). Inversion using the heterogeneous permeability field as the prior model generates a calibrated heterogeneous permeability that keeps the main shape of permeability distribution in the a priori information, but with values closer to the reference model. (Figure 4.26). Significantly higher magnitudes of permeability changes from the prior model can be observed approximately at the DOI than other regions during the 100hrs well test, which is especially obvious in the inversion with the homogeneous prior permeability with a low value of 20md (Figure 4.22d). This can be explained by the

maximum magnitudes of sensitivity coefficients of the well test derivative to permeability values within a specific τ-interval when the DOI passes by (Figure 4.10).

From Figure 4.22, Figure 4.24, and Figure 4.26, we can find that integration of pressure transient data into 2D reservoir models generates a calibrated permeability that is closer to the reference model in the near-well region than other regions of the reservoir model. This is mainly because that the well pressure is much more sensitive to reservoir properties near the production well within the depth of investigation (DOI) than regions far away. Reservoir permeability values beyond the DOI to the outer boundary can also be updated during history matching because of the small but still non-zero well test derivative sensitivities beyond the DOI (Figure 4.10). These results are consistent with previous studies in the estimation of reservoir properties using transient pressure data (Oliver, 1990, 1992).

In all the three cases above, the initial pressure drop profiles at the well (well test derivatives) are distinctively higher or lower than the "observational" data (Figure 4.21, Figure 4.23, and Figure 4.25). This indicates that the reservoir permeability can still be calibrated using the well test data even when the prior geologic model provided for inversion is totally wrong (Figure 4.22b and Figure 4.24b). Using a heterogeneous prior model, the calibrated reservoir permeability becomes more similar to the reference model, especially in the near-well region (Figure 4.26).

By comparison, it is evident that integration of the single-well pressure transient data into reservoir models using the τ-interval based analytic sensitivity coefficients can significantly improve the stability of the inversion result because the permeability within

the τ-intervals are updated with the same magnitude when the objective function is minimized (Figure 4.21 to Figure 4.26). In contrast, the grid-cell based analytic sensitivity calculation by means of the FMM calculated DTOFs can easily create adverse impacts upon the permeability calibration due to the sensitivity "preference" in certain directions (Figure 4.14 and Figure 4.16). In addition, inversion using τ-interval based analytic sensitivity calculation has more advantages over grid-cell based analytic sensitivity calculation in terms of the computational efficiency, especially for large-scale 3D reservoir models usually with millions of grid cells. Since the number of τ-intervals defined is independent of the number of grid cells within the geologic model, the computational cost can be tremendously reduced.

4.3.2 Brugge Field Application

After testing it on the 2D synthetic model, we demonstrate this inversion technology on the 3D Brugge full field reservoir model (Hegan, 2008). The reference model (FN-SS-KP-1-92 within the TNO Brugge data set) has heterogeneous permeability and porosity values, with an anisotropic permeability distribution that has different values in the x, y and z directions.

Two sets of reservoir parameters including porosity and permeability are used as the prior models for inversion. In the first prior model, the porosity is the same as in the reference model but the permeability is homogeneous. In the second prior model (FN-SS-KS-2-80 within the TNO Brugge data set), both the porosity and permeability are heterogeneous, and they are different to those of the reference model. The reference model

has a higher average permeability value compared with those of the two prior models. The porosity will not change during history matching of the 3D full field Brugge reservoir models with the well test data.

Orthogonal and non-uniform grid cells are used for the entire 3D Brugge model, with inactive cells located at the outer boundary and no faults considered. One vertical well is located at the grid cell (70, 23) and perforates the entire 9 layers, with a constant production rate of 10,000 res bbl/day (Table 4.2).

Table 4.2 Input parameters for the 3D Brugge full field models

NX	139	$\overline{DX}$	412.12	ft	μ	1	cp
NY	48	$\overline{DY}$	405.35	ft	c_t	1.0E-5	psi^{-1}
NZ	9	$\overline{DZ}$	22.92	ft	B_o	1	res bbl/STB
Well	(70, 23)				q_w	10,000	res bbl/day

	Reference Model		**Prior Model 1 (homogeneous)**		**Prior Model 2 (heterogeneous)**	
$\overline{KX}$	476.9	md	200.0	md	223.2	md
$\overline{KY}$	475.7	md	200.0	md	222.6	md
$\overline{KZ}$	34.2	md	20.0	md	18.3	md
$\overline{\phi}$	0.18		0.18		0.18	

Table 4.3 Dykstra-Parsons coefficients (VDP) for the 3D heterogeneous reference and prior permeability fields within the Brugge full field models

	Heterogeneous Reference Model	Heterogeneous Prior Model
VDP (KX)	0.8673	0.8079
VDP (KY)	0.8676	0.8087
VDP (KZ)	0.8569	0.8208

The reference and prior models have the same grid-cell geometry, which has an average cell length, cell width and cell thickness of 412.12ft, 405.35ft and 22.92ft, respectively. The permeability within the heterogeneous reference model has average values of 476.9md, 475.7md and 34.2md in the I, J, and K directions, respectively. Their corresponding Dykstra-Parsons coefficients (VDP) are 0.8673, 0.8676 and 0.8569, respectively. The permeability within the second prior model has average values of 223.2md, 222.6md and 18.3md in the I, J, and K directions, respectively, with the corresponding VDP of 0.8079, 0.8076 and 0.8208, respectively. Both the reference model and the second prior model are highly heterogeneous (Table 4.2 and Table 4.3).

The DTOFs to the grid nodes along the vertical well are all assigned zero values. With DTOF values evaluated at the cell center, cell vertex, face center as well as edge center of each cell within the reservoir model by solving the 3D anisotropic Eikonal equation (Eq.(4.2)) using the C27V27F11E11 FMM (Figure 4.11), we provide the basis for the 3D hybrid drainage volume construction. With more degrees of freedom of DTOF values evaluated at different locations of each grid cell, pressure drop in the 3D Brugge

reservoir model can be better represented by the DTOF contour, especially in the near-well region.

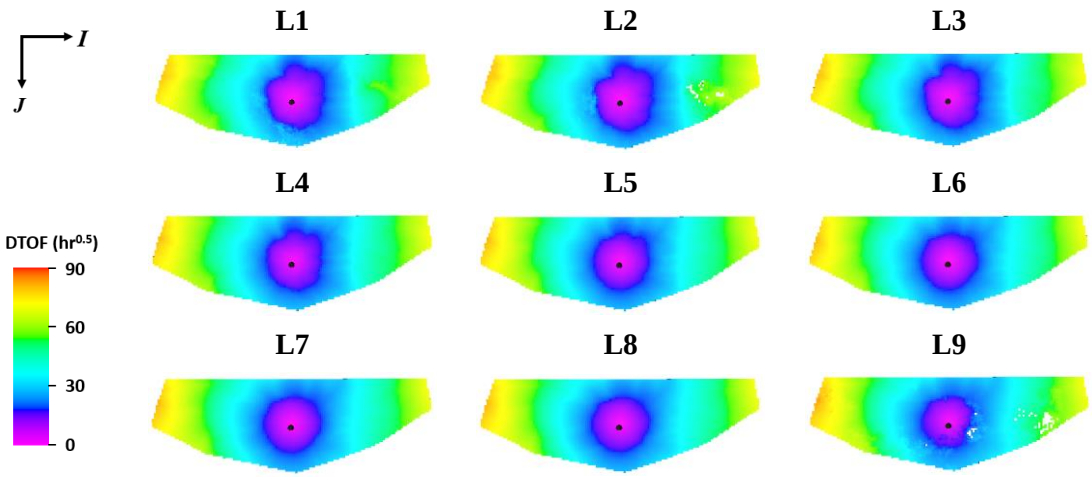

Figure 4.27 DTOFs calculated from the C27V27F11E11 FMM within the reference 3D Brugge full field model with heterogeneous and anisotropic media (back circle represents the vertically perforated well)

The DTOFs calculated from the C27V27F11E11 FMM for the heterogeneous reference Brugge model are shown in Figure 4.27, which have a minimum value of zero at the wellbore and maximum value of 88.52hr$^{0.5}$ at the outer boundary. In general, DTOF distributions in the nine layers of the reservoir model are quite similar, which indicates strong vertical pressure communication between them. This is mainly because that the ratios of grid-cell length to grid-cell permeability in the I, J, and K directions are quite close in general (Table 4.2), which makes pressure front propagation in three principal directions of anisotropy with almost equal ease.

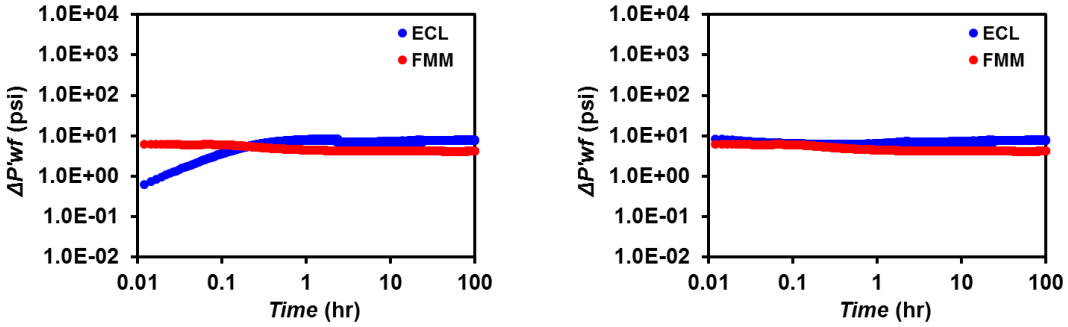

(a) Without LGR around the well in ECLISPE

(b) With LGR around the well in ECLISPE

Figure 4.28 Validation of the well test derivative calculated within the 3D heterogeneous and anisotropic Brugge full field used as the reference model for inversion

Figure 4.28 demonstrates the well test derivatives calculated using the asymptotic pressure approximation and a reservoir simulator (ECLIPSE) for the 3D Brugge reference model. Application of LGR in the near-well grid cells can significantly improve the accuracy of ECLIPSE simulation in early times (Figure 4.28b) by decreasing the wellbore radius effect (Figure 4.28a). At the very beginning of the simulation, the well test derivative calculated from the asymptotic pressure approximation is in good agreement with that generated from ECLIPSE. As time goes by, this pressure profile agreement deteriorates and the discrepancy between the FMM generated well test derivative and that from the ECLIPSE simulation becomes larger (Figure 4.28b).

Following the same procedure used for validating entire reservoir pressure calculated from the asymptotic pressure approximation with pressure generated from the numerical simulation before 2D inversions, we investigate the pressure drop within each grid cell of the 3D Brugge reference model (Figure 4.29). Reservoir pressures are recorded

at the simulation times of 30min, 3hrs, 24hrs and 100hrs, respectively. At each one of the four times, the FMM and ECLIPSE simulated reservoir pressure drops are compared, with an analysis focused on their correlation.

From Figure 4.29, we can observe that the pressure drop derivative with respect to time within the entire 3D Brugge reference model demonstrates the same transient pressure behavior that can be interpreted from the diagnostic plot (Figure 4.28b). Since the well is located at a region with relatively high and smoothly varying permeability values, the FMM calculated reservoir pressure is closely correlated with the ECLIPSE generated reservoir pressure at an early time of simulation. This indicates that the "τ-contour" generated from the FMM calculation can well approximate the pressure drop contour in the near-well region (Figure 4.29a), which can also explain the well pressure agreement between FMM and ECLIPSE simulations in the diagnostic plot of the well test at the very beginning (Figure 4.28b). At a later time, the discrepancy between pressure drops generated from the asymptotic pressure approximation and those from the ECLIPSE simulation becomes larger. Especially at the near-well region, the significantly higher time derivative of pressure drop generated from ECLIPSE compared with the FMM simulation represents strong local pressure front reflections between horizontal reservoir layers (Figure 4.29b, c and d). This is similar to the strong near-well reflections of the pressure front propagating in the 2D SPE10 model (Figure 3.44 to Figure 3.47), where multiple decreasing trends of the $w(\tau)$ function can be observed (Figure 3.21 to Figure 3.24).

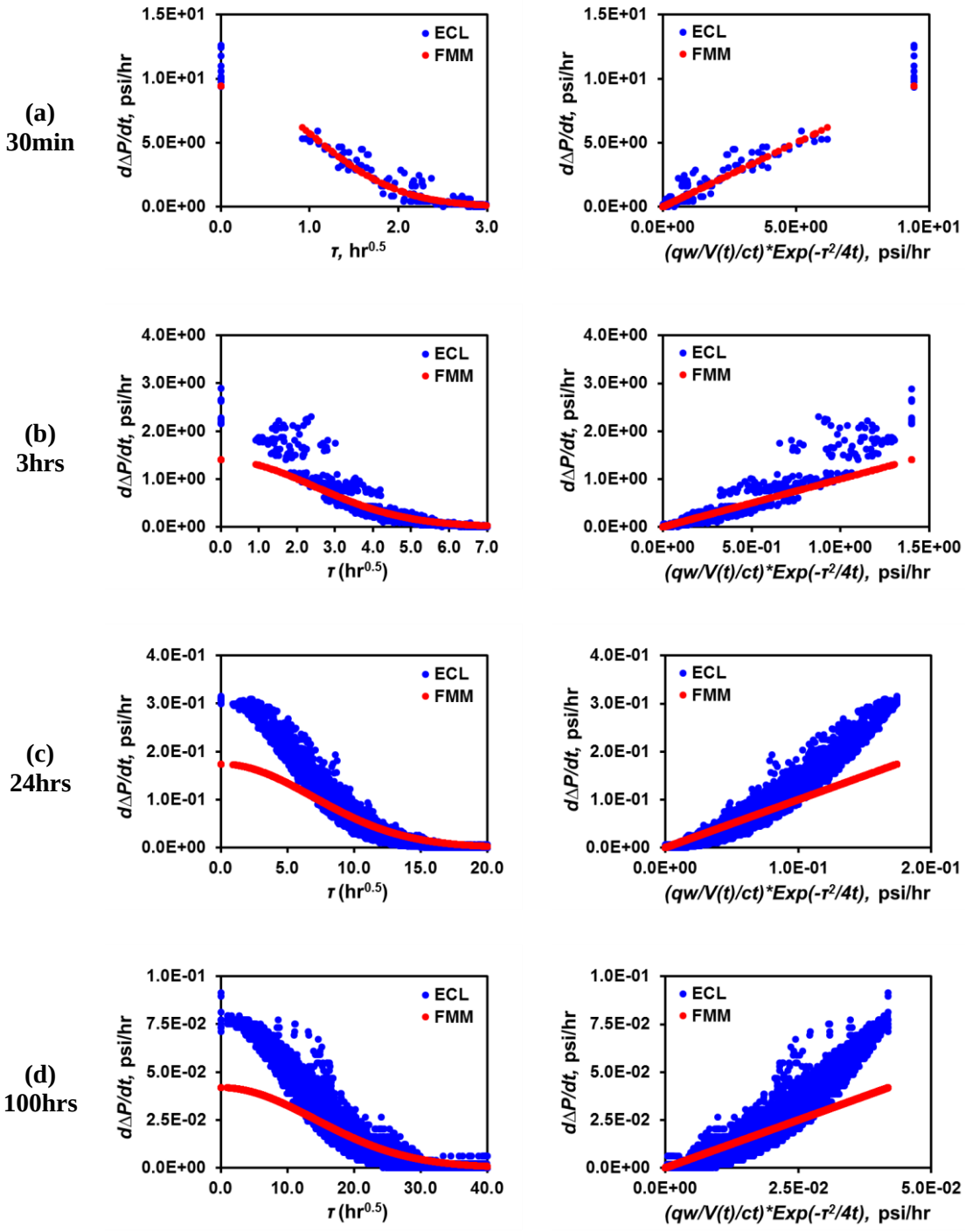

Figure 4.29 Validation of the asymptotic pressure approximation with ECLIPSE simulation within the 3D Brugge full field heterogeneous and anisotropic reference model (139x48x9, Well (70, 23, 1:9)) under a constant flow rate well test (q_w = 10,000 res bbl/day)

These results demonstrate that the validity of integrating pressure transient data into the 3D reservoir model based on the asymptotic pressure approximation is a function of time. Given that the forward modeling of the well test derivative using the FMM is not significantly different to that generated from ECLIPSE and no much boundary effect has been felt yet (Figure 4.28b), we can still calibrate the near-well reservoir permeabilities within the prior model from pressure transient analysis within 100hrs. The 3D Brugge reference model is only used to generate the "observational" data from ECLIPSE.

Similar to 2D inversions, we define 20 linearly distributed τ-intervals with equal widths from the vertical well to the outer boundary of the 3D reservoir model. The ECLIPSE generated pressure transient data are integrated into the prior reservoir model after formulating the well test derivative sensitivity coefficients with respect to reservoir permeabilities within the τ-intervals.

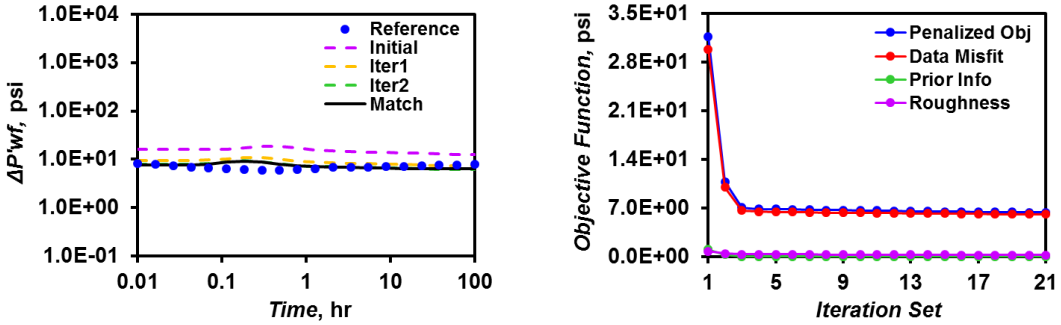

(a) Well Test Derivative **(b) Objective Function**

Figure 4.30 Integration of pressure transient data into the 3D homogeneous prior model during a constant flow rate well test with the 3D heterogeneous Brugge full field as the reference model using τ-interval based sensitivity coefficients (β_1 = 0.5 and β_2 = 150; linearly distributed τ-intervals; NTau = 20)

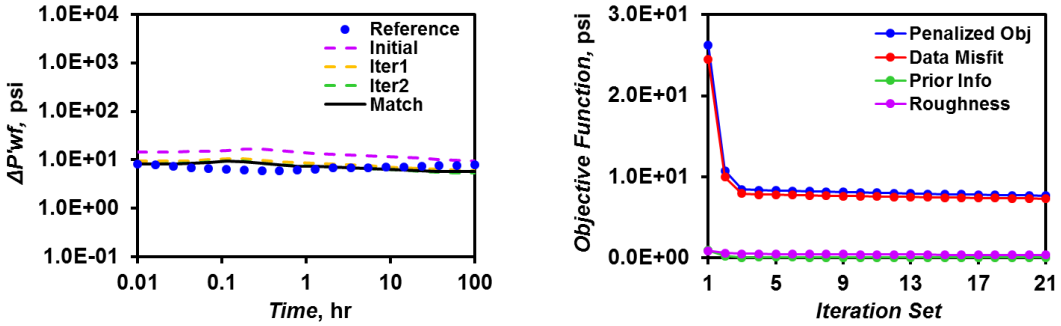

(a) Well Test Derivative **(b) Objective Function**

Figure 4.31 Integration of pressure transient data into the 3D heterogeneous prior model during a constant flow rate well test with the 3D heterogeneous Brugge full field as the reference model using τ-interval based sensitivity coefficients (β_1 = 0.5 and β_2 = 200; linearly distributed τ-intervals; NTau = 20)

From Figure 4.30 and Figure 4.31, we can observe the well test derivative variation when the penalized objective function is minimized during history matching of the 3D

Brugge reservoir model with the well test data. After several sets of iterations, the well test derivative after inversion can generally match the reference well response (Figure 4.30a and Figure 4.31a). However, there are still some discrepancies between the FMM and ECLIPSE generated well test derivatives after inversion. When the pressure front propagates beyond the well cell, the reduced hybrid drainage volume formulated based on the FMM calculated DTOFs will have some adverse impact upon the well test derivative curve, which will be slightly higher than the ECLIPSE generated well well test derivative. As the well test time is longer than 3hrs, strong local reflections of the pressure front can be felt in the near-well region within the reference model (Figure 4.29b, c and d) due to the high permeability contrast. This makes the well pressure profile calculated from the asymptotic pressure approximation at late times less valid compared with that calculated at the early times of well test, when the pressure front propagates mainly within the near-well high-permeability region (Figure 4.30a and Figure 4.31a). This explains why the data misfit within the penalized objective function stops decreasing after three sets of iterations in both cases of the 3D Brugge model inversion (Figure 4.30b and Figure 4.31b).

From Figure 4.32 to Figure 4.37, we demonstrate the inversion results after integrating the pressure transient data into the 3D Brugge full field model. The updated model has a permeability has a major modification of the prior permeability near the wellbore, which is also more similar to the reference permeability around it. This is because major drainage volume sensitivity occurs within the near-well region. Beyond that region, there are still some sensitivity and reservoir properties are updated with much smaller magnitudes from the prior model (Figure 4.32d to Figure 4.37d).

In the first inversion (Figure 4.32 to Figure 4.34), an ellipse-shaped permeability is distributed close to the wellbore in each horizontal layer since a homogeneous and anisotropic prior model is used for adjusting reservoir permeabilities (Figure 4.32c, Figure 4.33c and Figure 4.34c). This result demonstrates that the inversion methodology we propose can be efficiently used for the near-well permeability calibration using pressure transient data within general 3D heterogeneous and anisotropic reservoir models.

The second inversion result (Figure 4.35 to Figure 4.37) shows that the calibrated permeability is closer to the reference heterogeneous permeability, especially within those high-permeability layers (Layer 6, Layer 7 and Layer 8 in Figure 4.35c, Figure 4.36c and Figure 4.37c, respectively) where much more permeability changes from the prior model can be observed (Figure 4.35d, Figure 4.36d and Figure 4.37d). The is mainly because the pressure front propagates faster in those high-permeability regions, which will make the sensitivity of the drainage volume and well test derivative to reservoir properties higher compared to other regions (Figure 4.7b and d).

However, the overall calibrated permeability is still quite similar to the heterogeneous prior permeability (Figure 4.32 to Figure 4.37) even only a small coefficient is assigned to the prior term within the penalized objective function ($\beta 1 = 0.5$). Even the prior information given is completely wrong, the calibrated permeability still preserve large proportions of features within the prior model (Figure 4.32, Figure 4.33 and Figure 4.34). This reminds us the significant role the prior static geologic model plays during history matching of the reservoir model using pressure transient data.

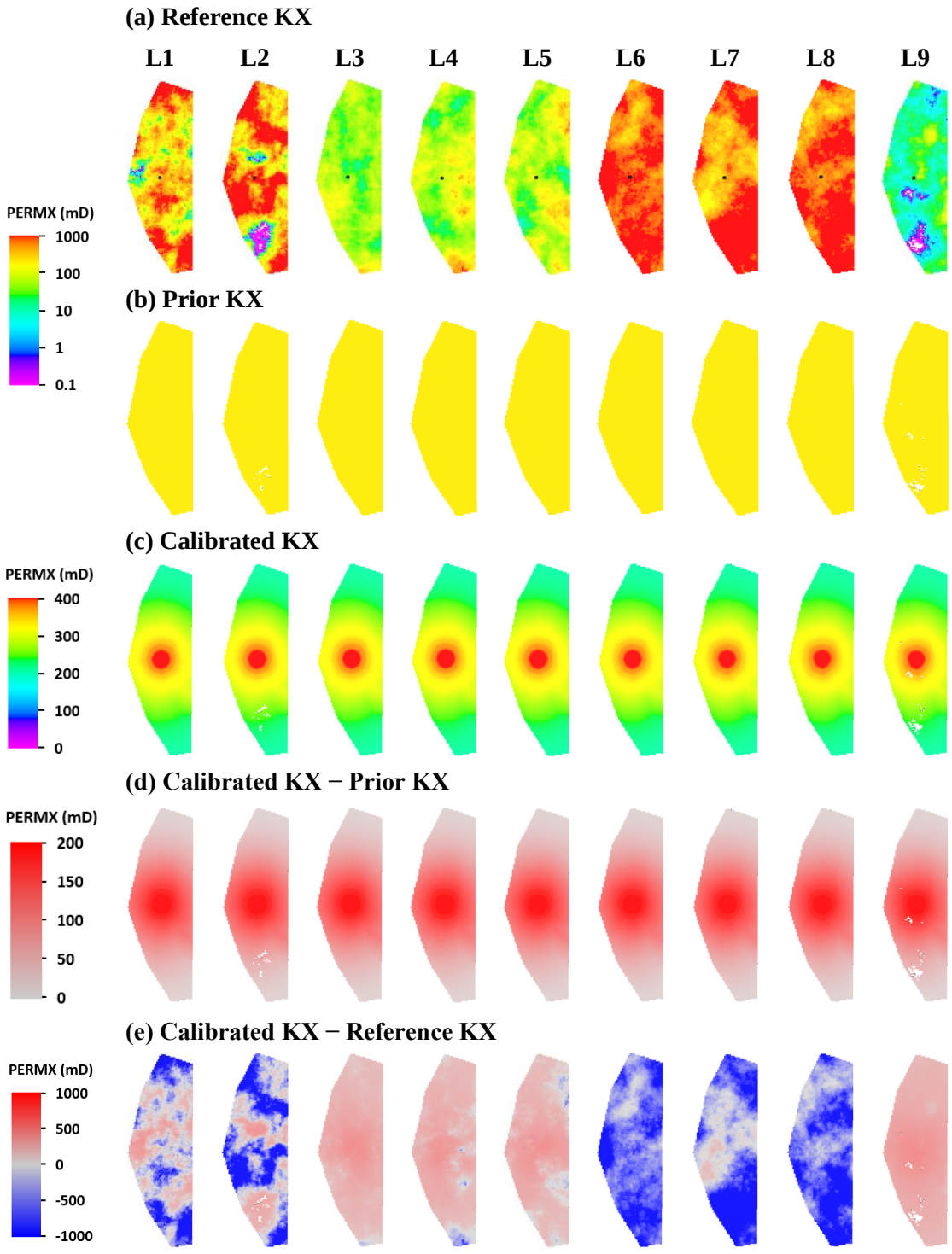

Figure 4.32 Anisotropic permeability inversion for 3D infinite-acting flow from the Brugge full field with a homogeneous prior permeability (PERMX inversion) using τ-interval based sensitivity coefficients (linearly distributed τ-intervals; NTau = 20)

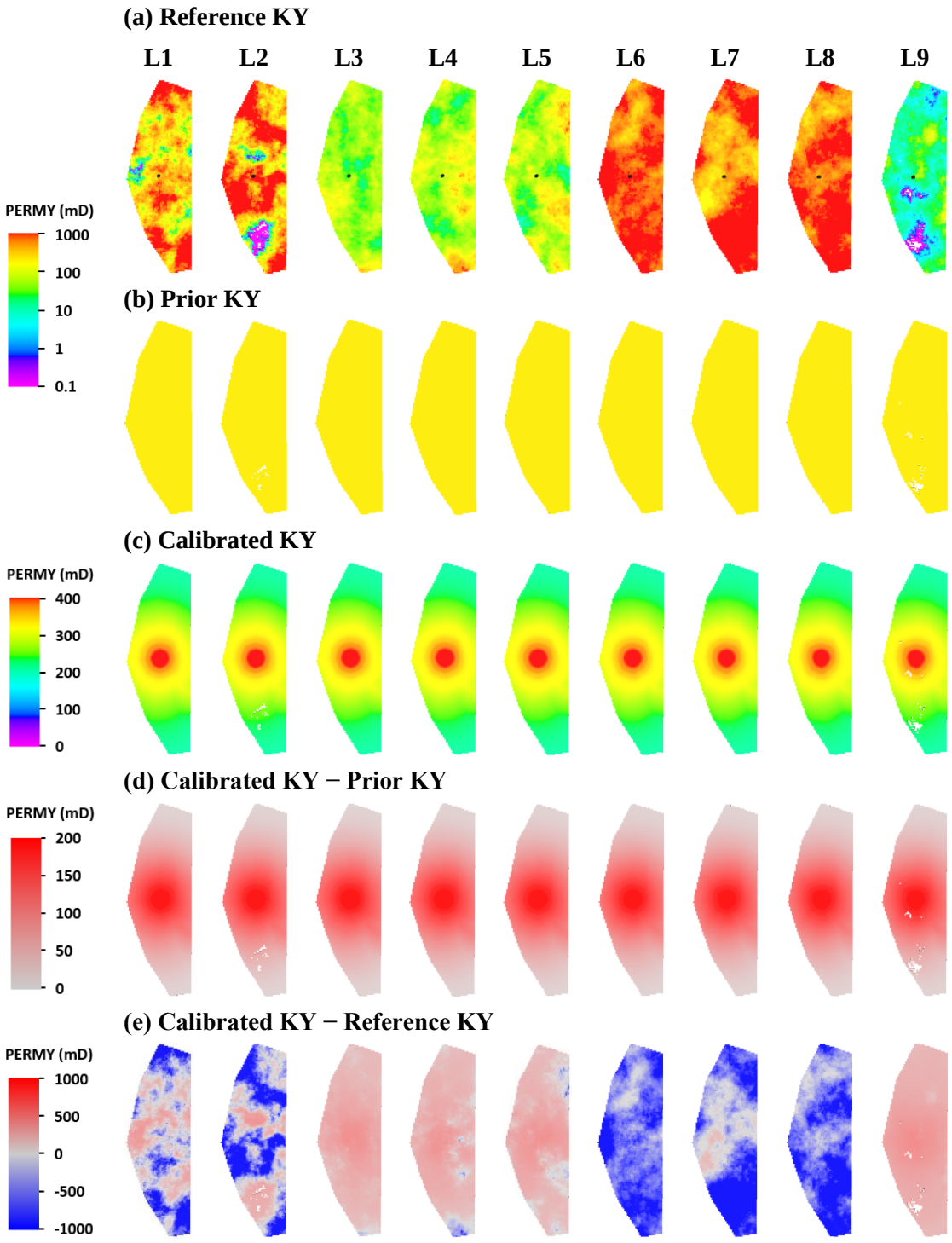

Figure 4.33 Anisotropic permeability inversion for 3D infinite-acting flow from the Brugge full field with a homogeneous prior permeability (PERMY inversion) using τ-interval based sensitivity coefficients (linearly distributed τ-intervals; NTau = 20)

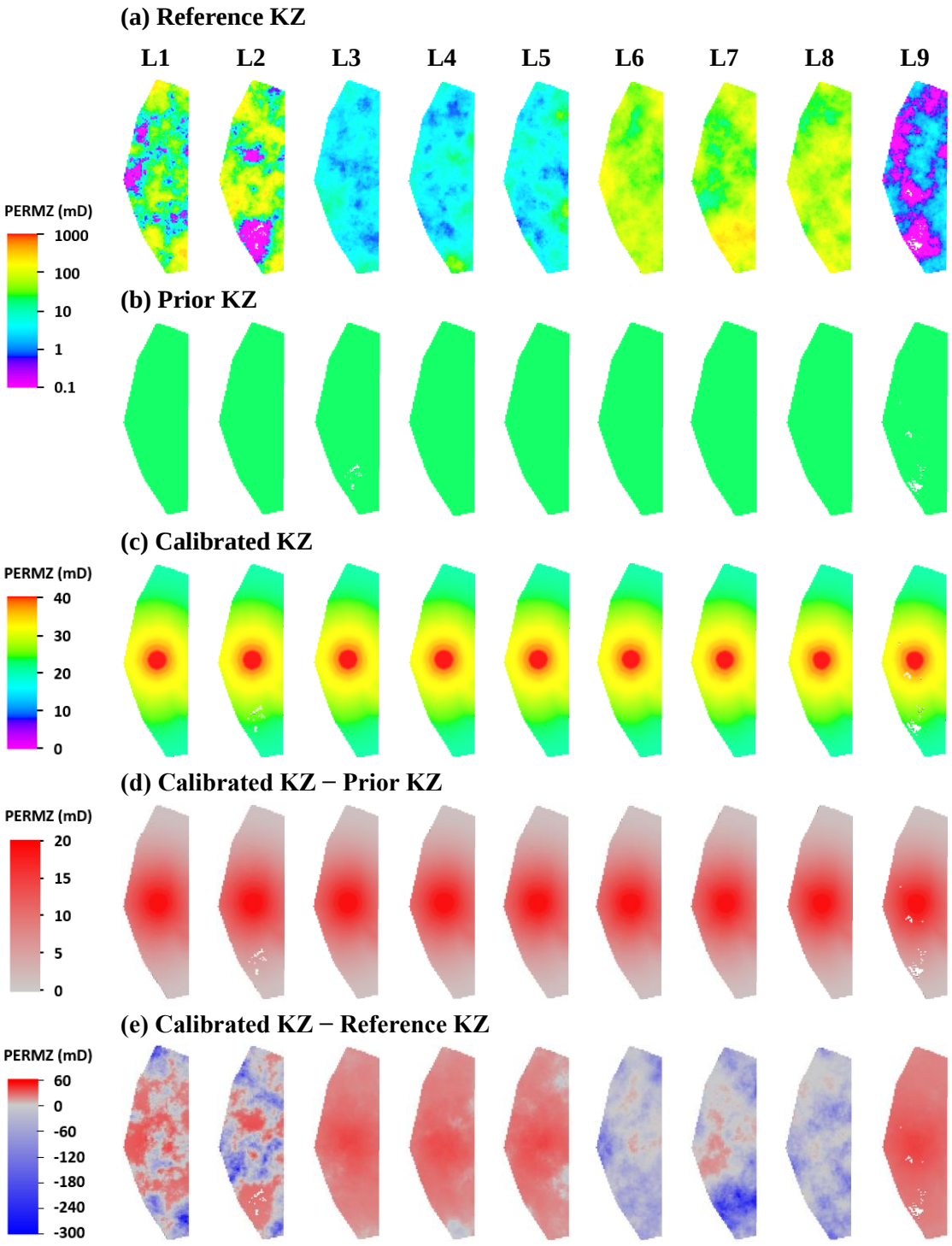

Figure 4.34 Anisotropic permeability inversion for 3D infinite-acting flow from the Brugge full field with a homogeneous prior permeability (PERMZ inversion) using τ-interval based sensitivity coefficients (linearly distributed τ-intervals; NTau = 20)

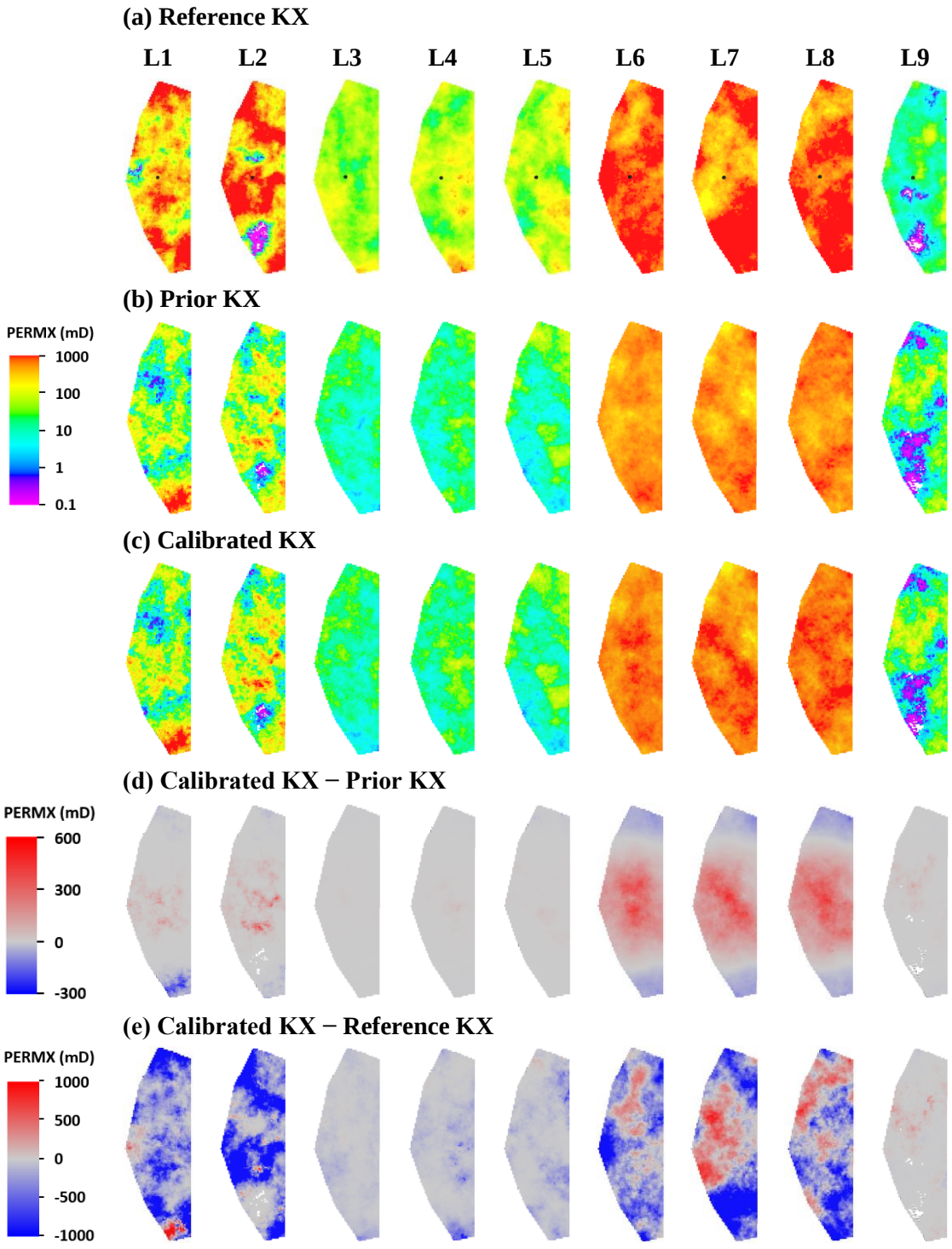

Figure 4.35 Anisotropic permeability inversion for 3D infinite-acting flow from the Brugge full field with a heterogeneous prior permeability (PERMX inversion) using τ-interval based sensitivity coefficients (linearly distributed τ-intervals; NTau = 20)

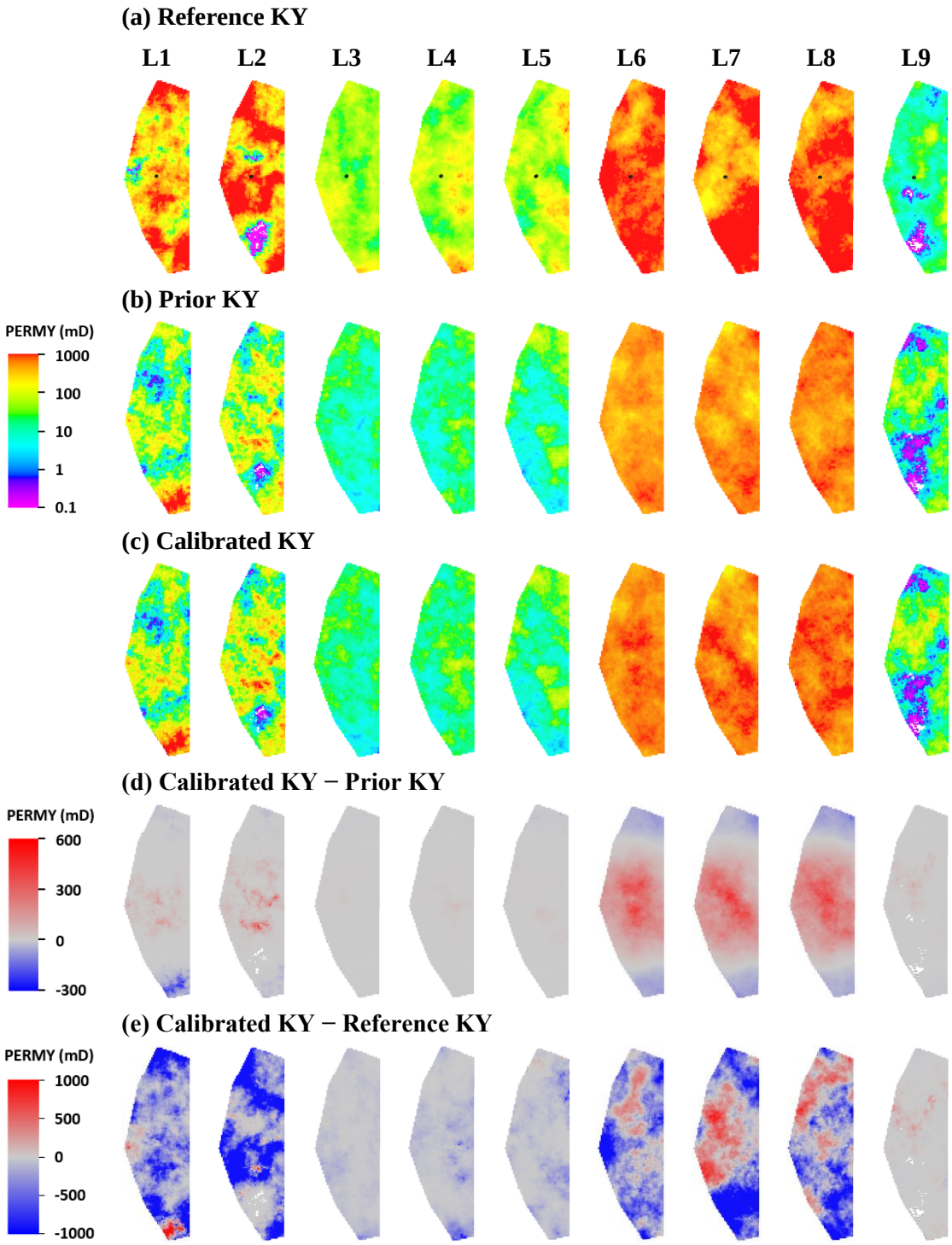

Figure 4.36 Anisotropic permeability inversion for 3D infinite-acting flow from the Brugge full field with a heterogeneous prior permeability (PERMY inversion) using τ-interval based sensitivity coefficients (linearly distributed τ-intervals; NTau = 20)

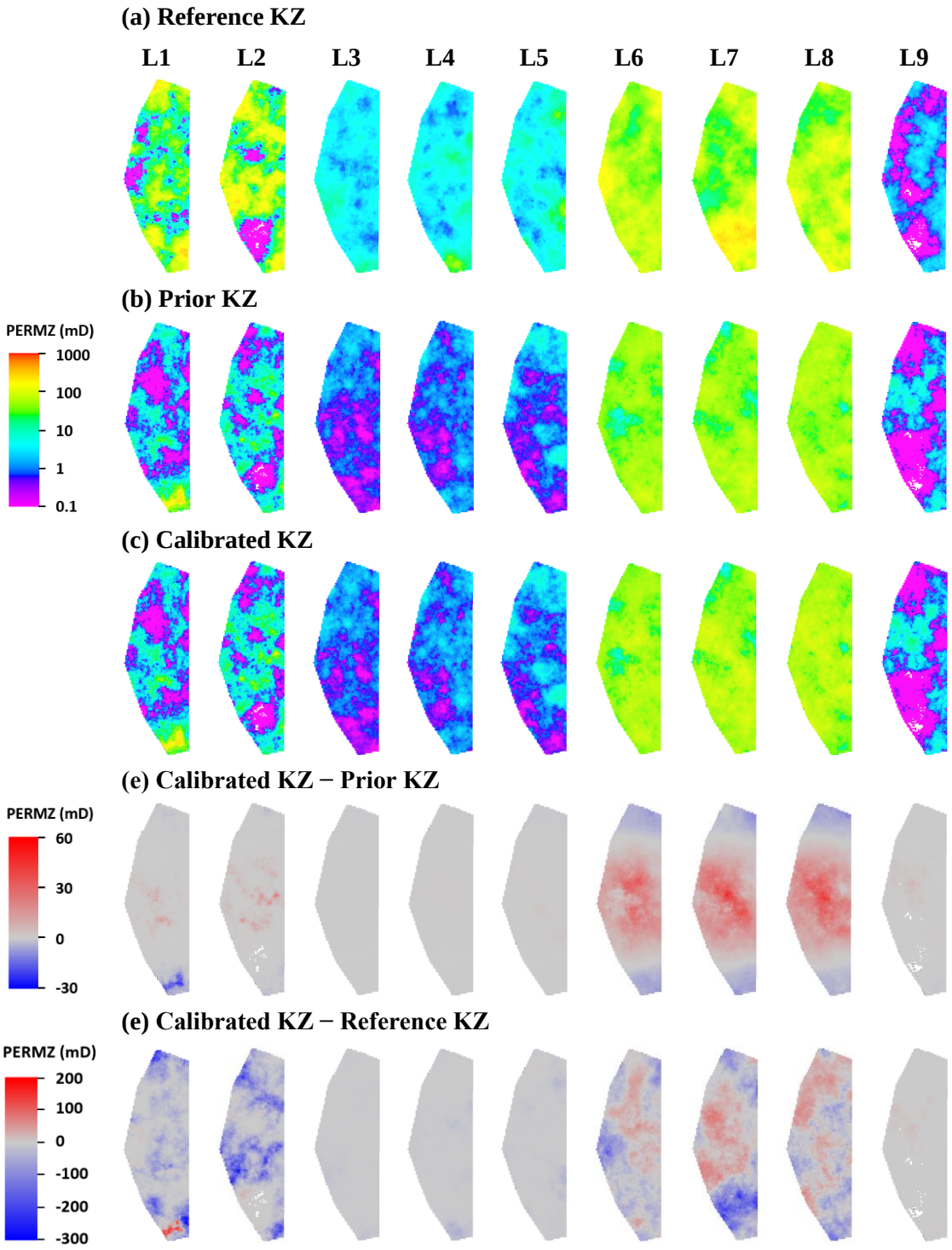

Figure 4.37 Anisotropic permeability inversion for 3D infinite-acting flow from the Brugge full field with a heterogeneous prior permeability (PERMZ inversion) using τ-interval based sensitivity coefficients (linearly distributed τ-intervals; NTau = 20)

4.4 Discussion

Successful application of the asymptotic pressure approximation in heterogeneous reservoir models relies on a "sufficiently" smooth distribution of the porous media. This will guarantee that the pressure gradient can be well approximated by the DTOF gradient. When the reservoir model heterogeneity increases, it is advisable to calculate the Dykstra-Parsons coefficient (VDP) for the reservoir permeability first, which can provide us a general idea of the applicability of our methodology for pressure transient analysis.

Calibrating reservoir permeability from well test data using the asymptotic pressure approximation relies upon an accurate drainage volume forward model, which is significantly impacted by the DTOF calculation. In this sense, discretization of the Eikonal equation and selection of a sufficiently accurate FMM becomes quite important.

Inversion with respect to grid-cell parameters fails because of the directional "preference" of the well test derivative sensitivity with respect to grid-cell reservoir parameters. The grid-cell based analytic sensitivity calculation easily leads to an unstable inversion even when comparable magnitudes of the prior information and roughness are included into the penalized objective function.

The τ-interval based analytic sensitivity calculation can significantly reduce the sensitivity "preference" in certain directions in 2D and 3D spaces. It proves to be more suited than the grid-cell based sensitivity calculation to calibrating the near-well permeabilities using the pressure transient data. From the wellbore to the reservoir outer boundary, only a limited number of τ-intervals needs to be defined. Hence, sensitivity calculation does not depend upon the size of the inverse problem.

Linearly distributed τ-intervals defined from the wellbore to the outer boundary of the reservoir model are recommended to be used in inversion because they can make the regularization of the penalized objective function easier compared with the logarithmically distributed τ-intervals. Using the logarithmically distributed τ-intervals to calibrate near-well permeaiblities can easily generate unstable inversion results, especially when the prior information is far from accurate. Except for the lower and upper limits, definition of the τ-intervals can be independent of the DTOFs calculated from the FMM.

4.5 Section Summary

We developed and demonstrated a new method for integrating well test derivative data into 3D heterogeneous and anisotropic reservoir models reconciled with a prior static geologic model. It relies upon a calculation of the drainage volume in terms of the "diffusive time of flight" (DTOF) using the fast marching method (FMM). This method takes advantage of the fast simulation speed of the FMM to calculate the analytic sensitivity coefficient of the DTOF (τ) with respect to reservoir parameters, which can be included into a penalized objective function to be minimized during inversion.

Application of the grid-cell based sensitivity calculation fails to generate stable inversion results. In steady, formulation of the analytic sensitivity coefficients of the well test derivative to reservoir parameters within the "τ-intervals" can significantly improve the inversion stability. Successful calculation of the τ-interval based analytic sensitivity coefficients can effectively help adjust permeability values within the depth of investigation (DOI) to a prior static geologic model.

The following conclusions can be drawn for this inversion study.

1) Application of the asymptotic pressure approximation relies significantly on the "smoothness" of the heterogeneous reservoir porous media. Before inversion, it is recommended to validate its applicability by comparing the pressure profile generated from the asymptotic pressure approximation with a reservoir simulator.
2) The well test derivative is shown to be inversely proportional to the drainage volume as a function of time. It is important to keep a predominantly transient-state flow within the reservoir model when using the well test derivative as the objective function to conduct history matching.
3) Analytic sensitivity coefficients of the DTOF with respect to reservoir parameters can be formulated from a functional derivative of the Eikonal equation, which can be numerically realized by tracking the "characteristic" direction of the local Eikonal solver using one single forward simulation of the FMM.
4) Analytic sensitivity coefficients have been validated with numerical ones. At a given time of the constant flow rate well test, magnitudes of the sensitivity coefficients of the well test derivative with respect to reservoir permeabilities in the near-well region are larger than those far away from the well. At a given location within the reservoir model, the well test derivative sensitivity with respect to reservoir permeability is a function of time. The well test derivative sensitivity coefficient will reach a "peak" magnitude when the DOI passes by.

5) Evaluation of the sensitivity coefficients using the FMM on a grid-cell basis leads to unstable inversion results due to the directional "preference" of the drainage volume sensitivity formulated in terms of the DTOF (τ).
6) Grid-cell based sensitivity formulation can help generate stable inversion results in 1D models, but fails in calibration of 2D and 3D reservoir models using the pressure transient data. By formulating the analytic sensitivity coefficients of well test data with respect to reservoir parameters within a limited number of τ-intervals defined, degrees of freedom of reservoir parameters to be calibrated in inversion can be significantly reduced and the computational efficiency of inverse modeling can be tremendously improved using the FMM.
7) Our inverse modeling approach will adjust the reservoir model to the average permeability as a function of distance "DTOF (τ)" to the wellbore within the drainage volume. Major modifications of the prior permeability occur within the DOI because major drainage volume sensitivity occurs within it. Beyond the DOI, reservoir permeability values can also be updated but with smaller magnitudes.
8) Large proportions of the geologic features within the prior model will be preserved during history matching of the reservoir model with pressure transient data, even when the prior information provided is completely wrong. Inverse modeling results remind us of the importance of the prior static geologic model.

5. AN ANISOTROPIC FAST MARCHING METHOD FOR RESERVOIR MODELS WITH COMPLEX GEOMETRIES IN FAULTED CORNER POINT GRIDS

Three-dimensional reservoir models often need to deal with geologic formations that are not horizontal with non-uniform thickness. The grid cells used to discretize the reservoir models with irregular shapes usually need to have sufficient flexibility that can adapt to the complex geometric features. The corner point grid (CPG) has been recognized as efficient in representing complex geologic features for reservoir simulation using distorted structures with an easy numerical implementation. It provides the basis for characterization of fluid and pressure communications between grid cells that have a mutual interface with complete or partial overlapping areas.

We propose a new algorithm for solving the Eikonal equation in general anisotropic and heterogeneous media using the fast marching method (FMM) in 3D reservoir models within the CPGs. It is an extension of the first-order local Eikonal solution implemented on 2D triangular meshes and 3D tetrahedral meshes. The new scheme relies upon an upwind finite difference approximation to the local gradient and ensures the causality relationship when the "diffusive time of flight" (DTOF) is updated within a simplex. Local Eikonal solutions in 1D, 2D, and 3D spaces are formulated in a general quadratic equation based on the tangent vectors within the CPG, the unknown of which has explicitly formulated coefficients. Solution of the quadratic equation for the unknown DTOFs requires an enforcement of the causality condition within the 2D triangular element and 3D tetrahedral element. The new Eikonal solver is included in a

FMM algorithm, which can be efficiently used to solve for the DTOF in reservoir models within the faulted CPG system.

5.1 Introduction

The fast marching method (FMM) has a wide application in seismology, where the solution of the Eikonal equation is used for prediction of seismic travel times and 3D teleseismic tomography (Rawlinson and Sambridge, 2004, 2005). Most of those grids used in travel time calculation and seismic tomography are orthogonal, where the media anisotropy can be treated without rotation of the speed (equivalently permeability or diffusivity in reservoir engineering) tensor matrix that defines its principal components in the 3D coordinate system. Thus, calculation of the arrival time or the time of flight (TOF) for general heterogeneous and anisotropic media using the FMM is easy to implement within the orthogonal grid system.

For unstructured grid meshes where the basic elements are triangular, the local solver of the Eikonal equation that can be used for updating the TOF value at one particular node is formulated either based on Fermat's principle or an Eulerian discretization. Both formulations can be used for either isotropic or anisotropic media. In isotropic media, the TOF gradient is aligned with the characteristic direction. In contrast, there usually exists a discrepancy between the TOF gradient and the characteristic direction in anisotropic media. In both methodologies, updating the TOF value at a specific node in 3D space replies upon one, two or three nodes whose TOF values are given. If the local solver is constructed based on Fermat's principle, the actual travel time to the unknown is

calculated by a minimization algorithm. It is easy for physical interpretations but the computational cost is expensive, especially when the model size is large. The local solver based on an Eulerian discretization is proven to be equivalent to the one based on Fermat's principle and is more straightforward to be implemented, especially for TOF calculation within anisotropic media.

The key to successful implementation of the FMM is to maintain the causality relationship, which means that the solution of each node to be updated depends only upon the smaller adjacent values (Sethian and Vladimirsky, 2000). This requirement is more likely to be violated when the anisotropic Eikonal equation is being solved within unstructured grids. Many research efforts had been made to avoid violation of the causality condition. Some of these efforts focus on approximating front propagation in triangulated meshes that contain simplexes with obtuse angles by a splitting section method, where any obtuse angle will be divided into acute angles (Sethian and Vladimirsky, 2000; Qian et al., 2007). Another commonly used technique to ensure the causality condition is the recursive correction, where TOF values of all neighboring nodes to a particular node being just accepted need to be re-computed using the newly and already accepted values (Konukoglu et al., 2007).

One effective strategy for maintaining the causality condition is enforcing the characteristic vector to pass through a triangular or tetrahedral element, where the 3D Eikonal solution often reduces into a 2D or 1D Eikonal solution (Qian et al., 2007). This process requires an efficient algorithm to compute travel time from one source point to another specific point in 3D homogeneous and anisotropic media, which can be achieved

using an iterative algorithm (Qian and Symes, 2001; Qian et al., 2007). However, this might lead to increased computational efforts when causality enforcement is required to be implemented extensively.

In this section, we propose a new local Eikonal solution that can be used to compute travel time in general anisotropic media. It is derived from the Eulerian discretization and much more straightforward to implement within the FMM algorithm. The causality enforcement can be more efficiently realized by an explicit formulation of a 1D or 2D Eikonal solution in 3D space, without the need to use iterative procedures. This new FMM is adaptive for unstructured and corner point grids, where complex geometric reservoir features like faults and pinch-outs can be easily represented.

5.2 Methodology: Corner Point Grid

Corner point grids (CPG) have wide applications in reservoir simulation because of its ready adaptability to structural variation in geologic formations and the capability to represent complex geologic features (Ponting, 1989). A typical 3D corner point is constructed by four pillars and the coordinate in the vertical direction (z-coordinate), with the top and base conforming to geologic strata.

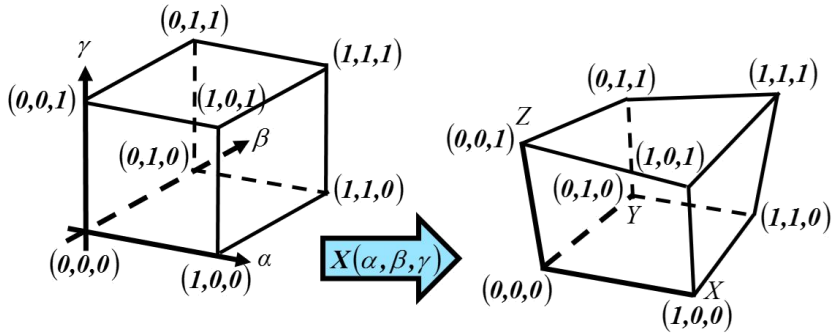

Figure 5.1 Tri-linear interpolation in (α, β, γ) from the 8 cell vertices (Zhang et al., 2013)

Its distorted geometry can be defined by the tri-linear isoparametric mapping from the reference unit space to the physical space (Figure 5.1). Given the point (X, Y, Z) within the physical space and its corresponding isoparametric coordinates (α, β, γ) within the unite space, it is convenient to specify the tangent vectors at any location within the CPG. The permeability tensor can be defined based on the tangent vectors and will also become location-dependent within the CPG.

5.2.1 Anisotropy and Cell Geometry

In anisotropic reservoir media, the Eikonal equation used for characterizing the pressure front propagation in the subsurface can expressed using the permeability tensor (Datta-Gupta et al., 2007).

$$\nabla\tau\left(\vec{x}\right)\bullet\vec{\vec{k}}\bullet\nabla\tau\left(\vec{x}\right)=\phi\mu c_t \tag{5.1}$$

By constructing the permeability tensor as a function of location within a CPG, we can reformulate the anisotropic Eikonal equation (Eq.(5.1)) using the tangent vectors and the isoparametric coordinates within it.

Zhang et al. (2013) represents the anistropic Eikonal equation (Eq.(5.1)) using the tangent vector of the CPG. Suppose that the principal directions of anisotropy for the reservoir media are along the tangent unit vectors $\vec{\boldsymbol{t}}_l / t_l$ ($l = 1,2,3$), where t_l is the norm of $\vec{\boldsymbol{t}}_l$. In the reference space, the permeability tensor can be formulated as a diagonal tensor $diag(k_l)$. By introducing a transformation matrix that consists of the unit vectors associated with the principal directions of anisotropy, $\boldsymbol{T} = \left[\vec{\boldsymbol{t}}_1 / t_1, \vec{\boldsymbol{t}}_2 / t_2, \vec{\boldsymbol{t}}_3 / t_3\right]$, the permeability tensor in the physical space can be written as $\vec{\vec{\boldsymbol{k}}} = \boldsymbol{T} diag(k) \boldsymbol{T}'$, which further reduces to

$$\vec{\vec{\boldsymbol{k}}} = \sum_{l=1}^{3} \frac{k_l}{t_l^2} \vec{\boldsymbol{t}}_l \vec{\boldsymbol{t}}_l \tag{5.2}$$

Then the Eikonal equation in the corner point grid can be expressed as

$$\sum_{l=1}^{3} \left(\frac{k_l}{\left|\vec{\boldsymbol{t}}_l\right|^2} \right) \cdot \left(\frac{\partial \tau}{\partial \alpha_l} \right)^2 = \phi \mu c_t \tag{5.3}$$

Here the unknown variable becomes dependent upon the isoparametric coordinate (α, β, γ) in the reference space.

The anisotropic Eikonal equation formulated in Eq.(5.3) sets up the basis for DTOF calculation within the CPG with complex geometries, which might even be used for pinch-out feature characterization. For example, if a CPG with a pinch-out feature

occurs in one of the three principal directions of anisotropy (I, J, or K), the magnitude of the tangent vector along that direction becomes zero and the norm of diffusivity tensor along that direction becomes infinity. This will lead to a zero value of DTOF increase along the direction where pinch-out occurs.

5.2.2 Pressure Communication

The pressure communication between adjacent CPGs relies upon their geometric features and the inter-cell transmissibility calculated. For a given DTOF value to be evaluated at the vertex of the CPG, it will be identical to DTOF to the vertex of the adjacent grid only when the inter-cell transmissibility is positive and share the same geometric position in space (Figure 5.2).

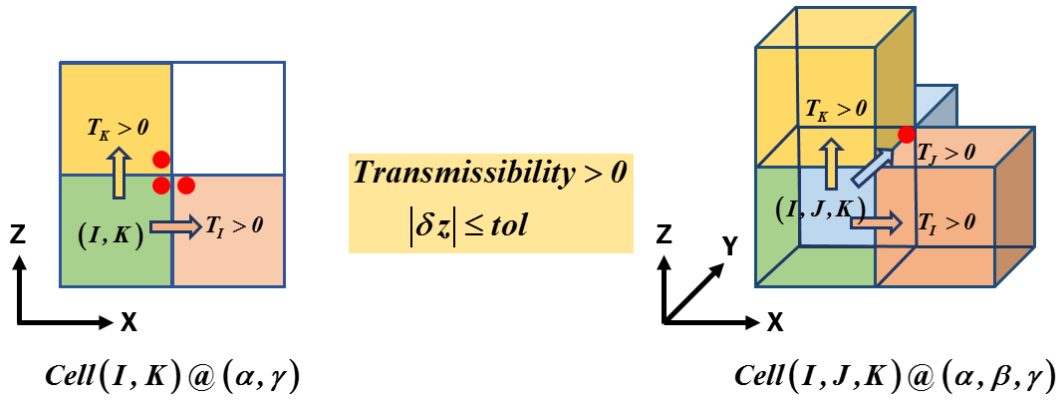

Figure 5.2 Pressure communication based vertex DTOF evaluation for adjacent CPGs sharing identical geometric positions in 2D and 3D spaces and having positive inter-cell transmissibilities

For the DTOF evaluated at a particular vertex (α,γ) of a CPG located at (I,K) in the 2D space, the location where pressure communicates with identical DTOFs calculated from the adjacent grid cells can be expressed as

$$\begin{aligned} &\textit{Adjacent Cell}\,(I):\ \textit{Cell}\,(I-1+2\alpha,K)\,@\,(1-\alpha,\gamma) \\ &\textit{Adjacent Cell}\,(K):\ \textit{Cell}\,(I,K-1+2\gamma)\,@\,(\alpha,1-\gamma) \end{aligned} \tag{5.4}$$

Similarly, the vertex location (α,β,γ) for pressure communication to occur with identical DTOF values calculated from the adjacent grid cells in the 3D space can be expressed as

$$\begin{aligned} &\textit{Adjacent Cell}\,(I):\ \textit{Cell}\,(I-1+2\alpha,J,K)\,@\,(1-\alpha,\beta,\gamma) \\ &\textit{Adjacent Cell}\,(J):\ \textit{Cell}\,(I,J-1+2\beta,K)\,@\,(\alpha,1-\beta,\gamma) \\ &\textit{Adjacent Cell}\,(K):\ \textit{Cell}\,(I,J,K-1+2\gamma)\,@\,(\alpha,\beta,1-\gamma) \end{aligned} \tag{5.5}$$

By such an identification of grid cells with potential common vertex DTOF values, the pressure communication will be ensured to occur only across adjacent grid cells with positive inter-cell transmissibilities. This is particularly important for the application of the transmissibility multiplier between faulted CPGs.

5.2.3 Grid Faulting and Non-Neighbor Connections

One of the major advantages of applying CPGs in reservoir simulation is its flexibility in defining non-neighbor connection (NNC) cells, which often occurs in the form that multiple cells stack together and share a mutual interface with another cell along complex fault-juxtapositions. The mutual interface area between two cells across a fault should be treated as a factor in inter-cell transmissibility calculation (Ponting, 1989).

Meanwhile, the transmissibility multiplier determined by permeability and thickness of the fault zones can be used to control the flow communications between cells separated by a fault (Manzocchi et al., 1999). In particular, application of realistic fault transmissibility multipliers within faulted reservoir models built using CPGs can significantly reduce the potential error in transmissibility formulation between partially-connected cells (Islam and Manzocchi, 2017).

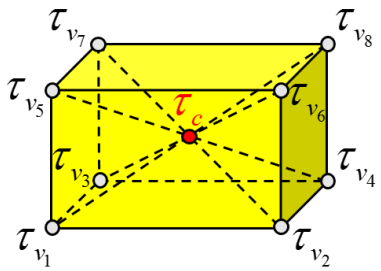

Figure 5.3 C9V5 Discretization of the Eikonal equation used for DTOF calculation within the FMM algorithm for 3D unfaulted grids

Given the NNC requirement for fault juxtaposition, we designed a new discretization scheme for the anisotropic Eikonal equation in corner point geometry models. The DTOF values are evaluated at the cell center and vertex of each CPG, which is name as a C9V5 discretization (Figure 5.3). Under such a discretization, each node at the cell center is connected with eight nodes at the cell vertices. Without faulted grid features, each node at the cell vertex is connected with fourteen nodes at cell centers and vertices. The basic element (simplex) used for constructing the local Eikonal solver is

triangular or tetrahedral in shape. Each unknown DTOF value is determined from the minimum local Eikonal solutions among neighboring elements.

The key to successful implementation of the C9V5 discretization scheme for the Eikonal equation is construction of a "next-node" variable used to store neighboring nodes for each node within the CPG reservoir model. The "next-node" variable is especially important for those nodes on the interface of partially juxtaposed cells across a fault. In the vertical direction (Z-direction), a node on the fault interface may not only have connections with the nodes within the cell it belongs to, it can also have immediate connections with nodes from adjacent grid cells along the fault interface (Figure 5.4).

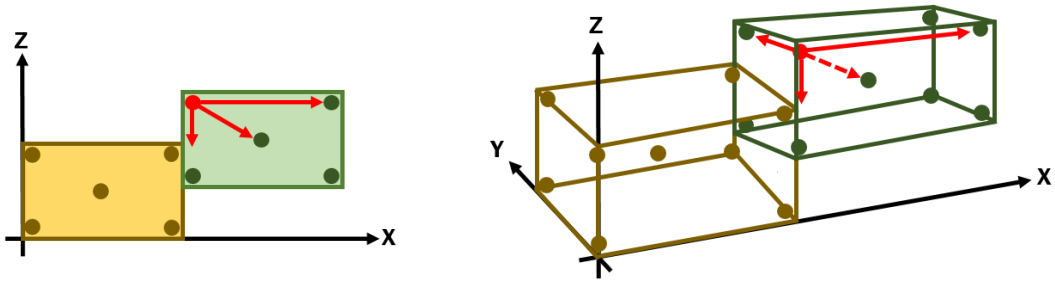

NNC in 2D coordinate **NNC in 3D coordinate**

Figure 5.4 Illustration of the nearest Z-node from the adjacent cell where pressure connection exists for faulted grids with NNC

DTOFs calculated for cells with neighbor and non-neighbor connections can represent the pressure communication across faulted grids. When the transmissibility multiplier is applied, the diffusivity can then be multiplied by an appropriate factor to

control the speed of pressure front propagation, which will have a significant impact on DTOF distributions across the faulted grids.

5.2.4 Extension to the Fast Marching Method

The corner point grid (CPG) has the flexibility in shape to conform to irregular geologic formations by a distorted cellular structure. Given the non-orthogonal shape of CPGs designed for reservoir models, we devised a new local Eikonal solver from an Eulerian discretization (Yang et al., 2017) that is easy for implementation within the FMM algorithm. This new local Eikonal solver is designed for the 2D triangular element and 3D tetrahedral element, so that the causality relationship can be easily maintained by enforcing the characteristic vector to fall within the simplex investigated (Figure 5.5).

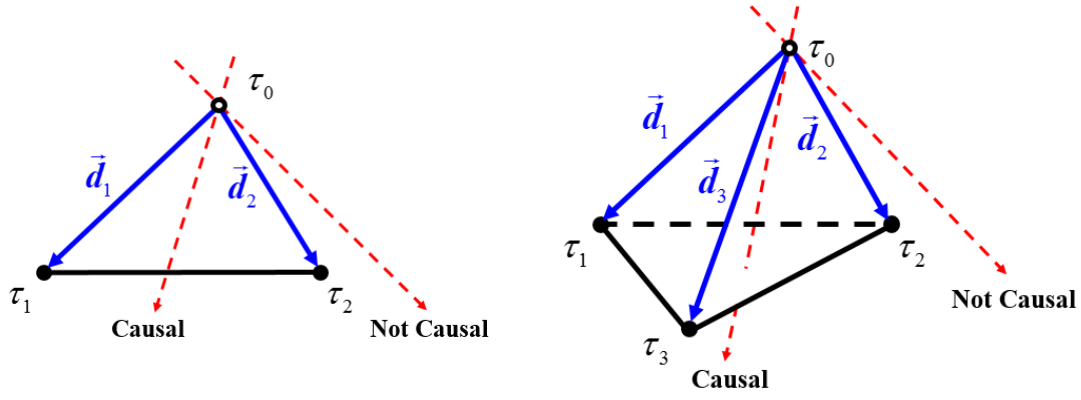

(a) 2D triangular element **(b) 3D tetrahedral element**

Figure 5.5 Local Eulerian causal solution to the Eikonal equation designed for the anisotropic FMM

Suppose we are computing the Eikonal solution to a node with an unknown DTOF value (τ_0) based on two known DTOF values (τ_1 and τ_2) in a 2D triangular element (Figure 5.5a) or based on three known DTOF values (τ_1, τ_2 and τ_3) in a 3D tetrahedral element (Figure 5.5b). The DTOF gradient within the element is assumed to be constant and can be related with the DTOF difference between two nodes with known and unknown DTOF values as

$$\vec{d}_i \bullet \nabla \tau = \tau_i - \tau_0 \tag{5.6}$$

where τ_i is referenced to the displacement vector $\vec{d}_i$ measured from the location of the unknown τ_0, and $i = 1,...,N \le 3$. The Eikonal characteristic vector can be defined as

$$-\vec{\vec{\alpha}}_D \bullet \nabla \tau = \sum_{j=1}^{N} a_j \vec{d}_j \tag{5.7}$$

where $\vec{\vec{\alpha}}_D = \dfrac{\vec{\vec{k}}_0}{\phi \mu c_t}$ and $\vec{\vec{k}}_0$ is the permeability tensor evaluated at the node where the DTOF is unknown. Thus, we can derive the DTOF gradient as

$$\nabla \tau = -\sum_{j=1}^{N} a_j \vec{\vec{\alpha}}_D^{-1} \bullet \vec{d}_j \tag{5.8}$$

The characteristic direction is constrained by the data support. If the solutions are causal then the weights satisfy $a_j \ge 0$. The data and the unknown τ_0 provide linear equations for the weights $\{a_i\}, i = 1,...,N$ as:

$$(\tau_0 - \tau_i) = -\vec{d}_i \bullet \nabla \tau = \sum_{j=1}^{N} a_j \left(\vec{d}_i \bullet \vec{\vec{\alpha}}_D^{-1} \bullet \vec{d}_j \right) \tag{5.9}$$

Based on above derivations, solution of the Eikonal equation can be represented by a quadratic equation for the unknown variable τ_0.

$$\nabla\tau \bullet \vec{\vec{\alpha}}_D \bullet \nabla\tau = \sum_{ij=1}^{N} a_i a_j \left(\vec{d}_i \bullet \vec{\vec{\alpha}}_D \bullet \vec{d}_j\right) = \sum_{i=1}^{N} a_i \left(\tau_0 - \tau_i\right) = 1 \tag{5.10}$$

To efficiently solve the quadratic equation, some implementation procedures are summarized below.

- If the unknown variable is supported by only one data point, a 1D local Eikonal solver can be derived from the elliptical solution (N = 1) for the anisotropic media $\left(\alpha_{D,x}, \alpha_{D,y}, \alpha_{D,z}\right)$. Since the elliptical solution is known to be a function of $\tau(r)$, where

$$r^2 \equiv \frac{x^2}{\alpha_{D,x}} + \frac{y^2}{\alpha_{D,y}} + \frac{z^2}{\alpha_{D,z}} \tag{5.11}$$

The DTOF gradient can be written as

$$\nabla\tau = \frac{1}{r}\left(\frac{x}{\alpha_{D,x}}, \frac{y}{\alpha_{D,y}}, \frac{z}{\alpha_{D,z}}\right) \tag{5.12}$$

The Eikonal equation becomes

$$\nabla\tau \bullet \vec{\vec{\alpha}}_D \bullet \nabla\tau = \left(\frac{d\tau}{dr}\right)^2 \tag{5.13}$$

And

$$\vec{\vec{\alpha}}_D \bullet \nabla\tau = \frac{1}{r}(x, y, z)\frac{d\tau}{dr} = \frac{1}{r}\vec{d}\,\frac{d\tau}{dr} \tag{5.14}$$

In such a way, the characteristic direction is aligned with the data support, $\vec{d}$.

- If the unknown variable is supported by two or three data points (Figure 5.5), then a 2D or 3D local Eikonal solvers need to be formulated. Let's define $\delta_{id}=1$ if data exists for point i; otherwise, $\delta_{id}=0$. Then Eq.(5.9) can be re-expressed in terms of a matrix form.

$$\begin{aligned}
&\left(\tau_0-\tau_i\right)=-\vec{d}_i\bullet\nabla\tau=\sum_{j=1}^{N}a_j\left(\vec{d}_i\bullet\vec{\vec{\alpha}}_D^{-1}\bullet\vec{d}_j\right)\\
&=\sum_{j=1}^{3}a_j\delta_{id}\left(\vec{d}_i\bullet\vec{\vec{\alpha}}_D^{-1}\bullet\vec{d}_j\right),\quad if\ \delta_{id}=1\\
&a_i=\sum_{j=1}^{3}a_j\delta_{ij}=0,\quad if\ \delta_{id}=0
\end{aligned}\tag{5.15}$$

In combination, for $i,j=1,...,N\le 3$

$$\delta_{id}\left(\tau_0-\tau_i\right)=\sum_{j=1}^{N}a_j\left\{\left(1-\delta_{id}\right)\delta_{ij}+\delta_{id}\delta_{jd}\left(\vec{d}_i\bullet\vec{\vec{\alpha}}_D^{-1}\bullet\vec{d}_j\right)\right\}\equiv\sum_{j=1}^{N}D_{ij}a_j \tag{5.16}$$

$$D_{ij}=\left(1-\delta_{id}\right)\delta_{ij}+\delta_{id}\delta_{jd}\left(\vec{d}_i\bullet\vec{\vec{\alpha}}_D^{-1}\bullet\vec{d}_j\right) \tag{5.17}$$

Here $\delta_{ij}=1$ if $i=j$; otherwise $\delta_{ij}=0$. If we define $M=D^{-1}$, the weights for causality satisfaction can be expressed as

$$a_i=\sum_{j=1}^{N}M_{ij}\cdot\delta_{jd}\left(\tau_0-\tau_j\right)=\sum_{j=1}^{N}\left(\delta_{id}M_{ij}\delta_{jd}\right)\cdot\left(\tau_0-\tau_j\right) \tag{5.18}$$

Specifically, $a_i=0$ if no data exist for point i. Substituting Eq.(5.18) into Eq.(5.10), the Eikonal equation can be obtained:

$$\nabla\tau\bullet\vec{\vec{\alpha}}_D\bullet\nabla\tau=\sum_{i=1}^{N}a_i\left(\tau_0-\tau_i\right)=\sum_{ij=1}^{N}\left(\delta_{id}M_{ij}\delta_{jd}\right)\left(\tau_0-\tau_i\right)\left(\tau_0-\tau_j\right)=1 \tag{5.19}$$

or

$$\tau_0^2 \sum_{ij=1}^{N} \left(\delta_{id} M_{ij} \delta_{jd} \right) - 2\tau_0 \sum_{ij=1}^{N} \left(\delta_{id} M_{ij} \delta_{jd} \tau_j \right) + \left\{ -1 + \sum_{ij=1}^{N} \left(\delta_{id} M_{ij} \delta_{jd} \tau_i \tau_j \right) \right\} = 0 \quad (5.20)$$

The coefficients for unknowns in Eq.(5.20) are easy to construct, leading to a local Eikonal solution that is much easier to implement within the FMM than that implemented by Qian et al. (2007) within the fast sweeping method (FSM). The latter often requires an iterative procedure to compute the wave or front propagation speed from a given direction when the unknown DTOF needs to be determined from two unknown points in the 3D space (Qian and Symes, 2001; Qian et al., 2007).

Since the diffusivity (or permeability) tensor in the CPGs depends upon the tangent vectors and varies within the cell, it is required that its value to be evaluated at the unknown points:

$$\vec{\vec{\alpha}}_{D,0} = \frac{\vec{\vec{k}}_0}{\phi \mu c_t} = \sum_{\ell=1}^{N} \frac{k_\ell}{\phi \mu c_t} \frac{1}{t_{\ell 0}^2} \vec{t}_\ell \vec{t}_\ell \equiv \sum_{\ell=1}^{N} \frac{1}{\tau_{\ell 0}^2} \vec{t}_\ell \vec{t}_\ell \quad (5.21)$$

When the characteristic vector falls within the 2D triangular element or the 3D tetrahedral element, the causality relationship is satisfied. In contrast, the causality relationship will be violated if the characteristic vector falls beyond the element. In this case, causality can be enforced by reducing the problem from $N = 3$ to $N = 2$ or from $N = 2$ to $N = 1$ (discarding one or more data points). It is always causal when $N = 1$. If the causality is still not satisfied within the triangular elements, the DTOF value to the unknown point can be updated by solving the Eikonal equation using the 1D elliptical solution. This causality enforcement has been used when DTOF values are calculated within the unstructured triangular meshes using the FSM (Qian et al., 2007).

5.3 Validation and Application

After formulating the causal Eulerian Eikonal solution, we applied it within the FMM algorithm and tested it with 3D reservoir models with heterogeneous and anisotropic porous media. We first applied this C9V5 FMM within a simple 3D synthetic model with heterogeneous but isotropic permeability and a uniform porosity distribution. There are pinch-out CPG geometries in the synthetic model and DTOFs evaluated at cell vertices are analyzed in detail. Then we test the C9V5 FMM on the Brugge benchmark model that has a highly heterogeneous and anisotropic permeability distribution as well as a heterogeneous porosity distribution. One main feature of the Brugge field is its faulted CPGs. We will show the DTOF distribution calculated from the anisotropic FMM across this fault and the potential impacts of the transmissibility multiplier across faulted grids have on pressure communication between them.

5.3.1 DTOF in Pinch-out Grid Geometry

A simple 3D reservoir model is built within a 5x5x5 CPG system, within which the central 3x3x3 grids have zero pore volume and are treated as inactive cells. This reservoir grid configuration leads to pinch-out geometry within grids on the outer boundary of the reservoir model. The horizontal permeabilities in the X (I) and Y (J) directions are identical and homogeneous, which have a uniform value of 100md. The permeability values in the Z (K) direction are 100md in the top and bottom layers, and are significantly lower within the second, third and fourth layers, which are only 0.1md. The reservoir porosity, viscosity and total compressibility are assumed to be 0.2, 1cp, and 1.0E-

5 psi^{-1}, respectively. All the 3D CPGs have an equal length and width of 50ft, and with a uniform height of 10ft in cells with no pinch-out geometries (Figure 5.6).

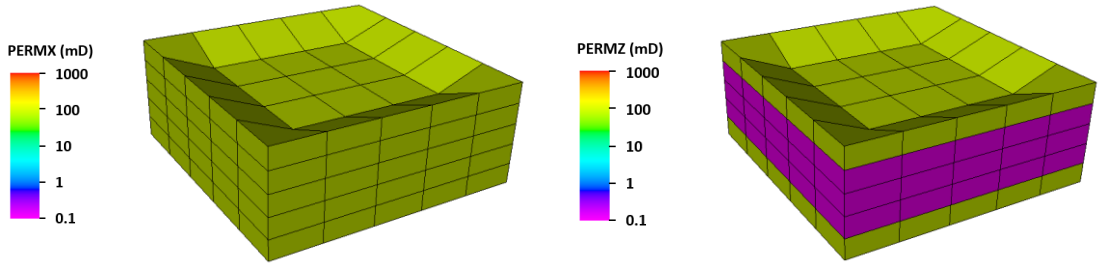

PERMX **PERMZ**

Figure 5.6 Anisotropic permeability distribution within the synthetic 3D reservoir model with pinch-out grid geometries

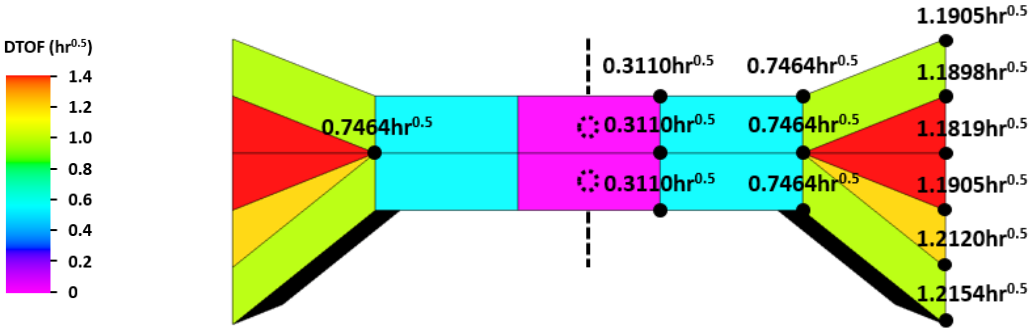

Figure 5.7 DTOFs calculated from the C9V5 FMM for the synthetic 3D reservoir model with pinch-out grid geometries and a fully-perforated vertical well (I =3; J = 3; K = 1:5)

Assume that a vertical well is placed the grid cell (3, 3) and perforates the 5 reservoir layers. Assigning the DTOFs at the grid-cell center of the top and bottom well

cell as zero, DTOFs at cell centers and vertices can be calculated using the C9V5 FMM. If we take a sectional view of a slice close to the well (between J = 2 and J = 3), we can observe the DTOF values at those pinch-out grid cells (Figure 5.7).

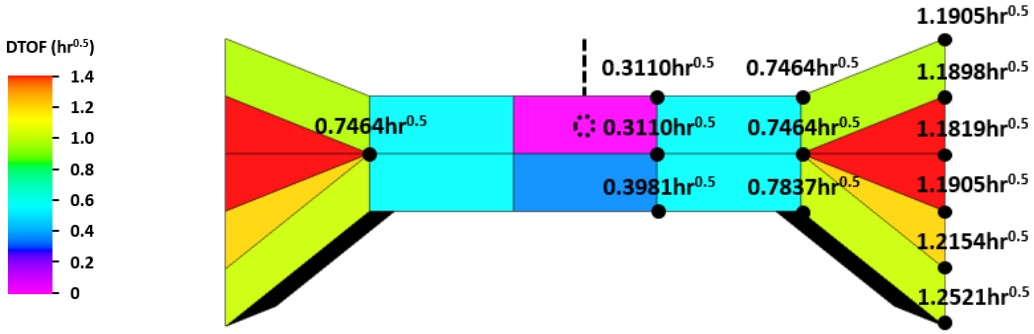

Figure 5.8 DTOFs calculated from the C9V5 FMM for the synthetic 3D reservoir model with pinch-out grid geometries and a partially-perforated vertical well (I = 3; J = 3; K = 1)

If the vertical well only perforates the first layer of the 3D reservoir model at the Cell (3, 3, 1), the DTOF values calculated from the C9V5 FMM at the bottom layer of the reservoir will increase. The DTOF value evaluated at the vertex where pinch-outs occur stays the same (Figure 5.8).

In both the model with a full-perforated well and the model with a partially-perforated well, the DTOF values are largest at those cells located at the reservoir outer boundary with peach-out features. The permeability in the Z (or K) direction within those cells is quite small (0.1md), which indicates the pressure front will arrive late at those cells mainly along the vertical direction (Figure 5.7 and Figure 5.8).

5.3.2 DTOF in Faulted Grid Geometry

The C9V5 FMM is tested on the Brugge full field model to solve for DTOFs within the CPGs and its distribution across the faulted grid cells with non-neighbor connections (NNC).

The Brugge model has a permeability field that is heterogeneous and anisotropic. The porosity within it is heterogeneous. The fluid viscosity and total compressibility of the reservoir are assumed to be 1cp and 1.0E-5 psi^{-1}, respectively. The reservoir model has a 3D dimension of 139x48x9 with a total number of 60048 cells, in which 44404 are active and 15644 are inactive with zero values of permeability and porosity. All active cells are located at the central reservoir region. Most of the inactive cells are located at outer boundary of the reservoir model. There is a major fault geometry within the active cell region, which is defined by (I = 64:95, J = 13:13, K = 1:9) and (I = 64:96, J = 14:14, K = 1:9), respectively. Grid cells with pinch-out features are all inactive and will have no impact on the DTOF calculation. In our study, a vertical well is placed at the (70, 23) location and perforates the entire nine reservoir layers (Figure 5.9).

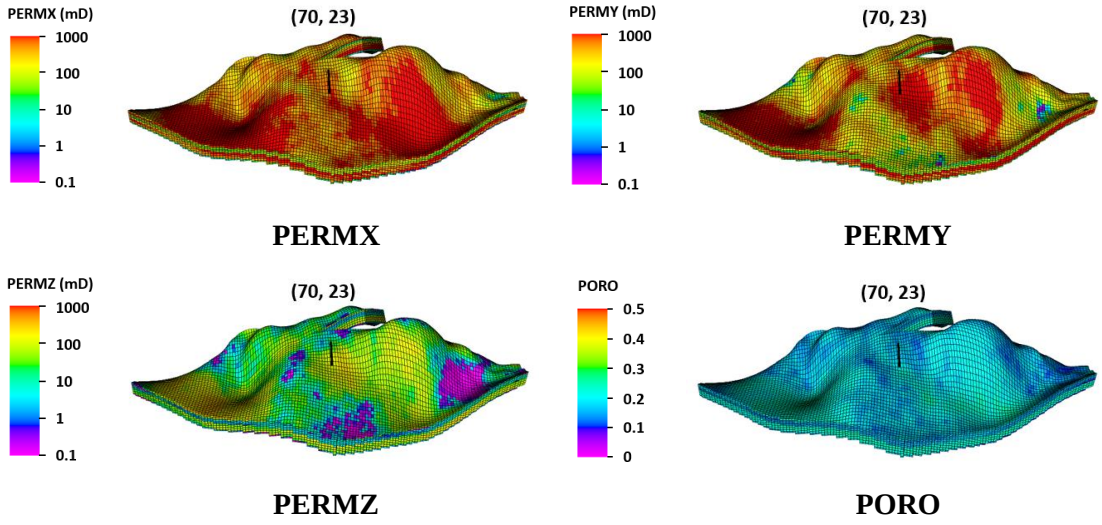

Figure 5.9 Permeability and porosity distributions within the Brugge full field model

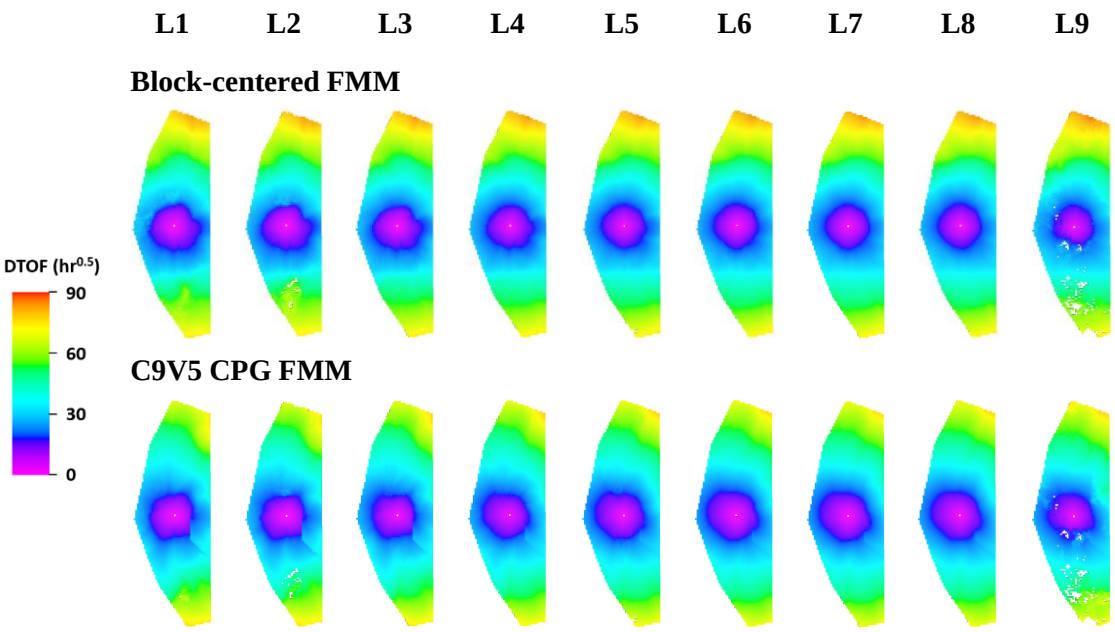

Figure 5.10 DTOFs generated from the Brugge full field model using the 3D block-centered FMM and the 3D C9V5 CPG FMM

Before simulation, we assign zero DTOF values to the centers of the nine cells where the vertical well perforates. In **Section 2**, we have calculated the DTOFs from the same Brugge model using a 3D block-centered FMM, which have a smooth variation across the fault region (Figure 5.10). By comparison, we can find that the DTOFs calculated from the 3D C9V5 CPG FMM are distinctively smaller than those generated from the 3D block-centered FMM. This indicates that accuracy of the Eikonal solution can be improved by adding more degrees of freedom of DTOFs to cell vertices. More importantly, abrupt changes of DTOF values across the fault structure can be clearly observed (Figure 5.10). This result demonstrates that the C9V5 CPG FMM can better capture pressure front propagation across faulted grids with NNCs.

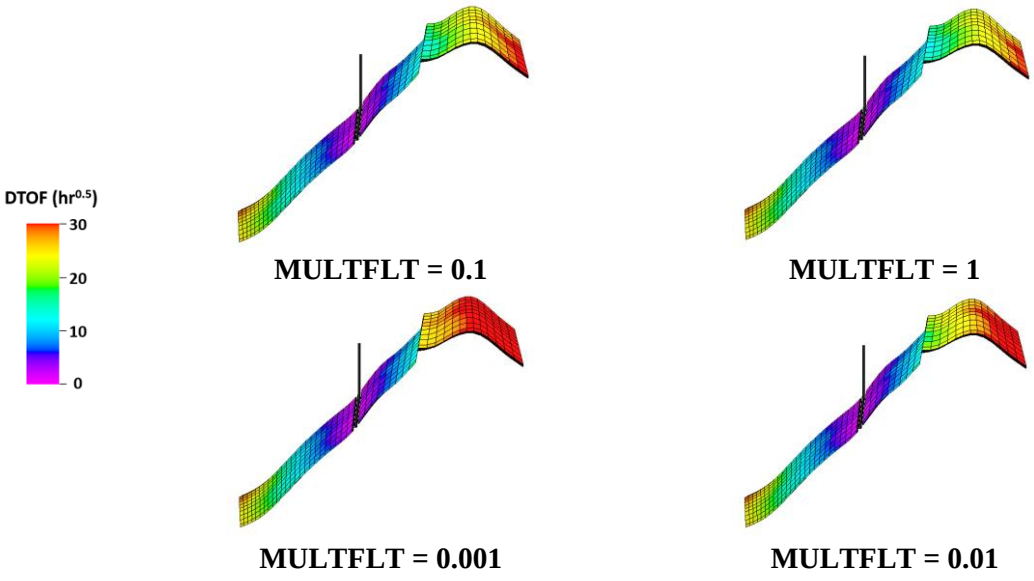

Figure 5.11 Illustration of DTOF distributions across faulted grids with NNCs influenced by the transmissibility multiplier implemented within the C9V5 CPG FMM within the Brugge full field model

Based on above analysis, we extended the C9V5 CPG FMM by including the transmissibility multiplier across the faulted grids. We take a slice (I = 70) across the fault in the Brugge model and compare the DTOF distribution on it when multiple values of transmissibility multipliers are implemented on the faulted grids with NNCs. The transmissibility multiplier is simply treated as a factor and multiplied by the permeability values within CPGs separated by the fault geometry (Figure 5.11).

From Figure 5.11, it can be observed that DTOF changes more abruptly across the fault when smaller values of transmissibility multiplier are assigned to the faulted grids. While the upstream DTOF values beyond the fault becomes larger as a result of stronger pressure barrier, the overall changes of DTOF in the downstream are not significant because of a closer distance to the wellbore. This result demonstrates that the C9V5 anisotropic FMM we propose for DTOF calculation can effectively capture pressure front propagation across fault features within 3D CPG reservoir models.

5.4 Discussion

Accurate calculation of the DTOF from the Eikonal equation in heterogeneous and anisotropic media is vital for characterization of pressure front propagation in the reservoir model. Discretization analysis of the Eikonal equation in previous sections has proven the importance of DTOF evaluation at both the cell center and vertex of orthogonal grids. It provides useful insights into more complex situations where faulted corner point grids (CPG) with distorted shapes are used for reservoir model discretization.

The Eikonal equation expressed in terms of the unknown DTOF variable and a symmetric permeability tensor forms the basis of DTOF calculation within general heterogeneous and anisotropic media. The permeability tensor expressed in terms of the tangent vector within a CPG makes it possible to evaluate the DTOF value at any location within the cell. Complex geometric features like faults and pinch-outs can be characterized by DTOFs calculated by solving the symmetric tensor Eikonal equation within the CPGs.

The transmissibility multiplier can be included into the CPG FMM to control the DTOF distribution separated by the fault, which can represent the ease of pressure communication between faulted grid cells. Abrupt DTOF changes between faulted CPGs with non-neighbor connections (NNC) indicate the pressure communication barrier between them.

The C9V5 FMM designed for general 3D heterogeneous and anisotropic reservoir models proves to be a fast and efficient numerical method for DTOF calculation from solving the anisotropic Eikonal equation, which is expressed in terms of reservoir properties and the tangent vectors within the CPGs. It provides us a convenient tool to characterize pressure communication between faulted CPGs with complex geometries using the DTOFs based on the asymptotic pressure approximation.

5.5 Section Summary

In this section, we presented a new local Eikonal solver based on Eulerian discretization and implemented it into the FMM for calculating the "diffusive time of flight" (DTOF) in reservoir models with anisotropic and heterogeneous media. It is readily

adaptable to unstructured triangulated meshes and has been successfully applied within faulted corner point grids (CPG).

After formulation of the causal local Eikonal solver and application to 3D reservoir models within the CPG system, following conclusions can be drawn.

1) The novel formulation of the local Eikonal solver can be successfully implemented on 2D triangular elements and 3D tetrahedral elements.
2) If the characteristic vector falls inside the elements in which the unknown point resides, the causality relationship is satisfied. If the causality is violated, it can be enforced by reducing the 3D local solver to the 2D or 1D local solver.
3) By solving a quadratic equation which has explicit coefficients of unknown variables, the new local Eikonal solution can be conveniently used to calculate the unknown DTOF based on three or two known DTOF values.
4) If the unknown DTOF is supported by only one data point, the elliptical solution can be used. This ensures that the DTOF is updated along the displacement vector from the unknown point to the known data point, which is aligned with the characteristic direction.
5) Solving for the DTOF using the 2D and 1D local Eikonal solvers within anisotropic media in the 3D space using the Eikonal solution we propose can be much more straightforward, without the need of an iterative algorithm to compute the front propagation speed from a given direction.

6) Based on the local causal Eulerian Eikonal solver we designed, we can calculate the DTOFs that can represent fault and pinch-out grid features in the CPG reservoir models with general heterogeneous and anisotropic media.

6. CONCLUSIONS AND FUTURE RESEARCH DIRECTIONS

6.1 Dissertation Contributions and Conclusions

In this dissertation, we presented the application of the fast marching method (FMM) to design a forward model as well as an efficient inversion scheme for pressure transient analysis. Detailed investigation of the FMM algorithm itself is the key to success of this research.

First, we investigate the asymptotic pressure approximation to the diffusivity equation based on the "diffusive time of flight" (DTOF) that can be calculated from solving the Eikonal equation using the FMM. A constant flow rate well test model is analyzed and related with drainage volume characterization. Discretization of both the Eikonal equation and the drainage volume is investigated and validated with the analytic solution. Pressure transient analysis is also related with the DTOF-based transient flow simulation. A hybrid drainage volume is constructed from the FMM calculated DTOFs, which relies significantly upon the analytic solution within the well cell to ensure an accurate characterization of the pressure transient behavior at very early times of flow simulation. The hybrid drainage volume construction leads to a stable DTOF derivative of the cumulative pore volume, which contributes to a significantly improved numerical solution to the DTOF-based one-dimensional diffusivity equation.

Second, we developed an inverse modeling method for integrating pressure transient data into reservoir models using the DTOF-based forward model. The inversion is realized by formulating the analytic sensitivity coefficients of the well test derivative

data with respect to reservoir parameters and by minimization of the objective function using a LSQR algorithm. The analytic sensitivity coefficients of the DTOF (τ) to reservoir permeability values can be obtained simultaneously with the DTOFs calculated from the FMM using one single forward simulation. Compared with the grid-cell based analytic sensitivity coefficient calculation, the "τ-interval" based sensitivity formulation can not only further improve the computational efficiency by decreasing the degrees of freedom of reservoir parameters to be calibrated, it also proves to help generate more stable inversion results.

Last, we presented a new formulation of the local Eikonal solution and extended the FMM to faulted corner point grids (CPG). The local solution to the Eikonal equation is derived from an Eulerian discretization that is consistent with Fermat's Principle. Complex geometric features are taken into account when the corner point grid FMM is designed.

The main findings in this research study are summarized below.

1) The novel local Eikonal solution formulated from an Eulerian discretization relies upon data support from nodal DTOF values already known. It can be used to solve for the DTOF of a specific point based upon one, two, or three data points with known DTOF values. Its implementation is straightforward and can be realized by solving a quadratic equation. In cases where the characteristic does not fall within the element in which the unknown nodal point reside, the causality condition can be enforced by reducing the number of data supports.

2) It has been proven that both discretization of the Eikonal equation and discretization of the drainage volume have significant impacts on pressure transient results. A hybrid version of drainage volume discretization leads to a much more accurate well pressure profile, especially during early times of simulation. The FMM that includes internal triangulation of grid cells proves to generate more accurate DTOF solutions than those Eikonal equation discretization schemes relying purely on corner point grids. Taking advantage of the analytic solution within the well cell and the more accurately calculated minimum and maximum DTOFs for each grid cell, a hybrid cumulative pore volume as a function of the DTOF can be used to better represent the pressure front propagation. Hence, the $w(\tau)$ function constructed from a local differentiation of the hybrid cumulative pore volume on individual τ-intervals can lead to a stable and consistent transient flow simulation.
3) The analytic sensitivity coefficients of the DTOF with respect to reservoir parameters can be efficiently formulated by taking the functional derivative of the Eikonal equation, which had been validated with the numerical computation and proves to be able to tremendously improve the computational speed in sensitivity-based inversion. For a given time during the constant flow rate well test, magnitudes of the well test derivative sensitivity to reservoir properties in the near-well region are larger than those in regions far away from the well. For a specific location in the reservoir model, the maximum magnitude of sensitivity coefficient of the well test derivative with respect to

permeability is found to occur approximately when the depth of investigation (DOI) passes by. Thus, largest magnitudes of reservoir parameter modifications in inversion occur approximately at the DOI, which is a function of time. Permeability values both within and beyond the DOI will be updated during history matching of the reservoir models with the pressure transient data, with major permeability modifications occurring within the DOI. Linearly distributed τ-intervals defined from the wellbore to the reservoir outer boundary are recommended to be used for calculation of the analytic sensitivity coefficients. Adjustment of reservoir parameters within equally spaced τ-intervals makes regularization of the penalized objective function much easier than logarithmically defined τ-intervals, especially when the prior information is far from accurate.

4) The anisotropic FMM that includes the local Eikonal solver we propose can be used to calculate the DTOF within corner point grid reservoir models. The DTOF generated can represent pressure and fluid communications between grid cells with complex geologic features like faults and pinch-outs.

6.2 Research Outlook

Although efficient numerical algorithms are designed for pressure transient analysis and integration of the well test data into reservoir models, the methodology we propose still has large room to improve. Recommendations for future work are provided below.

1) In most of the cases when the asymptotic pressure approximation is applied, it is assumed that the heterogeneous porous media are "sufficiently" smooth and the simulation is under the transient state. In field cases where the reservoir heterogeneity is high, the well response discrepancy between the asymptotic pressure approximation and the reservoir simulator becomes large. It is recommended to include more exponential terms in the asymptotic pressure approximation, which might represent pressure front reflection, so that the 3D forward model can more accurately represent the flow behavior in highly heterogeneous reservoir models.
2) The hybrid version of the drainage volume discretization we designed makes the flow simulation in the near-well region much more accurate. This hybrid drainage volume formulation might provide insights into the efficient well placement design.
3) The current FMM-based data integration technique works well for pressure transient analysis. It is recommended to extend this sensitivity-based inversion methodology to rate transient analysis where well pressure is fixed.
4) Meanwhile, data integration using analytic sensitivity coefficients of well test data with respect to reservoir permeability can be extended to multiple-well scenarios.
5) Aside from the deterministic approach, we might consider assimilating well pressure or production data into reservoir models using the ensemble Kalman filter (EnKF). Analytic sensitivity coefficients of the DTOF to reservoir

parameters calculated from the FMM can be applied to the "covariance localization" for history matching.

6) Tracking the characteristic vector within the local Eikonal solver within the FMM suggests that it might be related to the velocity (streamline) trajectory generated from the convection-diffusion equation. A projection method might be applied to the characteristic vectors, so that they can transform into a mass conservative velocity field.
7) Since integration of pressure transient data into reservoir models has been successfully achieved, it is recommended to consider calibrating reservoir model parameters by water-cut data using the FMM. Analytic sensitivity coefficients of the convective time of flight (TOF) with respect to velocity values within the reservoir grid cell can be derived through functional derivative of the Eikonal equation. Extra efforts are suggested to be made to investigate the relationship between the velocity field and reservoir permeability and porosity, so that the analytic sensitivity coefficients of the TOF and water-cut with respect to reservoir parameters can be established for inversion.

REFERENCES

Abacioglu, Y., Oliver, D., and Reynolds, A. 2001. Efficient reservoir history matching using subspace vectors. *Computational Geosciences*, 5 (2), 151-172.

Abbaszadeh, M.D., and Cinco-Ley, H. 1995. Supplement to Pressure-Transient Behavior in a Reservoir With a Finite-Conductivity Fault. Society of Petroleum Engineers. SPE-30227-MS.

Agarwal, R.G., Al-Hussainy, R., and Ramey, H.J., Jr. 1970. An Investigation of Wellbore Storage and Skin Effect in Unsteady Liquid Flow: 1. Analytical Treatment. *SPE Journal*, 10 (3), 279-290.

Blasingame, T.A., Johnston, J.L., Lee, W.J., and Raghavan, R. 1989. The Analysis of Gas Well Test Data Distorted by Well bore Storage Using an Explicit Deconvolution Method. Paper presented at the SPE Gas Technology Symposium, Dallas, Texas, USA, 7-9 June. Society of Petroleum Engineers. DOI: 10.2118/19099-MS.

Bonet-Cunha, L., Oliver, D.S., Redner, R.A., and Reynolds, A.C. 1998. A Hybrid Markov Chain Monte Carlo Method for Generating Permeability Fields Conditioned to Multiwell Pressure Data and Prior Information. *SPE Journal*, 3 (03), 261-271.

Bourdet, D., Ayoub, J.A., and Pirard, Y.M. 1989. Use of Pressure Derivative in Well Test Interpretation. *SPE Formation Evaluation*, 4 (02), 293-302.

Bourdet, D. 2002. *Well Test Analysis: The Use of Advanced Interpretation Models.* Amsterdam, The Netherlands: Elsevier. Original edition. ISBN: 978-0444509680.

Chen, Y. and Zhang, D. 2006. Data assimilation for transient flow in geologic formations via ensemble Kalman filter. *Advances in Water Resources*, 29 (8), 1107-1122.

Cheng, H., Datta-Gupta, A., and He, Z. 2005. A Comparison of Travel-Time and Amplitude Matching for Field-Scale Production-Data Integration: Sensitivity, Nonlinearity, and Practical Implications. *SPE Journal*, 10 (01), 75-90.

Chu, L., and Reynolds, A.C. 1994. Analysis of Pressure Data From Heterogeneous Reservoirs: Wellbore Storage and Skin Effects, Paper presented at the SPE Western Regional Meeting, Long Beach, California, USA, 23-25 March. Society of Petroleum Engineers. DOI: 10.2118/27902-MS.

Chu, L., Reynolds, A.C., and Oliver, D.S. 1995a. Computation of Sensitivity Coefficients for Conditioning the Permeability Field to Well-Test Pressure Data. *In Situ*, 19 (2), 179-223.

Chu, L., Reynolds, A.C., and Oliver, D.S. 1995b. Reservoir Description From Static and Well-Test Data Using Efficient Gradient Methods, Paper presented at the International Meeting on Petroleum Engineering, Beijing, China, 14-17 November. Society of Petroleum Engineers. DOI: 10.2118/29999-MS.

Chu, W.C., Garciarivera, J., and Raghavan, R. 1980. Analysis of Interference Test Data Influenced by Wellbore Storage and Skin at the Flowing Well. *Journal of Petroleum Technology*, 32 (1), 171-178.

Cinco-Ley, H. and Samaniego V, F. 1977. Effect Of Wellbore Storage And Damage On The Transient Pressure Behavior Of Vertically Fractured Wells. Paper presented at the SPE Annual Fall Technical Conference and Exhibition, Denver, Colorado, USA, 9-12 October. Society of Petroleum Engineers. DOI: 10.2118/6752-MS.

Crandall, M.G. and Lions, P.L. 1983. Viscosity Solutions of Hamilton-Jacobi Equations. *Transactions of the American Mathematical Society*, 277 (1), 1-42.

Crandall, M.G. and Lions, P.L. 1984. Two Approximations of Solutions of Hamilton-Jacobi Equations, *Mathematics of Computation*, 43 (167), 1-19.

Datta-Gupta, A., Lake, L.W., and Pope, G.A. 1995. Characterizing Heterogeneous Permeable Media with Spatial Statistics and Tracer Data Using Sequential Simulated Annealing, *Mathematical Geology*, 27 (6), 763-787.

Datta-Gupta, A. and King, M.J. 1995. A Semianalytic Approach to Tracer Flow Modeling in Heterogeneous Permeable Media. *Advances in Water Resources*, 18 (1), 9-24.

Datta-Gupta, A., Kulkarni, K.N., Yoon, S., and Vasco, D.W. 2001. Streamlines, ray tracing and production tomography: generalization to compressible flow. *Petroleum Geoscience*, 7, S75-S86.

Datta-Gupta, A. and King, M.J. 2007. *Streamline Simulation: Theory and Practice*. Richardson, Texas, USA: Society of Petroleum Engineers. Original edition. ISBN: 978-1555631116.

Datta-Gupta, A., Xie, J., Gupta, N., King, M.J., and Lee, W.J. 2011. Radius of Investigation and its Generalization to Unconventional Reservoirs. *Journal of Petroleum Technology*, 63 (07), 52-55.

Daungkaew, S., Hollaender, F., and Gringarten, A.C. 2000. Frequently Asked Questions in Well Test Analysis. Paper presented at the SPE Annual Technical Conference and Exhibition, Dallas, Texas, USA, 1-4 October. Society of Petroleum Engineers. DOI: 10.2118/63077-MS.

Denson, A.H., Smith, J.T., and Cobb, W.M. 1976. Determining Well Drainage Pore Volume and Porosity From Pressure Buildup Tests. *SPE Journal*, 16 (04), 209-216.

Deutsch, C.V. and Journel, A.G. 1994. The Application of Simulated Annealing to Stochastic Reservoir Modeling. *SPE Advanced Technology Series*, 2 (02), 222-227.

Duijndam, A.J.W. 1988a. Bayesian-Estimation in Seismic Inversion. Part I: Principles. *Geophysical Prospectecting*, 36 (8), 878-898.

Duijndam, A.J.W. 1988b. Bayesian-Estimation in Seismic Inversion. Part II: Uncertainty Analysis. *Geophysical Prospectecting*, 36 (8), 899-918.

Earlougher, R.C., Jr. 1971. Estimating Drainage Shapes from Reservoir Limit Tests. *Journal of Petroleum Technology*, 23 (10), 1266-1268.

Ehlig-Economides, C.A. and Joseph, J. 1987. A New Test for Determination of Individual Layer Properties in a Multilayered Reservoir. *SPE Formation Evaluation*, 2 (03), 261-283.

Feitosa, G.S., Chu, L.F., Thompson, L.G., and Reynolds, A.C. 1994. Determination of Permeability Distribution from Well-Test Pressure Data. *Journal of Petroleum Technology*, 46 (7), 607-615.

Fujita, Y., Datta-Gupta, A., and King, M.J. 2016. A Comprehensive Reservoir Simulator for Unconventional Reservoirs That Is Based on the Fast Marching Method and Diffusive Time of Flight. *SPE Journal*, 21 (06), 2276-2288.

Gringarten, A.C. and Ramey, H.J., Jr. 1974. Unsteady-State Pressure Distributions Created by a Well With a Single Horizontal Fracture, Partial Penetration, or Restricted Entry, *SPE Journal*, 14 (04), 413-426.

Gringarten, A.C., Ramey, H.J., Jr., and Raghavan, R. 1974. Unsteady-State Pressure Distributions Created by a Well With a Single Infinite-Conductivity Vertical Fracture. *SPE Journal*, 14 (04), 347-360.

Gringarten, A.C., Bourdet, D.P., Landel, P.A., and Kniazeff, V.J. 1979. A Comparison Between Different Skin And Wellbore Storage Type-Curves For Early-Time Transient Analysis. Paper presented at the SPE Annual Technical Conference and Exhibition, Las Vegas, Nevada, USA, 23-26 September. Society of Petroleum Engineers. DOI: 10.2118/8205-MS.

He, N., Reynolds, A.C., and Oliver, D.S. 1997. Three-Dimensional Reservoir Description From Multiwell Pressure Data and Prior Information. *SPE Journal*, 2 (03), 312-327.

He, Z., Parikh, H., Datta-Gupta, A., Perez, J., and Pham, T. 2004. Identifying Reservoir Compartmentalization and Flow Barriers From Primary Production Using Streamline Diffusive Time of Flight. *SPE Reservoir Evaluation & Engineering*, 7 (03), 234-247.

He, Z., Datta-Gupta, A., and Vasco, D.W. 2006. Rapid inverse modeling of pressure interference tests using trajectory-based traveltime and amplitude sensitivities. *Water Resources Research*, 42 (3), W03419, 1-15.

Hegan, D. 2008. Available online: https://share.tno.nl/Download/73d38836-8e3d-4e91-92c2-9a33ab260c48/02dcfa5e-7eca-4fe4-a1c3-fb72cf3f522f, TNO, Utrecht, The Netherlands. Accessed on: 31 March, 2018.

Horne, R.N. 1995. *Modern Well Test Analysis: A Computer-Aided Approach*. Palo Alto, California, USA: Petroway, Inc. Original edition. ISBN: 978-0962699214.

Horner, D.R. 1951. Pressure Build-up in Wells. Paper presented at the 3rd World Petroleum Congress, The Hague, The Netherlands, 28 May-6 June. World Petroleum Congress. WPC-4135.

Iino, A. 2018. Efficient History Matching and Optimization of Unconventional Reservoirs using the Fast Marching Method, Ph.D. Dissertation, Texas A&M University, College Station, Texas, USA.

Ikoku, C.U. and Ramey, H.J. 1980. Wellbore Storage and Skin Effects during the Transient Flow of Non-Newtonian Power-Law Fluids in Porous Media, *SPE Journal*, 20 (1), 25-38.

Islam, M.S. and Manzocchi, T. 2017. The transmissibility of faulted connections in corner-point geometry models. *Petroleum Geoscience*, 23 (1), 148-158.

Jin, S., Madariaga, R., Virieux, J., and Lambare, G. 1992. Two-Dimensional Asymptotic Iterative Elastic Inversion, *Geophysical Journal International*, 108 (2), 575-588.

Johnson, P.W. 1988. The Relationship Between Radius of Drainage and Cumulative Production. *SPE Formation Evaluation*, 3 (01), 267-270.

Jones, L.G. 1963. Reservoir Reserve Tests, *Journal of Petroleum Technology*, 15 (03), 333-337.

Jones, P. 1957. Drawdown Exploration Reservoir Limit, Well and Formation Evaluation. Paper presented at the Permian Basin Oil Recovery Conference, Midland, Texas, USA, 18-19 April. Society of Petroleum Engineers. DOI: 10.2118/824-G.

Jones, P. 1962. Reservoir Limit Test on Gas Wells. *Journal of Petroleum Technology*, 14(06), 613-619.

Joseph, J.A. and Koederitz, L.F. 1985. Unsteady-State Spherical Flow with Storage and Skin. *SPE Journal*, 25 (6), 804-822.

Kazemi, H., Seth, M.S., and Thomas, G.W. 1969. The Interpretation of Interference Tests in Naturally Fractured Reservoirs with Uniform Fracture Distribution. *SPE Journal*, 9 (04), 463-472.

King, M.J., Wang, Z., and Datta-Gupta, A. 2016. Asymptotic Solutions of the Diffusivity Equation and Their Applications. Paper presented at the SPE Europec featured at 78th EAGE Conference and Exhibition, Vienna, Austria, 30 May-2 June. Society of Petroleum Engineers. DOI: 10.2118/180149-MS.

Konukoglu, E., Sermesant, M., Clatz, O., Peyrat, J.-M., Delingette, H., and Ayache, N. 2007. A Recursive Anisotropic Fast Marching Approach to Reaction Diffusion Equation: Application to Tumor Growth Modeling. Paper presented at the Information Processing in Medical Imaging (IPMI): 20th International Conference, Kerkrade, The Netherlands, 2-6 July. Proceedings, Karssemeijer, N. and Lelieveldt, B (Eds.): 687-699. Springer-Verlag Berlin Heidelberg.

Kou, R., Moridis, G.J., and Blasingame, T.A. 2018a. Analysis and Modeling of Proppant Transport in Inclined Hydraulic Fractures. Paper presented at the SPE Hydraulic Fracturing Technology Conference and Exhibition, The Woodlands, Texas, USA, 23-25 January. Society of Petroleum Engineers. DOI: 10.2118/189856-MS.

Kou, R., Moridis, G.J., and Blasingame, T.A. 2018b. Field Scale Proppant Transport Simulation and Its Application to Optimize Stimulation Strategy. Paper presented at the SPE/AAPG/SEG Unconventional Resources Technology Conference, Houston, Texas, USA, 23-25 July. Unconventional Resources Technology Conference (URTEC). DOI: 10.15530/URTEC-2018-2878230.

Kuchuk, F.J. 2009. Radius of Investigation for Reserve Estimation From Pressure Transient Well Tests. Paper presented at the SPE Middle East Oil and Gas Show and Conference, Manama, Bahrain, 15-18 March. Society of Petroleum Engineers. DOI: 10.2118/120515-MS.

Kulkarni, K.N., Datta-Gupta, A., and Vasco, D.W. 2001. A Streamline Approach for Integrating Transient Pressure Data into High-Resolution Reservoir Models. *SPE Journal*, 6 (3), 273-282.

Lambare, G., Virieux, J., Madariaga, R., and Jin, S. 1992. Iterative Asymptotic Inversion in the Acoustic Approximation. *Geophysics*. 57 (9), 1138-1154.

Landa, J.L. and Horne, R.N. 1997. A Procedure to Integrate Well Test Data, Reservoir Performance History and 4-D Seismic Information into a Reservoir Description. Paper presented at the SPE Annual Technical Conference and Exhibition, San Antonio, Texas, USA, 5-8 October. Society of Petroleum Engineers. DOI: 10.2118/38653-MS.

Landa, J.L., Horne, R.N., Kamal, M.M., and Jenkins, C.D. 2000. Reservoir Characterization Constrained to Well-Test Data: A Field Example. *SPE Reservoir Evaluation & Engineering*, 3 (04), 325-334.

Lee, J. 1982. *Well Testing*. Richardson, Texas, USA: Society of Petroleum Engineers. Original edition. ISBN: 978-0895203175.

Lee, J., Rollins, J.B., and Spivey, J.P. 2003. *Pressure Transient Testing*. Richardson, Texas, USA: Society of Petroleum Engineers. Original edition. ISBN: 978-1555630997.

Lelievre, P.G., Farquharson, C.G., and Hurich, C.A. 2011. Computing first-arrival seismic traveltimes on unstructured 3-D tetrahedral grids using the Fast Marching Method, *Geophysical Journal International*, 184 (2), 885-896.

Li, C. and King, M.J. 2016. Integration of Pressure Transient Data Into Reservoir Models Using the Fast Marching Method. Paper presented at the SPE Europec featured at 78th EAGE Conference and Exhibition, Vienna, Austria, May-2 June. Society of Petroleum Engineers. DOI: 10.2118/180148-MS.

Li, G., Han, M., Banerjee, R., and Reynolds, A.C. 2010. Integration of Well-Test Pressure Data Into Heterogeneous Geological Reservoir Models. *SPE Reservoir Evaluation & Engineering*, 13 (03), 496-508.

Li, H. 2016. Wave Propagation Models Capture Pressure Behavior in Heterogeneous Unconventional Reservoirs. Paper presented at the SPE Annual Technical Conference and Exhibition, Dubai, UAE, 26-28 September. Society of Petroleum Engineers. DOI: 10.2118/184504-STU.

Luo, S. and Qian, J. 2012. Fast Sweeping Methods for Factored Anisotropic Eikonal Equations: Multiplicative and Additive Factors. *Journal of Scientific Computing*, 52 (2), 360-382.

Luo, S., Qian, J., and Burridge, R. 2014. High-Order Factorization Based High-Order Hybrid Fast Sweeping Methods for Point-Source Eikonal Equations, *SIAM Journal on Numerical Analysis*, 52 (1), 23-44.

Manzocchi, T., Walsh, J.J., Nell, P., and Yielding, G. 1999. Fault transmissibility multipliers for flow simulation models, *Petroleum Geoscience*, 5 (1), 53-63.

Matthews, C.S., Brons, F., and Hazebroek, P. 1954. A Method for Determination of Average Pressure in a Bounded Reservoir. Paper presented at the Petroleum Branch Fall Meeting, Dallas, Texas, USA, 19-21 October. Society of Petroleum Engineers. SPE-296-G.

Miller, C.C., Dyes, A.B., and Hutchinson, C.A. 1950. The Estimation of Permeability and Reservoir Pressure from Bottom Hole Pressure Build-up Characteristics, *Petroleum Transactions, AIME*, 189, 91-104.

Miller, C.W. 1980. Wellbore Storage Effects in Geothermal Wells. *SPE Journal*, 20 (6), 555-566.

Nunna, K., Zhou, P., and King, M.J. 2015. Novel Diffuse Source Pressure Transient Upscaling. Paper presented at the SPE Reservoir Simulation Symposium, Houston, Texas, USA, 23-25 February. Society of Petroleum Engineers. DOI: 10.2118/173293-MS.

Nunna, K. 2017. Application of Pressure Transient Concepts for Improved Upscaling of Geologic Models. Paper presented at the SPE Annual Technical Conference and Exhibition, San Antonio, Texas, USA, 9-11 October. Society of Petroleum Engineers. DOI: 10.2118/189293-STU.

Nunna, K. and King, M.J. 2017. Dynamic Downscaling and Upscaling in High Contrast Systems. Paper presented at the SPE Reservoir Simulation Conference, Montgomery, Texas, USA, 20-22 February. Society of Petroleum Engineers. DOI: 10.2118/182689-MS.

Nunna, K., Liu, C., and King, M.J. 2018. Application Of Diffuse Source Basis Functions To Multiscale Simulation. Paper presented at the ECMOR XVI-16th European Conference on the Mathematics of Oil Recovery, Barcelona, Spain, 3-6 September. EAGE. DOI: 10.3997/2214-4609.201802250.

Oliver, D.S. 1990. The Averaging Process in Permeability Estimation From Well-Test Data. *SPE Formation Evaluation*, 5 (03), 319-324.

Oliver, D.S. 1992. Estimation of Radial Permeability Distribution From Well-Test Data, *SPE Formation Evaluation*, 7 (04), 290-296.

Oliver, D.S. 1993. The Influence of Nonuniform Transmissivity and Storativity on Drawdown. *Water Resources Research*, 29 (1), 169-178.

Oliver, D.S. 1994. Application of a Wave Transform to Pressure Transient Testing in Porous Media. *Transport in Porous Media*, 16 (3), 209-236.

Oliver, D.S., He, N., and Reynolds, A.C. 1996. Conditioning Permeability Fields to Pressure Data. Paper presented at the ECMOR V-5th European Conference on the Mathematics of Oil Recovery, Leoben, Austria, 3-6 September, EAGE, 259-270.

Oliver, D.S. 1996. Multiple Realizations of the Permeability Field From Well Test Data. *SPE Journal*, 1 (02), 145-154.

Oliver, D.S., Cunha, L.B., and Reynolds, A.C. 1997. Markov Chain Monte Carlo Methods for Conditioning a Permeability Field to Pressure Data, *Mathematical Geology*, 29 (1), 61-91.

Oliver, D.S., Reynolds, A.C., Bi, Z.X., and Abacioglu, Y. 2001. Integration of production data into reservoir models, *Petroleum Geoscience*, 7, S65-S73.

Oliver, D.S., Reynolds, A.C., and Liu, N. 2008. *Inverse Theory for Petroleum Reservoir Characterization and History Matching*. The Edinburgh Building, Cambridge CB2 8RU, UK: Cambridge University Press. Original edition. ISBN: 978-0511398513.

Oliver, D.S. and Chen, Y. 2011. Recent progress on reservoir history matching: a review. *Computational Geosciences*, 15 (1), 185-221.

Ouenes, A., Brefort, B., Meunier, G., and Dupere, S. 1993. A New Algorithm for Automatic History Matching: Application of Simulated Annealing Method (SAM) to Reservoir Inverse Modeling. Society of Petroleum Engineers. SPE-26297-MS.

Paige, C.C. and Saunders, M.A. 1982. LSQR-An Algorithm for Sparse Linear-Equations and Sparse Least-Squares. *ACM Transactions on Mathematical Software*, 8 (1), 43-71.

Parker, R.L. 1994. *Geophysical Inverse Theory*. 41 William Street, Princeton, New Jersey, USA: Princeton University Press. Original edition. ISBN: 978-0691036342.

Pedrosa, O.A., Jr. and Aziz, K. 1986. Use of a Hybrid Grid in Reservoir Simulation. *SPE Reservoir Engineering*, 1 (06), 611-621.

Philip, J.R. 1989. The Scattering Analog for Infiltration in Porous Media. *Reviews of Geophysics*, 27 (4), 431-448.

Pierce, A. 1986. Wave Methods for an Inverse Problem in Diffusion. *Inverse Problem*, 2 (2), 205-217.

Ponting, D.K. 1989. Corner Point Geometry in Reservoir Simulation. Paper presented at the ECMOR I-1st European Conference on the Mathematics of Oil Recovery, Cambridge, UK, 1 July. EAGE. DOI: 10.3997/2214-4609.201411305.

Press, W.H., Teukolsky, S.A., Vetterling, W.T., and Flannery, B.P. 1988. *Numerical Recipes: The Art of Scientific Computing*. The Edinburgh Building, Cambridge CB2 8RU, UK: Cambridge University Press. Original edition. ISBN: 978-0521354653.

Qian, J. and Symes, W.W. 2001. Paraxial Eikonal Solvers for Anisotropic Quasi-P Travel Times, *Journal of Computational Physics*, 173 (1), 256-278.

Qian, J., Zhang, Y.T., and Zhao, H.K. 2007. A fast sweeping method for static convex Hamilton-Jacobi equations. *Journal of Scientific Computing*, 31 (1-2), 237-271.

Ramey, H.J., Jr. 1970. Short-Time Well Test Data Interpretation in Presence of Skin Effect and Wellbore Storage. *Journal of Petroleum Technology*, 22 (01), 97-104.

Rawlinson, N. and Sambridge, M. 2004. Wave front evolution in strongly heterogeneous layered media using the fast marching method. *Geophysical Journal International*, 156 (3), 631-647.

Rawlinson, N. and Sambridge, M. 2005. The fast marching method: an effective tool for tomographic imaging and tracking multiple phases in complex layered media, *Exploration Geophysics*, 36 (4), 341-350.

Reynolds, A.C., He, N., Chu, L., and Oliver, D.S. 1996. Reparameterization Techniques for Generating Reservoir Descriptions Conditioned to Variograms and Well-Test Pressure Data. *SPE Journal*, 1 (04), 413-426.

Reynolds, A.C., He, N., and Oliver, D.S. 1999. Reducing Uncertainty in Geostatistical Description With Well Testing Pressure Data. *Reservoir Characterization-Recent Advances, AAPG Memoir* 71, 149-162.

Rodrigues, J.R.P. 2005. Calculating Derivatives for History Matching in Reservoir Simulators. Paper presented at the SPE Reservoir Simulation Symposium, The Woodlands, Texas, USA, 31 January-2 February. Society of Petroleum Engineers. DOI: 10.2118/93445-MS.

Rodrigues, J.R.P. 2006. Calculating derivatives for automatic history matching. *Computational Geosciences*, 10 (1), 119-136.

Romero, C.E., Carter, J.N., Gringarten, A.C., and Zimmerman, R.W. 2000. A Modified Genetic Algorithm for Reservoir Characterisation. Paper presented at the International Oil and Gas Conference and Exhibition in China, Beijing, China, 7-10 November. Society of Petroleum Engineers. DOI: 10.2118/64765-MS.

Sagar, R.K., Kelkar, M.G., and Thompson, L.G. 1995. Reservoir Description by Integration of Well Test Data and Spatial Statistics. *SPE Formation Evaluation*, 10 (04), 267-274.

Sen, M.K., Datta-Gupta, A., Stoffa, P.L., Lake, L.W., and Pope, G.A. 1995. Stochastic Reservoir Modeling Using Simulated Annealing and Genetic Algorithm. *SPE Formation Evaluation*, 10 (01), 49-56.

Sethian, J.A. 1996. A fast marching level set method for monotonically advancing fronts. *PNAS*, 93 (4), 1591-1595.

Sethian, J.A. 1999. Fast Marching Methods. *SIAM Review*, 41 (2), 199-235.

Sethian, J.A. and Vladimirsky, A. 2000. Fast methods for the Eikonal and related Hamilton-Jacobi equations on unstructured meshes. *PNAS*, 97 (11), 5699-5703.

Sevink, A.G.J. and Herman, G.C. 1996. Three-dimensional, nonlinear, asymptotic seismic inversion. *Inverse Problems*, 12 (5), 757-777.

Silin, D. and Goloshubin, G. 2010. An Asymptotic Model of Seismic Reflection from a Permeable Layer. *Transport in Porous Media*, 83 (1), 233-256.

Silin, D.B., Korneev, V.A., Goloshubin, G.M., and Patzek, T.W. 2006. Low-frequency Asymptotic Analysis of Seismic Reflection From a Fluid-Saturated Medium, *Transport in Porous Media*, 62 (3), 283-305.

Sun, Y. and Fomel, S. 1998. Fast-marching Eikonal Solver In the Tetragonal Coordinates. Paper presented at the 1998 SEG Annual Meeting, New Orleans, Louisiana, 13-18 September. Society of Exploration Geophysicists. SEG-1998-1949.

Tarantola, A. 2005. *Inverse Problem Theory and Methods for Model Parameter Estimation*. 3600 University City Science Center, Philadelphia, Pennsylvania, USA: Society for Industrial and Applied Mathematics. Original edition. ISBN: 0-89871-572-5.

Thompson, L.G. and Reynolds, A.C. 1997. Well Testing for Radially Heterogeneous Reservoirs Under Single and Multiphase Flow Conditions. *SPE Formation Evaluation*, 12 (01), 57-64.

Tiab, D. and Puthigai, S.K. 1988. Pressure-Derivative Type Curves for Vertically Fractured Wells. *SPE Formation Evaluation*, 3 (01), 156-158.

Tiab, D. 1994. Analysis of pressure and pressure derivative without type-curve matching: Vertically fractured wells in closed systems. *Journal of Petroleum Science and Engineering*, 11 (4), 323-333.

Tongpenyai, Y. and Raghavan, R. 1981. The Effect of Wellbore Storage and Skin on Interference Test Data. *Journal of Petroleum Technology*, 33 (1), 151-160.

Vasco, D.W., Keers, H., and Karasaki, K. 2000. Estimation of reservoir properties using transient pressure data: An asymptotic approach. *Water Resources Research*, 36 (12), 3447-3465.

Vasco, D.W. and Finsterle, S. 2004. Numerical trajectory calculations for the efficient inversion of transient flow and tracer observations. *Water Resources Research*, 40 (1), W01507, 1-17.

Vasco, D.W., Datta-Gupta, A., Behrens, R., Condon, P., and Rickett, J. 2004. Seismic imaging of reservoir flow properties: Time-lapse amplitude changes. *Geophysics*, 69 (6), 1425-1442.

Vasco, D.W. 2004. Seismic imaging of reservoir flow properties: Time-lapse pressure changes. *Geophysics*, 69 (2), 511-521.

Vasco, D.W., Ferretti, A., and Novali, F. 2008. Estimating permeability from quasi-static deformation: Temporal variations and arrival-time inversion. *Geophysics*, 73 (6), O37-O52.

Virieux, J., Floresluna, C., and Gibert, D. 1994. Asymptotic Theory for Diffusive Electromagnetic Imaging. *Geophysical Journal International*, 119 (3), 857-868.

Wang, Z., Li, C., and King, M. 2017. Validation and Extension of Asymptotic Solutions of Diffusivity Equation and Their Applications to Synthetic Cases. Paper presented at the SPE Reservoir Simulation Conference, Montgomery, Texas, USA, 20-22 February. Society of Petroleum Engineers. DOI: 10.2118/182716-MS.

Wang, Z., Malone, A., and King, M.J. 2018. Quantitative Production Analysis and EUR Prediction From Unconventional Reservoirs Using a Data-Driven Drainage Volume Formulation. Paper presented at the ECMOR XVI-16th European Conference on the Mathematics of Oil Recovery, Barcelona, Spain, 3-6 September. EAGE. DOI: 10.3997/2214-4609.201802244.

Wattenbarger, R.A. and Ramey, H.J. 1970. An Investigation of Wellbore Storage and Skin Effect in Unsteady Liquid Flow: II. Finite Difference Treatment. SPE Journal, 10 (03), 291-297.

White, B.S. 2005. Asymptotic Theory of Electroseismic Prospecting. *SIAM Journal on Applied Mathematics*, 65 (4), 1443-1462.

Wijesinghe, A.M. and Culham, W.E. 1984. Single-Well Pressure Testing Solutions for Naturally Fractured Reservoirs With Arbitrary Fracture Connectivity. Paper

presented at the SPE Annual Technical Conference and Exhibition, Houston, Texas, USA, 16-19 September. Society of Petroleum Engineers. DOI: 10.2118/13055-MS.

Wijesinghe, A.M. 1985. Green's Functions for Solving Unsteady Flow Problems in Naturally Fractured Reservoirs With Arbitrary Fracture Connectivity: Part I-Theory. Paper presented at the SPE California Regional Meeting, Bakersfield, California, USA, 27-29 March. Society of Petroleum Engineers. DOI: 10.2118/13626-MS.

Wijesinghe, A.M. and Kececioglu, I. 1986. Green's Functions for Solving Unsteady Fluid Flow Problems in Naturally Fractured Reservoirs With Arbitrary Fracture Connectivity: Part II-Applications. Paper presented at the SPE California Regional Meeting, Oakland, California, USA, 2-4 April. Society of Petroleum Engineers. DOI: 10.2118/15113-MS.

Wong, D.W., Harrington, A.G., and Cinco-Ley, H. 1986. Application of the Pressure Derivative Function in the Pressure Transient Testing of Fractured Wells. *SPE Formation Evaluation*, 1 (05), 470-480.

Xie, J., Yang, C., Gupta, N., King, M.J., and Datta-Gupta, A. 2015a. Depth of Investigation and Depletion in Unconventional Reservoirs With Fast-Marching Methods. *SPE Journal*, 20 (04), 831-841.

Xie, J., Yang, C., Gupta, N., King, M.J., and Datta-Gupta, A., 2015b, Integration of Shale-Gas-Production Data and Microseismic for Fracture and Reservoir Properties With the Fast Marching Method. *SPE Journal*, 20 (02), 347-359.

Xue, X., Yang, C., Sharma, V.K., Datta-Gupta, A., and King, M.J. 2016. Reservoir and Fracture Flow Characterization Using a Novel W(τ) Formulation. Paper presented at the SPE/AAPG/SEG Unconventional Resources Technology Conference, San Antonio, Texas, USA, 1-3 August. Unconventional Resources Technology Conference. DOI: 10.15530/URTEC-2016-2440083.

Xue, X., Yang, C., Park, J., Sharma, V.K., Datta-Gupta, A., and King, M.J. 2018. Reservoir and Fracture-Flow Characterization Using Novel Diagnostic Plots. *SPE Journal*, (Preprint). DOI: 10.2118/194017-PA.

Yang, C., Xue, X., King, M.J., and Datta-Gupta, A. 2017. Flow Simulation of Complex Fracture Systems With Unstructured Grids Using the Fast Marching Method. Paper presented at the SPE/AAPG/SEG Unconventional Resources Technology Conference, Austin, Texas, USA, 24-26 July. Unconventional Resources Technology Conference. DOI: 10.15530/URTEC-2017-2691393.

Yaxley, L.M. 1987. Effect of a Partially Communicating Fault on Transient Pressure Behavior. *SPE Formation Evaluation*, 2 (04), 590-598.

Yeh, W.W.G. 1986. Review of Parameter-Identification Procedures in Groundwater Hydrology: The Inverse Problem. *Water Resources Research*, 22 (2), 95-108.

Zafari, M. and Reynolds, A.C. 2007. Assessing the Uncertainty in Reservoir Description and Performance Predictions With the Ensemble Kalman Filter. *SPE Journal*, 12 (03), 382-391.

Zhang, F. and Reynolds, A.C. 2002. Optimization Algorithms for Automatic History Matching of Production Data. Paper presented at the ECMOR VIII-8th European Conference on the Mathematics of Oil Recovery, Freiberg, Germany, 3-6 September. EAGE. DOI: 10.3997/2214-4609.201405958.

Zhang, F., Reynolds, A.C., and Oliver, D.S. 2002. Evaluation of the Reduction in Uncertainty Obtained by Conditioning a 3D Stochastic Channel to Multiwell Pressure Data. *Mathematical Geology*, 34 (6), 715-742.

Zhang, Y., Yang, C., King, M.J., and Datta-Gupta, A. 2013. Fast-Marching Methods for Complex Grids and Anisotropic Permeabilities: Application to Unconventional Reservoirs. Paper presented at the SPE Reservoir Simulation Symposium, The Woodlands, Texas, USA, 18-20 February. Society of Petroleum Engineers. DOI: 10.2118/163637-MS.

Zhang, Y., Bansal, N., Fujita, Y., Datta-Gupta, A., King, M.J., and Sankaran, S. 2016. From Streamlines to Fast Marching: Rapid Simulation and Performance Assessment of Shale-Gas Reservoirs by Use of Diffusive Time of Flight as a Spatial Coordinate. *SPE Journal*, 21 (05), 1883-1898.

Zhang, Y.T., Zhao, H.K., and Qian, J. 2006. High Order Fast Sweeping Methods for Static Hamilton-Jacobi Equations. *Journal of Scientific Computing*, 29 (1), 25-56.

Zhao, H.K., Osher, S., Merriman, B., and Kang, M. 2000. Implicit and Nonparametric Shape Reconstruction from Unorganized Data Using a Variational Level Set Method. *Computer Vision and Image Understanding*, 80 (3), 295-314.

Zhao, H.K. 2004. A Fast Sweeping Method for Eikonal Equations. *Mathematics of Computation*, 74 (250), 603-627.